VIBRATIONAL SPECTROSCOPY OF SOME ORGANIC COMPOUNDS

by

H. A. Majid

B.Sc. Hons., M.Sc., M.A.

A thesis in support of candidature

for the Degree of Doctor of Philosophy

at

The University of Southampton

April 1976

بسم الله الرحمن الرحيم

In the name of Allah, the Beneficient,
the Merciful.

To my parents

ساحل افتادہ گفت گرچہ بسی زیستم
ہیچ نہ معلوم شد آہ کہ من چیستم!

موج ز خود رفتہ تیز خرامید و گفت
ہستم اگر می روم گر نہ روم نیستم

A desolate seashore said "Alas! I have lived a long time
Nevertheless I am unaware of my being"

A violent wave moved fast and said
"My being is due to motion, if I do not move I do not exist".

Sir Dr. M. Iqbal

Acknowledgement

The author wishes to express his gratitude for the following persons and organisations without whose help this work would not have been completed.

Dr. P.J. Hendra for suggesting the topic and providing supervision.

Professor G.J. Hills for providing guidance and supervision.

The Chemistry Department of the University of Southampton for provision of research facilities.

My colleagues, Dr. D.S. Bedborough, Dr. A.J. McQuillan and Dr. E.P. Marsden for much stimulating discussions and encouragement.

My parents for their continued patience, encouragement and financial support throughout the research course.

British Council, Wali Muhammad fellowship trust and Sir Ernest Cassel educational trust for financial contributions.

Mrs. A. Lampard for her ever ready services to type the manuscript. (See section 2.8 also).

ABSTRACT

FACULTY OF SCIENCE

CHEMISTRY

Doctor of Philosophy

VIBRATIONAL SPECTROSCOPY OF SOME ORGANIC COMPOUNDS

by Hafiz Abdul Majid

In the work reported in this thesis, Raman spectroscopy in conjunction with infra red spectroscopy and other physical techniques such as D.S.C and X-ray diffraction has been used to study the structure of organic compounds and polymers.

Characteristic Raman frequencies have been deduced for a variety of molecular backbones and groups belonging to substituted benzenes. These have been shown to be particularly useful where polar substituents such as carbonyl and nitro groups are involved. Nevertheless, the joint use of Raman and IR frequencies usually provides much more information than either Raman or IR.

Considerable expertise has been developed in the synthesis of a large number of polymers and their subsequent handling and processing.

The observation of correlation band splitting and longitudinal acoustic modes which occur at very low frequencies in the Raman spectrum have been particularly emphasised because of their significance to the interpretation of polymer structure. Conclusions reached from the analysis of vibrational spectra of polyethers and polythioethers of the series $\{(CH_2)_m\text{-}Y\}_n$ (m = 1-6,10; Y = O or S), may be summarised as follows:

A careful analysis of the molecular vibrations of these polymers has been carried out before looking for correlation band splitting in their spectra. Assignments for the observed bands have

been made on the basis of reported calculations or on tentative basis. Correlation band splitting has been observed in the spectra of polyethylene oxide, polydecamethylene oxide and polythioethers with m = 2-6 and 10. It has been shown, however, that its occurrence in the spectra of polydecamethylene oxide and polythioethers with $m \geq 4$ is dependent upon the mode of crystallization and annealing. These observations have been applied to deduce molecular and crystal structures of these polymers.

The longitudinal acoustic modes observed at very low frequencies in the Raman spectra of polyethers with m = 4, 6 and 10 and polythioethers (with m = 2-6 and 10) indicate that the crystallization of these polymers is predominantly lamellar. Crystallization from solution results in very thin lamellae which thicken on annealing just below T_m. Melt crystallization, however, gives rise to well developed lamellae which thicken further on annealing. Although the application of Raman technique to this field is limited because of experimental difficulties, it offers a number of advantages over other techniques such as low angle X-ray diffraction, electron microscopy etc.

It is concluded that Raman spectroscopy is a powerful analytical technique which when applied in conjunction with other techniques, yields very much valuable information about the structure of organic compounds and polymers.

CONTENTS

TABULATED DATA

ILLUSTRATIONS

CHAPTER I

INTRODUCTION

1.1 Historical aspects

About 52 years ago Smekal[1] predicted a light scattering effect which was practically demonstrated by Raman[2] in 1928. The effect which allowed the investigation of molecular structure, was so significant that it soon caught the attention of physicists and chemists alike. Over 2000 publications reporting the spectra of more than 4000 compounds appeared in the first decade[3]. In those days IR spectroscopy was no more than a primitive technique. Although discovered in the beginning of the century, it could make little progress due to instrumentation problems. Other spectroscopic techniques such as NMR, EPR, NS and MS which now play a significant role in solving various analytical problems were almost nonexistent. The newborn technique was comparatively easy and simple, though not without difficulties. In the late 1940s and early 1950s, advances in IR instrumentation led to the introduction of IR spectrometers which offered the spectroscopist an easier, quicker and less expensive method for routine structural analysis. Raman instrumentation could not compete with IR spectroscopy in this field and subsequently underwent a steady decline. It was not until mid 1960s that the advent of continuous wave lasers and other instrumental and sampling improvements brought about a radical change in this situation and stimulated a resurgence of activity in this field.

The early work on Raman spectroscopy upto 1960 has been covered in a number of monographs including those by Hibben[3], Kohlrausch[4], Jones and Sandorfy[5], Brandmuller and Moser[6]. Theoretical aspects have been discussed in the texts of Plackzeck[7], Herzberg[8], Wilson, Decius and Cross[18] and Colthup, Daly and Wiberly[29]. The recent developments

have occasioned the publication of numerous review articles and books which deal with various aspects of theory, experimental methods and applications of this technique. General survey of the applications of laser-Raman spectroscopy has been made by Hendra et al[9] and more recently by Schrader[10]. Reviews of recent developments in the field appear annually in the annual reports on the progress of chemistry and biennially in the review issues of analytical chemistry. "Raman news letter" exchanges current developments between active workers and includes a current bibliography on Raman literature. The state-of-the-art expertise has been reviewed in the books of Szymansky[11], Gilson and Hendra[12] Tobin[13] and more recently Freeman[14], Hummel[15], Durig[16] and Ivin[17].

1.2 Fundamentals of vibrational spectroscopy

Although detailed accounts on vibrational spectroscopy have been given in the references cited above, it is appropriate to introduce some of the fundamental principles in view of their relevance in the subsequent discussions.

Raman effect

The Raman effect is a member of a group of spectral techniques which provide information on molecular vibrations. Fig. 1.1 shows energy level diagram of a diatomic molecule which represents potential energy v as a function of interatomic distance q. It is clear that a molecular vibration can be excited either by absorption of an energy quantum equivalent to the difference of ground and exicted states (a)e.g.IR spectrum,or by inelastic scattering in which the incident light quantum is partially consumed between ground and excited states before scattering (b) e.g. Raman spectrum.

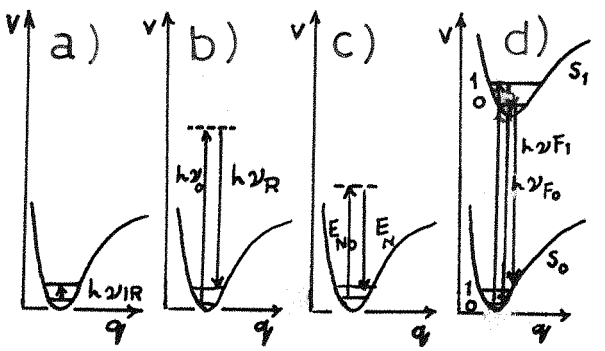

FIG. 1.1 Term diagrams of different methods for the observation of vibrational states: a) by IR spectroscopy ($h\nu_s = h\nu_{IR}$), b) by Raman spectroscopy ($h\nu_s = h\nu_o - h\nu_R$), c) by neutron spectroscopy ($h\nu_s = E_{N_D} - E_{N'}$), d) by fluorescence spectroscopy ($h\nu_s = h\nu_{F_o} - h\nu_{F_1}$), S_o = ground state, S_1 = excited state of the valence electrons.

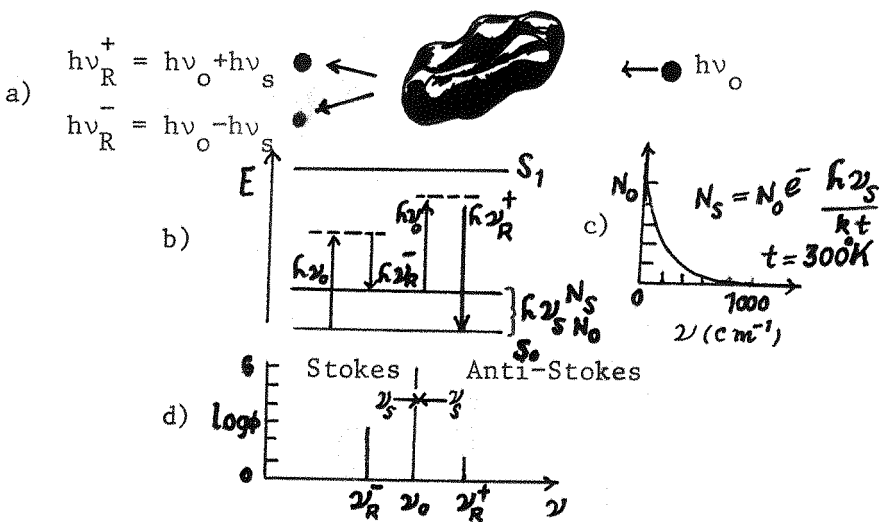

FIG. 1.2 Raman effect as inelastic impact of a light quantum with a molecule, a) impact process, b) energy level diagram, c) relative occupation of vibration level at $\tilde{\nu}$ cm^{-1} and 300°K, d) Stokes and anti-Stokes Raman spectra.

Other possible methods for the study of molecular vibrations are analysis of the inelastic scattering of mono energetic neutrons of energy E_{No} (Fig. 1.1c) and of the fluorescence spectrum (Fig. 1.1d). However, these methods are by no means as generally applicable as IR and Raman spectroscopy. The Raman effect is generated when molecules are illuminated with monochromatic light of frequency ν_o. The scattered light consists of both elastic (Raleigh) and inelastic (Raman) scatter at frequencies ν_o and $\nu_o \pm \nu_s$ respectively. Since the molecular population in ground and electronic states is described by the Boltzmann distribution law, $I\nu_o+\nu_s$ is much weaker than $I\nu_o-\nu_s$ and the intensity ratio

$$\frac{I\nu_o + \nu_s}{I\nu_o - \nu_s}$$

falls rapidly with ν. (Fig. 1.2)

Tentative values of intensity ratios are:

$$I(\text{Raman scattering}) \approx I(\text{Raleigh scattering}) \times 10^{-4}$$
$$< I(\text{Source}) \times 10^{-7}$$

In the scattering process the incident light wave represented by the electric field E induces a dipole moment P in the molecule. E and P are related as below

$$P = \alpha E$$

where α is known as the polarizability. Since E and P are vectors α is a tensor so that with respect to a system of cartesian coordinates x,y,z

$$P_x = \alpha_{xx} E_x + \alpha_{xy} E_y + \alpha_{xz} E_z$$

$$P_y = \alpha_{yx} E_x + \alpha_{yy} E_y + \alpha_{yz} E_z$$

$$P_z = \alpha_{zx} E_x + \alpha_{zy} E_y + \alpha_{zz} E_z$$

The polarizability tensor is generally a symmetric one which implies that for a special set of mutually perpendicular axes x',y',z', all terms except the diagonal ones, $\alpha_{x'x'}$, $\alpha_{y'y'}$, $\alpha_{z'z'}$, are zero. If arrows are drawn from a common origin in any direction having lengths proportional to $1/\sqrt{\alpha}$, the heads of the arrows will define a polarizability ellipsoid whose axes x',y',z' are parallel to $\alpha_{x'x'}$, $\alpha_{y'y'}$ and $\alpha_{z'z'}$ respectively. For a completely isotropic molecule the polarizability will be the same in all directions whereas for a completely anisotropic molecule $\alpha_{x'x'} \neq \alpha_{y'y'} \neq \alpha_{z'z'}$. A Raman spectrum results, if the polarizability ellipsoid changes in size, shape or orientation with vibration, rotation or rarely due to an electronic transition in the molecule.

Depolarization ratio

The polarizability tensor is made up of an isotropic or spherical part $\bar{\alpha}$ and the completely anisotropic part $\bar{\beta}$. Depolarization of a Raman mode is defined in terms of $\bar{\alpha}$ and $\bar{\beta}$ as below,

$$\rho = \frac{3\beta^2}{45\alpha^2 + 4\bar{\beta}^2}$$

while the minimum value of ρ is zero for the totally symmetric vibration which scatters only polarized radiation ($\bar{\beta} = 0$), a maximum figure of $\frac{3}{4}$ is obtained when a vibrational mode completely depolarizes the incident light($\alpha = 0$).

Obviously depolarization ratio can play a significant role in determining the symmetry of a vibration. As will be seen later it serves as an additional aid in group frequency analysis.

Selection rules: Comparison with IR

Although Raman effect basically provides the same kind of information as IR i.e. normally on molecular vibrations and rotations, a

number of intrinsic complementary differences exist between Raman and IR effects arising from basic dissimilarities in the participating physical processes.

Raman spectra arise because the polarizability ellipsoid changes in size, shape or orientation during a vibration or rotation. Quantum mechanically this is equivalent to having non zero values of the Raman transition moment integral

$$M = \int \psi_b \frac{\partial \alpha}{\partial q_k} \psi_a \, dV \neq 0$$

where

ψ_b and ψ_a are the upper and lower vibrational state functions and $\frac{\partial \alpha}{\partial q} \simeq \alpha_o + \sum_k (\frac{\partial \alpha}{\partial q_k})_o q_k$ at any instant of time during the transition; the subscript o refers to values when the nuclei are at the equilibrium positions and q_k is a normal coordinate.

In contrast, a vibrational transition giving rise to IR absorption takes place when

$$M = \int \psi_b \frac{\partial \mu}{\partial q} \psi_a \, dV \neq 0$$

where

$\frac{\partial \mu}{\partial q}$ is the dipole moment operator at any instant of time during the transition i.e. $\frac{\partial \mu}{\partial q} \simeq \mu_o + \sum_k (\frac{\partial \mu}{\partial q_k})_o q_k$.

Since the operators $\frac{\partial \alpha}{\partial q}$ and $\frac{\partial \mu}{\partial q}$ are symmetric and antisymmetric respectively, they connect the zeroeth vibrational states to the upper states which are also symmetric and antisymmetric respectively. In molecules with high effective symmetry such as those with a centre of inversion, this selectivity is such that Raman and IR active transitions are mutually exclusive (Mutual Exclusion Rule). To demonstrate the

latter, take the example of CO_2 molecule. CO_2 is a linear and centro-symmetric molecule. It is capable of performing the following vibrations.

		$\frac{\partial\mu}{\partial q}$	IR activity (ν cm^{-1})	$\frac{\partial\alpha}{\partial q}$	Raman activity ($\Delta\nu$ cm^{-1})
ν_1	O ← C → O	zero	None	Finite	1286
ν	O ↔ C → ← O	Finite	2349	zero	None
ν_3	O — C — O	Finite	667 (degenerate)	zero	None

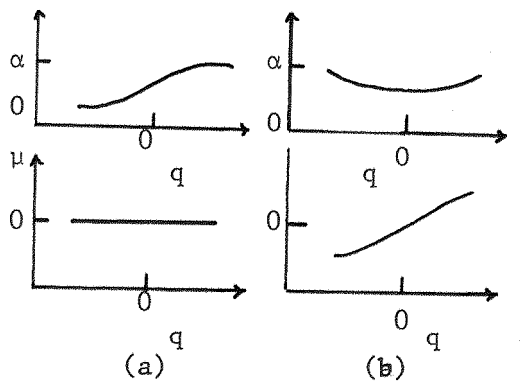

FIG. 1.3 Change of the polarizability α and the dipole moment μ of a) the symmetric, and b) the antisymmetric stretching vibration of the CO_2 molecule.

The polarizability and dipole moment functions are given in Fig. 1.3 from which it is clear that ν_1 will give rise to a Raman line but that the other modes have zero values of $(\frac{\partial\alpha}{\partial q})$ (Fig. 1.3a); the reverse is true for changes in dipole moment function $(\frac{\partial\mu}{\partial q})$ in IR absorption (Fig. 1.3b). This means that vibrations active in the Raman are inactive in the IR absorption and vice versa or the vibrations in both effects are mutually exclusive. In some molecules, some of the normal vibrations are forbidden both in the Raman and IR spectra. There are cases of molecules, however, where some normal vibrations are active both in the Raman and IR effects. These molecules usually possess little or no symmetry and are in fact very common in the realm of organic chemistry.

Raman and IR-complementary techniques

The Raman and IR techniques which form the major part of vibration spectroscopy are complementary in nature. A general purview of vibrational spectroscopy in Table 1.1 would facilitate the visualization of this fact.

Table 1.1

A general purview of vibrational spectroscopy

Characteristic features of the Vibrational spectrum	Properties of molecules or unit cells
Number of vibrations : Z	Number of atoms: n Z = 3n-6; 3n-5 (for linear molecules)
Frequencies	Mass of atoms, geometry, force constants
Intensities	Changes in properties of the electron system with changing position of atoms
In the	
IR spectrum	Change of dipole moment*
Raman spectrum	Change of polarizability*
	IR and Raman activities are dependent upon the symmetry of the vibration and the molecules or unit cells.

* The so called "silent" modes which are fortunately rare give rise to neither change of dipole moment nor polarizability and must, therefore, be measured by other techniques.

Types of vibrations

Covalently bonded atoms give rise to two types of vibrations (a) a periodic extension and contraction (stretching) and (b) a periodic bending or deformation. More complex types of vibrations also occur involving the simultaneous stretching and bending of several bonds linked to the same atom. Fig. 1.4 shows various types of vibrations associated with $> CH_2$ and $-CH_3$ groups as typical examples.

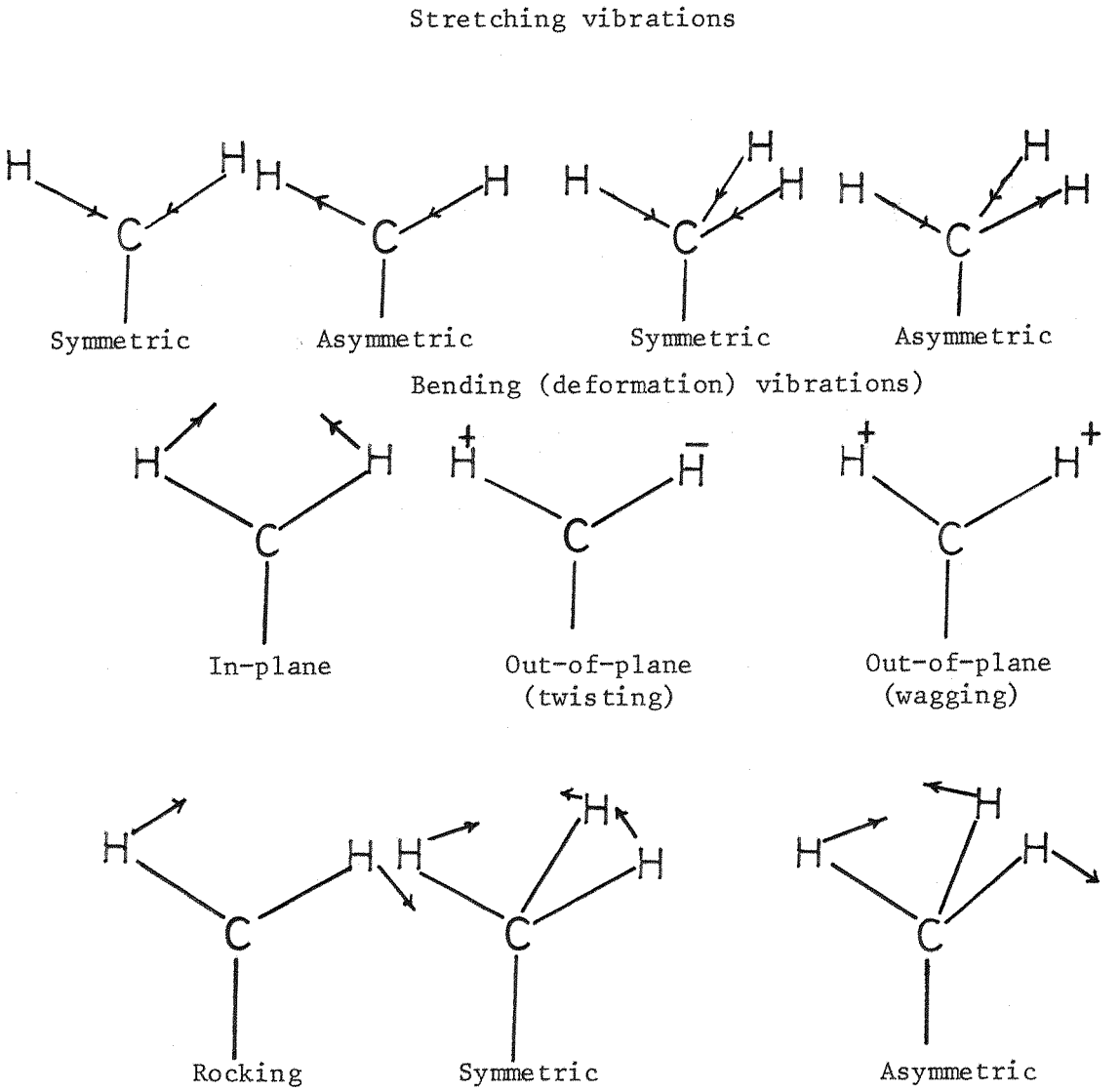

FIG. 1.4 Various types of vibrations associated with > CH_2 and $-CH_3$ groups.

1.3 The nature of vibrational group frequencies*

Molecular vibrations though complex in nature occur in clearly defined ways. The frequency of a vibration depends upon the bond strength or force constant and inversely on the masses of the vectors involved. In the case of a diatomic molecule (X - Y)

$$\nu = 1303 \frac{\left(\frac{k}{M_X M_Y}\right)^{\frac{1}{2}}}{M_X + M_Y}$$

where ν = frequency, k = force constant, M_X and M_Y are atomic weights, Calculations show that C = C group will vibrate at $\nu \approx 1650\ cm^{-1}$ and C - F, C - Cl and C - I at $\nu \approx 750\ cm^{-1}$, $\nu \approx 550\ cm^{-1}$ and $\nu \approx 350\ cm^{-1}$ respectively[28]. For most vibrations of a complex molecule, however, several bonds or angles are deformed simultaneously. Even in these cases, it is often possible to assume that a vibration may be localized in one group of the molecule when the vibrational frequency of this group taken as an isolated oscillator is different from the frequencies of the neighbouring groups. This may not hold true in the presence of severe interactions explained later. In the former case, the frequency and intensity of the vibration in the Raman and IR spectra, however, is characteristic for that group i.e. the vibration is independent of the rest of the molecule and may therefore be useful for the detection of that group. Whilst a single characteristic frequency is able to detect a particular molecular group in a compound e.g. a band between ν1650 - 1860 cm^{-1} will show the presence of a carbonyl group, a collection of group frequencies may be used to determine the structure of a molecule e.g. characteristic frequencies of the benzene ring discussed later.

* The terms "group frequency" and "characteristic frequency" will be used as synonyms in the subsequent discussions.

1.3.1 Characteristic frequencies - Raman vs IR

The first IR characteristic frequencies were compiled by Coblenz[19] in the beginning of this century. Since then IR characteristic frequencies have been deduced for a vast variety of molecular groups[20] and are used as a matter of routine in the analytical laboratories. With the birth of Raman technique due attention was given to the development of similar deductions in the Raman effect[3,4,5,6] but the eventual decline of this technique resulted in diminished activity in this field too. Though a number of characteristic Raman frequencies have been existing for a variety of groups as a result of this work, yet most of them have not been well-substantiated experimentally. The renaissance of the technique has again drawn the attention of some laboratories to this subject[21]. A compilation of Raman frequencies from the old work in comparison with the IR ones has been published by Szymansky[35]. Recent developments in this field have been combined with the old work in a book by Dollish et al[22]. Freeman[14] has published his own laser Raman work in a book recently, and a number of papers have appeared from several other workers[23,24,25,26]. A compendium of Raman group frequencies was published by U.S. air force materials laboratory in 1971 and 1973 from an analysis of $\sim$ 400 compounds[21]. Catalogues[14] giving a large variety of spectra have been compiled and computers are also being applied for this work[27].

The recent activity in the investigation of Raman group frequencies has emerged not only because of practical reasons but also because of theoretical reasons. Some of these reasons may be stated as follows:

a) The Raman spectrum predominently gives information about the molecular skeleton and the IR about the side groups. Because of the shape of μ against q (Fig. 1.5) the magnitudes of $\frac{\partial \mu}{\partial q}$ can vary widely as a function of the relative value of q* and q_{eq}. Thus vib rations of

highly polar groups may not necessarily give rise to intense absorption and different intensities of absorption may occur for similar modes in a homologous series of molecules. In contrast $\frac{\partial\alpha}{\partial q}$ and α are related (see Fig. 1.3(a)). The value of $\frac{\partial\alpha}{\partial q}$ for C-C is about $0.1nm^2$, C=C, $0.2nm^2$ and for C---C (in the benzene ring) $\sim 0.154nm^2$ in wide ranges of molecules. Thus when such a group is present in a series of molecules, the intensity of the Raman line assigned to the group will be about the same for each member of the series e.g. νC-C spectral modes give rise to strong Raman bands between 900-1150 cm^{-1} in straight chain polymers.

b) The relative activity, intensity and polarization of a vibration in the Raman and IR spectra depend upon the symmetry of both the molecule and the vibration concerned. For example a molecule AB_3 may possess either pyramidal or planar structure represented by C_{3v} or D_{3h} symmetry groups respectively[30] (Table 1.2).

Table 1.2

The vibrations of an AB_3 molecule under the D_{3h} and C_{3v} Groups

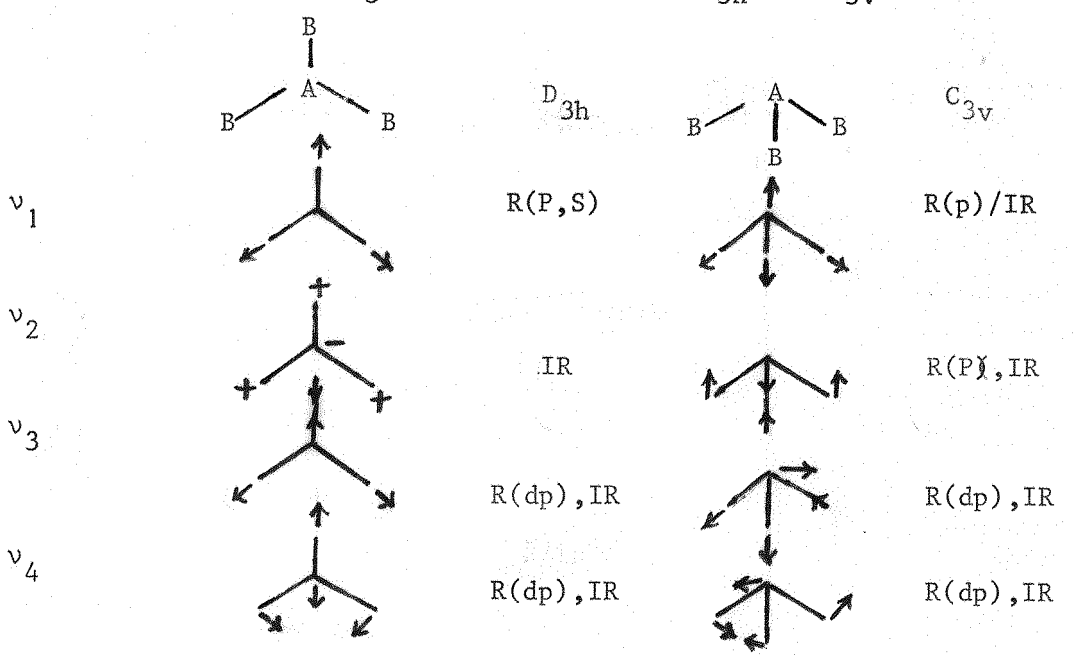

Nitrogen trichloride which is an AB_3 molecule, was found to be pyramidal by similar considerations[36] (Fig. 1.6).

For a vibration involving an X-Y group in a molecule, the stretching vibration will be stronger in the IR absorption if the X-Y bond is polar, a bending vibration will be weaker than the stretching vibration and may be absent in the Raman. The symmetric vibrations or those vibrations which are associated with bonds having symmetric charge distribution will generally give rise to stronger bands in the Raman than in the IR and reverse will hold for the asymmetric vibrations. Due to this reason S-H, C=S, C-S, S-S, C=C, C≡C, C≡N, O-O, Se-Se and N=N groups give rise to very intense bands in the Raman but O-H and N-H groups display weaker bands; the reverse happens in the IR. Because of the covalent character of these groups an empirical relation has also been suggested between the Raman intensity (I) to the ionic character (P) and atomic weight (Z) as follows[11]:

$$I = CP(Z_x + Z_y)$$

where C is a constant and X and Y are atoms forming X-Y bond. Sometimes, the high symmetry of a vibration e.g. C≡C in symmetric acetylenic compounds would result in complete disappearance of the corresponding band in the IR, but it would display a strong Raman band.

c) Whereas in the IR some vibrations such as νC-F, νO-H and νC-O give rise to very broad and strong bands and thus obscure large parts of the spectrum, this does not seem to be the case in the Raman.

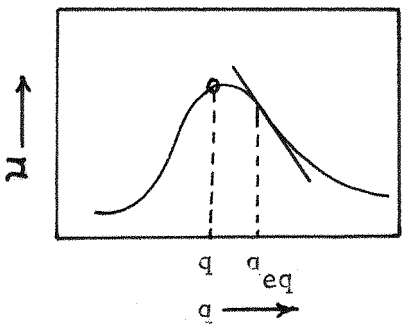

FIG. 1.5 Curve for μ against q; q_{eq} is the equilibrium interatomic distance

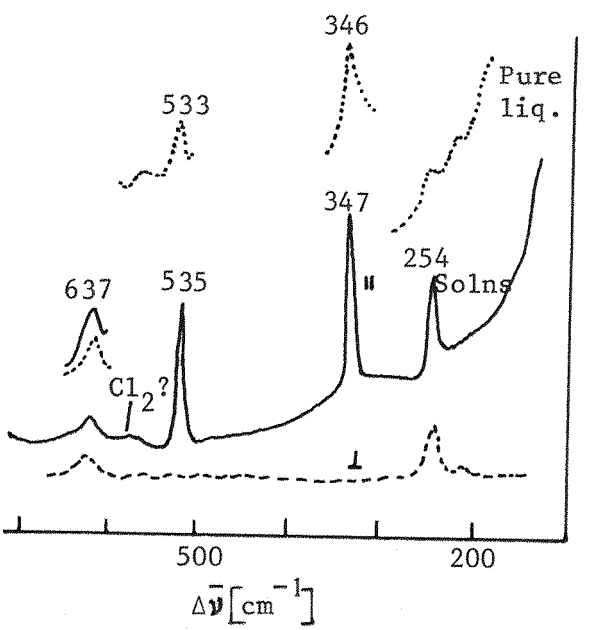

FIG. 1.6 The Raman spectrum of nitrogen chloride

∥ : parallel

⊥ : perpendicular

1.3.2 Factors influencing vibrations in complex molecules

Although the frequencies are determined primarily by the forces within the molecule, they are also affected by intermolecular forces. The spectrum of a substance, for example, will be different in gaseous liquid and solid states for the same reason.

Similarly the characteristic frequency of a group, though largely it reflects the vibration of the latter, is influenced by the environments of the associated molecular structure. Such environments may either cause the characteristic frequency band vary in intensity or position or its absence altogether. It is appropriate here to discuss some of these environments.

Vibrational coupling

The vibration of an X-Y bond would produce a band at a characteristic frequency only when the masses X and Y are largely different. If in a molecule such as X-C-Y, the masses of X, C and Y are close the X-Y and C-Y vibrations will couple and interact with each other and the resulting two bands will be displaced from their expected positions. Further their intensities will also be altered to a degree depending upon the extent of coupling. Coupling also occurs between two identical groups in the same molecule even when the groups are separated by several atoms. Almost all anhydrides gi ve rise to two carbonyl bands in the ν1750-1850 cm^{-1} region due to coupling between the in phase and out-of-phase vibrations[20]. Inter and intra molecular hydrogen bonding between a hydroxyl group and a carbonyl group of an acid, also generates symmetric and asymmetric vibrational bands due to coupling[20].

Conjugation

It has been observed that the intensities of bands associated with double or triple bonds such as C=C, C≡C, C≡N etc. are increased consider-

ably when conjugated with a system of alternate single and multiple bonds. This occurs due to the delocalization of electrons within the bonds concerned[33].

Chemical and physical effects[20]

The chemical properties affecting intensity arise from variations in the distribution of the electrons within the system resulting from replacement by substituents e.g. inductive effects. Physical effects operate due to changes in the substituent mass and interbond angles and further from intervibrational coupling.

Inductive effects[34]

An atom or a group which attracts electrons more strongly than hydrogen is said to have a negative inductive effect (-I) and any atom or group which attracts electrons less strongly than hydrogen is said to have a positive effect (+I). On this basis certain atoms and groups have been classified as follows:

a) electron attracting (-I): $NO_2 > F > Cl > Br > I > OCH_3 > C_6H_5 > H$

b) electron repelling (+I): $H > CH_3 > C_2H_5 > CH(CH_3)_2 > C(CH_3)_3$

The influence of above (a) and (b) series of inductive groups on some mono and disubstituted benzenes has been investigated by some workers. In general, (-I) effects tend to decrease the intensity of bands resulting from vibrations of neighbouring groups, and (+I) effects in contrast tend to increase the intensity.

1.3.3 Conclusion

It is clear from the above considerations that Raman technique may be developed profitably in the field of characteristic group frequencies.

Though the latter work is being carried out actively in some laboratories, a considerable effort is needed to fill the gap in this field created by the steady decline of Raman technique previously.

This work was aimed to deduce characteristic frequencies from various groups of organic compounds. Over 300 compounds belonging to a variety of structures were analysed with this purpose in mind. A list of these compounds has been presented in appendix II. The lack of space and time, however, has allowed the discussion of only a limited number of results which were the most substantiated on the basis of numerical and structural multiplicity of compounds (Chapter 3).

1.4 Organic polymers

1.4.1 Morphology[37]

Most properties of polymers are determined by their morphology which may be broadly expressed as their macro and microconformations in the bulk material.

Macroconformation

The term macroconformation refers to the overall conformation of a polymer. A number of distinct morphological units belonging to the macroconformation have been identified during the crystallization of polymers from the solution as well as melt e.g. single crystals, dendrites, hedrites, spherulites etc.

Fringed micelle model[36]

The first attempts to explain the crystallization of a polymer in the bulk produced a model called fringed micelle model consisting of ordered or crystalline regions ($\sim$ 100-200 $\mathring{A}$) within a continuous amorphous matrix. The chain was envisaged as meandering throughout the system entering and leaving several ordered regions embedded randomly in a continuous amorphous matrix (Fig. 1.7). This concept

accounted for the X-ray diffraction patterns, the density variations, the broad transition temperatures and the flexibility usually associated with the polymers. It was, however, discarded in the light of more recent developments which revealed features incompatible with this picture.

Single crystals[38,39,40]

When a polymer is crystallized from the melt, imperfect polycrystalline aggregations are formed in association with a substantial amorphous content. This is a consequence of chain entanglement and the high viscosity of the melt combining to hinder the diffusion of chains into the ordered arrays necessary for crystallite formation. If these restrictions to free movement are reduced and a polymer is allowed to crystallize from a dilute solution, it is possible to obtain well defined single crystals. The study of single crystals of a number of polymers has revealed that they are made up of thin lamellae, often lozenge shaped, sometimes oval, about 10 to 20 nm thick depending upon the temperature of crystallization . The most significant feature of these lamellae is that while the molecular chains may be as long as 1000 nm, the direction of the chain axis is across the thickness of the platelet. This indicates that the chain must be folded many times like a concertina to be accommodated in the crystal.

For a polymer such as polyethylene[37], the fold in the chain is completed using only 3 or 4 monomer units whilst the extended portions in between have about 40 monomer units.

The crystals, thus formed, have a hollow pyramid shape, because of the requirement that the chain folding must involve a staggering of the chains if the most efficient packing is to be achieved. There is also a remarkable constancy of lamellar thickness but this increases

as a function of crystallization or subsequent annealing temperatures. While opinions vary between kinetic and thermodynamic reasons for this constancy of fold length, it is suggested that the fold structure allows the maximum amount of crystallization of the molecule at a length which produces a free energy minimum in the crystal.

Measurement of the enthalpy of fusion of single crystals[42] and nitric acid oxidation studies[43] have shown that a significant amorphous content is still associated with each crystal. This must be on the surface and it has been suggested that it arises from the disordered folding planes produced by the emergence and reentry of a chain in the crystal. Various models such as regular adjacent reentry, irregular adjacent reentry and random switchboard type reentry of folds have been suggested to describe this (Fig. 1.8) .

The inadequacy of the fringe-micelle theory thus becomes obvious and modern concepts centre on the models described above. A judicious compromise of the more extreme proposition that a crystalline polymer is a single phase with defects leads to a reasonable view that this only applies to very highly crystalline polymers . The less crystalline polymers are considered to be two phase systems, one ordered, one disordered, in which the loops and folds on the crystal surface, together with the defects, contribute to an additional amorphous phase .

Hedrites[48]

If the concentration of the polymer solution is increased, a crystalline polyhedral structure emerges composed of lamellae joined together along a common plane. These have also been detected growing from a melt which suggests that lamellar growth can take place in the melt and may be a sub-unit of the spherulite.

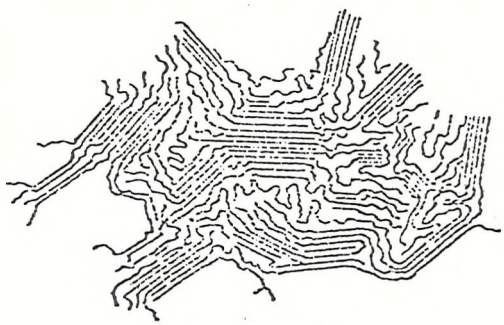

FIG. 1.7 FRINGED MICELLE MODEL OF THE CRYSTALLINE-AMORPHOUS STRUCTURE OF POLYMERS

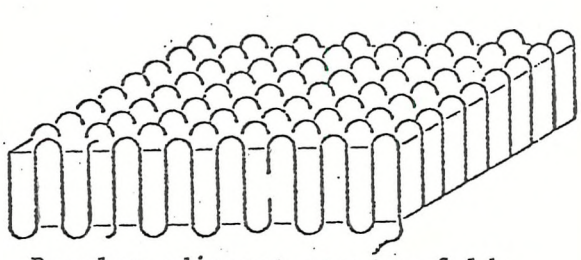

Regular adjacent reentry folds

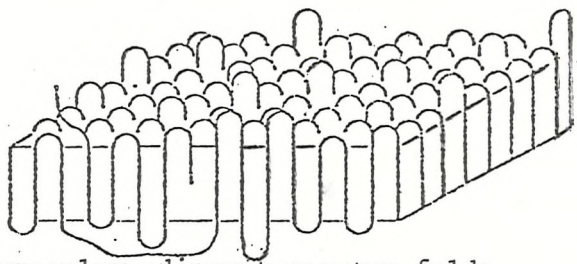

Irregular adjacent reentry folds

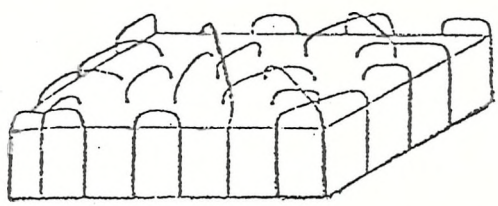

Switchboard or non-adjacent reentry folds

FIG. 1.8 THREE MODELS FOR THE LAMELLAR CRYSTALS IN POLYMERS

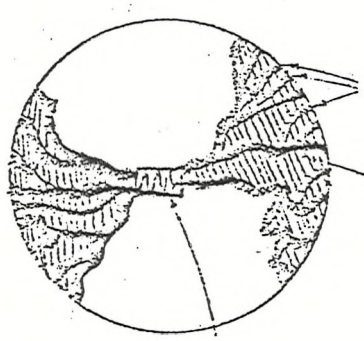

Fibrils with low angle branching

Amorphous regions between branches

Single crystal nucleus

FIG. 1.9 SCHEMATIC DIAGRAM OF A SPHERULITE BASED ON THE STRUCTURE PROPOSED BY SHARPLES

Spherulites[49]

Examination of thin sections of semicrystalline polymers has revealed that the ordered regions or crystallites are not arranged randomly, but form regular birefringent structures with circular symmetry. These structures which exhibit a characteristic Maltese cross optical extinction pattern, are called spherulites.

Each spherulite grows radially from a nucleus formed either by the density fluctuations which result in the initial chain ordering process or from an impurity in the system. The number, size and fine structure depend on the temperature of crystallization which determines the critical size of the nucleating centre. Thus large fibrous structures form near T_m, whereas greater numbers of small spherulites grow at lower temperatures.

A study of the fine structure of a spherulite shows that it is built up of fibrous sub units, growth takes place by the formation of fibrils which spread outwards from the nucleus in bundles, into the surrounding amorphous phase. As this fibrillar growth advances branching takes place, and at some intermediate stage in the development, the spherulite often resembles a sheaf of grain (Fig. 1.9). This forms as the fibrils fan out and begin to create the spherical outline. Although the fibrils are arranged radially, the molecular chains lie at right angles to the fibril axis. This has led to the suggestion that the fine structure is created from a series of lamellar crystals winding helically along the spherulite radius.

General purview of the macroconformational features of a melt-crystallized polymer[49]

Sharples has proposed a picture of the main morphological features produced during the crystallization from the melt of a polymer .

This is shown schematically in Fig. 1.8 as a spherulite, which he suggests is the major unit. Growth proceeds from a small crystal nucleus which develops into a fibril. Low branching and twisting then produces bundles of diverging and spreading fibrils which eventually fill out into the characteristic spherical structure. In between the branches of the fibrils are amorphous areas and these, along with the crystal defects, make up the disordered content of the semicrystalline polymer.

(b) Microconformations

Conformations about the constituent backbone bonds may be termed as microconformations. Macroconformations come about by sequences of microconformations (usually trans or gauche) along the polymer chain.

The trans and gauche conformations of a molecule arise as a result of rotation about a carbon single bond as axis. The Newman and 'Saw Horse' projections of butane in Fig. 1.10(a), for example, show the trans position with the dihedral angle $\phi = 180^{o}$. Rotation about the C_2-C_3 bond alters ϕ and moves the methyl groups past the opposing hydrogen atoms so that an extra repulsive force is experienced when an eclipsed position (Fig. 1.10(b)) is reached.

These rotations produce 3 potential minima at $\phi = \pi$, $\pi/3$ and $5\pi/3$ called the trans and $\pm$ gauche states respectively, and the greater depth of the trans position indicates that this is the position of maximum stability (Fig.1.10(c)). Although the gauche states are slightly less stable, all three minima can be regarded as discrete rotational states. The maxima correspond to the eclipsed positions and are angles of maximum instability. These diagrams vary with the type of molecule and need not be symmetrical, but the butane diagram is very similar to that for polyethylene, $\left[-CH-CH_2-\right]_n$, if the $-CH_3$ groups are replaced by the two sections of the chain adjoining the bond of rotation. The backbone of this polymer is composed of a chain of tetrahedral carbon atoms

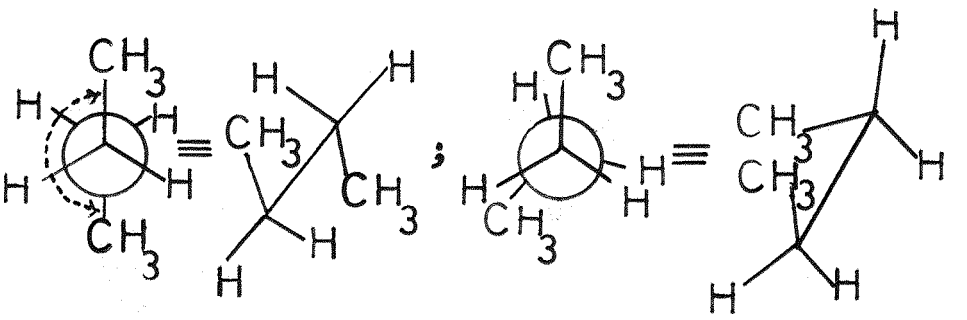

(a) Staggered (b) Eclipsed

Newman and "saw horse" projections for n-butane:

a) a staggered state with $\phi = \pi$

b) an eclipsed position

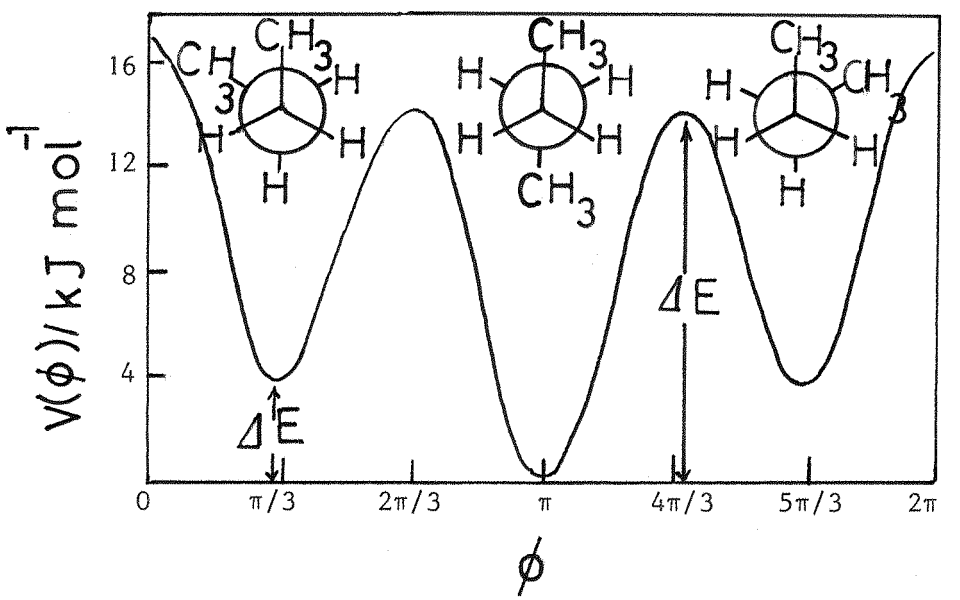

c) Potential energy $V(\phi)$ as a function of the dihedral angle ϕ for n-butane

FIG. 1.10

covalently bonded to each other so that the molecular can be represented as an extended all trans zig zag chain as shown below:[50]

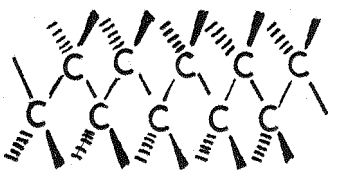

Conformational regularity

The repetition of one microconformation or a sequence of a few microconformations along a polymer chain gives rise to a regular macroconformation e.g. planar zig zag chains - trans(T) sequences of polyethylene (as shown above) and polyethers with $m \geq 4$ [52,52]; helical chains - gauche (G) or a mixture of T and G sequences in the case of polyethers with $m \leq 3$.[53,54,55] Various helical conformations of isotactic vinyl polymers are illustrated in Fig. 1.11.

Configurations

These are part of the chemical state of a polymer chain. In contrast to a microconformation, a configuration can be transformed into the other one only by breaking chemical bonds. Examples for the configurations are the cis or trans structure of ethylene[56] or cyclopropane derivatives[57].

Stereoregularity

This is produced by the repetition of one configuration or a sequence of a few configurations along a polymer chain. Isotactic polypropylene and syndiotactic polypropylene provide two such examples.

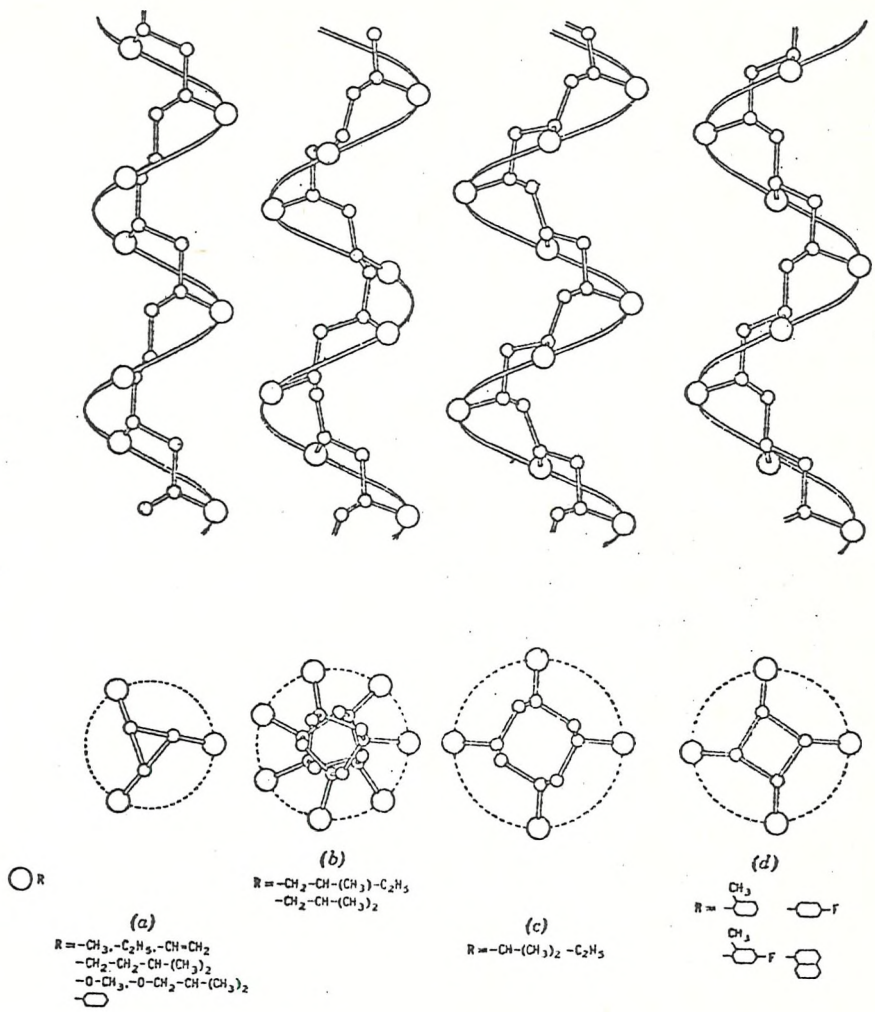

FIG. 1.11 Helical conformations of isotactic vinyl polymers [56]

1.4.2 Investigation of structure by X-ray diffraction[58]

Diffraction occurs when radiation is scattered from centres whose separation is of the same order as the wavelength of the incident radiation and arises from the constructive and destructive interference of the scattered rays.

Similarly an array of atoms or ions in a crystal will cause a similar effect when the incident radiation is an X-ray (Fig. 1.12).

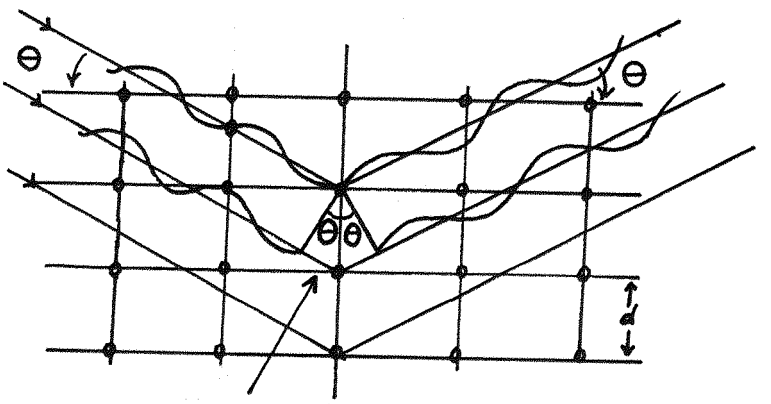

For constructive interference
$2d \sin \theta = n\lambda$
$n = 1,2,3 - - -$

FIG. 1.12

X-ray diffraction is the definitive method of determining the structure of a crystalline material. It enables the crystal class, the dimensions of the unit cell and the space group to be elucidated. The latter determines the vibrational selection rules and thus the observed spectrum can be interpreted or predicted. Low angle X-ray diffraction can be used to study larger periodicities within a substance and the crystallite size in polycrystalline material can be measured by application of the Debye-Scherrer equation to the band widths of its wide angle diffraction pattern.

1.4.3 The structure and vibrational spectra of polymers

Due to the instrumental superiority of the IR technique over the Raman in pre 1966 era, the former has been mainly applied for the structural analysis of polymers until recent years[59-61]. However, there are several reasons which now justify the preferred use of Raman spectroscopy for this purpose. Apart from the experimental advantages which laser Raman spectroscopy now offers over the IR, usually more vibrational modes are active in the Raman effect than in the IR. Further, in the case of a centrasymmetric molecule only half of the vibrational modes are active in the IR, the remaining giving rise to Raman bands. It is, therefore, necessary in most cases to use the IR technique together with the Raman to achieve satisfactory results.

In a polymer chain, every monomer unit, chain end, chemical irregularity and chain branch vibrates but the selection rules for the Raman and IR activity of these vibrations depend upon the associated macro and microconformational structures.

The following discussion is intended to introduce briefly the impact of structure on vibrational spectra of polymers with reference to polyethylene and n-paraffins, because of their simple structure and relevance in the subsequent discussions.

Polymers in common with all nonlinear, nonpolymeric molecules have 3N-6 possible vibrational modes where N is the number of atoms in the molecule. Since a polymer has the general formula $(X)_n$ where X is the structural repeat unit and since n is a large number typically of the order 10^3, the expected number of modes will be very large, becoming infinite for an infinitely long molecular chain. In fact the observed vibrational spectrum of the simplest polymer i.e. polyethylene, is extremely simple, less complex than that of most n-alkanes which are the low molecular weight homologues of polyethylene.

1.4.3a Chain vibrations of polyethylene and the n-alkanes

Snyder and Schachtschneider[57,62] have investigated the vibrational behaviour of the n-alkanes. They have shown that the multiplicity of the bands increases as the chain length increases such that whereas C_3 has a few bands, higher homologues have a more complex spectrum and the relative intensities of the components change. For instance, as the chain length increases, effects due to end groups decrease in relative importance and features due to skeletal motions increase in relative importance. In polyethylene this results in a distribution rather than in distinct bands, which are, however, still relatively sharp (of the order of $20cm^{-1}$). These effects are shown diagrammatically in Fig. 1.13.

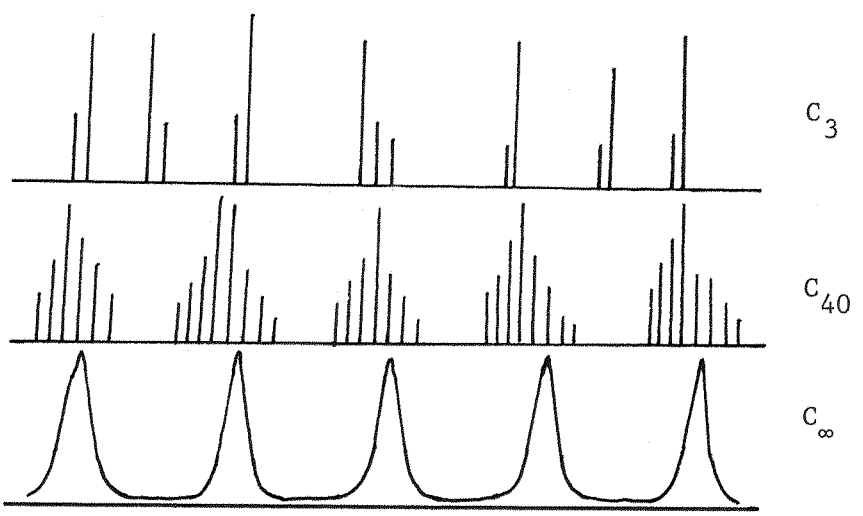

FIG. 1.13

FIG. 1.14 Symmetric stretching mode of polyethylene

For any mode there are an infinite number of possible phase relationships between vibrations on adjacent atoms. These can be exemplified by the two possible extremes as shown in Fig. 1.14 for the $C H_2$ symmetric stretching mode of polyethylene. The spectrum would thus be expected to show bands due to these extremes plus those due to all the possible intermediate phase relationships. Tasumi et al[63] have calculated these frequency-phase curves for a polymethylene chain as shown in Fig. 1.15. In these curves, only those modes are optically active which correspond to $\theta = 0$ and $\theta = \pi$ i.e. totally in phase and out-of-phase. n-alkanes, however, would give rise to bands corresponding to all possible phase relationships in the form of band progressions in various spectral regions due to the finite molecular length. Considering these relationships, Snyder and Schachschneider[57,62] developed a model which successfully explained the IR spectra of n-alkanes through $C_{30}H_{62}$. In this approximate analysis, the vibrational mode of each individual CH_2 group is replaced by a harmonic oscillator with the frequency characteristic of the mode under consideration, and the end groups e.g. CH_3 can be regarded as the fixed ends. The vibrational frequency ν of a linear array of m identical oscillators depends upon the phase difference θ between adjacent oscillators. The phase difference allowed for the vibration is expressed by

$$\theta = \frac{k\,\pi}{m+1} \qquad (k = 1,2,3,\ldots\ m)$$

Assignments of integers k to the observed bands can be made on the basis of the selection rules which are expressed in terms of the values of k and the number of methylene groups m for each vibrational mode. The relation between k and the symmetry species is given in Table 1.3 alongside the frequencies of the limiting modes on the frequency phase curves of polyethylene shown in Fig. 1.15.

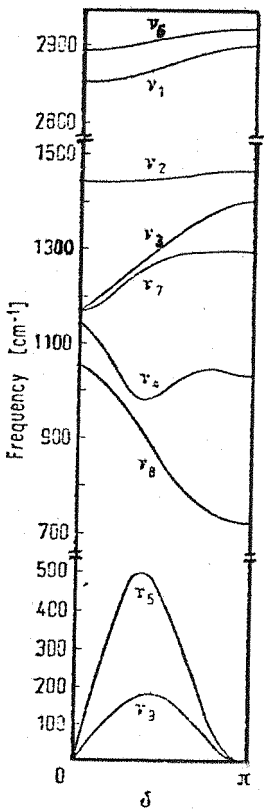

FIG. 1.15 Frequency-phase difference curves of polyethylene (Tasumi et al)

Table 1.3

The relation between k and symmetry species for n-paraffins

Vibrational mode	m odd (C_{2v})		m even (C_{2h})		M ∞ (D_{2h})		Fig.1.15)
	k odd	k even	k odd	k even	θ=0 (cm^{-1})	θ=π(cm^{-1})	
CH_2 sym. stretching	A_1	B_1	A_g	B_u	A_g (2848)	B_{2u}(2851)	ν_1
CH_2 asym. stretching	B_2	A_2	B_g	A_u	B_{3g}(2883)	B_{1u}(2919)	ν_6
CH_2 bending	A_1	B_1	A_g	B_u	A_g (1418)	B_{2u}(1463, 1473)	ν_2
CH_2 wagging	B_1	A_1	B_u	A_g	B_{3u}(1175)	B_{1g}(1370)	ν_3
Skeletal (C-C) stretching	A_1	B_1	A_g	B_u	A_g (1131)	B_{1g}(1061)	ν_4
Skeletal (C-C) deformation	A_1	B_1	A_g	B_u	$B_{3u}(T_x)$(0)	$B_{2u}(T_y)$(0)	ν_5
CH_2 twisting-rocking	A_2	B_2	A_u	B_g	B_{3g}(R)(1168)	B_{2g}(T)(1295)	ν_7
CH_2 rocking-twisting	B_2	A_2	B_g	A_u	A_u(T)(1053)	B_{2u}(R)(720)	ν_8
Skeletal (C-C) torsion	A_2	B_2	A_u	B_g	$B_{3g}(R_x)$(0)	$B_{1u}(T_z)$(0)	ν_9

Of the symmetry species in Table A_1, B_1, B_2, A_u, B_u, B_{1u}, B_{2u} and B_{3u} are IR active, whilst A_1, A_2, B_1, B_2, B_{1g}, B_{2g} and B_{3g} are Raman active. Strictly speaking, polyethylene has a finite molecular chain thus giving rise to a number of weak bands which apart from the stronger bands resulting from totally in phase and out-of-phase modes are associated with intermediate phase relationships. The above analysis, therefore, has also been useful in the interpretation of these bands.

Although this approach has been extended to model compounds of polymers[64,138] other than polyethylene, the results are fragmentary, because

of the difficulty in preparing a series of oligomers with increasing chain length having the same conformation. As will be seen in Chapter 5, polyethers and polythioethers with $m \geq 4$ conform to this requirement, because the length of the methylene sequence between O or S atoms increases as m increases, and hence may be expected to give rise to the frequency phase curves similar to polymethylene chain.

The total number of vibrations and their activity in Raman and IR effects is derived from group theoretical considerations. For example, an isolated chain of polyethylene has the symmetry group d_{2h}. The fibre period (CH_2-CH_2) consists of n = 6 atoms thus giving rise to (3 x 6 - 6) vibrations, of which those symmetric to the centre of symmetry (gerade) are Raman active and those asymmetric to the centre of symmetry (ungerade) are IR-active. Details of the vibrational analysis of both planar zigzag and helical polymers may be seen in reviews by Koenig et al[65] and Tadokoro[66].

1.4.3(b) The effect of different conformations on molecular vibrations

The simplest example for the influence of different conformation on molecular vibrations is a polar end group of the type

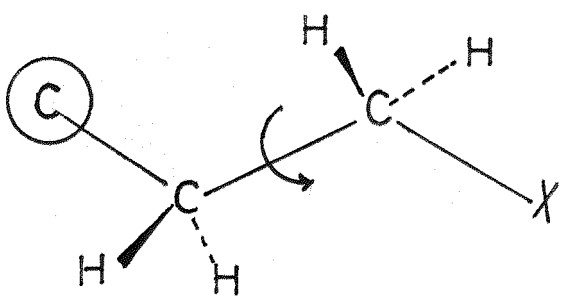

By rotating, the end group around the ultimate C-C bond, 3 potential minima are reached, two of them having the same energy. These minima belong to the conformations: X trans to C and X trans to one of the two H atoms at the penultimate C. Usually, the latter two (identical conformations have the high energy and are, therefore, "high temperature

conformations". In this situation at least one vibration of the end group, frequently the C-X stretching vibration, is sensitive against the conformation of the C-X group with respect to the neighbouring units due to different coupling conditions. Thus instead of one C-X band, two of them will appear. If C-X is situated somewhere within the chain, it will be necessary to consider the conformations of the neighbouring groups on both sides with respect to the C-X group.

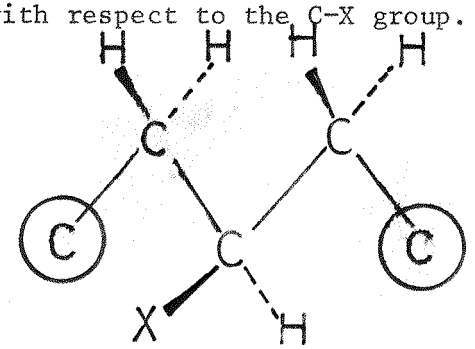

Potential minima are reached with the following conformations: X_{HH} (H trans to X on both sides (X_{HC} and X_{CH} (identical conformations) and possible X_{CC}. The latter one has usually a rather high potential energy and is therefore a "high temperature conformation". Considering again the C-X stretching vibration, splitting into two or three components is therefore expected. Whilst the bands sensitive to certain conformations are called conformational bands, the phenomenon itself is known as conformational splitting by Hummel[67]. However, Zerbi calls conformational bands as "regularity bands".[68]

In a chain molecule with a certain conformational order, the number of possible conformations on both sides of any group is very small. Thus, the conformational splitting of certain bands is well defined i.e. the bands being characteristic for this long range conformational order are sharp.

Conformational order in a polymer may be considered as one-dimensional crystallinity. This means that a single chain has reached minima both in energy and entropy when it has a regular conformation. If a

polymer chain can assume different regular conformations this is known as one dimensional polymorphism[67]. In a number of cases, these transformations are enantrotropic and take place in a narrow range of temperatures. A well known example is polytetrafluoroethylene which forms a (13/1) helix below 19°C and a (15/1) helix above this temperature[69]. One dimensional polymorphs always give rise to characteristic vibrational spectra. Even the minor transition of PTFE at 19°C, (13/1) to (15/1) helix, is accompanied by a shift of the CF_2 wagging vibration from 638 to 625 cm^{-1}. More obvious are spectral changes in the cases of isotactic polybutene-1[70] and trans 1-4 polyisoprene[71]. The (3/1) helix of the former one is characterised by bands at 921-, 847- and 797 cm^{-1}.

A similar phenomenon has been observed in the case of PES (Chapter 4).

Irregularities in one dimensional crystallinity may assume several conformations which would give rise to characteristic bands. Since long range conformational order is usually predominant in contrast to these irregularities in polymer chains, the bands associated with the latter are usually weak. These may be recognised by their defiance to selection rules applicable to long range order conformations. Additional weak bands may also arise due to chemical irregularities.

1.4.3.(c) The effect of crystalline environments on chain vibrations

Three dimensional crystallinity can have several effects on the vibrational spectrum of a polymer which will depend upon the symmetry of the crystal as well as the strength of the interchain interactions. The crystal field may split each band of the isolated chain into a number of closely spaced components depending upon the number of chains in the primitive unit cell. Further, bands due to lattice modes may also appear at low frequencies ($\sim$ 150 - 20 cm^{-1}).

The experimental observation of these effects, however, is fraught with several problems. In some cases, the intermolecular forces may be too weak to sufficiently resolve the components of the split band, whereas in some other cases, one of the resolved components may be too weak to be observed. This latter reason was first thought to be the cause of the failure in observing the expected doublets in the Raman spectrum of polyethylene[72]. The selection rules may also prevent the observation of splitting when one of the components is either active in the Raman or IR and the other is inactive in either of these effects e.g. polyvinyl chloride[72].

Polyethylene crystal

Crystalline polyethylene forms a primitive orthorhombic lattice, space group (Pnma - D_{2h}^{16}) with two chains translating the unit cell[50]. The space group is isomorphous to the line group d_{2h}.

Fig. 1.16 shows polyethylene unit cell with reference to line and space group axes.

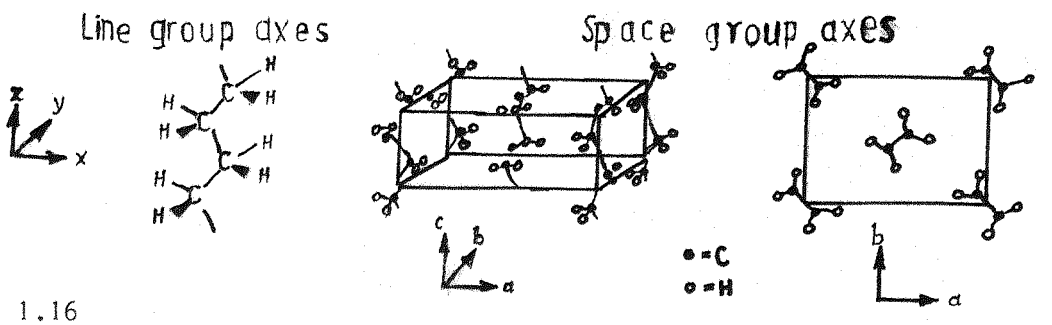

FIG. 1.16

The line group characteristics of this molecule fall into 4 classes of Raman activity, i.e. a_g, b_{1g}, b_{2g} and b_{3g} and 4 of IR activity i.e. a_u, b_{1u}, b_{2u} and b_{3u} (see Table 1.2). Thus each line group mode can vibrate in phase or out-of-phase with its neighbour in the unit cell and would have a doublet in the crystalline case with the following symmetry properties:

Line	Space	Line	Space
a_g	$A_g + B_{1g}$	a_u	$A_u + B_{1u}$
b_{1g}	$B_{1g} + A_g$	b_{1u}	$B_{1u} + A_u$
b_{2g}	$B_{2g} + B_{3g}$	b_{2u}	$B_{2u} + B_{3u}$
b_{3g}	$B_{3g} + B_{2g}$	b_{3u}	$B_{3u} + B_{2u}$

The interaction forces between PE chains have been discussed by by several authors[74,75,122,151]. and the splittings have been anticipated at 25°C and -196°C. Table 1.3 gives the observed and calculated Raman and IR splittings at these temperatures.

Table 1.4

Correlation splitting in the vibrational spectrum of polyethylene[75,122]

		25°C		-196°C	
Species	Mode	Calculated (ν cm^{-1})	Observed (ν cm^{-1})	Calculated (ν cm^{-1})	Observed (ν cm^{-1})
A_g	$\delta(CH_2)$	1429.4 1452.9	1418 1441	1429.2 1455.5	1414 1442
B_{2g}	ν(C-C)	1060.4 1055.7	1066	1061.7 1056.2	1068 1065
B_{3g}	T (CH_2)	1294.1 1299.4	1296	1295.9 1301.2	1295 1297
B_{2u}	R (CH_2)	-	720 730	-	719 732
B_{1u}	$\delta(CH_2)$	-	1460 1470	-	1459 1472

The correlation effect is enhanced when the temperature is lowered, since the lowering of temperature among other effects causes the con-

traction of the unit cell thus bringing the two chains closer together and resulting in more vigorous interaction.

Another effect which further complicates the consequences of correlation splitting and occurs in PE and other molecules is known as Fermi resonance. Fermi resonance occurs when an overtone or combination vibrational frequency which usually gives rise to a Raman or IR band has a frequency close to that of a fundamental of appropriate symmetry. In this case, interaction can occur and uncharacteristically strong features are observed. In polyethylene, the first overtone of the CH_2 rocking mode near 725 cm^{-1} has a frequency close to the α_g CH_2 deformation near 1440 cm^{-1}. The symmetry characteristics arising as a consequence of this situation have been summarized by Hendra[41] as follows:

Line	b_{2u} rock	725 cm^{-1}		
Space		731 cm^{-1}	720 cm^{-1}	
		B_{1u}	B_{2u}	
1450	1440	1430		overtones and combinations
	B_{3g}	A_g		
Line	a_g CH_2 def	1440		
Space		1447	1433	
		B_{3g}	A_g	

Thus a complex band profile is in fact observed in the Raman spectra of crystalline PE and other systems between $\Delta\nu$1400-1500 cm^{-1} with band heads in the former case occurring close to $\Delta\nu$1455,1440- and 1415 cm^{-1}. The shape of this band system is very sensitive to crystallinity and hence can be used as a good indicator of PE-like crystallization.

Some trans planar n-paraffins (m > 20) can be crystallized in two forms. In the orthorhombic habit they have a PE-type unit cell whilst in the triclinic form they have a PTHF-type unit cell consisting of one chain only. In the latter case no correlation splitting can occur and also complex interactions described above are simplified in the 1450 cm^{-1} region. Consequently the band shapes in the CH_2 region due to these crystalline forms are quite different from each other as shown below[75].

2 chain/unit cell 1 chain/unit cell

These band shapes may be used for studying unknown systems.

1.4.4 Low frequency Raman spectra (Longitudinal acoustic vibrations)

In 1967, two papers appeared[76-77] describing low frequency Raman shifts characteristic of an accordion-like vibration of planar zig zag polymethylenic chains (Fig. 1.17). In the first, Schaufele and Shimanauchi[76] showed that regular sequences of weak bands are observed for n-paraffins close to the exciting line whose frequencies ν are given by the relation:

$$\nu = (^{m}/_{2L})(^{E}/_{\rho})^{\frac{1}{2}} \qquad \ldots (1)$$

where m is the order of the mode and has odd integral values for Raman activity, ρ is the density of the hydrocarbon, E is Young's elastic modulus and L is the length of the planar zig zag polymethylene chain.

For $C_{36}H_{74}$, bands were observed at:

m :	1	3	5	7	9
$\Delta\nu cm^{-1}$:	67.4	189	303	403	475

From this the value of E was estimated as $(3.58 \pm 0.25) \times 10^{12}$ dynes/cm^2, which agreed closely to the experimental value along the fibre axis determined by X-ray diffraction. Whenthis value was later used to calculate ν for a series of n-paraffins upto $C_{94}H_{190}$ in conjunction with equation 1, the observed and calculated frequencies were found in close agreement.

In mechanical terms, this vibration has been considered as one of a string of beads with antinodes at the chain ends and has been termed as the longitudinal acoustic mode. (L.A.M.)

Although unlike n-paraffins, the polymers usually crystallize in chain folded lamellae-like structures, the straight stem segments between the folds have a close similarity to polymethylenic chains in n-paraffins (see section 1.4.1). A straight stem segment within a lamellar unit of polyethylene, for example, will comprise several monomer units which implies that the observation of a similar vibration as that in n-paraffins should provide a direct measure of the length of this segment. The accuracy of such a measurement, however, will depend upon the effective decoupling of the accordion motion between the adjacent fold segments.

It is now a well-established fact that the Raman spectrum of polyethylene contains bands with low frequency shifts which are characteristic of longitudinal acoustic vibrations of the planar zig zag segments in the crystalline case. Further, the frequency of the vibration is sensitive to the length of the planar zig zag system (Fig. 1.17).

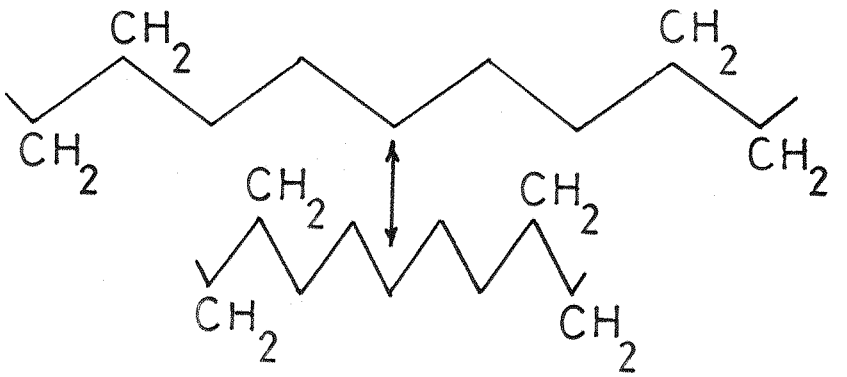

(a)

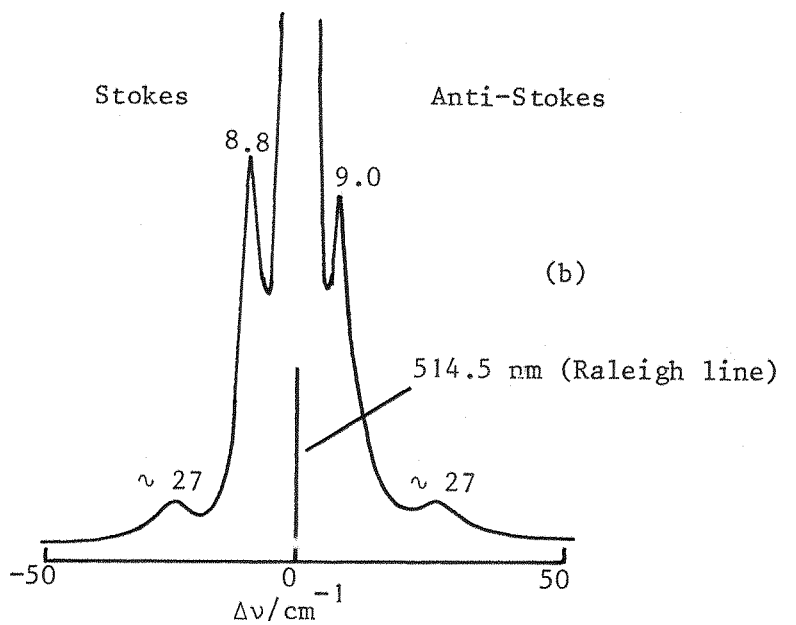

FIG. 1.17 Longitudinal acoustic mode (LAM) of vibration of a polyethylene chain (a). Raman spectrum of polyethylene showing low frequency shifts associated with LAM (b).

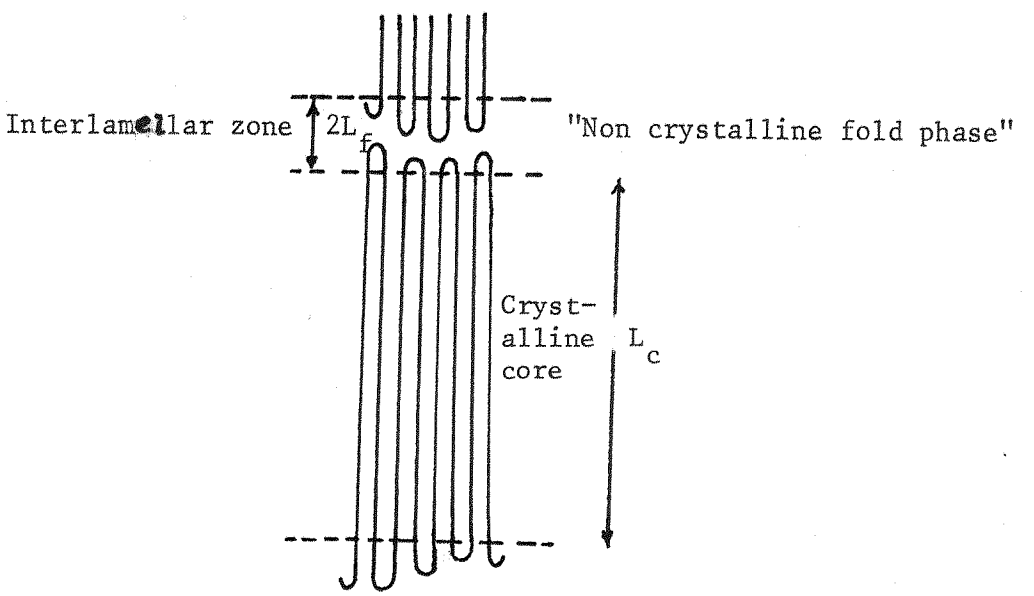

FIG. 1.18 Definitions of 'core' and fold zone thicknesses

The potential of the Raman technique for measuring lamellar thickness in polymers is vast since unlike other conventional techniques, as will be seen below, it offers a precise measurement of lamellar thickness and experimental ease and versatility. The conventional techniques available for determining the structure of lamellae include:

Low angle X-ray diffraction (LAXD)[78]

In this method the lamellar thickness is determined by the measurement of long spacings from LAXD patterns.

Electron microscopy (EM)[78,79]

It provides data on lamellar thickness from replicas of fractured surfaces by measuring the step height and is normally used to support LAXD results.

Chemical methods[80]

Usually these involve oxidative destruction of the chain folds at the lamellar surface followed by analysis of the molecular fragments.

Wide angle X-ray diffraction (WAXD)[58,81]

This method is widely used to identify the repeat structure in the crystalline lamellar core and for crystallite size determination through line width measurements.

Vibrational spectroscopy[32,82]

This is a much more limited technique and is applicable by inference only.

Density and thermal data[83,84]

These tend to be only vaguely connected to the presence or otherwise of lamellar features.

None of these techniques is capable of measuring the magnitude of L_c or L_f within a given lamellar unit as defined in Fig.1.18. The long spacing from LAXD patterns gives $L_c + 2L_f$ which when combined with chemical data can indicate a rough value of L_c. The Raman technique, on the other hand provides a precise value of L_c from the measurement of LAM frequency. This is based upon the assumption that the acoustic vibration of a planar zig zag polymethylenic segment is restricted by the first gauche CH_2-CH_2 unit encountered at the interface between the crystalline and fold phases. It is possible even to calculate the value of L_f, if Raman data are combined with good LAXD data. Early promise was, however, not realized since it was observed that the thickness determined by the Raman method agreed roughly with that from LAXD but was not strictly comparable with it.

Recently Peterlin and coworkers[85] have contradicted the assumption regarding the lack of involvement of the fold phase in the acoustic vibration. They have analysed the problem of the three-zone vibrator comprising an upper fold phase and have allowed for probable density differences between the phases (Fig. 1.18). They conclude that the vibrational antinode assumed to lie at the fold-core interface is likely to be lying within the fold zone i.e. the length calculated from the measurement of the acoustic mode may be significantly greater than L_c. Recent experimental and theoretical evidence, however, suggests that the antinode lies close to the fold-core interface. The vibrational force constant, however, may not be exactly the same as for n-paraffins. This evidence may be summarized as follows:

(i) LAM frequency in polyethylene is not temperature sensitive.[44,85] The modulus of elasticity (E) and the density (ρ) of the fold phase is expected to be temperature dependent. If this phase contributed signif-

icantly to the vibration, a shift in frequency would occur on cooling (see Equation 1).

(ii) 'Etching' with fuming nitric oxide which removes the fold zone, does not alter the LAM frequency.[44]

(iii) Tilting the chains with respect to the lamellar surfaces does not alter their LAM frequency.[45]

(iv) Calculations by Fanconi[46] suggest that a gauche CH_2-CH_2 unit or similar structural discontinuity will confine the LA mode but a methyl side group will have a very little effect.

Thus, it may be concluded that the LAM frequency is related to the lamellar thickness L_c but the relationship may not be exactly the same as in n-paraffins.

The experimental versatility gives this technique an added advantage over other techniques. The sample can be heated, cooled, mechanically manipulated or even exposed to high pressures all with comparative ease. Whilst this method can be applied to minute samples or large samples, it has excellent spatial resolution.

Thus it becomes clear that Raman technique has a considerable value as an analytical tool for the investigation of lamellar crystallization in polymers. Its application to the polyethylene problem has been the main attraction to polymer chemists in the last few years. These applications may be discussed briefly as follows, in order to appreciate the scope of this technique.

Applications

Polyethylene has been studied at temperatures between $-180^{\circ}C$ and $+140^{\circ}C$ using this technique.[85,86] One advantage in studying specimens at low temperatures is that the Raleigh band narrows thus allowing to approach

closer to the exciting line. The LAM frequency remains unaltered on lowering or raising the temperature until annealing temperatures are reached.

On heating to annealing temperatures ($100^{o}C$), the LAM frequency falls due to lamellar thickening until near T_m, the band belonging to the LA mode disappears in the background scattering.

The frequency of the LAM mode is the function of lamellar thickness which in turn is the function of annealing temperature i.e. the higher the annealing temperature, the lower the frequency of the LA mode.[85,86] Rolled and drawn polyethylene have also been studied with particular reference to the breakdown of extended polymethylenic chains of regular length on passing through the deformation neck or as a function of extension ratio in rolling.[47] Recently lamellar build up at low temperatures has been demonstrated in quenched polyethylene melt using this technique which resulted in the determination of glass transition temperature of polyethylene.[73] Under similar circumstances such an observation is quite inaccessible to study by other techniques.

Raman bands due to fundamental (i.e. m=1) LA mode in melt crystallized polyethylene is relatively intense but the higher order modes (e.g. m=3) gives rise to only weak bands. Further, these bands tend to be broad and it may well be that the intensity and band width data can be made to yield information on the distribution of lamellar thicknesses within a specimen.

Finally it may be concluded that the Raman method of measuring lamellar thickness is now an established tool in polyethylene and potentially it may prove of significant value in many other synthetic polymers.

1.4.5 Conclusion

It has been indicated from the above discussion that the interpretation of vibrational spectra of polymers is closely associated with molecular structure which includes micro as well as macroconformations.

Microconformations give rise to bands due to long range as well as short range order in the polymer chain. Whilst the bands associated with long range order or one dimensional crystallinity, are characteristic of predominant symmetry of the molecule, the bands associated with short range order i.e. amorphous region, are characterised by their defiance to the selection rules applicable to the latter. Further, bands associated with long range order would arise from totally in phase or out of phase modes if the chain is of considerable length. These may , however, arise from all possible phase relations if the chain is short or effectively so.

Bands associated with macroconformations may arise either from three dimensional crystallinity as in the case of interchain interactions in a unit cell containing two or more than two chains, or from longitudinal acoustic vibrations of chain stems within lamellar structures.

Micro as well as macroconformations may vary with temperature or crystallization conditions e.g. melt, solution annealing or stress. These variations, therefore, cause corresponding variations in the observed vibrational spectrum.

The vibrational spectra of a series of polyethers and polythioethers with the general formula $\left[(CH_2)_m-Y\right]_n$ (m = 1-6, 10 and Y = O or S respectively) have been discussed in Chapters 4, 5 and 6, with these implications in mind.

In order to substantiate the results, wide angle X-ray diffraction (WAXD), low angle X-ray diffraction (LAXD), density and D.S.C. derived melting point (T_m) measurements have also been carried out at appropriate occasions.

CHAPTER II

EXPERIMENTAL

2.1 Introduction

Although the first Raman experiment was performed using sunlight as the source and human eye as the detector, extremely poor scattering which gives rise to Raman effect, has always been a problem in practice. Ways have been devised over the years to tackle this problem by developing more and more efficient radiation sources and detecting devices. Nevertheless, it was not until 1966 that considerable development in this field could be achieved. Post 1966 era saw the development of continuous wave laser sources which could emit monochromatic radiation (a basic requirement) at various wavelengths with high powers, and a wide range of detecting devices with highly efficient electronic and optical systems. Though ideality may still not be claimed and may never be so in view of the ever increasing demands of Raman spectroscopy, much has been done to get closer to it. Several reviews and monographs discussing instrumentation and sampling with regard to past and present developments are available[11,12,13,87].

This chapter describes the instruments, experimental arrangements, samples used, their preparation, processing and characterization, and the experimental problems encountered during the experimentation.

2.2 Instruments

2.2.1 Laser Raman spectrometers

Three spectrometers have been used in this work, all manufactured by Cary Instruments Inc. U.S.A. They are the Cary-81L, Cary-82 and Cary-83.

The Cary-81 was originally designed for use with the mercury Toronto arc source but was later modified for use with lasers. The

Cary-82 is a research instrument being solely designed for use with lasers. The Cary-83 is a bench top analytical instrument incorporating a built in laser and has been designed for routine laboratory work.

The main differences in instrumentation of these spectrometers are:

a) The wave number and recorder scan of the Cary-81 is driven by a $^{1}/_{20}$ h.p. squirrel cage a.c. motor at a range of selected constant speeds. The Cary-82 uses a small d.c. motor and a techo-generator driven from it as a constant speed device. The scanning speeds on this instrument are continuously variable (0.01 - 100 cm^{-1}/sec) but the scan rate is not as constant as on the Cary-81.

b) The optical system in the Cary-81 and Cary-83 involves a double monochromator, whilst Cary-82 incorporates a triple monochromator. Thus stray light characteristics of the Cary-82 are much better than those of Cary-81 and -83.

c) The Cary-82 and the Cary-83 incorporate illumination of the sample at 90^{o} to the viewing direction (Fig. 2.1a) whereas the Cary-81 has an illumination system involving illumination and viewing at 180^{o} (Fig. 2.1b).

d) The optics (b) and (c) on the Cary-81 and (b) on the Cary-83 seldom allows the recording of spectra below 100$\div$150 cm^{-1}. On the other hand the spectra may be recorded down to 3 cm^{-1} on the Cary-82 in favourable circumstances.

e) The Cary-81 has manually adjustable slits calibrated in cm^{-1} band pass at 435.8 nm. When using alternative laser lines, a correction has to be applied owing to the change of dispersion of the monochromator. The Cary-82 has a built in correction for dispersion and can be operated

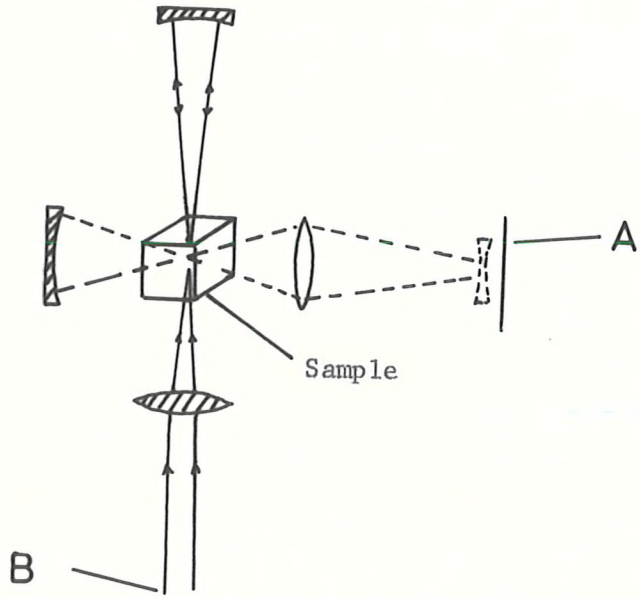

90° SYSTEM (CARY-82 & -83)

(a)

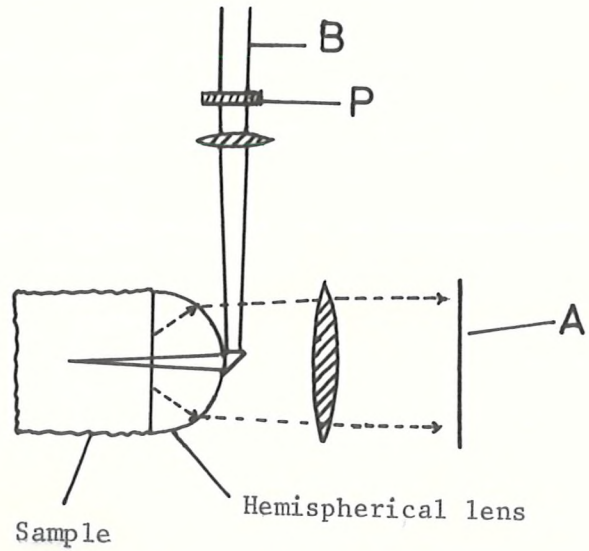

180° SYSTEM (CARY-81)

(b)

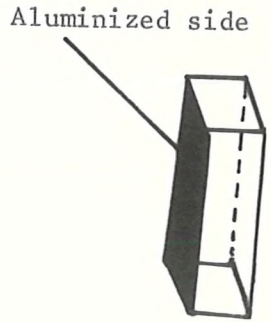

(c)

FIG. 2.1 (a) and (b) VIEWING AND ILLUMINATING SYSTEMS ON THE CARY 81-, 82- and -83 RAMAN SPECTROMETERS; (c) ALUMINIZED UV CELL

either at constant mechanical slit width or at constant monochromator band pass.

f) The resolution on the Cary-82 is generally greater than on the Cary-81 and -83.

g) The alignment of the sample in the Cary-82 is facilitated by using back illumination of the sample through the monochromator slit. The alignment in the Cary-81 presents no difficulty whilst it is much more difficult on the Cary-83. In the Cary-81, it simply involves the placing of the sample firmly against the flat surface of the hemispherical lens. In the Cary-83, on the other hand, adjustment of the sample is made by maximising the intensity of a known peak. In the case of fluorescent samples or where the spectrum is completely unknown, the whole operation may become highly tedious.

The analytical work involving simpler organic compounds was carried out exclusively using the Cary-81 and -83, whereas the polymer work was done using the Cary-82 only. The use of particular instruments with regard to the type of work is justified in view of the following reasons.

(i) Spectral resolution required for simpler organic compounds is much lower than for polymers.

(ii) Spectral measurements down to the low frequency range are not required in the case of simpler organic compounds while they are needed down to the very low frequencies in the case of polymers.

(iii) Simpler organic compounds scatter relatively more in the Raman than in the Raleigh effect as compared with polymers. Thus greater discrimination between Raman and Raleigh scattering is required in the latter case than in the former.

Clearly, the requirements for simpler organic compounds are

adequately met by the Cary-81 and -83, whereas those for polymers by the Cary-82.

The spectrometers were calibrated occasionally according to the method devised by Hendra and Loader.[93] For organic compounds, usually 2- and 4 cm^{-1} constant double slits were used in the case of solids and liquids respectively on the Cary-81 and 4-6 cm^{-1} on the Cary-83. For polymers, usually 2 to 1.5 or occasionally less cm^{-1} slits were used on the Cary-82 strictly in accordance with Schubert's formula[88] i.e.

$$\frac{1}{4} \times \frac{\text{Slit Width } (cm^{-1})}{\text{Pen period (sec.)}} = \text{Scanning speed } (cm^{-1}/\text{sec.}$$

2.2.2 Lasers

The lasers used in tandem with the spectrometers are listed below together with the main wave lengths and power outputs.

Laser	Main Wavelengths (λ/nm)	Power* outputs (~mW)
125 Ne/Ne Spectra physics	632.8, red	70
164 Ar^+ " "	488, blue	1000
52B Ar^+ Coherent Radiation	514.5, green	1000
165 Kr^+ Spectra physics	568, yellow	100
	647, red	700
52 Mixed gas(Ar^+,Kr^+) Coherent Radiation	488, blue	250
	514.5, green	250
	568, yellow	50
	647, red	100

* Experimental

They were all continuous wave gas lasers giving coherent polarized radiation tunable to the above listed wavelengths plus some other wavelengths with weaker outputs. When tuning to a particular wavelength spurious plasma lines were also emitted. However, they could be filtered using an interference filter on the Cary-81 and -83, whereas Cary-82 employed a premonochromator to get rid of them.

The He/Ne laser was not as useful as the others because of the ν^4 law [11], its low power and poor response of the photomultiplier tube in the red region (Fig. 2.2). With the ion lasers, the main problem was stability particularly with the CRL lasers which had a tendency for the overall power to drop gradually throughout a single run. This could be as much as 40% over 2-3 hours. Apart from this, the output tended to vary in the short term also, often producing choppy spectra. The most useful laser has been the Spectra Physics 164 Ar^+ one which maintained a stability both in the short and long term of approximately better than 2%.

Simpler organic compounds were excited mostly with 4880 Å and 5145 Å, whilst polymers were excited mostly with 5145 Å. 6471 Å and 6328 Å wavelengths were used for those materials which were either coloured or absorbed in the 5145 Å or 4880 Å wavelength regions. The optimum power for exciting good spectra of most polymers has been 100-120 mW. Most polymers burnt if the power level was raised beyond 160 mW.

2.2.3 IR spectrometer

Perkin Elmer IR-225 spectrometer equipped with grating optics was used for standard experiments. This spectrometer scans between ν4000-200 cm^{-1} and provides high resolution ($\sim$ 1 cm^{-1}).

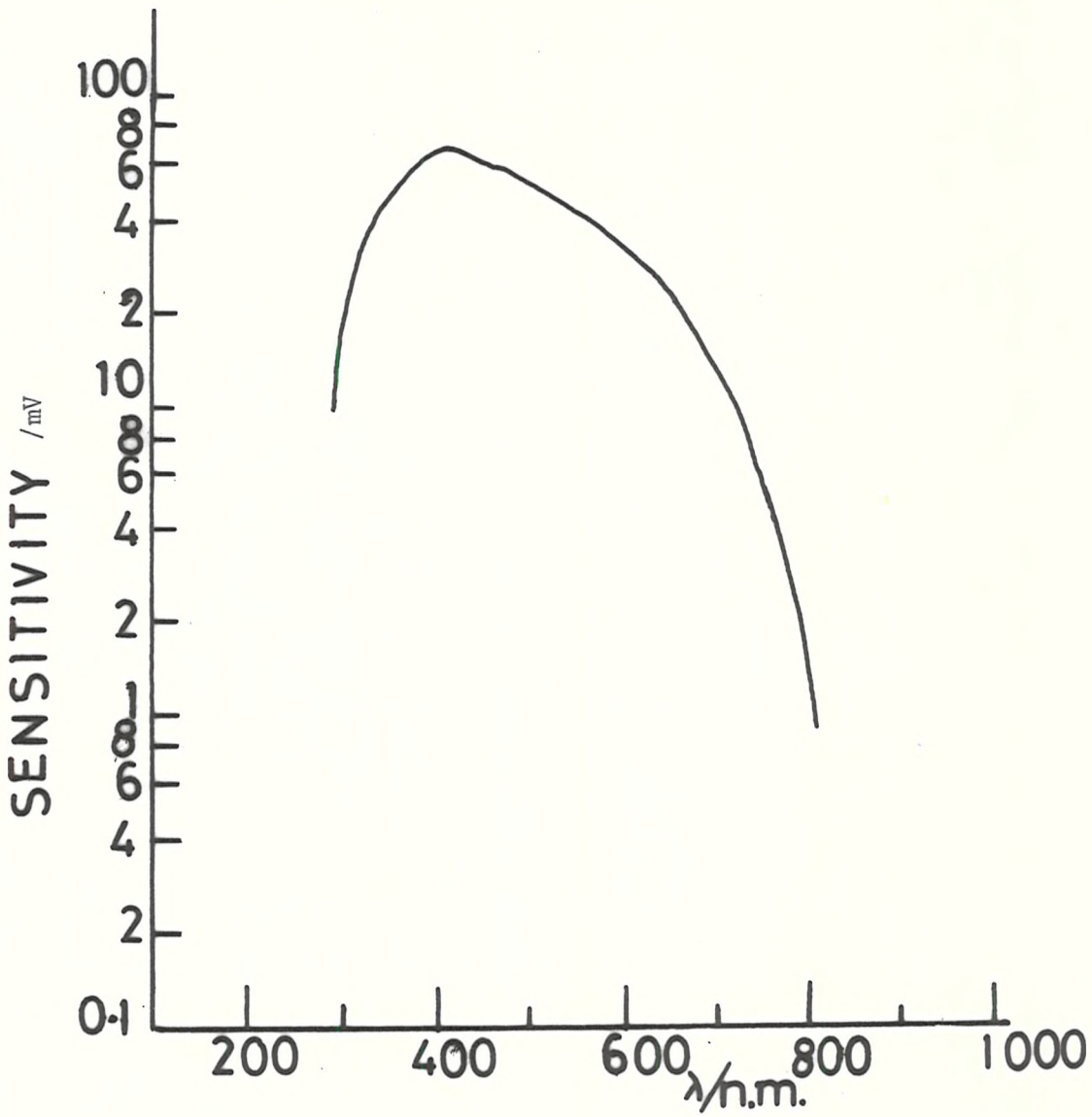

FIG. 2.2 SPECTRAL RESPONSE OF S-20 PHOTOMULTIPLIER TUBE

2.3 Depolarization ratio

When appropriate, depolarization ratio was measured for simpler organic compounds because of its analytical value. On the Cary-81, a half wave plate P was used to rotate the plane of polarization of the laser beam B and the polarization of the Raman light was then examined by means of an analyser A in front of the main optics compartment of the spectrometer (Fig. 2.1b). Two measurements were made by rotating the half wave plate through 45^{o} and the analyser through 90^{o}. On the Cary-83, these measurements were made by simply rotating the polarizer A through 90^{o} (Fig. 2.1a). Depolarization ratio (ρ_s) was then obtained as follows:

$$\rho_s = \frac{\text{Band intensity with polarizer perpendicular to vector}}{\text{Band intensity with polarizer along vector}}$$

$$= \frac{I_{\perp}}{I_{\parallel}}$$

2.4 IR dichroism

IR dichroic data for the polymers were obtained by using a gold wire AgCl polarizer between an oriented polymer film and the entrance slit. Two measurements were taken in each case with the direction of draw or fibre axis along the polarizer or the electric vector of the radiation beam, and perpendicular to it.

2.5 Experimental arrangements

2.5.1 Simpler organic compounds

On the Cary 81, the solids were examined in 0.6 cm soda glass tubes whilst liquids were presented in a 1 cm standard UV-visible spectroscopic cell, one side of which was aluminized (Fig. 2.1c).

On the other hand, both solids and liquids were viewed transversely in glass capillaries on the Cary 83.

The use of aluminized UV cell on the Cary 81

Although the sensitivity of the spectrometer while using a capillary is 6-8 times that when using the UV-visible cell, the multiple reflections involved in enhancing the instrument sensitivity in the former case destroy the polarization characteristics of the scattered radiation. Thus depolarization data obtained by using a capillary will not be reliable. On the other hand, no such problem is encountered in the case of a UV-visible cell. Further, the aluminized side of the UV-visible cell allows more scattered light to go to the entrance slit thus enhancing the sensitivity of the instrument.

2.5.2 Polymers

Raman

Room temperature measurements were made using a holder with a kinematic mount.

Low temperature measurements were made using a cell shown in Fig. 2.3 . This cell has been designed to avoid evacuation necessary in a conventional cell. Although early low temperature experiments were carried out using a conventional low temperature cell, later experiments were made exclusively with this cell because of the ease with which the sample is fitted and cooled down to $-180^{\circ}C$ by convection currents.

High temperature measurements were made using a furnace of the type shown in Fig. 2.4 . A heating rate of $5^{\circ}C$/min was employed

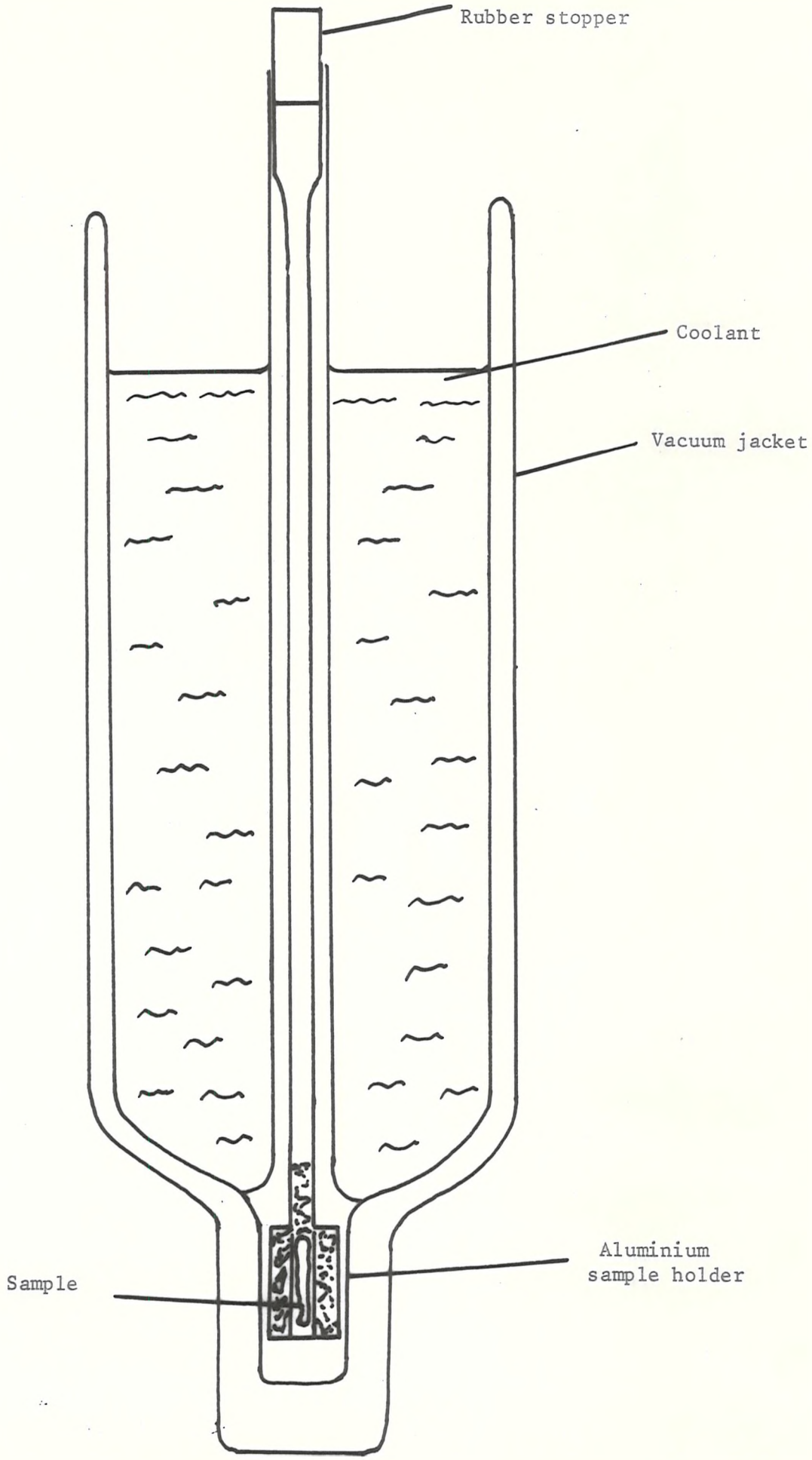

FIG. 2.3 LOW TEMPERATURE RAMAN CELL

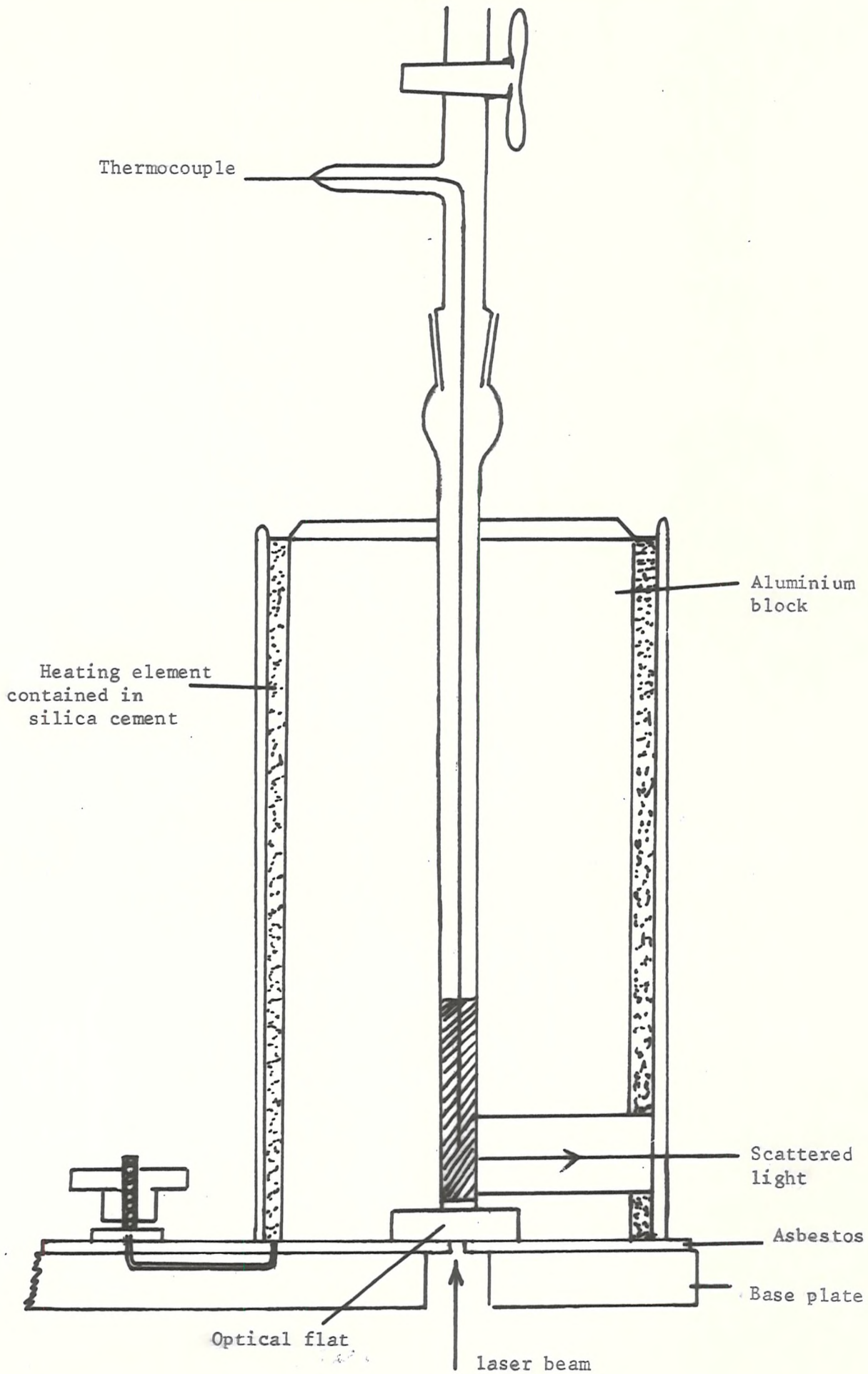

FIG. 2.4 LOW TEMPERATURE RAMAN CELL

and a period of 5 minutes was allowed to elapse before the spectrum was measured at a particular temperature. A transitrol device was used in order to control and guarantee the reliable measurement of temperature.

IR

Low and high temperature IR measurements were made using the cell shown in Fig. 2.5. When using the high temperature device, a heating rate of $5^{o}C$/min between 25 and $200^{o}C$ and $3^{o}C$/min between 200 and $220^{o}C$ was maintained. A period of 5 minutes was allowed to elapse before the spectrum was recorded at a particular temperature.

2.6 Materials

2.6.1 Availability and synthesis

Simpler organic compounds

The majority of the samples were supplied by BDH, the remainder being supplied mainly by Kotchlight and William and Hopkins Chemical organizations. They were mostly of reagent grade and less commonly of analytical grade. No further purification was carried out before use.

Polymers

Polymer samples were obtained either from commercial or academic sources, or synthesised when required.

The details are as follows:

Polyethers

Polyoxymethylene: This was supplied by Du Pont Co. Ltd. U.K. in the form of Delrin 500. Single crystals were prepared according to Geil by dissolving 0.2% of this material in phenol at $\sim 100^{o}C$ and then

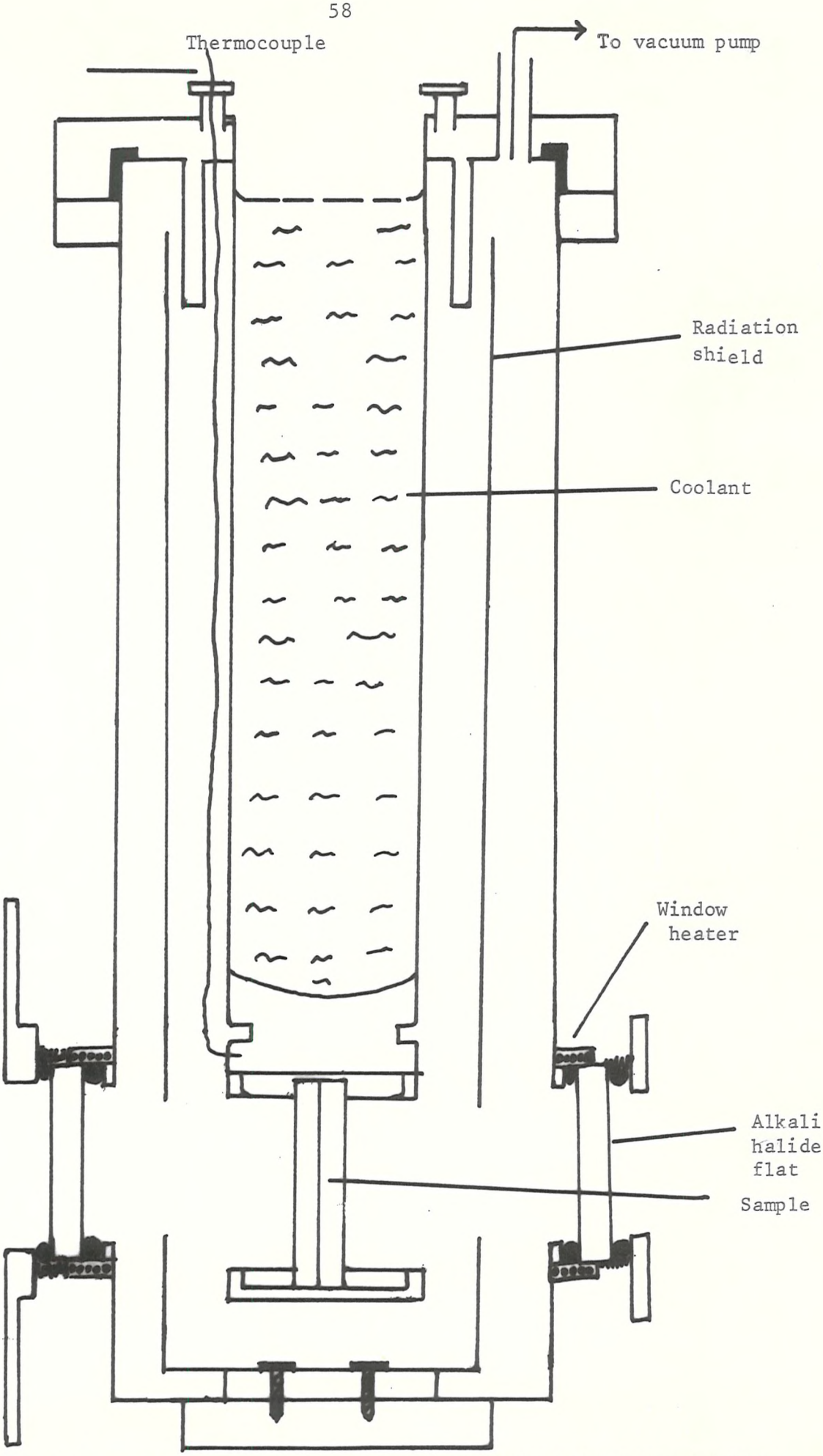

FIG. 2.5 BICC VARIABLE TEMPERATURE IR CELL USED FOR BOTH LOW AND HIGH TEMPERATURE EXPERIMENTS

allowing to crystallize at 60°C.

Perdeutero paraformaldehyde was kindly supplied by Mark, Sharp and Dhome of Canada as a gift.

Orthorhombic polyoxymethylene:

The orthorhombic form of POM is metastable and transforms into the hexagonal form on heating to 70-80°C.[125] This transformation has been considered to be irreversible. Preedy et al[133] however, claimed in 1972 that the transformation of POM_{Hex} to POM_{orth} could be affected by rolling the former at subambient temperatures. When a sample prepared in this way was examined by comparing its Raman spectrum with the reported one[130], it failed to show any such transformation. It was thought that failure could be due to a very low degree of transformation which was not detectable spectroscopically.

In this study the transformation of the ordinary material i.e. POM_{Hex} to POM_{orth} was affected by the application of pressure in view of the mechanism of transformation proposed by Preedy et al. A hydraulic press was used to press several samples of the single crystal material of POM_{Hex} in a metal die (13 mm. dia.) at 25°C as well as -180°C. The pressure was varied and the samples thus prepared were examined for transformation to POM_{orth} by means of Raman spectroscopy. The intensities of the bands near $\Delta\nu$ 598- and 624 cm^{-1} [130] were calibrated against per cent transformation. The results are plotted in Fig. 2.6. It is clear that maximum transformation does not exceed 40% against optimum pressures (10 to 15 K bars). These results have been recently supported from an independent inquiry in which a diamond anvil cell was used[134].

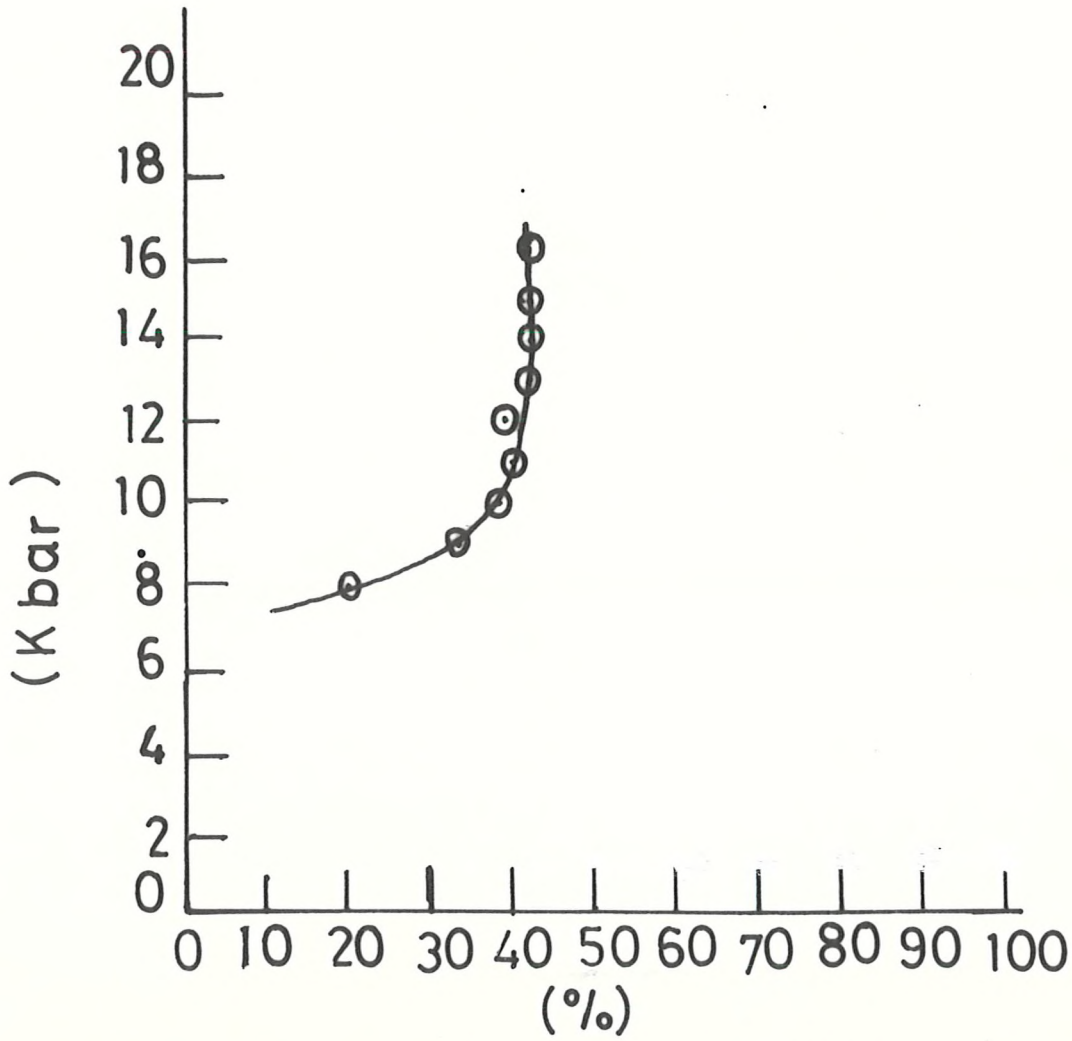

FIG. 2.6: Transformation of P.O.M. to P.O.M. Hex Ortho as a function of pressure

Polyethylene oxide: A high molecular weight (600,000) specimen was purchased from BDH and was subsequently annealed at 60°C for 18 hours to increase the degree of crystallinity. Tm:66°C, Degree of crystallinity:- ∿ 70%.

Polyoxacyclobutane: A sample of this polymer was kindly supplied by Professor H. Suga of Osaka University, Japan. This was purified by repeated precipitation from methanolic solution with water and then drying at high vacuum (10^{-3} mm). The three structural modifications were prepared as follows:[55]

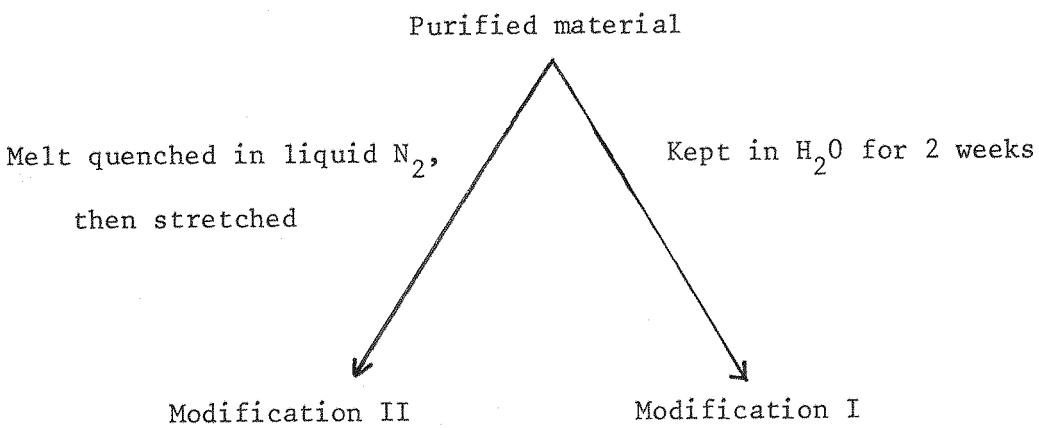

Since modifications I and II obtained in this manner were not amenable to Raman studies owing to high absorption characteristics, they were not investigated any further. The purified sample was identified as modification III from its IR spectrum and was used for Raman studies: Tm: 37°C.

Polytetrahydrofuran: A sample of this polymer was supplied by Mr. Fielding Russel of Loughborough University but was found to be highly fluorescent.

A second sample was provided by Dr. G.V. Frazer of Bristol University. It had a low Tm (∿ 41°C) but was quite amenable to Raman

studies.

Synthesis of polyhexamethylene oxide and polydecamethylene oxide

The procedure of Lal and Trick[89] was followed to synthesise these polymers. This involves poly condensation of glycols in an acidic medium according to the following reaction

$$n\ HO(CH_2)_mOH \xrightarrow{\text{Acid}} HO\left[(CH_2)_m-O\right]_nH + n-1\ H_2O$$

The reagents were supplied by BDH in the reagent grade and were used without further purification.

Polyhexamethylene oxide was synthesised by heating a mixture of 18 g of hexamethylene glycol, 0.15 g of boron trifluoride diethylether complex and 0.1 g of con. H_2SO_4 at the temperature of refluxing ethylene glycol under N_2 atmosphere. The apparatus described by Lal and Trick was modified to accommodate a stirrer as shown in Fig. 2.7. The heating was continued for 3 hours at the atmospheric pressure followed by heating for an additional 2 hour's period under high vacuum. The reaction vessel, however, was shaken from time to time during this period. After the reaction was over, the reaction product was treated with hot methanol and the insoluble fraction was crystallized from hot ethyl alcohol to give ∿ 1 g of white powdery material. Yield: 7% Tm: 56°C.

Polydecamethylene oxide was also prepared similarly by heating a mixture of 45 g of decamethylene glycol, 0.34 g of boron trifluoride diethyl ether complex and 0.22 g of con. H_2SO_4. The reaction product was treated with boiling ethyl alcohol and the insoluble fraction was crystallized from n-butanol to give ∿ 15 g of light grey powder. The material was later crystallized from a dilute ehtanolic solution. Yield: 37%, Tm: 75°C, Degree of crystallinity: > 90%.

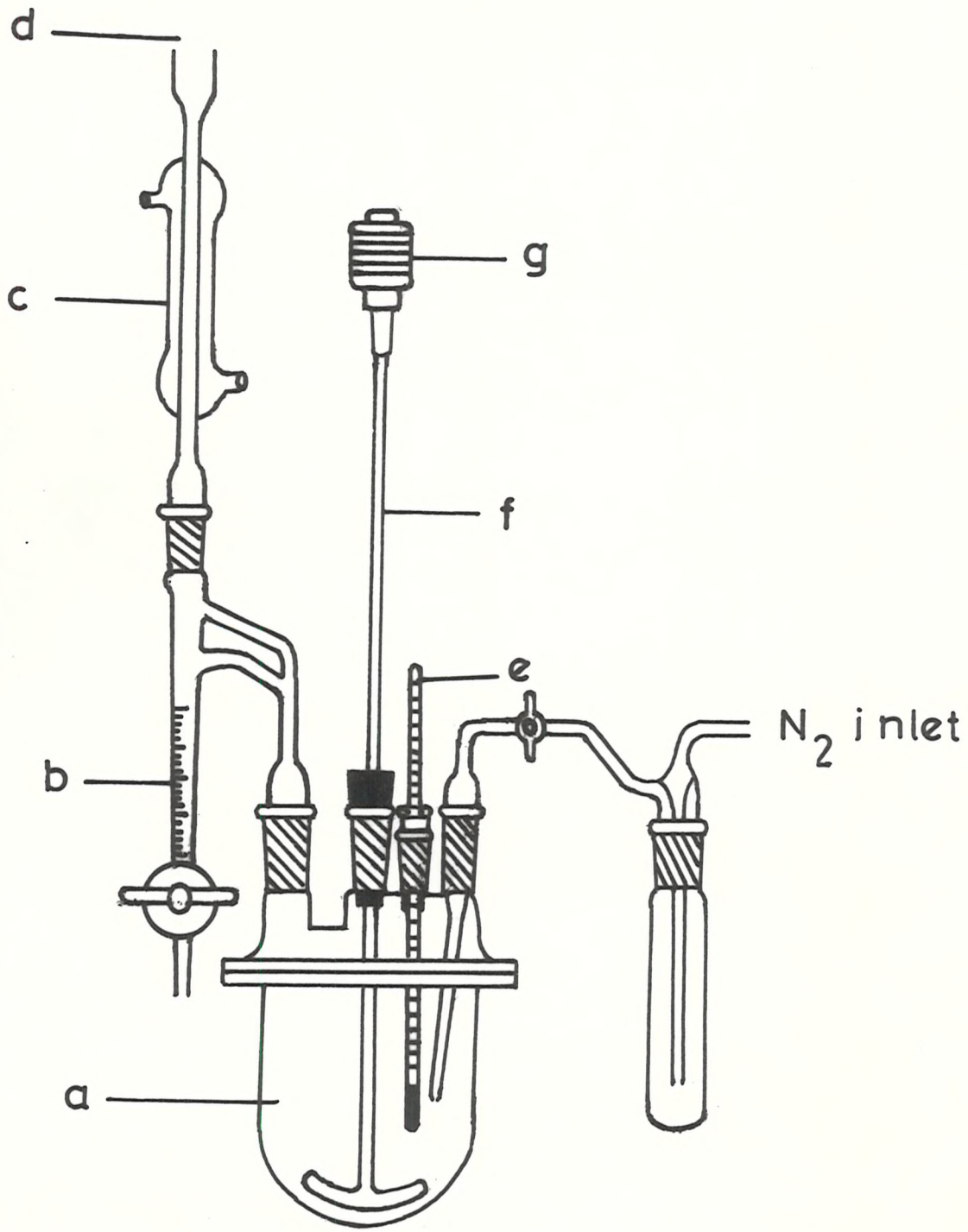

FIG. 2.7 APPARATUS USED FOR POLYCONDENSATION REACTIONS:
a - the reaction kettle, b ; Dean and Stark tube, c - condenser, d - to vacuum pump, e - thermometer, f - stirrer, g - stirring motor

The identities of these polymers were established by comparing their IR spectra with the reported ones.[52]

Polythioethers

Polythiomethylene: A sample was provided by Professor M. Mammi of Italy. Tm: 252°C.

Polyethylene sulphide: Melt quenched and stabilized samples of polyethylene sulphide were supplied by Dr. R.H. Gobran of Thiokol Chemical Corporation, U.S.A. and Dr. P.R. Sewell of Dunlop Co. Ltd., U.K. and had the following specifications.

Supplier	Designation	Stabilizer	Molecular Weight
Dr. R.H. Gobran	XP 6469	Polyamine	235,00 (by melt index)
Dr. P.R. Sewell	Thiolon M-180	Polyamine	Probably the same

These behaved similarly with regard to spectroscopic measurements.

Synthesis

Another sample of this material was synthesized for studying in the "as prepared" form as follows:

The synthesis was carried out in two steps i.e. the preparation of the monomer (ethylene sulphide) and its polymerization.

The monomer was prepared by heating equimolar quantities of dry KSCN and ethylene carbonate in a flask equipped with a thermometer and connected to a receiver through a water cooled condenser[156]. The product was obtained in high yield through following reaction.

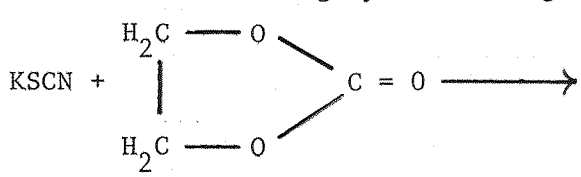

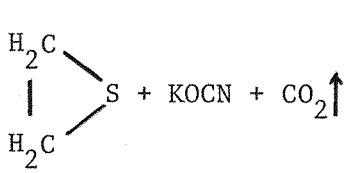

The IR spectrum of the product showed a very strong band near $\nu 1800\ cm^{-1}$ indicating the absorbed carbonate material as the main source of impurity. Refluxing over CaH_2 for ½ hour and subsequent distillation twice, resulted in complete removal of this material.

The monomer was then polymerised in methanolic NaOH (∿ 1%). The mixture was kept at $-10^{o}C$ overnight but no appreciable polymerization occurred. When the temperature was subsequently raised to $25^{o}C$, a hyper explosion took place and the whole mixture was converted into a white powder in a few seconds evolving a considerable amount of heat. Later, spectroscopic analysis showed it to be highly pure and crystalline. Yield: ∿ 100%, Tm: $202^{o}C$.

In view of the high Tm, the material is believed to be of very high molecular weight.

Ethylene carbonate (reagent grade) and KSCN (Analar) were purchased from BDH.

Polytrimethylene sulphide: A number of French concerns supplied specimens of this material. The details are as follows.

Supplier	Designation	Particulars
Dr. J.P. Machon (Ethylene Plastique)	$P49A_2$	Catalyst: Sodium Naphthalenide Mn: 120,000 $[\eta]$: 1.75 dl/g Tm: 61-62°C
	P49B	Catalyst: Sodium Naphthalenide Mn: 30,000 $[\eta]$: 0.70 dl/g Tm: 60-62°C
Dr. Y. Eitienne Dr. R. Paulet	-	Catalyst: Sodium Naphthalenide Mn: 100,000
Dr. S. Boileau	-	Not provided

Synthesis

Another sample was prepared as follows:

Trimethylene sulphide purchased from Ralph N. Emanuel Co. was purified by distilling from CaH_2. 5 g of the purified material was then heated with 0.2 g of sodium metal at 80°C under N_2 atmosphere for 5 minutes.[90] The product was purified by repeated precipitation with methanol from dichloromethane solution. Yield: ∿ 80%, Tm: 60°C.

All samples behaved similarly on spectroscopic examination and were found to be 65 to 70% crystalline.

Synthesis of polythioethers with $m \geq 4$

Polythioethers with m = 4, 5, 6 and 10 were synthesised by condensation polymerization of the disodium salt of a dimercaptan with a corresponding polymethylene dibromide in absolute alcohol-dry benzene medium according to the procedure of Marvel and Kotch.[91]

$$n\ \overset{+}{Na}\ \overset{-}{S} - (CH_2)_m - \overset{-}{S}\ \overset{+}{Na} + n\ \overset{-}{Br} - (CH_2)_m - Br \longrightarrow$$

$$\left[(CH_2)_m - S \right]_{2n} + 2nNaBr$$

Absolute alcohol was prepared by refluxing a mixture of ordinary absolute alcohol and Mg turnings for ½ hour in the presence of a trace of I_2 and then distilling in dry atmosphere. Dry benzene was prepared simply by introducing Na wire in Analar benzene and subsequently storing for a few days. 1,4 tetramethylene dibromide and 1,5 pentamethylene dibromide were purchased from BDH; 1,6 hexamethylene dibromide and 1,6 hexane dithiol were purchased from Kotchlight Co.; 1,4 butane dithiol and 1,5 pentane dithiol were purchased from Fluka Co.; 1,10 decane dithiol and 1,10 decamethylene dibromide were purchased

from Rolph N. Emanuel Co. The purity of these materials as indicated by the suppliers ranged between 97.5 to 99%. They were used without further purification.

A general procedure followed for the synthesis of polytetramethylene sulphide, polypentamethylene sulphide, polyhexamethylene sulphide and polydecamethylene sulphide may be described typically for polytetramethylene sulphide as follows:

The apparatus used was similar to that shown in Fig. 2.7 with the exception of Dean Stark tube. It was repeatedly evacuated and filled with dry N_2 before the start of experiment to ensure an oxygen and moisture-free atmosphere. 60 ml of absolute alcohol were then added into the flask with 0.84 g of Na under a constant flow of dry N_2. Na was dissolved by stirring and then heating to $60^{o}C$. After cooling to room temperature, 4.9 g of tetramethylene dithiol was added which produced disodium salt of the dithiol. The mixture was boiled to complete the reaction and diluted with 100 ml of dry benzene. After cooling to room temperature 8.6 g of tetramethylene dibromide were added. Immediately a vigorous reaction started with effervescence. When the reaction subsided, the reaction mixture was diluted with an additional 100 ml of benzene and refluxed overnight with continued stirring. The fraction insoluble in the reaction medium was separated by filtration and the filtrate was diluted with methanol to precipitate another fraction soluble in the medium. Both fractions were washed with distilled water repeatedly to free from NaBr and then with methanol. Finally, they were crystallized from benzene solution and dried under high vacuum (10^{-3} mm.). Yield $\sim$ 60%.

Solution crystallized materials had crystallinities greater than 90% (90-95%).

The insoluble fraction is considered to have a higher molecular weight than the soluble one[89]. Nevertheless they behaved similarly spectroscopically and had almost the same melting points.

The identity of polypentamethylene sulphide was determined by comparing its IR spectrum with the reported one[92]. The identities of polytetramethylene sulphide, polyhexamethylene sulphide and polydecamethylene sulphide were, however, established by microanalysis for carbon, hydrogen and sulphur contents, since no spectral data have been reported for these materials. The results of microanalysis are as follows:

Table 2.1

Microanalysis of polythioethers

Polythioether (m)	Element	Calculated (%)	Found (%)
4	H	9.09	9.04
	C	54.55	53.87
	S	36.4	37.32
6	H	10.30	10.21
	C	62	61.27
	S	27.60	26.90
10	H	11.63	11.49
	C	69.76	69.54
	S	18.60	17.95

Although these data are derived from microanalysis of the soluble fractions, the insoluble or high molecular weight fractions may be assumed to give almost the same results in view of the following facts:

(i) Vibrational spectra of both fractions are similar

(ii) Microanalysis of both fractions of polyhexamethylene sulphide have yielded similar results.

2.6.2 Processing

Raman: The samples used in Raman experiments were either solution crystallized or as prepared or melt quenched, which were annealed below Tm when required.

Melt crystallization or melt quenching was conducted using a hydraulic press as follows:

A mould was made by cutting a hole of the required shape and size in a stainless steel disc. The mould was placed between two sheets of aluminium with the sample in the mould and the whole assembly was put between two thick metal sheets in order to avoid damage to the platens of the press. This assembly was placed between electrically heated platens of the press. The sample was melted by controlling the temperature, pressed into shape and then slowly cooled or quenched. Quenching was carried out either by rushing cold water into the platens or by plunging the assembly into an ice-water mixture, liquid N_2 etc.

When powder samples had to be examined in their original form, they were lightly pressed into pellets.

Annealing at various temperatures was carried out using a thermostatically heated furnace under conditions of forced convection. The temperature was controlled (within $\pm$ 1^{o}C) using a thermometer in conjunction with a Sunvic EA4M electronic relay. The samples were sealed in glass ampoules under N_2 and placed in the vicinity of thermometer bulb.

IR: IR experiments were carried out on (25 - 50 μ thick) films of polymers made either by evaporating the solution or by pressing a mixture (polymer + K Br) or molten material. Oriented films were, however, prepared as follows:

Polyethylene sulphide: A small specimen was heated very close to Tm until it was soft and drawn rapidly.

Other polymers were oriented by rolling at room temperature using a hand driven roller.

2.6.3 Characterisation

Differential Scanning Calorimetry (D.S.C)

The melting points (Tm) for the polymer samples were measured using a Perkin Elmer D.S.C. model-2 instrument. This instrument allows a programming of the initial temperature, the heating or cooling rate (0.312 to 320 degrees/min) and the final temperature. The sensitivity varies from 0.1 to 20 M cals/sec. and the temperature is controlled and displayed within 4 digits to a tenth of a degree. Only a few mg of sample are required.

N_2 gas is used to purge the holders and to prevent the oxidation of the sample. The normal temperature range is 323 to 1000^{o}K. Calibration is carried out using standard transitions.

In a D.S.C. instrument, a thermal transition e.g. melting, boiling or crystallization, is displayed as a peak on a recorder and results from the change in power required to maintain a sample in a holder and a reference holder at the same temperature. The area under the curve indicates the energy supplied to or removed from the sample.

Crystalline melting point (Tm) is a first order transition. The temperature of the sample does not change during a first order transition- hence Tm may be determined as shown below:

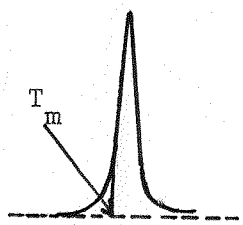

FIG. 2.8

In the usual experiments, a sample weighing ~10 mg was pressed into a small aluminium holder and placed in the sample compartment of the instrument. The heating rate was $5^{o}C$/min and the sensitivity 5-10 M cals/sec. Tm was measured as shown in Fig.2.8, by joining the slope and base of the endothermic peak.

Density

The densities of various samples were measured by the floatation method usually in aqueous $Na_2S_2O_3$ solution at $25^{o}C$.

X-ray diffraction patterns and degree of crystallinity

Wide angle X-ray diffraction patterns were recorded on a Phillips diffractometer using Ni filtered CuK_{α} radiation (λ = 1.54 $\AA$). Low angle X-ray measurements were made by Dr. G.V. Frazer on the author's request.

The degree of crystallinity is a function not only of the sample treatment but also of the technique used for its measurement.[94] Presently, however, this parameter for various samples was measured from wide angle X-ray diffraction patterns as the relative per cent crystallinity[93].

A crystalline but unoriented polymer specimen gives a typical X-ray pattern as shown in Fig. 2.9. In this pattern sharp peaks are considered to arise from crystalline regions and the broad diffused area under the peaks from the amorphous regions.

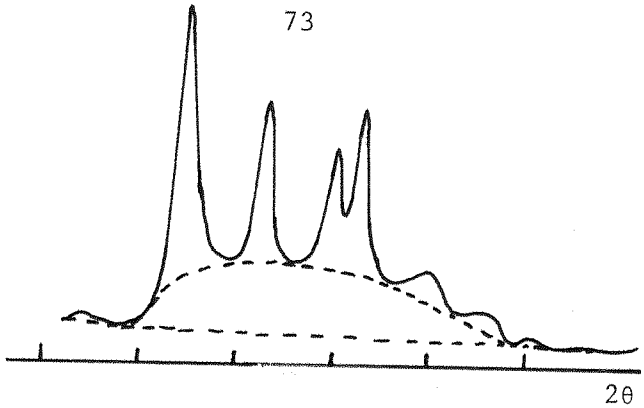

FIG. 2.9

The degree of crystallinity is defined as the ratio of the intensity of X-rays diffracted by the crystalline regions to that diffracted by the material as a whole. The relative per cent crystallinity is obtained by multiplying the product by 100.

The accuracy of the results thus obtained is sometimes not good because of the uncertain base line and nonsymmetrical peaks. Since high accuracy is not required in this work, such results are quite acceptable.

2.7 Fluorescence

The most troublesome problem encountered in Raman spectroscopy of polymers is the background emission which sometimes overlaps the whole spectrum, and is believed to arise mainly from fluorescence. It takes the form of a very broad background spectrum which reaches a maximum height at a cm^{-1} shift which is dependent on the wavelength of the exciting line (Table 2.2). A typical background spectrum (Stokes-Anti Stokes) is shown in Fig. 2.10 from which it can be seen that this phenomenon occurs mainly to the red side of the exciting line.

Table 2.2

Dependence of Fluorescence Background on the Exciting Line

Exciting Line (cm^{-1})	Fluorescence Maximum (cm^{-1})	Shift (Δcm^{-1})
20945	17850	3095
20430	17690	2740
19490	17370	2120
17600	16270	1330
15800	15200	600

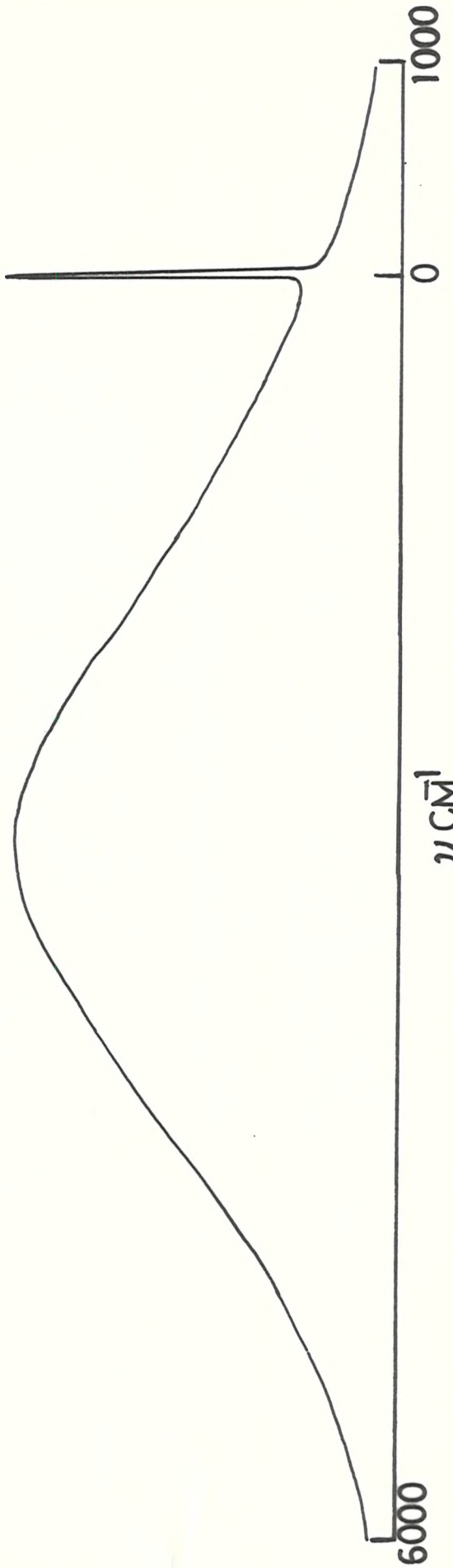

FIG. 2.10 STOKES AND ANTI-STOKES SPECTRUM OF FLUORESCENCE FOR THE 514.5 nm LASER LINE

The main reason for the occurrence of this phenomenon appears to be the presence of impurities e.g. trace amounts of foreign materials. Some impurities seem to be particularly destructive e.g. silicon grease.

A number of methods have been devised to combat this problem. No method seems, however, universally applicable.

In the present work following methods were employed to remove fluorescence.

Removal by exposure to the laser beam

Usually it decays when the sample is exposed to the laser beam for some time before recording the spectrum and does not return even if the laser is temporarily extinguished provided the sample remains firmly in position. The extent of removal varies not only with a particular sample but also wavelength, power and period of exposure. The reason for this behaviour seems to be the oxidation of impurities as indicated by a bleached spot at the focus of the laser beam.

Though this method proved to be particularly useful for polyethylene sulphide, polytrimethylene sulphide and polydecamethylene oxide, it brought about no improvement in the case of polyphenylene oxide.

Removal by Soxholet extraction

If the impurities and the polymer have different solubilities, the most convenient method to remove them consists of Soxholet extraction using a suitable solvent. This method was employed to polyphenylene oxide and high molecular weight polytetrahydrofuran but no improvement was indicated.

Removal by E.D.T.A.

In a private communication Atalla[95] proposed that spurious metal

ions might cause fluorescence in view of the fact that the spectra of some cellulose materials containing trace amounts of Fe, Ni and Co ions showed considerable improvement after treating with aqueous solution of E.D.T.A. Therefore, a small specimen of polyphenylene oxide known to consist of trace amounts of Cu and Na ions was mixed with aqueous solution of E.D.T.A. and after storing for two days washed several times with deionised water. The sample was then dried under high vacuum and examined. No improvement in the spectrum was, however, observed.

Removal by the addition of quenching materials

It has been suggested that the addition of trace amounts of some chemicals e.g. dinitrobenzene can quench fluorescence[96]. No success could, however, be achieved even with this method in the case of polyphenylene oxide.

Removal by activated charcoal

This method consists in shaking a polymer solution with activated charcoal followed by filtration and seems to be valuable for many purposes. The polymer is recovered from the filtrate by precipitation and dried under high vacuum.

Sometimes a difficult situation may arise when fine particles of charcoal pass to the filtrate and become an additional source of impurity. This may be avoided either by using several layers of filter paper and repeating the filtration or by centrifuging the filtrate before precipitation. Very great care is needed to wash the containers before subsequent filtration since fine charcoal particles may remain stuck to the walls and may not be visible with naked eye.

This method was successfully applied to a number of polythioethers.

This too, however, failed to give any good results in the case of polyphenylene oxide. The failure in the latter case may be assumed to have resulted from the solubility of polyphenylene oxide at elevated temperatures only ($80^{\circ}C$) in certain solvents at which temperatures the absorption characteristics of activated charcoal might be less effective.

Thus it is clear that none of these methods is universally applicable. Polyphenylene oxide did not show any spectrum in spite of the concerted efforts described above. Nevertheless, considerable evidence has emerged that fluorescence is caused mainly by impurities.

2.8 Acknowledgement

The author wishes to thank the following persons and organizations in connection with the experimental work performed outside the Department of Chemistry.

Dupont Co. Ltd. U.K. for a sample of polyoxymethylene.

Professor M. Mammi of Italy for a sample of polythiomethylene

Dr. R.H. Gobran of Thiokol Chemical Corporation, U.S.A. and Dr. P.R. Sewell of Dunlop Co. U.K. for the samples of polyethylene sulphide.

Professor H. Suga of Osaka University, Japan, for a sample of polyoxacyclobutane. Dr. J.P. Machon of Ethylene Plastique, Dr. Y. Etienne, Dr. R. Paulet and Dr. S. Boileau all of France, for the samples of polytrimethylene sulphide.

Mr. Fielding Russel and Dr. G.V. Frazer, for the samples of polytetrahydrofuran. The latter also for measuring low angle X-ray diffraction patterns of polytetrahydrofuran and polydecamethylene sulphide.

Dr. E.P. Magré of AKZO, Netherlands, for a sample of polyphenylene oxide.

Professor F. Hodson, Department of Geology, University of Southampton for permission to use his X-ray diffractometer.

Mr. J. Clayton and other staff of the Engineering Department, Southampton College of Technology, for permission to use their roller and for their cooperation.

CHAPTER III

CHARACTERISTIC RAMAN FREQUENCIES OF ORGANIC COMPOUNDS

3.1 Substituted benzenes

Upon substitution of the benzene molecule, the symmetry is in most cases lowered and the degenerate vibrations are split into their components (See Varsanyi[168] for normal coordinate analysis of benzene and its derivatives). The symmetry of each of the various types of monoatomic substituted benzenes is given in Fig. 3.1.

Characteristic vibrations in substituted benzenes are those in which the carbon atom(s) linking the benzene ring with the substituent(s) and the atom(s) of the substituent(s) undergo insignificant displacements during the vibration. The vibration itself is localized on the atoms of the benzene ring that are removed from the point(s) of substitution. Nonspecific vibrations are those that are essentially localized on the bond joining the ring with the substituent(s) and on the angles nearest to it, all of which undergo considerable displacements. See Bogomolov[169-173] for a classification of the characteristic vibrations of mono, ortho, meta, para and 1,2,3 trisubstituted benzenes.

Nevertheless, it is a collection of characteristic frequencies rather than a single one which determines the type of substitution.

Despite the fact that Raman frequencies are more useful than the IR ones for skeletal characterization, they have been investigated less extensively in the case of substituted benzenes.

3.1.1 Review of literature

Raman

Several authors including Hibben[3], Kohlrausch et al[4] and Jones and Sandorfy[5] have reviewed moderately extensive series of substituted benzenes mostly with alkyl substituents at mono, 1,2; 1,3 and 1,4 positions. Their results may be summarized as follows;

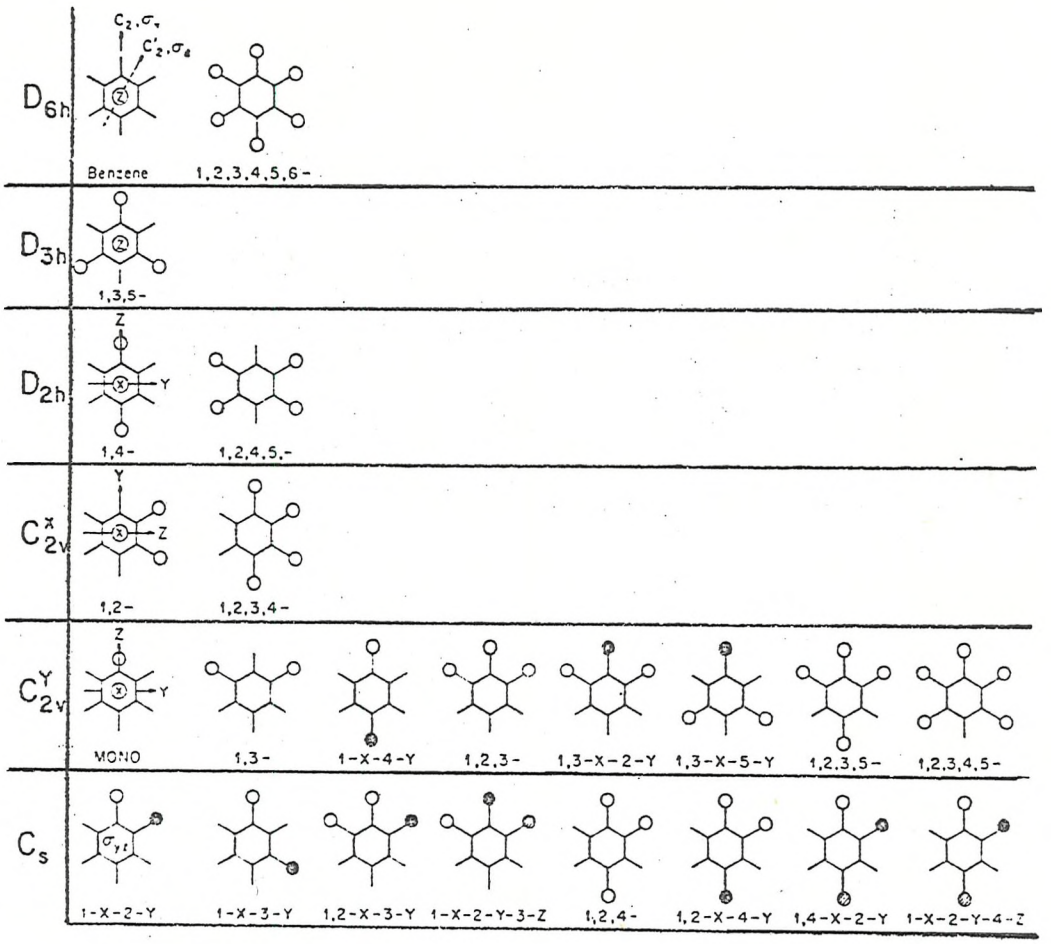

FIG. 3.1[22] SYMMETRY CLASSIFICATION OF SUBSTITUTED BENZENES

Table 3.1

Classical Raman group frequencies for mono and disubstituted benzenes

Type of substitution	$\Delta \nu$ cm^{-1}	Mode
Mono	620 ± 3(W)	Ring deformation
	1000 ± 3 (S)	Ring breathing
	Higher in some molecules e.g. toluene (1022 cm^{-1})	
	1027 ± 2(W)	β(C-H), In plane C-H deformation
	1155 ± 5(V)	γ(C-H), out-of-plane C-H deformation
	1195 ± 15(V)	
1,2	711 - 736	γ(C-H)
	1030 ± 4	β(C-H)
1,3	711 - 736	γ(C-H)
	1000 ± 3	Ring breathing
1,4	796 - 824	β(C-H)

In the late sixties Green et al[174-188] reported a series of fifteen papers on the vibrational spectra of various benzene derivatives. Very recently, Schrader et al[97], Dollish et al[22] and Freeman[14] have reported their conclusions specifically on the characteristic Raman frequencies of substituted benzenes. Although these latter sets of conclusions are based upon larger number of compounds, it is felt that various substituent groups are still not represented or insufficiently represented in their derivations.

IR

On the other hand, although IR group frequencies exist for almost all substituted benzenes they are subject to different sorts

of limitations. The most characteristic band patterns in the IR spectra of substituted benzenes occur in the frequency ranges of 700 to 850 cm^{-1}[89,99,107,189] and 1650 to 2000 cm^{-1}[100] (Fig. 3.2), and arise from the out-of-plane CH deformations and their overtones respectively. The bands arising from polar groups in the frequency range of 650 to 1900 cm^{-1}, however, tend to deform or overlap them thus making the identification of the substitution type difficult and sometimes impossible[20].

Due to these facts, Raman characteristic frequencies have been deduced in the present work from an analysis of >200 substituted benzenes with substituents belonging to a large variety of molecular groups.

3.2 Monosubstituted benzenes

3.2.1 Results

The Raman correlations derived from more than 70 spectra have been given in table 3.2 together with the IR ones. The latter correlations have been adopted from Bellamy[20]. Fig. 3.3 represents typical Raman and IR spectra of monosubstituted benzene.

3.2.2 Discussion

Evidently the present correlations do not differ much from the already existing ones. However, these suggest more relaxed and meaningful spectral ranges for the characteristic bands but cast doubts on the diagnostic validity of some characteristic bands referred to above. The depolarized band near $\Delta\nu$ 620 cm^{-1} classically recognised as a particularly characteristic band[3,4,5] can not be recommended firstly because of its too low intensity in certain cases and secondly because of a coincident

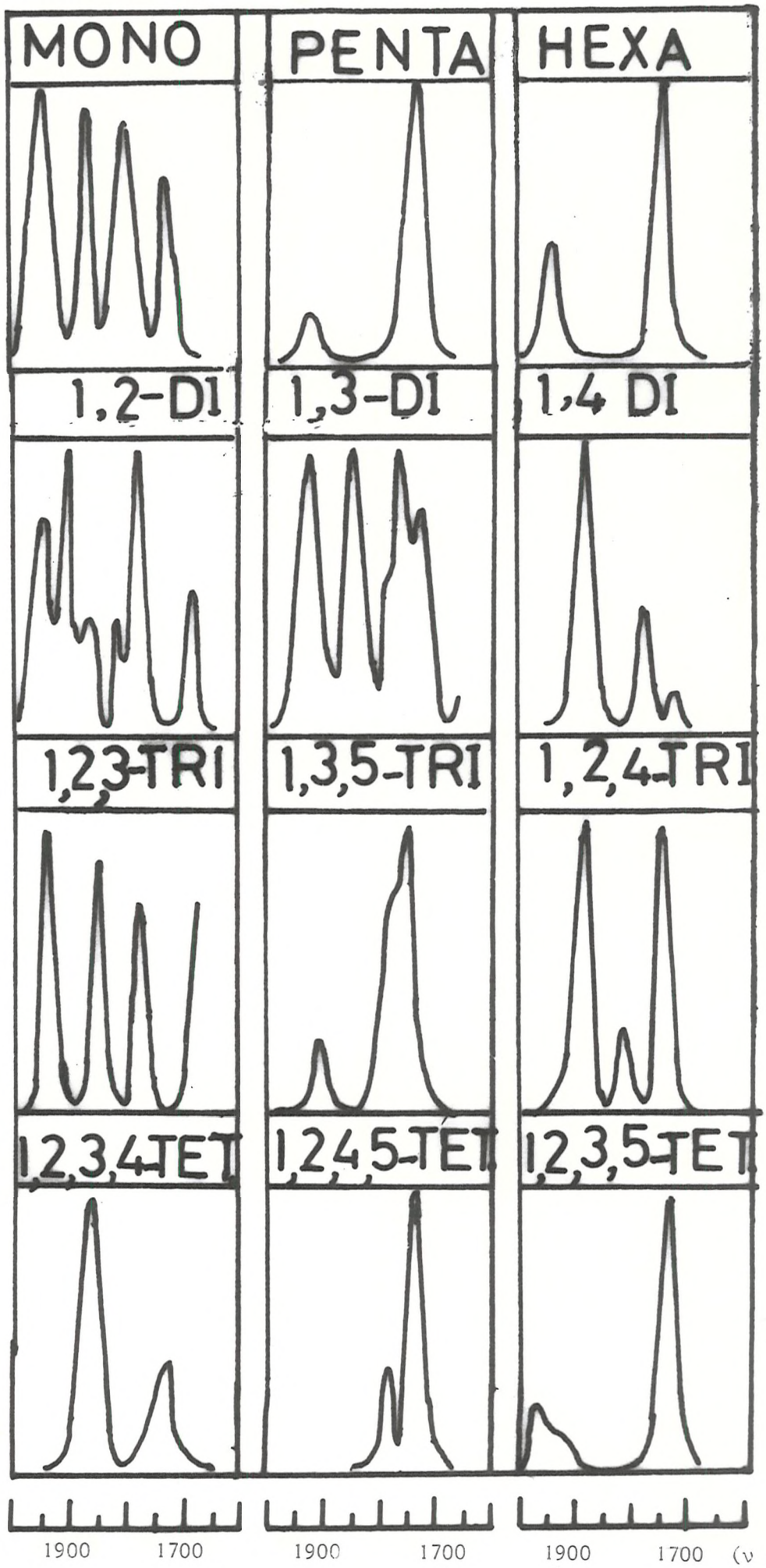

FIG. 3.2 CHARACTERISTIC IR PATTERNS OF SUBSTITUTED BENZENES BETWEEN ν1650-2000 cm^{-1}

Table 3.2

Raman and IR correlations of monosubstituted benzenes

Vibrational Type	Raman Correlations $\Delta\nu cm^{-1}$	Comments	IR Correlations νcm^{-1}	Comments
ϕC-C	$620^{\pm}8$	VW-MW, (dp)	680-710	M-S
γC-H	720 840	VW-M, (P)	737-747	S For Ar CH=CHA* systems the range changes to 758-763 cm^{-1}, NO_2 and carbonyl groups shift the band to still higher values.
Ring	$1003^{\pm}6$	S, (P)		
βC-H	$1028^{\pm}10$	W-M, (P) The above pair is the most characteristic of monosubstitution.		
νC=C	$1600^{\pm}10$	W or M-S, dp Usually weak but conjugation with substituents, increases the intensity	1450 M 1500 S	Monophenyl compounds
			1495 S 1500 S 1520 M	Bi or polyphenyl compounds
		Alkyl monophenyl and di or polyphenyl compounds give rise to more than one band. Lower frequency with heavy substituents e.g. $(C_6H_5)_3AS$-1570 cm^{-1}	1570-1600 1650-2000	VW - intensity increases due to conjugation. VW summation bands due to γC-H Very characteristic.
νC-H	3050-3080	MW-S, P Lower frequency with alkyl or metalloid substituents. Usually 1-3 bands; one of them being stronger than others.	3030-3080	Weaker than Raman
2νC=C	(i) 3140-3180	VW, P		
	or (ii) 3240-3280	VW-MW, P Occur usually but may be absent.		

* Ar = Aryl or phenyl

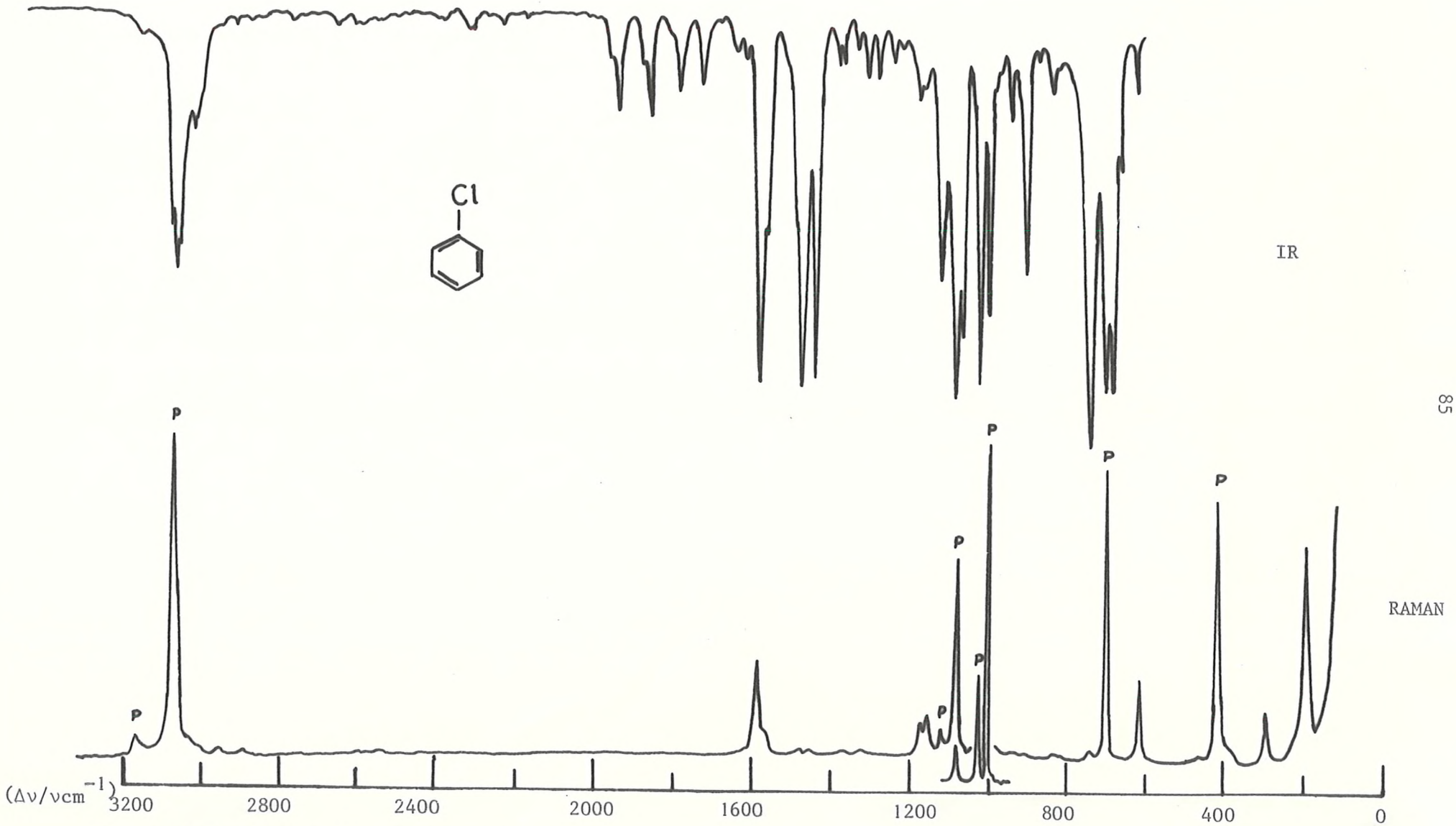

FIG. 3.3 RAMAN AND IR SPECTRA OF A MONO SUBSTITUTED BENZENE

medium intensity band due to the NO_2 bend. Its narrow range, however, suggests its validity particularly for liquids where polarization measurements are possible. The intensity of this band increases with electron withdrawing groups.

The low intensity of the Raman bands between $\Delta\nu$ 650-850 cm^{-1} is a remarkable characteristic of monosubstituted benzenes. Despite their low intensity they eventually give some useful information about the related molecular features. The molecules associated with heavy substituents like halogens, metals and metalloids give rise to an X-sensitive band between $\Delta\nu$ 650-720 cm^{-1}. The frequency of this band appears to decrease with increase in the weight of M-ϕ (M = atom of X attached to ϕ) and its intensity appears to decrease with increase in the electronegativity of M. Almost all alkyl or partially alkyl substituted compounds show W-MW polarized band between $\Delta\nu$ 720-790 cm^{-1}. Very electronegative substituents drive the frequency of this band upto $\Delta\nu$ 850 cm^{-1}.

The pair of polarized bands between $\Delta\nu$ 1000-1030 cm^{-1}, are the most spectacular bands in the spectra of monosubstituted benzenes. The band near $\Delta\nu$ 1000 cm^{-1} is the strongest in the whole spectrum apart from those due to the conjugated functional groups. It also occurs in spectra of M-disubstituted and 1,3,5 trisubstituted benzenes wherefrom it can be easily distinguished by the occurrence of the weaker companion band near $\Delta\nu$ 1028 cm^{-1}. Abnormally high frequencies of this band for alkyl benzenes as referred to in the literature[3], were not observed. However, slight variations in the frequency of this band are very difficult to interpret. These are perhaps connected with both electronegative and steric effects of the substituent. A more recent proposal[15] that oxygen and nitrogen containing substituents cause this band to appear below about $\Delta\nu$ 1000 cm^{-1} while others drive it to slightly

higher frequencies, is not correct in view of the present investigation. The variations in the frequency and the intensity of the band near$\Delta\nu$ 1028 cm^{-1}, seem to be induced by the X-sensitive mode occurring close to it in frequency, in an analogous manner to the corresponding IR band[101,102].

The classical proposal[103] that the bands near$\Delta\nu$ 1150 cm^{-1} and 1195 cm^{-1} have some analytical value is incorrect because of the occurrence of similar bands in other types of substituted benzenes.

The depolarized $\nu C{=}C$ band near$\Delta\nu$ 1600 cm^{-1} is usually weak but its intensity increases considerably if the substituent is capable of becoming involved in delocalization with the ring. Monophenyl alkyl benzenes and di and polyphenyl monosubstituted benzenes show more than one band in this region, of which one near$\Delta\nu$ 1600 cm^{-1}, is usually the strongest. Heavy substituents like halogens, metals or metalloids cause downward shifts in frequency. The increased intensities of these bands in the case of some di and triphenyl compounds like $(C_6H_5)_2SO_2$, $(C_6H_5)_2SO$, $(C_6H_5)_3As$, $(C_6H_5)_3P$ can be attributed to the donating of the ring electrons into the vacant P or d orbitals of the substituents which causes delocalization of the ring electrons.

The C-H stretching bands ($\Delta\nu$ 3050-3080 cm^{-1}) are only slightly polarized probably because of the coincidence of A and B class fundamentals. Monophenyl alkyl benzenes and di and polyphenyl compounds show more than one band in this region; that at a moderately high frequency being the strongest.

In the IR absorption, the bands given in table 3.2 can be regarded as characteristic for monosubstitution. The band near ν740 cm^{-1} also occurs in O-disubstituted benzenes and can be distinguished by noting the absence of that nearν700 cm^{-1} in the latter type of compounds. Like other substituted benzenes, monosubstituted benzenes show a

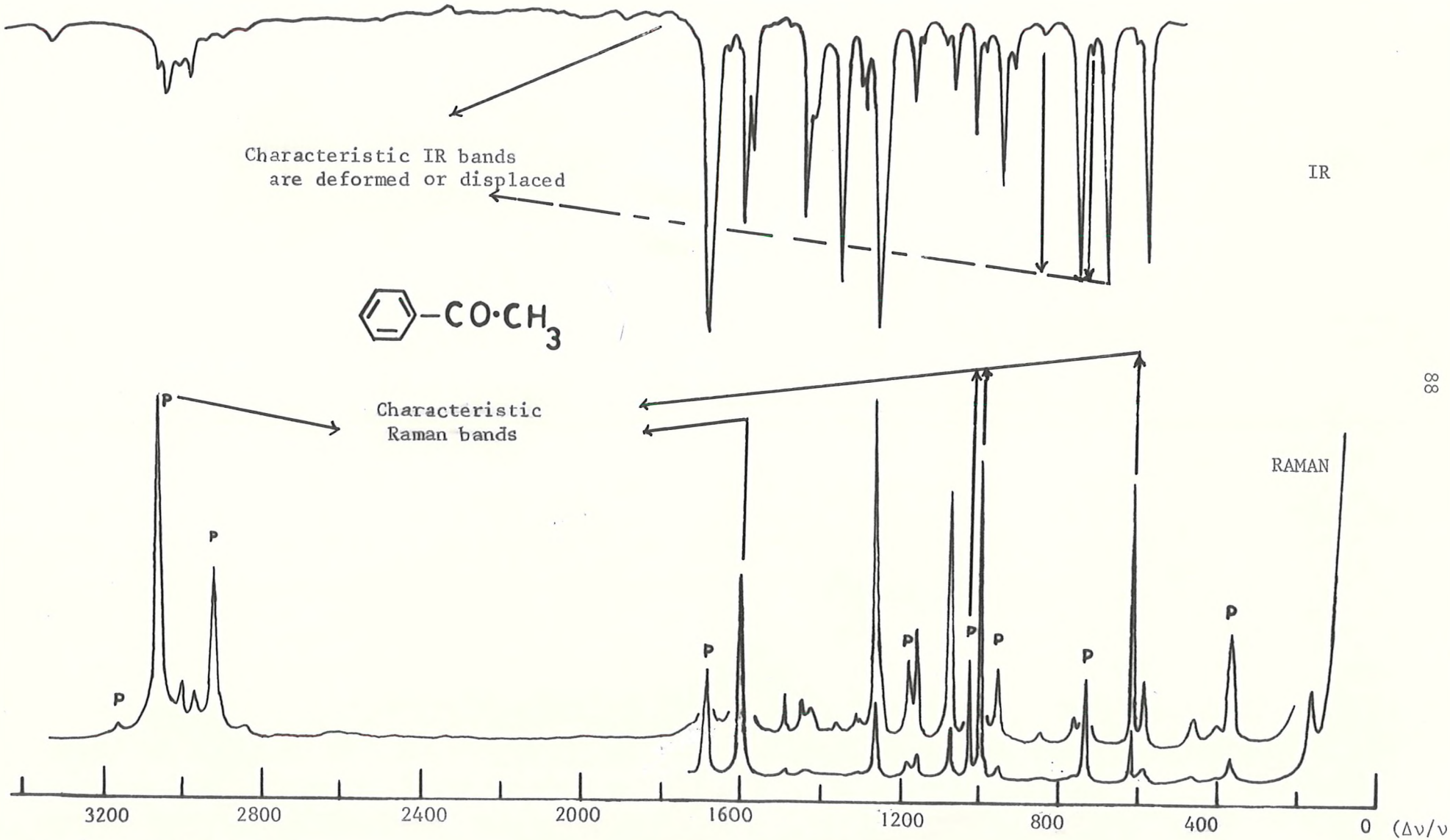

FIG. 3.4 RAMAN AND IR SPECTRA OF BENZOYL METHYL SHOWING THAT RAMAN CORRELATIONS ARE RELIABLE EVEN WHEN THE IR CORRELATIONS FAIL DUE TO POLAR SUBSTITUENT GROUPS

characteristic pattern of bands between ν 1650-2000 cm^{-1} (see Fig. 3.2). The number and intensity of these bands are very characteristic of the type of substitution[100].

While no exception to the Raman correlations has been noted in more than 70 compounds examined, the IR correlations can be regarded as holding good in a limited number of cases only. The lower frequency bands undergo considerable anomalous shifts and the band pattern between ν 1650-2000 cm^{-1} is overlapped or deformed in the case of nitro and carboxylic compounds (see Fig. 3.4). However, it is clear that the use of both of these correlations together can yield an unambiguous analysis of the substituted benzenes.

3.3 Disubstituted benzenes

3.3.1 Results

Tables 3.3, 3.4 and 3.5 give Raman correlations derived from an analysis of more than 70 disubstituted aromatics together with the IR ones. The latter refer to Bellamy. Figs 3.5, 3.6 and 3.7 show typical Raman and IR spectra of ortho-, meta- and para disubstituted benzenes respectively.

3.3.2 Discussion

The tables 3.3, 3.4 and 3.5 reveal that the classical Raman correlations (Table 3.1) are limited in application to alkyl benzenes only i.e. the source of their derivation. The present correlations extend over larger spectral ranges representing progressive changes in the regions: $\Delta\nu$ 700-900 cm^{-1} and $\Delta\nu$ 1000-1100 cm^{-1} subject to the type of disubstitution (see Tables 3.6, 3.7 and Fig. 3.8). The latter region is particularly significant for recognizing the type of substitution.

The strong polarized band near $\Delta\nu$ 1000 cm^{-1} due to symmetric ring

breathing mode (see Table 3.5, Fig. 3.5) is given by all monosubstituted, M-disubstituted and 1,3,5 trisubstituted phenyl compounds as stated before, but that given by M-disubstituted compounds can be distinghished from others as follows: Like monosubstituted benzenes no similar band is given by M-compounds near $\Delta\nu$ 1030 cm^{-1} and 1,3,5 trisubstituted aromatics show no comparable band near $\Delta\nu$ 1095 cm^{-1} as given by the M-compounds. This band can be further characterised for M-compounds only by noting the absence of any medium to strong intensity band in the out-of-plane C-H deformation region i.e. $\Delta\nu$ 700-800 cm^{-1} in the spectra of mono and 1,3,5 trisubstituted aromatics.

The identification of O-substitution is exceedingly simple. The strong polarized band near $\Delta\nu$ 1040 cm^{-1} (see Table 3.3, Fig. 3.5) is unique in position and strongly points towards O-disubstitution. This band sometimes splits into two as observed in the case of alkyl or partially alkyl substituted benzenes. This is perhaps due to interaction with the aliphatic C-H deformation mode of the substituents.

No intense band is given by the P-disubstituted benzenes in the region between $\Delta\nu$ 1000-1070 cm^{-1} (see Table 3.5, Fig. 3.7). Nevertheless, in contrast to other types of substitution the GAP represented by this region in the spectra of P-substituted aromatics, hints towards P-substitution.

The characteristic bands in the $\Delta\nu$ 700-900 cm^{-1} region (γC-H) (see Tables 3.3, 3.4, 3.5, and Fig. 3.5, 3.6, 3.7) further support the above conclusions especially in the case of P-substituted benzenes where these bands are not likely to be confused with those in other compounds because of their occurrence at sufficiently elevated positions.

The identification of P-substitution is further facilitated by two

Table 3.3

Raman and IR correlations of O-disubstituted Benzenes

Vibrational Type	Raman Correlations $\Delta\nu cm^{-1}$	Comments	IR Correlations $\nu\ cm^{-1}$	Comments
νC-H	740-800	S, P Halogen Substd. aromatics give VW bands in this region	735-770	S 690-710 cm^{-1} band absent
βC-H	1030-1055	S, P Very characteristic. Occasionally a pair of strong bands perhaps due to interaction with other vibrations.		
νC=C	1575-1625	W, dp Strong due to conjugation. Higher frequencies with phenols, esters and amines. Lower frequencies with halogens and nitro groups.	1450 1500 1600 1650-2000	M V Very strong due to conjugation Characteristic summation bands
νC-H	3050-3100	MW-S, P 2-4 unresolved bands or 1 broad band.	Same range	Weaker than Raman

Table 3.4

Raman and IR correlations of M-disubstituted Benzenes

Vibrational Type	Raman Correlations $\Delta\nu$ cm^{-1}	Comments	IR Correlations ν cm^{-1}	Comments
νC-H	700-765	MS-M, P	770-800	S
		Very electronegative groups drive this band to $\Delta\nu$810 cm^{-1}.	710-690	S
Ring	1000±5	S or VS, P Not accompanied by a weaker band near $\Delta\nu$ 1025 cm^{-1}.	-	-
νC-H	1095±10	W, P Distinction from monosubstitued.		
νC=C	1585-1610	W, dp Strong with conjugation.	1585-1610	VW - strong with conjugation.
		Lower and higher frequencies as stated before	1650-2000	Characteristic weak summation bands
νC-H	3060-3105	MW-MS, P More than 1 band may occur.	3040-3100	Weaker than Raman

Table 3.5

Raman and IR correlations of P-disubstituted benzenes

Vibrational Type	Raman Correlations $\Delta\nu_{cm}^{-1}$	Comments	IR Correlations ν_{cm}^{-1}	Comments
νC-H	790-880	M-S, P 1-2 strong bands, halogens directly attached to the ring lower the frequency upto $\Delta\nu$ 700 cm^{-1}. Halogens in the β position affect less.	800-860	S
	625-640 VW-M			
βC-H	1000-1070	VW or NO band (GAP)	1000-1070 1090-1125 1195-1125	2 W bands
X-sensitive		Usually 1-2 M-S substituent sensitive bands in the region $\Delta\nu$ 1070-1300 cm^{-1}	1650-2000	Characteristic weak summation bands.
	1580-1625	W, dp Strong with conjugation		
νC-H	3060-3100	M-S, P Unresolved 2-4 bands	3040-3100	Weaker than Raman

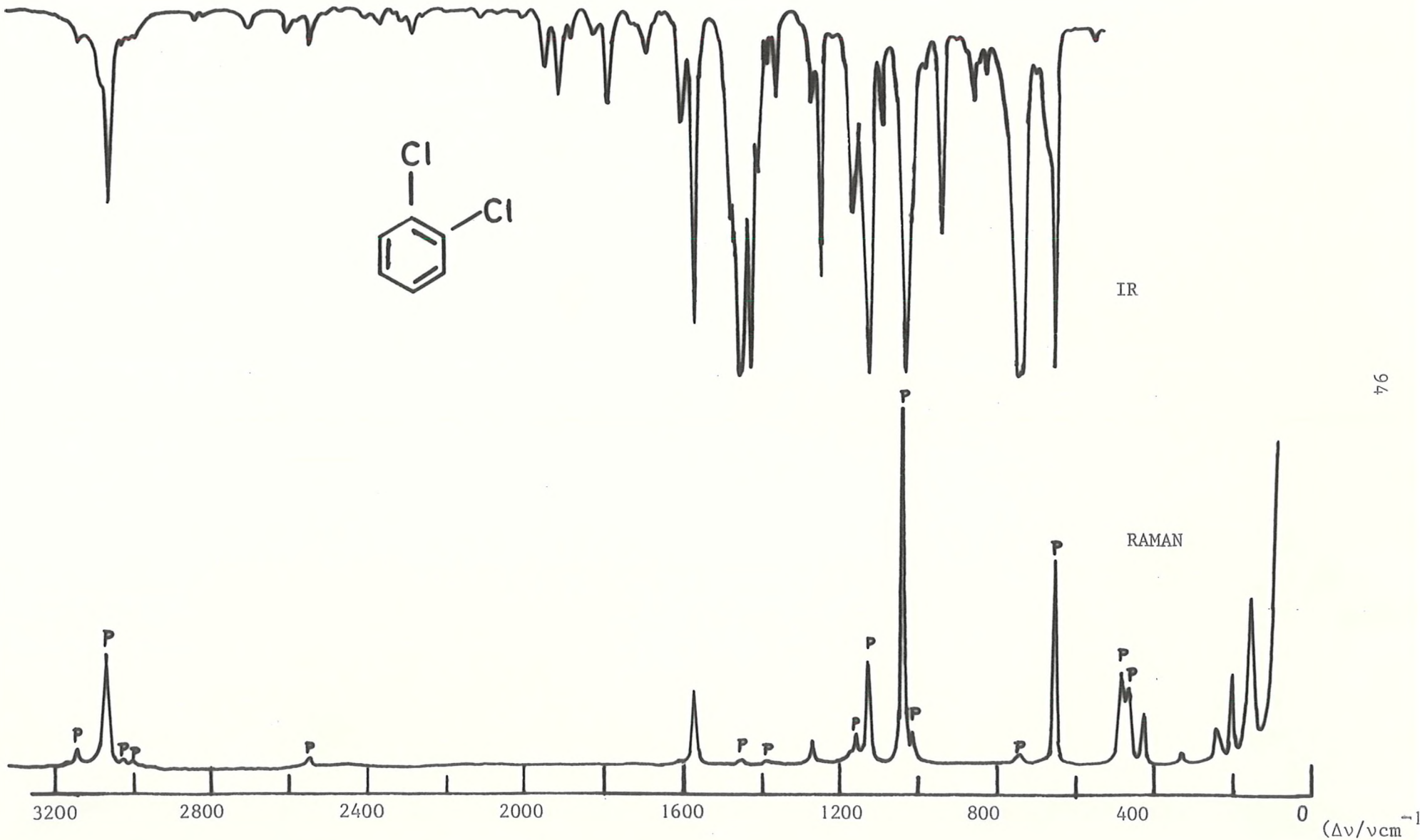

FIG. 3.5 RAMAN AND IR SPECTRA OF AN O-DISUBSTITUTED BENZENE

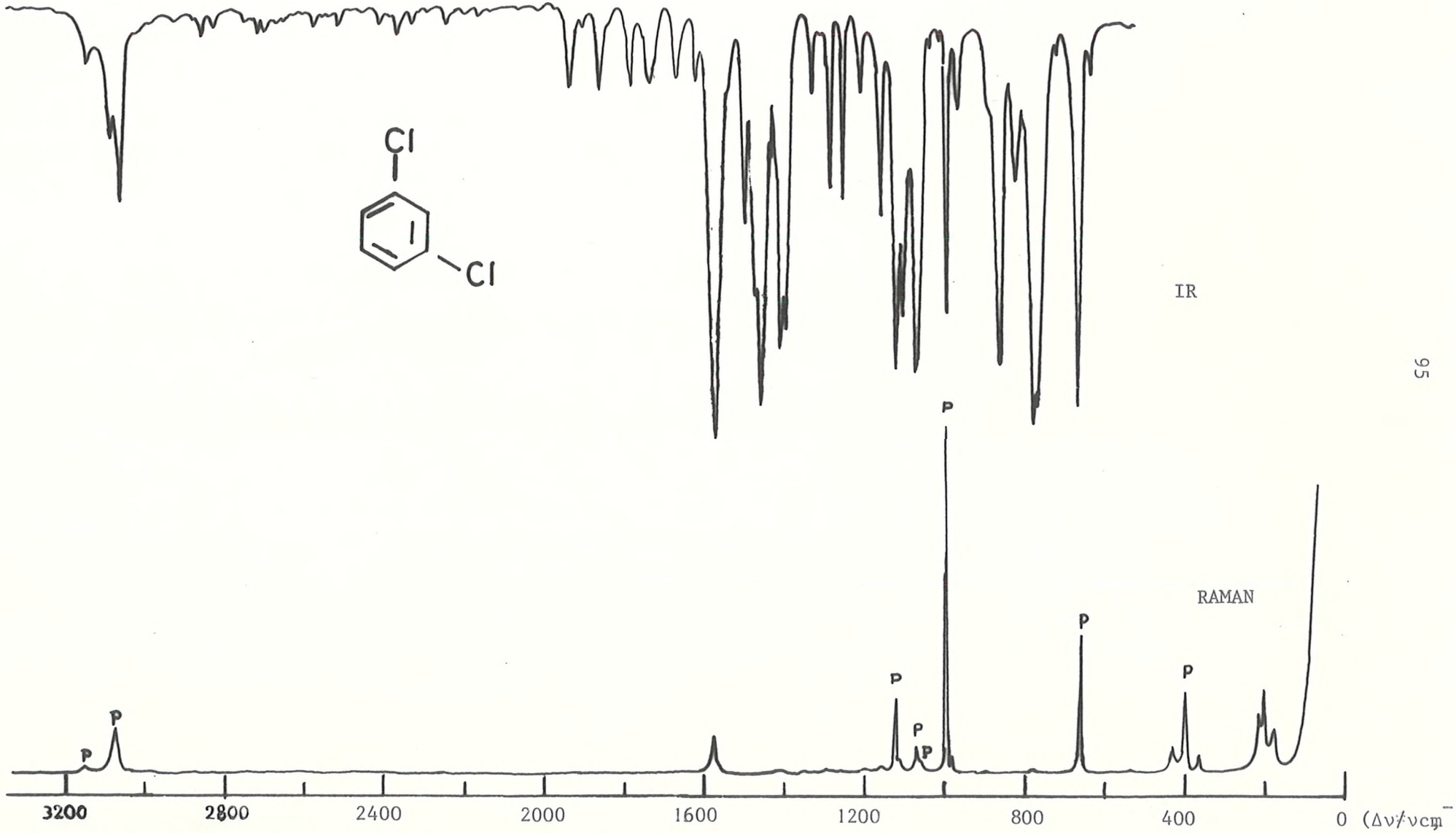

FIG. 3.6 RAMAN AND IR SPECTRA OF A M-DISUBSTITUTED BENZENE

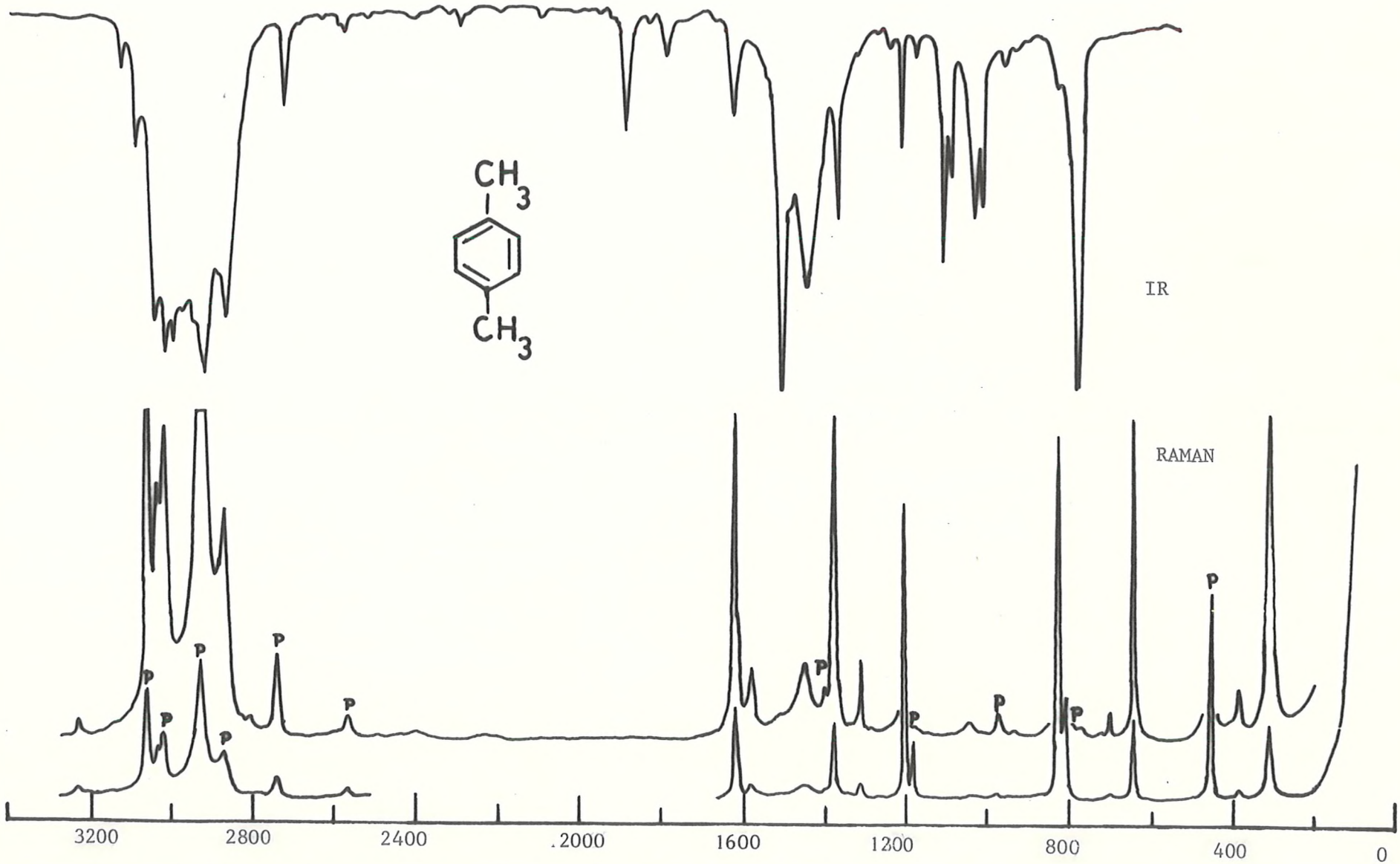

FIG. 3.7 RAMAN AND IR SPECTRA OF A P-DISUBSTITUTED BENZENE

Table 3.6

Progressive changes in the γC-H region $\Delta\nu$ 700-900 cm^{-1}

XC_6H_4Y

X	Y	O-	M-	P-
		$\Delta\nu cm^{-1}$	$\Delta\nu cm^{-1}$	$\Delta\nu cm^{-1}$
OH	COOH	775 S	760 MS	843 MS 853 MS
OH	OH	780 S	750 M	860 S
Cl	Cl	756 VW	?*	750 S
CH_3	OH	838 S	749 S	?
OH	CO-H	775 S	788 S	850 M
CH_3O	CH_3O	762 S	?	824 S
Cl	NH_2	840 M	700 M	?

Table 3.7

Progressive changes in the region between ν 1000-1100 cm^{-1}

XC_6H_4Y

X	Y	O-	M-	P-
		$\Delta\nu cm^{-1}$	$\Delta\nu cm^{-1}$	$\Delta\nu cm^{-1}$
Cl	Cl	1040 S	999 S 1068 W	-
Cl	NH_2	1028 S	1003 S 1087 W	?
OH	OH	1048 M	1006 W 1092 W	-
OH	COOH	1035 S	1000 S 1079 VW	-
OH	CO-H	1034 S	1000 S 1120 VW	1050 W

? = Not investigated.

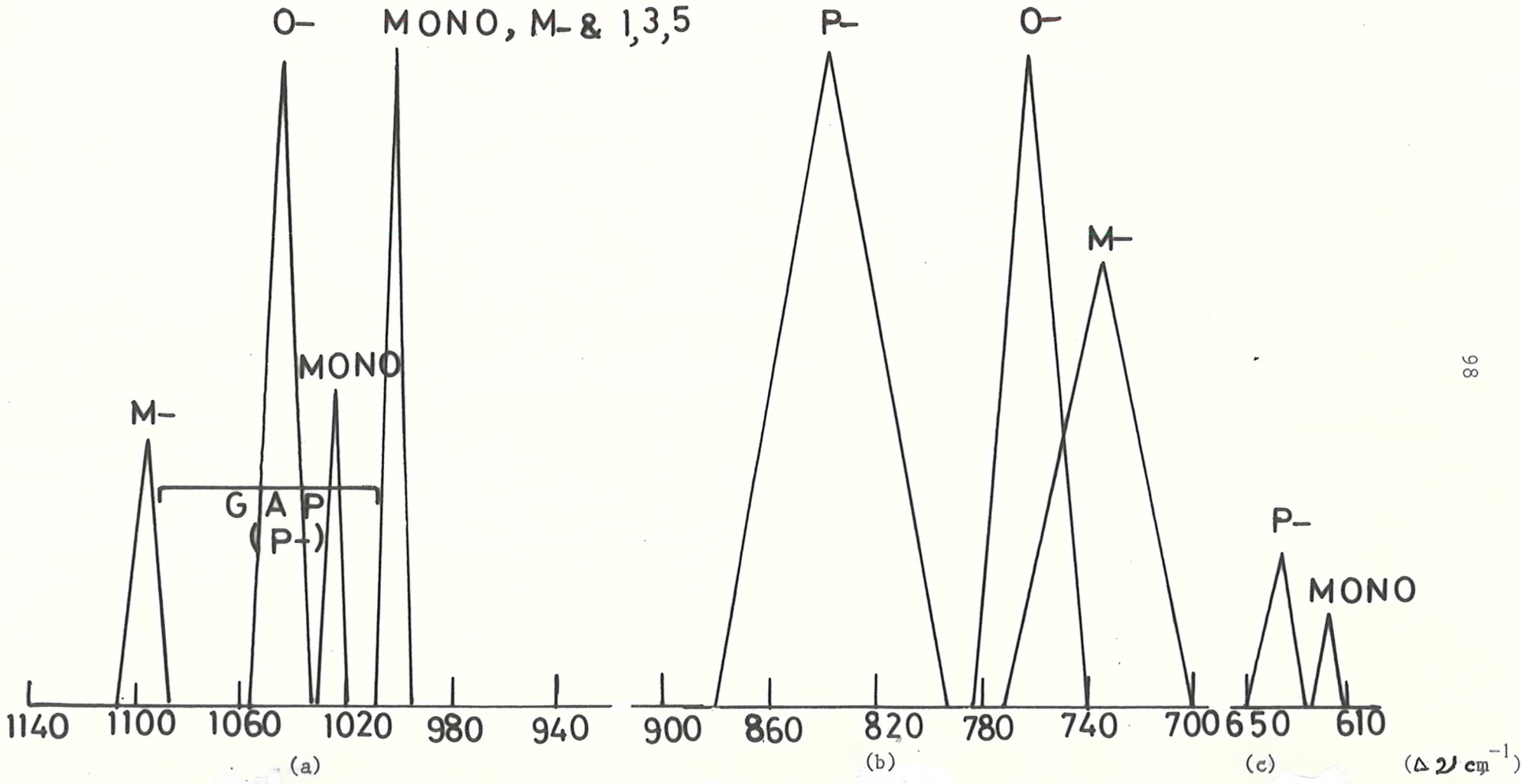

FIG. 3.8 PROGRESSIVE CHANGES IN THE RAMAN SPECTRUM OF A DISUBSTITUTED BENZENE BETWEEN (a) $\Delta\nu$ 7720-990 cm^{-1}; (b) $\Delta\nu$ 900-700 cm^{-1} and (c) $\Delta\nu$ 610-660 cm^{-1} as a function of the type of disubstitution

other features i.e. bands between (i)$\Delta\nu$ 625-640 cm^{-1} (ii)$\Delta\nu$ 1070-1300 cm^{-1} (see Table 3.5). Despite the weakness of the bands between $\Delta\nu$ 625-640 cm^{-1} they seem to have great utility in the diagnostic analysis because of their recurrence within a narrow range.

The depolarized weak band near$\Delta\nu$ 1600 cm^{-1} is usually accompanied by 1-2 weaker bands in its vicinity in the spectra of all disubstituted benzenes (see Tables 3.3, 3.4, 3.5). This band undergoes slight variations in frequency depending upon the type of substitution as below:

$$O - < M - < P -$$

The intensity of this band increases considerably when the substituent is conjugated with the ring. Hydroxy, ester, amino and alkyl groups cause upward frequency shifts of this band as follows:

Hydroxy > Amino> Ester > Alkyl

On the contrary, the groups such as halogens, NO_2, COOH, CO-H and CH_3O cause downward frequency shifts in the following order:

$$\text{Halogens} < NO_2 < CH_3O < CO\text{——}H < COOH$$

Most of these conclusions are consistent with the results of prior studies on ethylenic compounds[104,105,106].

The C-H stretching vibrations give rise to a pattern of one to four partially resolved bands between$\Delta\nu$ 3060-3110 cm^{-1}, the strongest being between$\Delta\nu$ 3070-3095 cm^{-1}. (See Tables 3.3, 3.4, 3.5). These bands are only slightly polarized probably because of the coincidence of the A and B class fundamentals. Unless the presence of the ring is confirmed by other features, the precise assignment of these bands may not be diagnostic because of the coincident bands due to νC-H and

$\nu \equiv$ C-H in the case of aliphatic molecular groups. Slight variation in the frequency of these bands follow this order according to the type of substitution:

P - > O - > M -

Alkyl and halogen substituents cause downward frequency shifts. Fermi interaction with the summation tones and overtones of $\nu C = C$, sometimes seem to cause an immense increase in the intensity of these bands.

In the infra red absorption the bands between (i) ν 700-900 cm^{-1} (ii) ν 1500-1610 cm^{-1} (iii) ν 3040-3100 cm^{-1} and (iv) the characteristic pattern of bands between ν 1650-2000 cm^{-1} (Tables 3.3, 3.4,3.4, and Figs 3.5, 3.6, 3.7) represent the counterparts of the characteristic bands in the Raman discussed presently.

The out-of-plane C-H deformation ranges in the IR suffer from the same shortcomings as discussed before. Therefore only the joint use of Raman and the IR characteristics can yield the best results.

3.4 Trisubstituted benzenes

3.4.1 Results

The characteristic Raman frequencies for various types of trisubstitution are given in Table 3.8 together with some IR results. The latter refer to Bellamy[20]. Typical Raman and IR spectra are shown in Figs 3.9, 3.10 and 3.11.

3.4.2 Discussion

It is clear from Table 3.8 and Figs 3.9, 3.10 and 3.11 that the identification of 1,3,5 trisubstitution is relatively more easy than other types of trisubstitution because of the recurrence of a very strong feature near 1000 cm^{-1}. The latter also forms the basis for the identification of mono and meta substitution. The distinction of 1,3,5 substitution from mono and meta substitution may, however, be

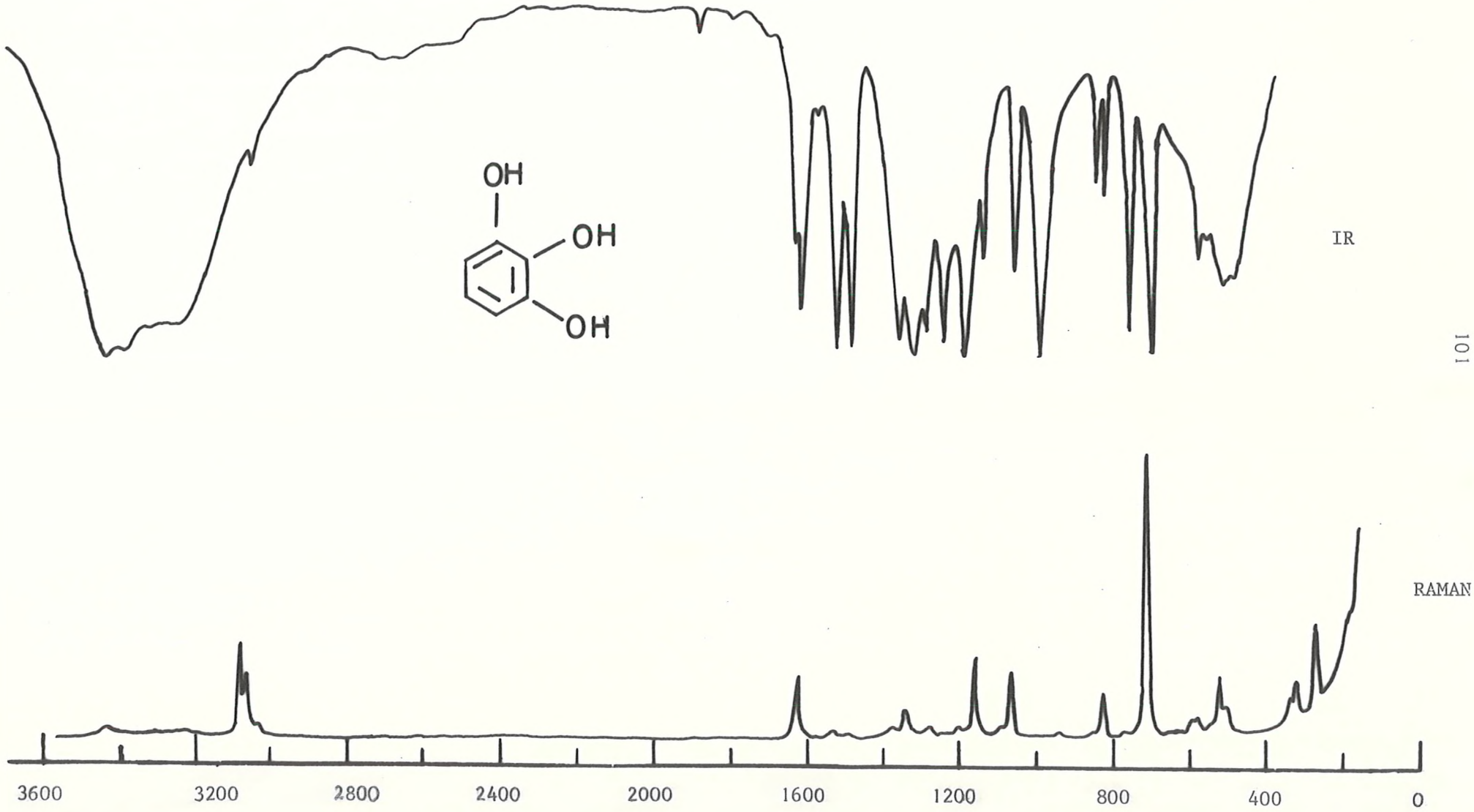

FIG. 3.9 RAMAN AND IR SPECTRA OF A 1,2,3 TRISUBSTITUTED BENZENE

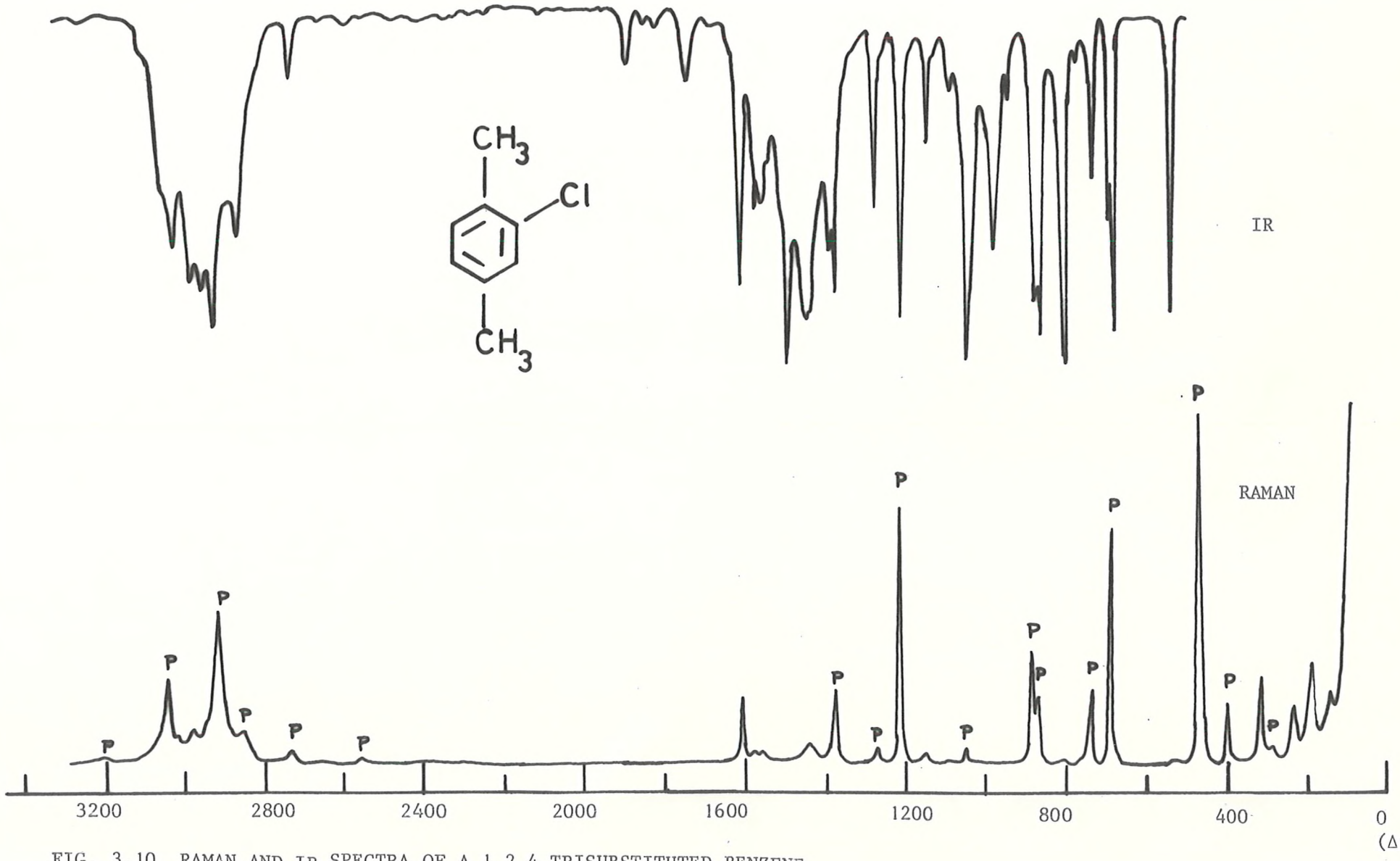

FIG. 3.10 RAMAN AND IR SPECTRA OF A 1,2,4 TRISUBSTITUTED BENZENE

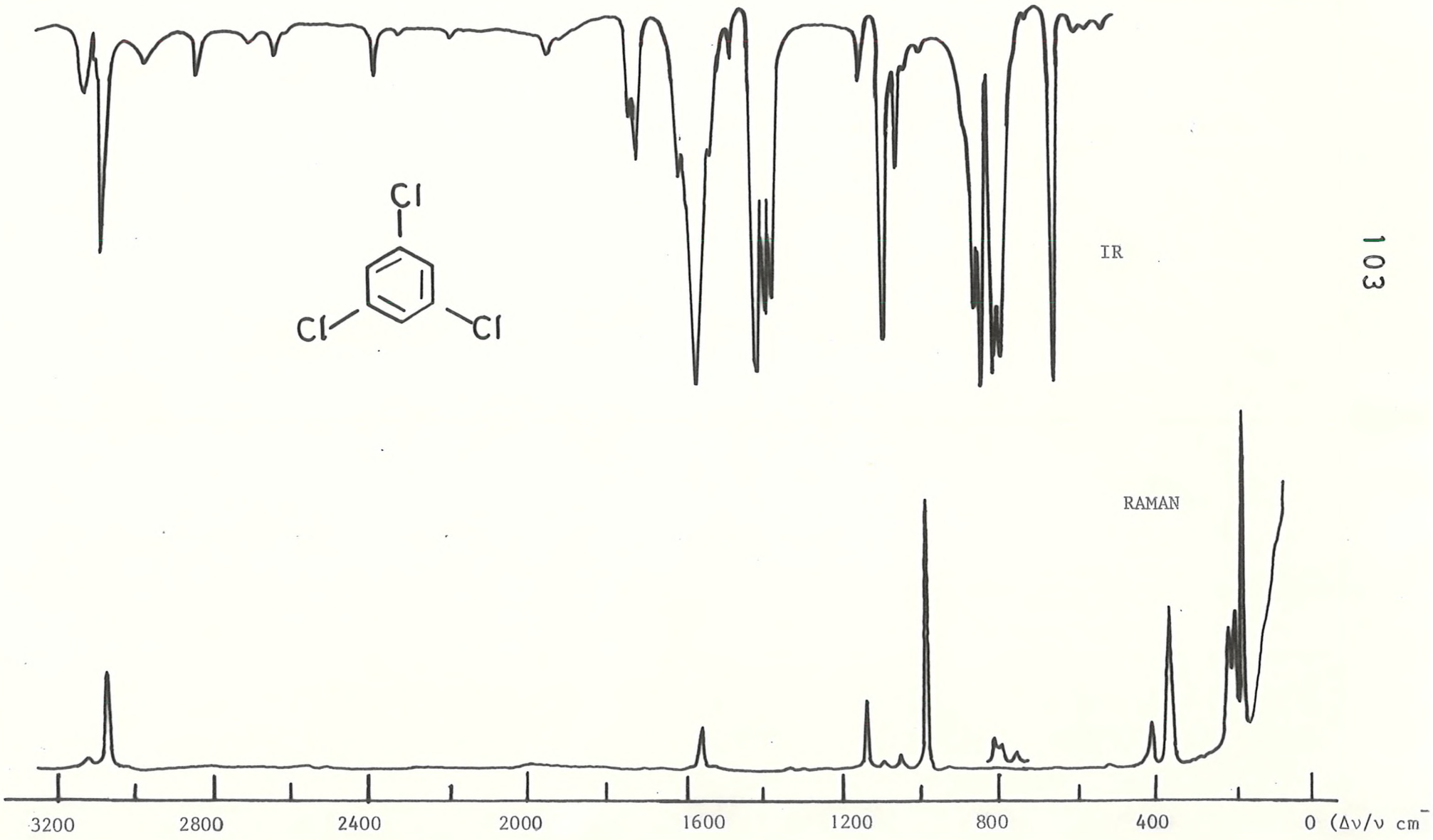

FIG. 3.11 RAMAN AND IR SPECTRA OF A 1,3,5 TRISUBSTITUTED BENZENE

made by noting the absence of characteristic features which appear only in the spectra of mono and meta substituted compounds (Table 3.2 and 3.4).

The distinction between 1,2,3 and 1,2,4 trisubstitution may be made by the characteristic bands between $_{\Delta}\nu$ 650-850 cm^{-1}. The number, intensity and frequency of these bands seem to be highly characteristic of 1,2,3 and 1,2,4 trisubstitution. This may be seen more clearly from the details of the prominent features in some of the analysed compounds belonging to the two classes of trisubstituted benzenes as below.

Substitution	Molecule	Characteristic Frequencies $\Delta\nu cm^{-1}$
1,2,3	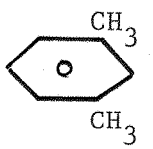	708(S), 824(MS), 1081(M), 420(W)
	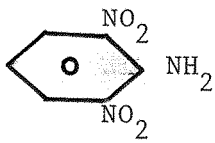	600(S), 817(S), 1110(M), 410(W)
	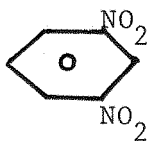	600(S), 820(M), 1110(M), 400(W)
	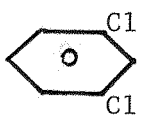	600(S) 830(W) 1060(M) 450(M)
	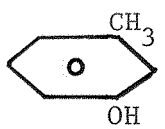	630(S),730(S),845(W),1080(M) 430(W)
	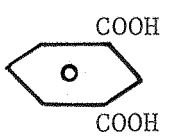	790(S) - 1070(M)
	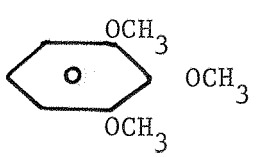	700(S) 802(W), 1095(MS), 370(W)

Substitution	Molecule	$\Delta\nu$ cm^{-1}
	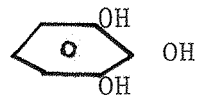	710(S) 824(W) 1062(M), 450(W)
	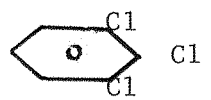	500(S), 800(W) 1080(M), 400(W)
	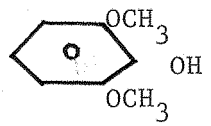	710(S), 820(MS) 1080(M), 370(W)
1,2,4	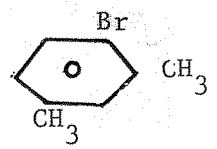	730(VS), 1026(W), 308(MW)
	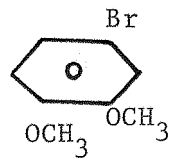	741(VW), 1085(M), 282-302(M)
	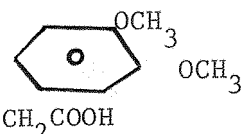	763(VS) 1036(VW), 274(MW)
	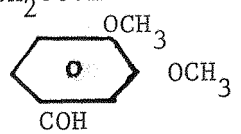	774(M) 1020(VW), 290(VW)
	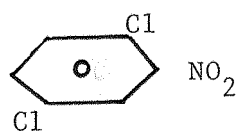	771(MS) 1050(W), 298(MW)
	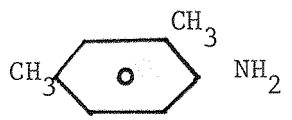	721(VS),776(MS), 988(VW), 288(W)
	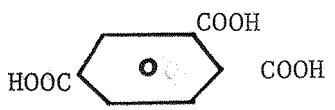	774(S),782(S), 1075(MW), 240(S)
	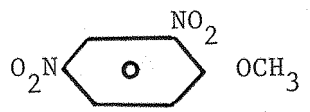	792(W),834(S), 1073(VW), 342(VW)
	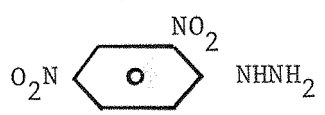	834(S), 1104(VW) 304(VW)

Although IR characteristic frequencies exist for different types of trisubstituted benzenes (Table 3.8) they are far less reliable than those belonging to mono and disubstituted benzenes[20].

The characteristic Raman frequencies in contrast to the IR ones, are though relatively less reliable than those of mono and disubstituted benzenes, can play an important role for the characterization of trisubstituted benzenes.

3.5 Tetra, penta and hexa substituted benzenes

3.5.1 Results

The characteristic frequencies for various types of tetra substitution and penta and hexa substitution are listed in Table 3.8. The IR results are also given from references 98 and 99. Typical Raman and IR spectra are presented in Figs. 3.12, 3.13, 3.14, 3.15 and 3.16.

3.5.2 Discussion

Tetrasubstitution

The characteristic frequencies for tetrasubstitution seem to be far less conclusive than even those for trisubstitutions. Their utility may, however, be enhanced if the following qualifications pertaining to them are considered:

Whilst 1-2-4-5 tetra substituted benzenes give rise to a strong to very strong band between $\Delta\nu$ 740-800 cm^{-1}, 1-2-4-6 tetra substituted benzenes rarely give rise to any strong band between $\Delta\nu$ 700-790 cm^{-1}. [a very strong band occurs in this case between $\Delta\nu$ 830-845 cm^{-1} if at least one of the substituents is a halogen or a NO_2 group].

On the other hand, the frequency range 700-800 cm^{-1} is not characteristic for 1-2-3-4 tetrasubstitution since strong or weak bands may occur randomly in this range.

Penta and hexa substitution

Although only a few new compounds of these classes could be analysed because of the scarcity of these compounds, it may be concluded that the band patterns occurring in the spectra of various compounds do not show any common features. However, the vanishing of the bands associated with C-H stretching between $\Delta\nu$ 3030-3100 cm^{-1} in the case of hexasubstituted benzenes, and their weakness in the case of pentasubstituted benzenes may serve as a useful clue for the identification of hexa and penta substitution.

Unfortunately, the IR characteristic band patterns are also unrealiable in the case of tetra, penta and hexa substitution because of their complication with increasing substitution. Therefore, it may be suggested that the joint use of Raman and IR results especially in these cases may yield more useful information than the use of any single set of results.

3.6 Aromatic carbonyl groups

The aromatic carbonyl groups give rise to bands of variable intensity between $\Delta\nu$ 1630-1870 cm^{-1} due to $\nu C = 0$ and between $\Delta\nu$ 1200-1300 cm^{-1} due to $\nu C-O$ in both the Raman and IR. The frequency and intensity of these bands varies in almost the same way as of those due to $\nu C=C$. The electronegative groups on other positions also modify their frequency or intensity due to induction. The bands are almost always polarized.

3.6.1 Aromatic acids

Aromatic acids exist in two forms! associated and unassociated. The associated acids almost always occur as dimers and possess a centre of symmetry[108,109]. The symmetric band occurs near $\Delta\nu$ 1650 cm^{-1} in the

Table 3.8

Characteristic frequencies of tri, tetra, penta and hexa substituted benzenes.

Type of substitution	Vibrational mode	Raman correlations[a] ($\Delta \nu cm^{-1}$)	IR correlations[b] (νcm^{-1})
Trisubstituted benzene			
1,2,3		370-450 (W-M)	
		600-710 (S),p	780-760
	γ(CH)	800-840 (W-M)dp	745-705
	β(CH)	1060-1100 (M)	
		1260-1300 (V)	
1,2,4		270-310 (V)	
	γ(C-H)	765-775 (MS-S),P	825-805 885-870
	β(CH)	1020-1050 (W)	
1,3,5	Ring breathing	1000 ± 5	
		Weaker bands characteristic of mono and meta disubstitution absent	
			850-830
			700-680
Tetrasubstituted benzenes			
1,2,3,4		(i) 350-390 (W-S)	
	γ(C-H)	(ii) 740-800 (S),P	870-855
1,2,4,6		No strong band between $\Delta\nu$ 700-900 cm^{-1} except when the substituents are either halogens or NO_2 groups	850-840
1,2,3-4		No characteristic band patterns	810-800 (By inference only[107])
Penta		No characteristic band patterns. The C-H stretching bands between 3050-3100 cm^{-1} are weak	870
Haxa		No characteristic band patterns. The C-H stretching bands between 3050-3100 cm^{-1} are absent.	None

a: Bands between 1540-1610 cm^{-1} and 3040-3100 cm^{-1} are not given:
b: Most characteristic bands

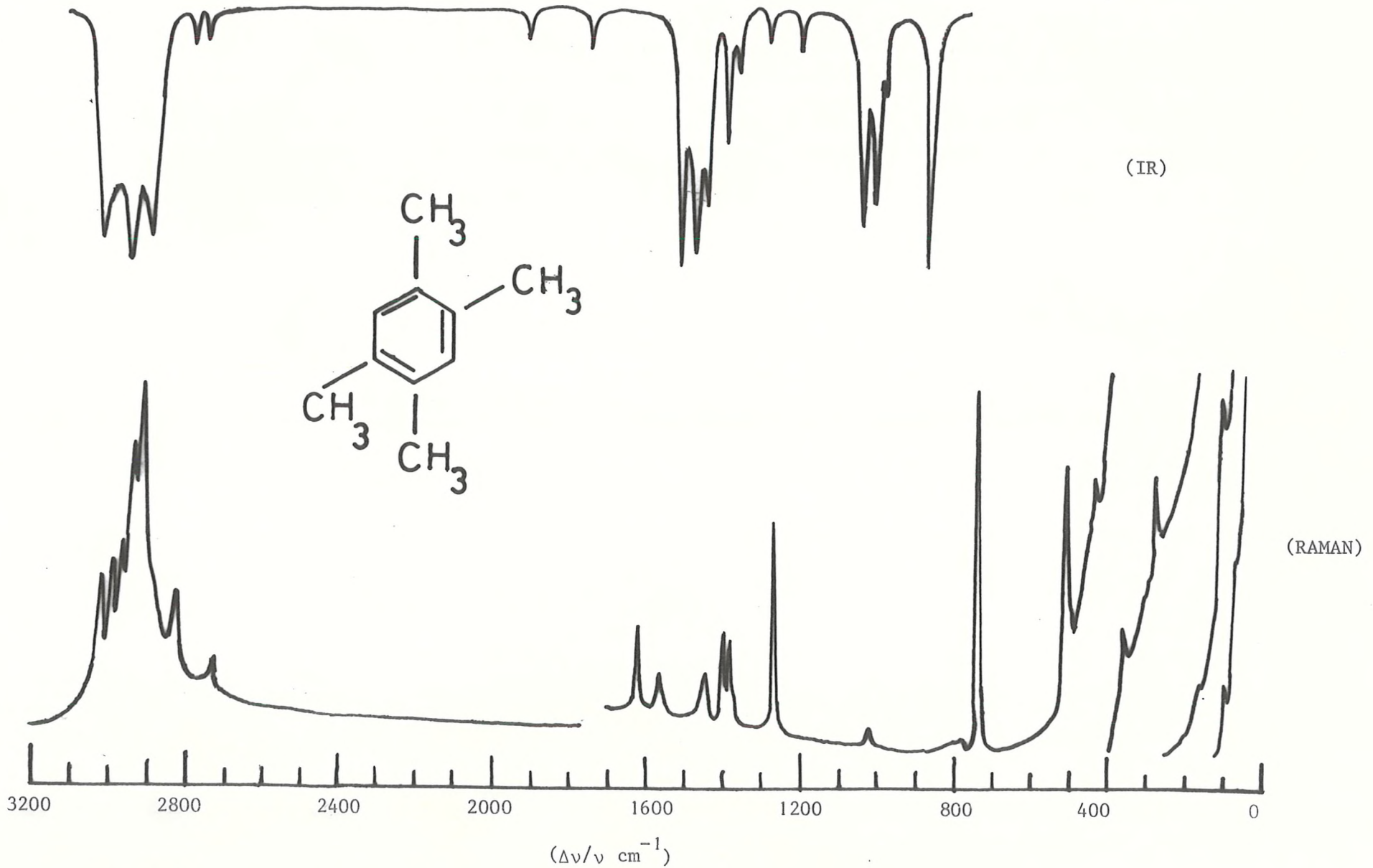

FIG. 3.12 RAMAN AND IR SPECTRA OF A TETRA SUBSTITUTED (1,2,4,5) BENZENE

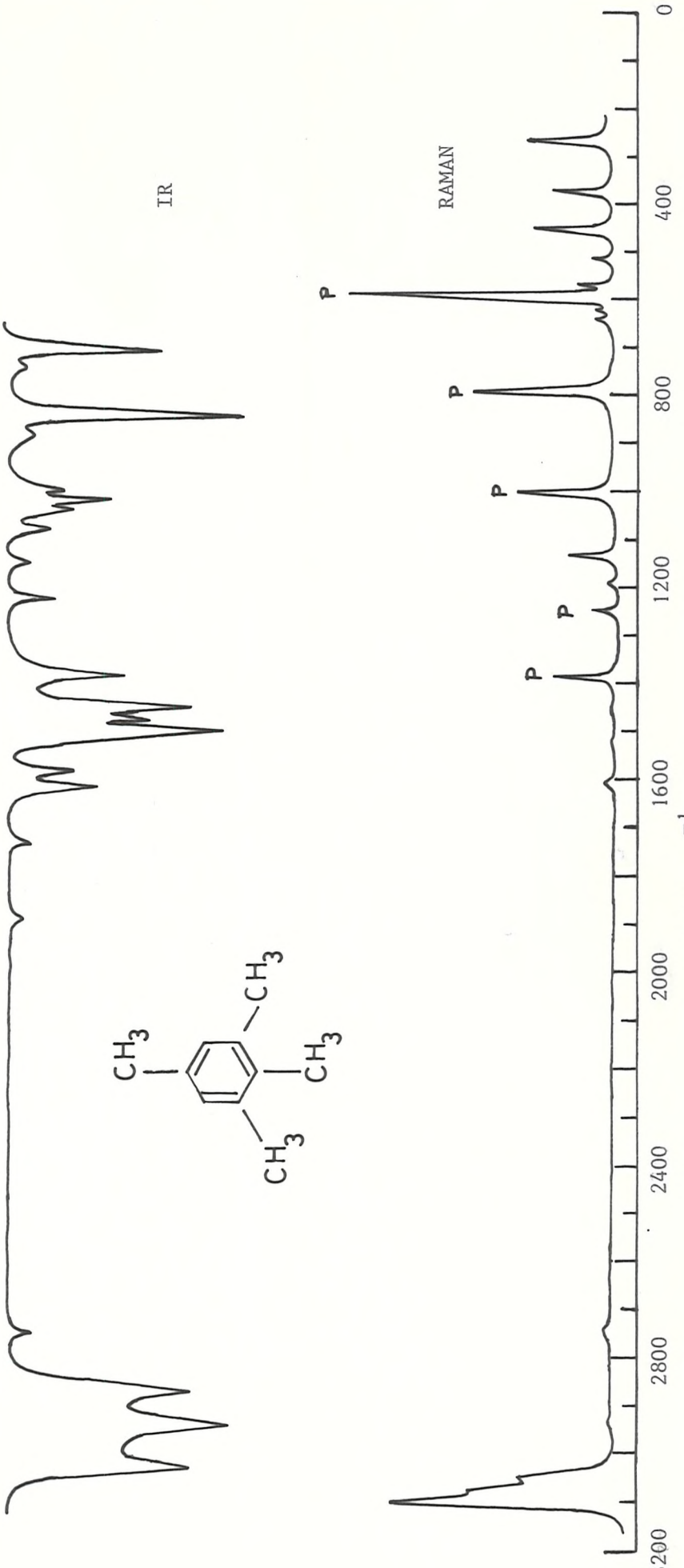

FIG. 3.13 RAMAN AND IR SPECTRA OF TETRA SUBSTITUTED (1,2,4,6) BENZENE

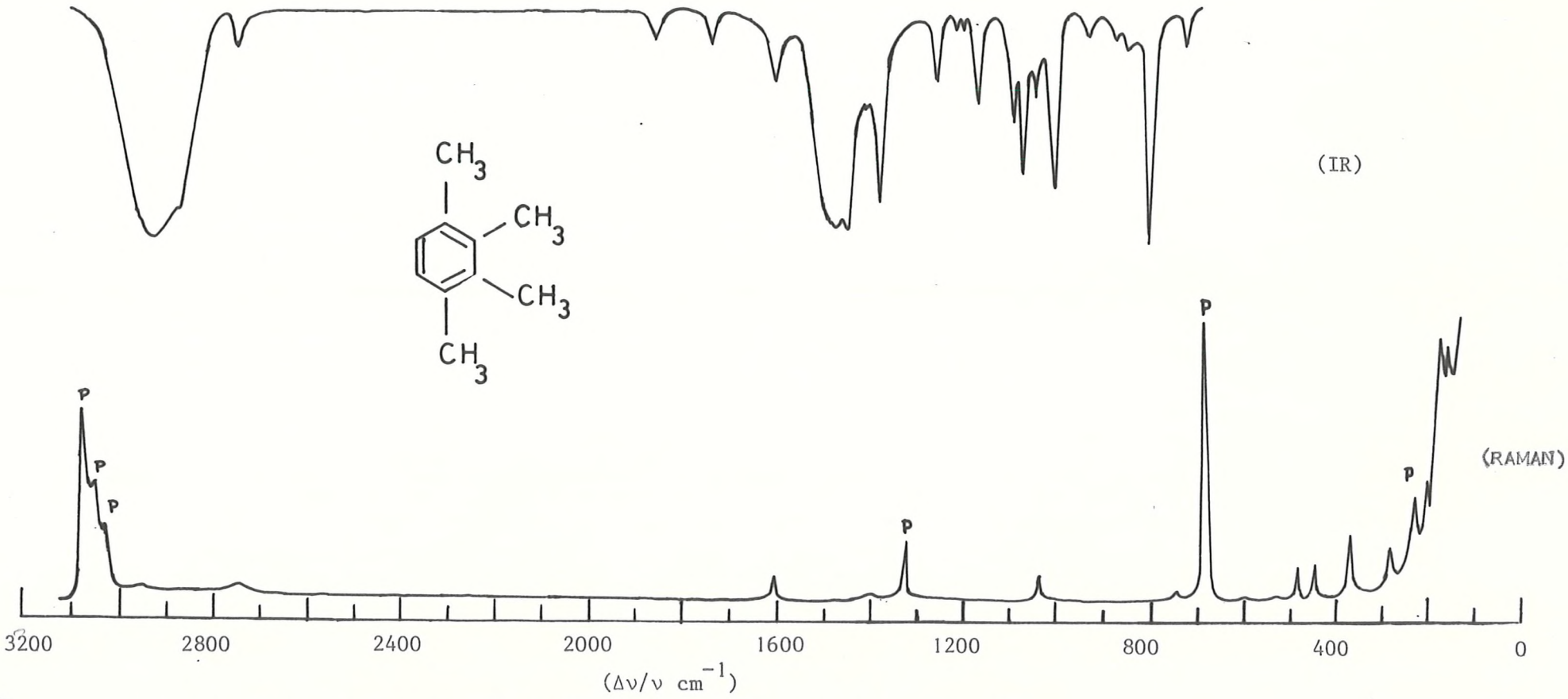

FIG. 3.14 RAMAN AND IR SPECTRA OF A TETRA SUBSTITUTED (1,2,3,4) BENZENE

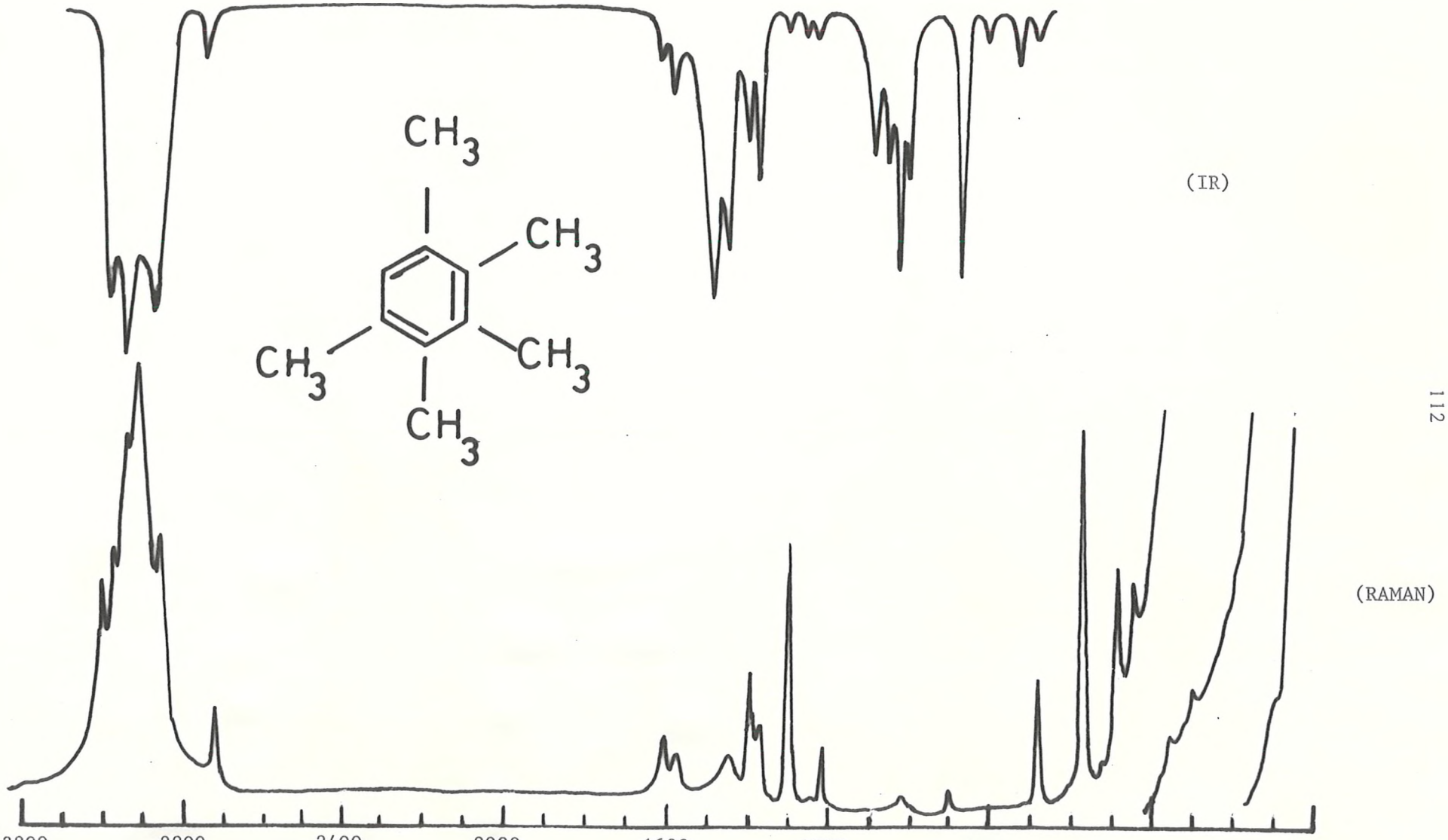

FIG. 3.15 RAMAN AND IR SPECTRA OF A PENTASUBSTITUTED BENZENE

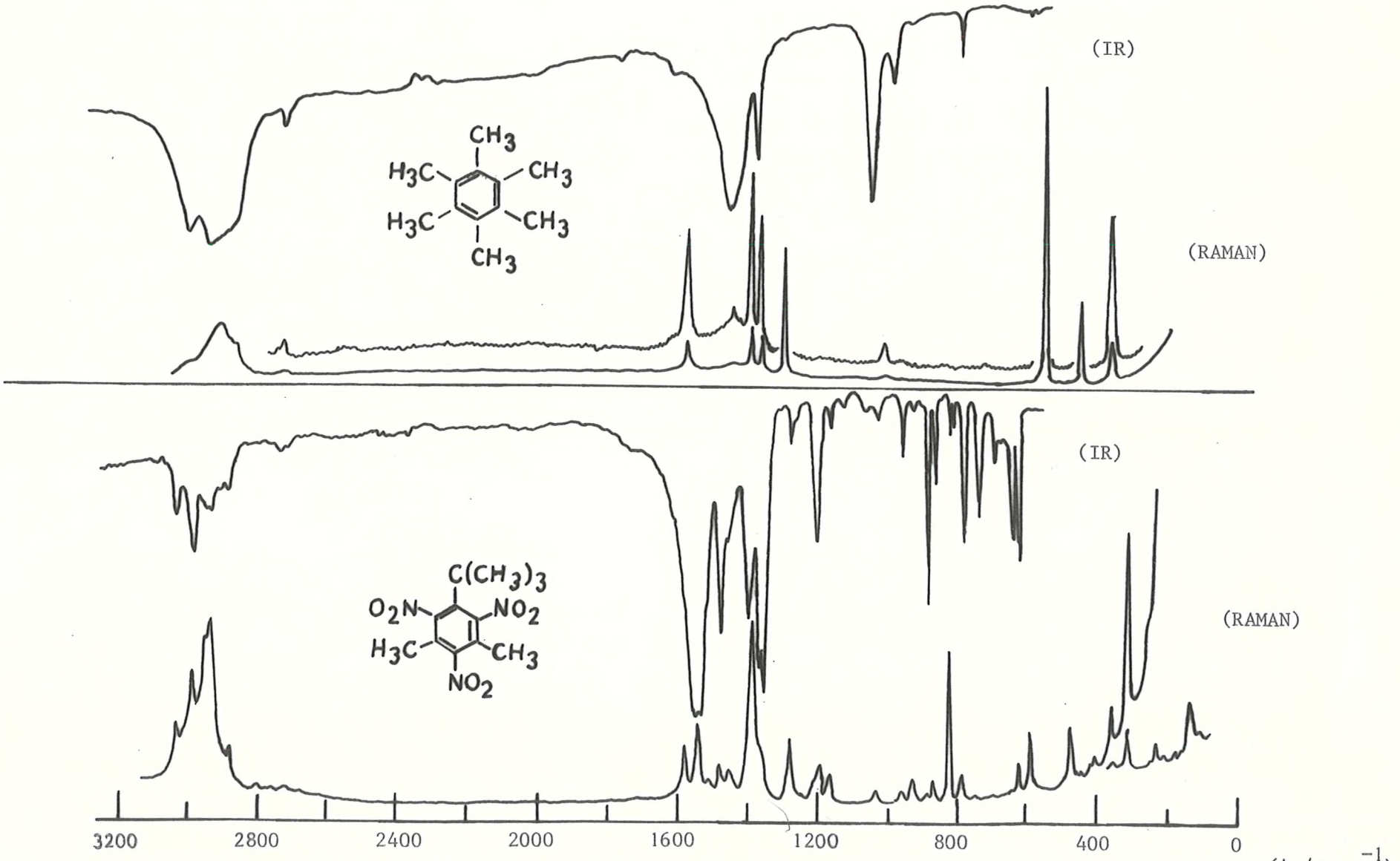

FIG. 3.16 RAMAN AND IR SPECTRA OF HEXASUBSTITUTED BENZENES

Raman which on dilution shifts to $\Delta\nu$ 1730 cm^{-1} and is assigned to the unassociated molecule. The asymmetric band occurs near $\Delta\nu$ 1720 cm^{-1} in the IR and does not vary much for the unassociated molecule. Halogen groups on other positions of the ring elevate $\nu C=O$ whilst nitro and hydroxy groups cause downward shifts. The complementary nature of the Raman and the IR correlations is evident from the various frequencies of the carbonyl bands. The symmetric and the asymmetric frequencies which indicate the association or nonassociation of an acid, can be known only by the simultaneous use of two techniques. Further, sometimes it is very difficult to identify an acid or carbonyl group because of the just coincidence of the carbonyl band with the $\nu C=C$ band in the Raman [e.g. Hippuric acid: ν1602 cm^{-1}].

Apart from the carbonyl stretching vibrations several other characteristic vibrations occur which are strong pointers towards the presence of an acidic group. (Table 3.9)

3.6.2 Aromatic aldehydes

The aldehydes have been investigated in detail by Kohlrausch and Kopple[110]. They have noted the changes in the carbonyl shift occurring due to substitution with other groups on various positions of the molecule. Thompson et al.[111,112] have investigated the IR characteristics of the aldehydes.

The present findings in general agree with the previous results. The aldehydes generally give rise to two carbonyl bands: one near $\Delta\nu$ 1650 cm^{-1} and the other between $\Delta\nu$ 1670-1700 cm^{-1}. The duplicity of the carbonyl bands can be attributed to the interaction of the C-H deformation summation tone with $\nu C=O$. The weak maxima between $\Delta\nu$ 2720-2840 cm^{-1} due to $\nu C-H$ of the aldehyde group further confirms the presence of this group. (Table 3.9)

Table 3.9

AROMATIC ACIDS			AROMATIC ALDEHYDES		
	Raman	IR		Raman	IR
Bond Type	$\Delta\nu cm^{-1}$	νcm^{-1}	Bond Type	$\Delta\nu cm^{-1}$	νcm^{-1}
(Associated) $\nu C=O$	1645 ± 15, V,P	1710 S	$\nu C=O$	1650 ± 5,V	1700
Monobasic	1 Band			1685 ±15,V	
Dibasic	2 or more bands		$\nu C-O$	1200-1300,M,P	1200-1300 M
(Unassociated $\nu C=O$	1730 ± 20 V,P	1720,S	$\nu C-H$	2720-2840 W,B	-
Sym. $\nu C-O$	1260 - 20,M,P	1300,S			
Asym.ν C-O	1297 ± 5,M,P				
$\beta O-H$	1445 ± 15,W,B	1450,B*			
$\gamma O-H$		900S,B			
Hindered rotation of C-O	180 ± S,dp				
ν(OH)	3000-2800 S,B				

B = Broad.

3.6.3 Aromatic esters

The Raman spectra of esters have been reported by Cheng[113] and the IR ones by several others[114,115]. The aliphatic esters show higher carbonyl shifts than the aromatic ones. The carbonyl frequencies in the esters are uniquely placed as compared to the acid, aldehyde and the Ketonic carbonyl groups. (Table 3.10). R and X greatly modify the overall frequency (see below). In general, the frequency decreases with X as follows:

—Ester > COOH > NO_2 > Halogens > NH_2 > OH

The O-substituted esters show slightly higher carbonyl frequencies than the corresponding M and P-substituted ones. The inductive effect of R seems to inhibit the conjugation effect on the intensity of these bands.

3.6.4 Aromatic anhydrides

The anhydrides have been only slightly investigated in the Raman so far[116]. The IR carbonyl frequencies of these compounds have been reported by Kartritzky and Jones[117,118].

The occurrence of the carbonyl bands [more than one] at uniquely elevated positions, $\Delta\nu$ 1720-1880 cm^{-1} strongly indicate the presence of an anhydric group (Table 3.10).

Table 3.10

Raman and IR group frequencies of aromatic esters and anhydrides

Mode	Raman (νcm^{-1})	IR (νcm^{-1})
	(Esters)	
νC=O	1720 ±30 S,P	1710 ± 25, S
νC-O	1200 -1300 M,p	1200- 1300, S
νC-O	1000-1100 W,P	1000-1100 (S) (1 or more bands may occur)
	(Anhydrides)	
νC=O	1770 -1870,S-M (1-2 bands) 1710 -1770 S-M,P (1-2 bands)	Almost same as Raman frequencies
νC-O	1200 -1300 MW,P (1 band)	
νC-O	1000 -1130, MW,P	

3.7 Aromatic methyl and fluoride groups

It has been observed in a large number of cases that when Methyl or Fluoride groups occur at 1,3 positions on the benzene ring such that the substituents on the adjacent neighbouring positions are different, they give rise to a very strong polarized band between $\Delta\nu$ 560- and 580 cm^{-1} (Table 3.11). The frequency and often the intensity of this band, however, decreases abnormally when the substituents on the adjacent neighbouring positions are similar. (Table 3.11) This band will, therefore, be characteristic in the (a) case and not in the (b) as shown below:

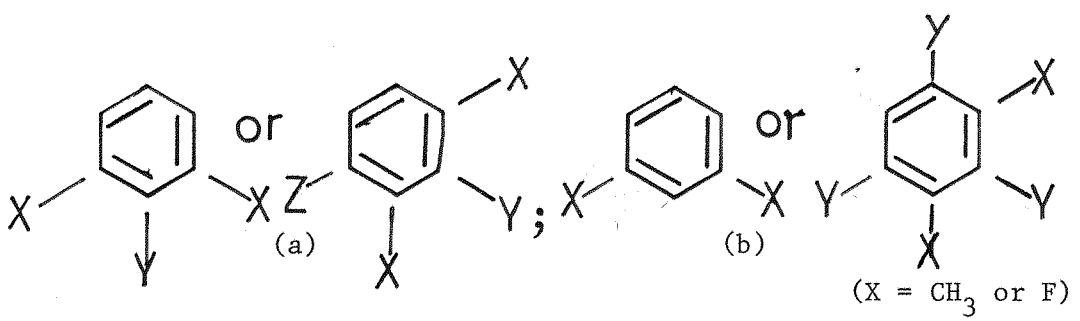

The frequency range in the (a) case is so tight and the intensity and polarization is so unmistakable that this band may be regarded as one of the most important group frequency correlations in the Raman effect.

Although Methyl and Fluoride groups give rise to similar features in other spectral parts also, distinction between them may be made by a careful study of some minor differences. Both groups give rise to the following characteristic bands, apart from the one between $\Delta\nu$ 560- and 580 cm^{-1}.

(i) $\Delta\nu$ 1370-1385 cm^{-1} (symmetric deformation)

(ii) $\Delta\nu$ 2550-2740 cm^{-1} (overtone of symmetric C-H deformation)

In addition they cause an upward shift in the frequency of the band near 1600 cm^{-1} (νC=C).

Whilst the frequencies of the bands associated with the Fluoride groups are generally higher than those of the Methyl, the difference in the frequencies of 1370-1385 cm^{-1} band is too small to be of any analytical value. The difference in the frequencies of the other two bands i.e. 1610-1640 cm^{-1} and 2550-2740 cm^{-1} however, is large enough to make distinction between the two groups as indicated below:

CH_3	$\Delta\nu$ 1605-1610 cm^{-1}	
	$\Delta\nu$ 2725-2740 cm^{-1}	(VW)
F	$\Delta\nu$ 1630-1640 cm^{-1}	
	$\Delta\nu$ 2550-2650 cm^{-1}	(VW)

Table 3.11

Characteristic Raman frequencies of the Methyl (X) and Fluoride (F) groups attached to the benzene ring at 1,3 positions.

Molecule	(cm^{-1})
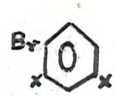	564, MW, P
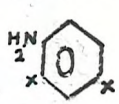	568, S, P
	578, VS, P
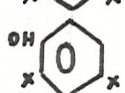	582, VW, P
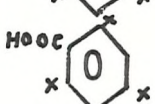	569, VW, P
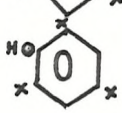	581, Vw, P
	560, S, P
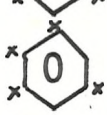	570, S, P
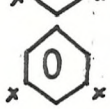	540, M, P

Table 3.11 (Contd)

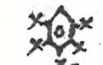	504, MS, P
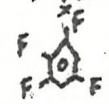	573, VS, P
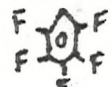	572, VS, P
	552, VS, P
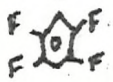	490, M, P

3.8 Conclusion

It is obvious that the substituted benzenes give rise to characteristic Raman bands in the frequency ranges of 600 to 900 cm^{-1} and 100-1040 cm^{-1}. Further, every substituted benzene gives rise to characteristic bands in the frequency ranges of 1540 to 1610 cm^{-1} and 3040 to 3100 cm^{-1}, except hexasubstituted ones which give rise to $\Delta\nu$ 1540 to 1610 cm^{-1} bands only. The use of the latter bands together with the former is essential since while the former bands may arise in the spectra of organic compounds other than substituted benzenes also, the latter are observed in the spectra of substituted benzenes only. Whilst the characteristic bands of mono di and tri substituted benzenes are very reliable, those of tetra, penta and hexa substituted benzenes may only be used as hints.

Highly polar groups e.g. NO_2 and halogens have the effect to disturb or widen the frequency ranges for the characteristic bands whilst other polar groups e.g. carbonyl groups, NH_2, OH etc. seem to cause no such disturbances. In a particular set of correlations the frequency seems to decrease in the following order

NO_2 < carbonyl groups < OH < OCH_3 < alkyl < halogens

Generally, Raman frequencies seem to be more characteristic than IR ones. However, the joint use of both Raman and IR techniques is expected to yield more reliable results than from a single technique.

The molecular groups attached to the benzene ring also give rise to highly characteristic frequencies. Apart from the carbonyl groups, Methyl and Fluoride groups at 1,3 positions have been observed to produce one of the most important characteristic frequencies in the Raman effect.

These findings constitute a large fraction of the results obtained under this project. Their versatility and usefulness may be realized from the list of compounds given in appendix II from which they were derived.

CHAPTER IV

STRUCTURAL STUDIES OF POLYETHERS AND POLYTHIOETHERS WITH m = 1 - 3

4.1 Introduction

Polyethers and polythioethers are members of the polymer series with general formula $\left[(CH_2)_m-Y\right]_n$ where Y = O or S respectively. This series gives polyethylene as the limiting case when m becomes infinity. It has been shown that these polymers undergo remarkable variations in physical properties as m increases[89] (Fig. 4.1 and Table 4.1). These variations in physical properties do not occur simply because of different chemical structures of these polymers viz one by one increase of methylene units between O or S atoms, since these are not steady and regular. In fact, X-ray analysis of polyethers (m = 1-12)[51-55] and polythioethers (m = 1-3,5)[119-121,92] has shown that the cause of variation in physical properties is rooted in different molecular and crystal structures of these polymers. This may be conveniently seen from Table 4.1, which also gives a summary of their structures. Since variations in the structural order may cause corresponding variations in the associated physical properties, it is important to determine the former by some convenient means, in order to follow the latter.

Since vibrational spectrum of a polymer fingerprints its molecular and crystal structures, vibrational spectroscopy offers such a means.

The purpose of this study has been to investigate the effect of various conditions on the structures of the above series of polymers, (with m = 1-6,10), using vibrational spectroscopy.

This work

The discussion in this chapter is concerned with lower members of the series i.e. m = 1-3. There are a number of reasons which justify this work as follows:

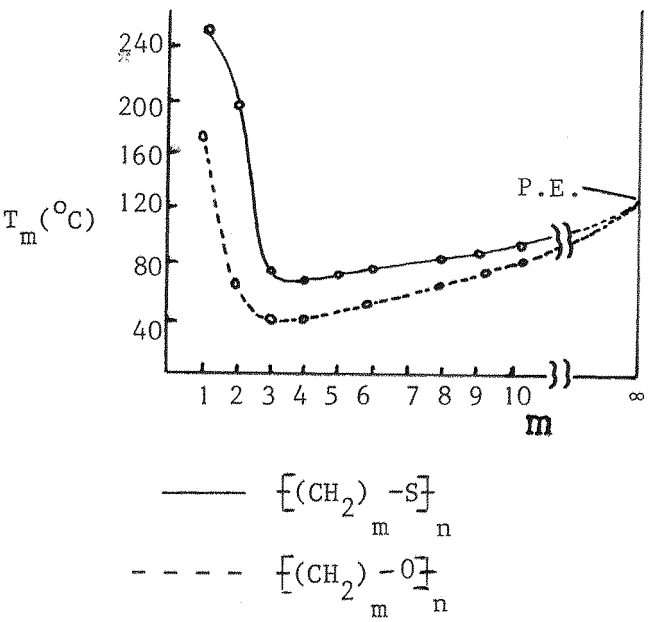

FIG. 4.1 MELTING POINTS OF POLYETHERS AND POLYTHIOETHERS PLOTTED AGAINST THE NUMBER m

Table 4.1

Crystallographic data of polyethers and polythioethers: $\{(CH_2)_m-Y\}_n$; Y = O or S

Polyether / Polythioether	T_m (°C)	Density (g/cm^3) observed	Density (g/cm^3) X-ray	Crystal system, space group, lattice constants and no. of chains per unit cell (N)	Molecular Conformation	Ref.
$\{(CH_2)-O\}_n$	180	1.40-1.45	1.49	Trigonal; $P3_1-C_3^2$ a=4.47 Å; c(f.a.) = 17.39 Å, N = 1	Helix; $G'_{18}(78^\circ)$ -D(9/5)	53
				Orthorhombic; $P222_{111} — D_2^4$; a = 4.77 Å; b=7.65 Å; c(f.a.) =3.56 Å;N=2	Helix; G_4— D($^2/_1$)	53
$\{(CH_2)_2-O\}_n$	66	1.20-1.22	1.234	Monoclinic; a=8.16 Å; b=12.99 Å; c(f.a.)= 19.30 Å; β=126°5'; N=4	Helix; (T_2G'); (172°-65°) -D($^7/_2$)	54
$\{(CH_2)_3-O\}_n$	37	∿ 1.11	-	Modification I; f.a. = 4.80 Å	Planar zig zag; T_4 - $C_2(^1/_0)$	55
			1.20	Modification II; Trigonal; $R3_c-C_{3v}$ a=14.13 Å; c(f.a.)= 8.41 Å; N=9	$T_3GT_3\bar{G}$ $C_s(^2/_0)$	
			1.20	Modification III: Orthorhombic; $C222_1-D_2^5$; a=9.23 Å; b=4.82Å; c(f.a.)= 7.21 Å; N=2	Helix; $(T_2G_2)_2-D_2(^2/_1)$	
$\{(CH_2)_4-O\}_n$	43	1.06	1.11	Monoclinic; $C2/c-C_{2h}^6$; a=5.59 Å; b= 8.90 Å; c(f.a.)= 12.07 Å; β=134.2;N=2	Planar zig zag; $T_{10}-D_{2h}(^2/_1)$	57

Table 4.1 (Contd)

$+[(CH_2)_6-O]+_n$	55-58	1.04	1.06	Monoclinic C2/c-C^6_{2h}; a;5.65 Å; b=9.01 Å; c(f.a.)=17.28 Å; β= 134.5°; N=2	Planar zig zag; T_{14}-$D_{2h}(^2/_1)$	52
$+[(CH_2)_{10}-O]+_n$	75-79	1.02	1.03	Orthorhombic; P_{nam}-D^{16}_{2h}; a=7.40 Å; b= 4.94 Å; c(f.a.)=27.49Å; N=2	Planar zig zag; T_{22}-$D_{2h}(^2/_1)$	52
$+[(CH_2)-S]+_n$	150	1.52	1.60	Triclinic; P_1-C^1_1; a=5.07 Å; c(f.a.)= 36.52 Å; N=1	Helix; G_{34}-$(^{17}/_9)$	119
$+[(CH_2)_2-S]+_n$	202-10	1.33-1.34	1.41	Orthorhombic; Pbcn-D^{14}_{2h}; a=8.50 Å; b= 4.95 Å; c(f.a.)=6.70 Å N=2	$TG_2T\bar{G}_2$-$D_{2h}(^2/_1)$	120
$+[(CH_2)_3-S]+_n$	58-62	1.27	1.32	Monoclinic; PC-C^2_s a=5.16 Å; b(f.a.)= 4.06 Å; c=10.33 Å; β=120.5° N=2	Helix; G_4- $\sim C_2(^2/_1)$	121
$+[(CH_2)_5-S]+_n$	75			Monoclinic-$P2_1/a(C^5_{2h})$ a=9.61 Å, b=19.78Å c(f.a.)=7.84 Å, β=131° N=4	Planar zig zag; T_{12}-$C_{2v}(^1/_1)$	98

(i) Combined Raman and IR studies have been reported on polyethers[124-131] and polythioethers[137,138,140,141] with m = 1-2 only. Further, the previous Raman measurements have lacked resolution and detail. This precluded not only the observation of a number of predicted bands in the high frequency region ($\sim \Delta\nu$ 100-3000 cm^{-1}) , but also provided no information on the modes occurring at lower frequencies.

(ii) No Raman spectrum of polyoxacylobutane, $\left[(CH_2)_3-O\right]_n$, has been reported.

(iii) Neither Raman nor IR spectra of polytrimethylene sulphide have been reported.

(iv) The vibrational analysis has so far been mostly confined to the features arising from an isolated chain. The effects of thermal treatment, cooling or heating or interchain interactions have been scarcely investigated.

Features arising from disordered structures have been occasionally explored.

Thus detailed Raman and where required IR vibrational analysis is needed either to supplement the already existing results or to contribute towards not-yet-investigated structural aspects of these polymers.

4.2 Polyoxymethylene (POM); $\left[(CH_2)\ O\right]_n$

POM has two crystal modifications; hexagonal and orthorhombic (Table 4.1). Both modifications are helical but the helix of the hexagonal form is more tightly coiled than that of the orthorhombic one. Further, hexagonal POM has only one molecular chain per unit cell, whereas orthorhombic POM has two chains per unit cell. These structural differences cause significant variations in their vibrational spectra.

4.2.1 Hexagonal polyoxymethylene - POM_{Hex}

The fundamental vibrations of POM_{Hex} may be treated under the factor group isomorphous to the point group D10 /9.[123] This gives $5A_1, 5A_2$, $11E_1$ and $12E_2$ symmetry species, of which A_1 and E_2 are Raman active only, A_2 are IR active only whilst E_1 species are both Raman and IR active.

The Raman and IR spectra of POM_{Hex} have been measured and analysed by a number of authors[125-131]. Zerbi and Hendra[130] published the first laser-Raman spectrum with the assignments based upon normal coordinate analysis. Their assignments were later revised by Sugeta[131]. The previous Raman studies however lacked detail and resolution which precluded the observation of a number of predicted vibrational modes, and features associated with amorphous and extraneous structures.

Results and Discussion

The results of the present study have been presented in Fig. 4.2 which shows Raman spectrum of the solution crystallized (single crystals) POM at 25°C and -180°C , and that of POM-d_2 at 25°C. A number of new bands have been observed in these spectra. These occur between $\Delta\nu$ 10-80- and at 553-, 1020-, 1119- 1325-,~1336- and between 2800-3000cm^{-1} in the spectrum of POM; and between $\Delta\nu$10-130- and at 616-, 987-, 1158- and between 2100-2350 cm^{-1} in the spectrum of POM-d_2. The resolution seems to be more pronounced at -180°C due to a considerable decrease in the band widths which also results in shifting the band heads to higher frequencies by 1-4 cm^{-1}. In view of the present data, the revised assignments for POM are collected in Table 4.2 together with the calculated and observed frequencies from reference 130. A few of the suggestions require justification as follows:

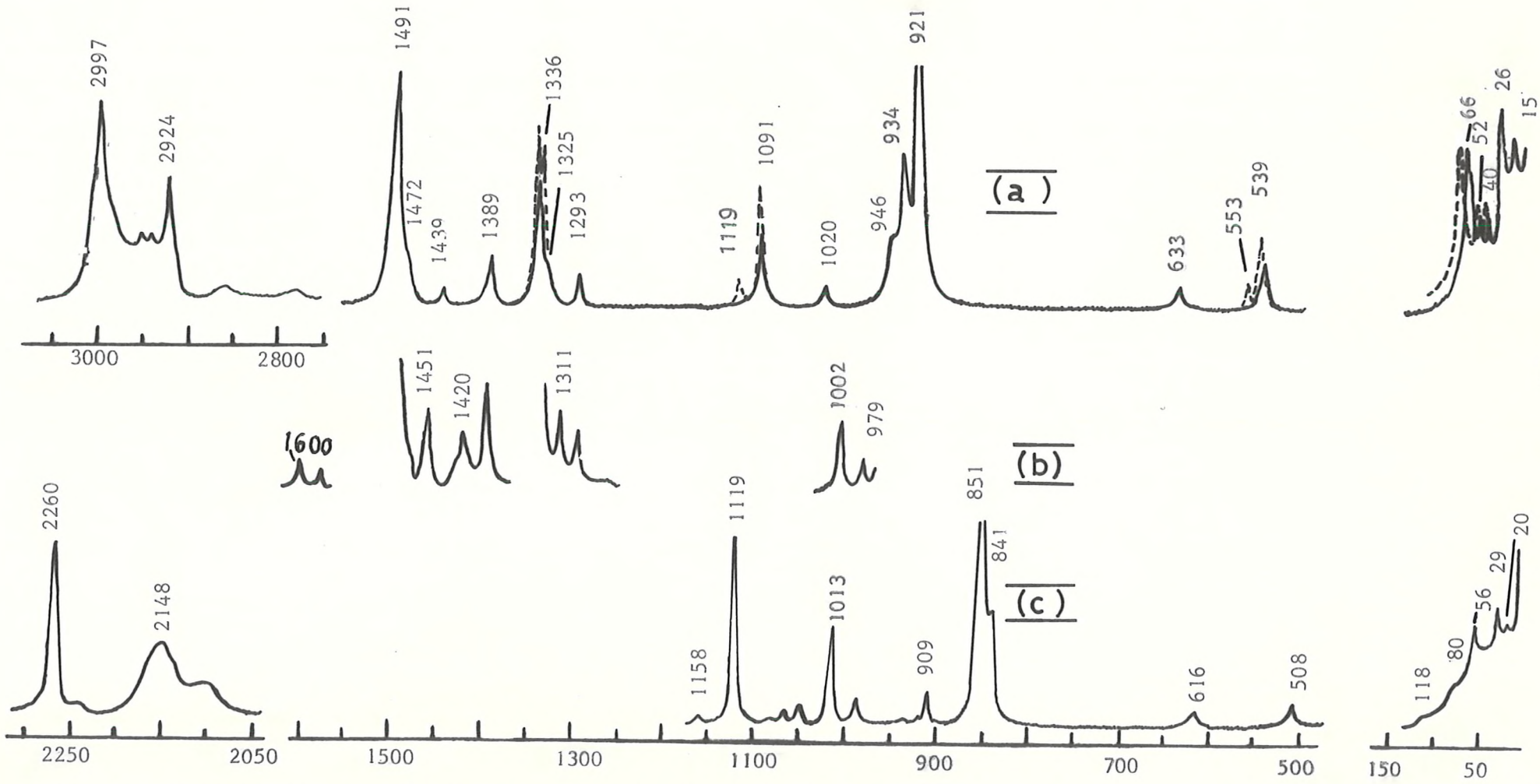

FIG. 4.2 RAMAN SPECTRA OF (a) Solution crystallized POM, (b) Delrin 500 (partial) (c) POM-d_2
(Broken line (- - - -) indicates features measured at -180°C)

Table 4.2

Raman spectrum of POM_{Hex}
(A revised assignment)

Present study ($\Delta\nu$ cm^{-1})	Zerbi and Hendra[130] ($\Delta\nu$ cm^{-1})	Calculated (ν cm^{-1})	Species	Assignment
2924-29	-	2910	A_1	$\nu(CH_2)_S$
1491	1492	1491		$\delta(CH_2)$
1336	1338	1324		$T(CH_2)$
919	923	962		$\nu(COC)_S+\delta(OCO)$
539	539	499		$\delta(COC)_S+\delta(COC)$
2997	-	2979	E_1	$\nu(CH_2)$
2929	-	2919		$\nu(CH_2)_S$
1472	-	1486		$\delta(CH_2)$
1439	1434	1418		$W(CH_2)$
1293	1295	1303		$T(CH_2)$
-	-	1224		$R(CH_2)+\delta(COC)+\nu(COC)_S$
1091	(1095) 1106	1077		$\nu(COC)_\alpha+\delta(OCO)$
934	936	916		$\nu(COC)_S$
633	635	649		$\delta(OCO)$
-	-	466		$\delta(COC)+R(CH_2)$
27	-	26		$\tau(COC)$
2990	-	2972	E_2	$\nu(CH_2)_S$
2952	-	2929		$\nu(CH_2)_S$
1491	1492	1490		$\delta(CH_2)$
1389	-	1419		$W(CH_2)$
1325	-	1321		$T(CH_2)$

Table 4.2 (Contd)

1119	-	1137	$R(CH_2)+\nu(COC)_a$
1020	946	956	$\nu(COC)_a+R(CH_2)+\delta(OCO)_a$
946	-	931	$\nu(COC)$
553	-	552	$\delta(COC)+\delta(OCO)$
-	190*	191	$\delta(OCO)+\delta(COC)$
-	180*	175	$\tau(COC)$
60-66	-	57	$\tau(COC)$

* Spurious bands arising from the exciting line

Nongenuine bands

$\Delta\nu$ 979-, 1002-, 1311-, 1420-, 1452-, 1574- and 1600 cm^{-1}.

The frequencies of the observed Raman bands in the low frequency region of POM [15-(,S),27-(S),40-(W),50-(W),60-66 cm^{-1} (M)] are very different from those of the predicted ones [26-(E_1), 57-(E_2), 175-(E_2), 191 cm^{-1}(E_2)]. The observed bands at $\Delta\nu$27- and 60-66 cm^{-1} may, however, be assigned to the calculated ones at 26-(E_1) and 57 cm^{-1}(E_2) respectively. Nevertheless the assignment of the other observed bands is not possible, not only because their frequencies are widely different from the calculated ones but also they are more numerous than the predicted ones.

A band near $\Delta\nu$ 1020 cm^{-1} seems to arise from a fundamental mode since its intensity does not seem to vary appreciably with specimens of various crystallinity e.g. crystallized from solution, quenched from the melt and annealed close to T_m. This band may not be assigned to any mode but the nearest one of E_2 species calculated at $\Delta\nu$ 956 cm^{-1}.

The band resolved near $\Delta\nu$ 1336 cm^{-1} at -180°C finds no explanation on the basis of the calculated data.

The predicted bands near $\Delta\nu$ 466-(E_1) and 1224 cm^{-1}(E_1) have not been observed in spite of the much greater resolution achieved in this study. These observations clearly point out to the fact that considerable discrepancies exist in the normal coordinate analysis. This conclusion is in full agreement with a previous assessment[94] which indicated that neither Urey Bradley force field nor valence force field seemed to explain the observed vibrational spectrum of POM.

Non genuine bands

In order to study the effect of crystallinity on Raman spectrum, 3 various samples of POM_{Hex} have been examined. From a comparison of the spectra of 'as supplied' (Delrin 500), melt quenched and annealed samples, it has been concluded that although bands generally broaden on melt quenching and sharpen again on annealing close to T_m, no band could

be associated with the so called crystallinity or regularity bands.

A number of bands having considerable intensities, however, have been observed in the spectrum of the 'as supplied' sample which could not be assigned to any predicted vibrational modes. These bands (bottom of Table 4.2 and Fig. 4.2) persisted even in the spectra of melt-quenched and annealed samples. To clarify the situation, these spectra were compared with that of the single crystal material. Since the latter spectrum shows no such bands, they may be regarded as arising from impurities e.g. additives etc. Probably, these were the bands which Zerbi and Hendra[130] thought as arising from irregular structures.

4.2.2 Orthorhombic polyoxymethylene - POM_{orth}

Since POM_{orth} has two chains per unit cell structure; every line group mode is expected to split into a doublet under the factor group of the space group isomorphous to the point group D_2. Correlation splitting for a number of IR bands has been observed[125]. No Raman band, however has shown splitting in a previous study[130].

POM_{orth} was prepared in this study by a novel method (see section 2.6.1) to reexamine the expected correlation splitting in the Raman spectrum. The Raman spectrum of the transformed sample of POM_{orth}, however, failed to show any splitting probably because it was not possible in many cases to distinguish between the spectral features belonging to either POM_{orth} or POM_{Hex} due to the low content of the former.

4.2.3 Conclusion

Several new bands have been observed in the Raman spectrum of POM_{Hex}. Since a number of them may not be reconciled with the predictions, a reassessment of the normal coordinate analysis is required. A number of bands observed in the Raman spectrum of Delrin-500 may be

attributed to the additives etc.

In view of the predicted interchain forces[129], correlation splitting in the Raman spectra of POM_{orth} is worth investigating using a sample having a high content of the latter.

4.3 Polythiomethylene - PTM, $\{CH_2-S\}_n$

The molecular and crystal structure of PTM is given in Table 4.1. The IR spectrum of PTM has been measured by a number of authors[135,136]. Hendra et al[137] have reported laser Raman and IR spectra and tentatively suggested some assignments of the observed bands. Recently Masaru Ohsaku[138] has carried out a normal coordinate analysis of PTM and the related simple molecules of the type $CH_3S(CH_2S)_n CH_3$ (n = 1-3). Since the predicted vibrational modes were assigned on the basis of the IR spectrum measured by these authors and incomplete Raman data from Hendra et al, the measurement of a detailed Raman spectrum is required to complete these assignments. Further, it would be interesting to investigate the variations in Raman spectrum as a result of degradation which seems to occur in this polymer even on ageing. Mass spectroscopic study[139] has shown that thermal degradation involves homolytic cleavage of the C-S-C bonds evolving CS_2 and H_2CS. A similar degradative mechanism for ageing would result in the accumulation of various chain lengths on the surface of an aged specimen. Since the symmetry of the resulting short molecular chains will be lowered, optically inactive vibrational modes (degenerate vibrations) may become active, thus giving rise to extra features in the spectrum.

4.3.1 Results and Discussion

The spectroscopically active vibrations of this molecule fall into 4 symmetry species i.e. A_1, A_2, E_1 and E_2, of which A_1 and E_2 are Raman active only, A_2 are IR active only and E_1 are active both in the Raman as well as IR spectrum. Fig. 4.3 shows Raman spectra at (a) 25°C and (b) -180°C. A few new bands are resolved in the (b) spectrum which may be attributed to the decreased half band widths on cooling. The revised assignments are given in Table 4.3 together with the previous[137,138] ones and the calculated results. A few comments regarding the justification of some of these are as follows:

The assignments to A_1 and E_1 species have been made on the basis of calculated results and spectroscopic activity. Since no calculations exist for E_2 species, the corresponding assignments have been made on different basis. Whilst spectroscopic activity is the main consideration for these assignments, it has also been checked that the concerned bands do not arise from the vibrations of amorphous structures. The calculated frequencies of A_1 (ν 1406-, 1129- and 331 cm^{-1}) and E_1 species (ν 1406-, 1129- and 343 cm^{-1}) fall close to the strong features near $\Delta\nu$ 1375-, 1177- and 354 cm^{-1}. Since the observed bands are relatively broader than the other bands in the spectrum and calculated frequencies due to the above A_1 and E_1 species are almost coincident, these bands may be assigned to A_1 as well as E_1 species. This view will receive indirect support from the discussion in the next section.

4 bands are predicted in the low frequency region $\Delta\nu$ 100-0 cm^{-1}:

$$\left.\begin{array}{l}(A_1)\ \ 2 \text{ —, } 78\ cm^{-1} \\ (E_1)\ 27 \text{ —, } 90\ cm^{-1}\end{array}\right] \quad \text{Torsion}$$

The calculations in this region seem to be rather misleading since the observed bands are far too removed from the calculated frequencies as

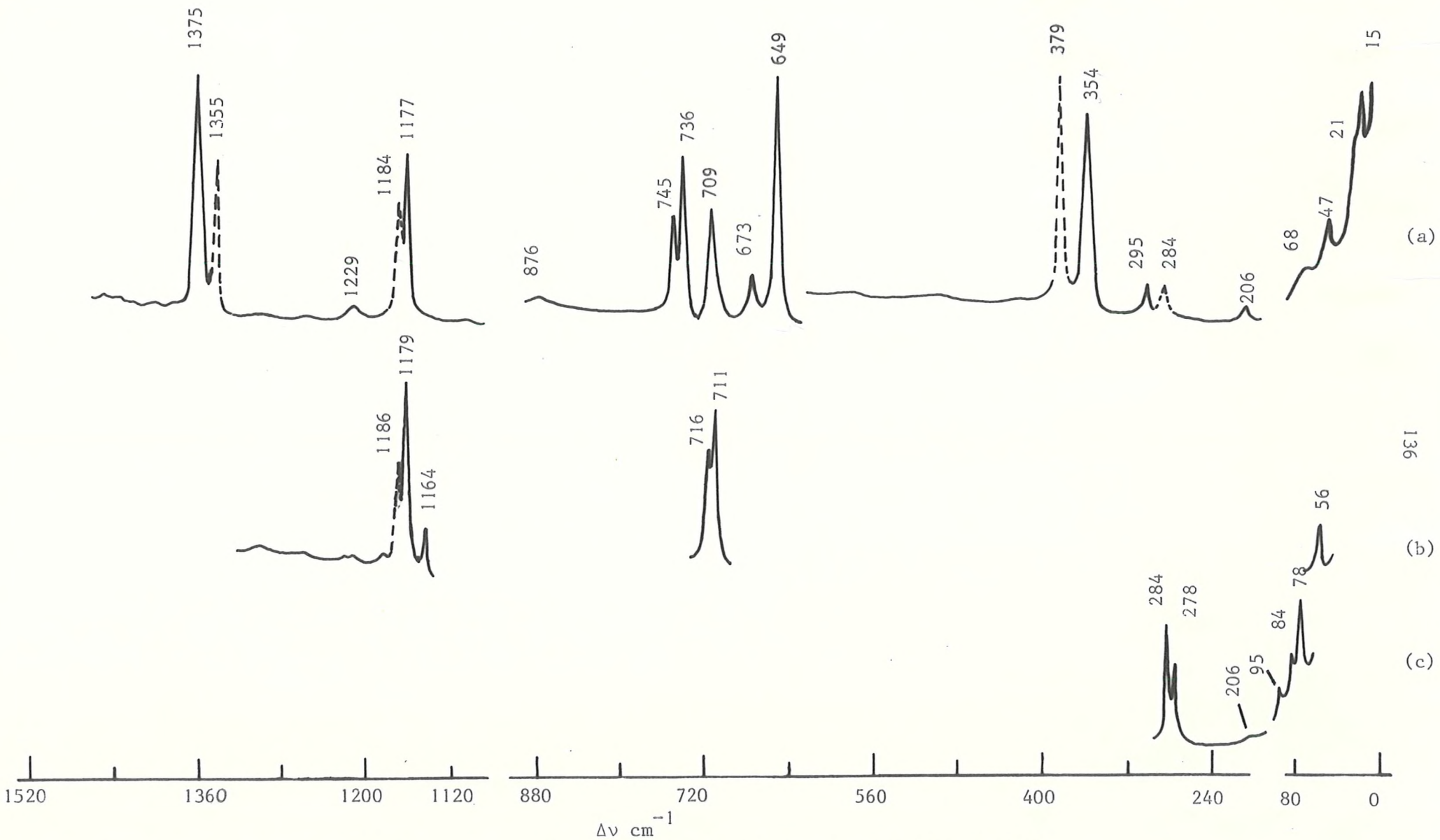

FIG. 4.3 RAMAN SPECTRUM OF PTM (a) at 25°C, (b) at -180°C (c) after melt-quenching in H_2O

Table 4.3

Raman spectrum of PTM

Present study (ν cm^{-1})	Hendra et al[139] ($\Delta\nu$ cm^{-1})	Masaru Ohsaku[138] (ν cm^{-1})	(calculated)	Species	Mode
1375	1373	-	(1406)	A	$\delta(CH_2)$
1177	1180	-	(1129)		$T(CH_2)$
649	648	-	(614)		$\nu(CSC),\delta(SCS)$
354	355	-	(331)		$\delta(CSC),\delta(SCS)$
47	-	-	(78)		$\tau(CSC)$
14.5	-	-	(2)		$\delta(SCS),\delta(CSC)$
1375	-	*1368	(1406)	E_1	$\delta(CH_2)$
1166	-	*1173	(1187)		$W(CH_2)$
1177	-	*1155	(1129)		$T(CH_2)$
876	-	*882	(821)		$R(CH_2)$
709	711	*708	(723)		$\nu(CSC)$
673	674	*671	(624)		$\nu(CSC),\delta(SCS)$
354	-	*355	(343)		$\delta(CSC),\delta(SCS)$
206	-	-	(177)		$\delta(SCS),\delta(CSC)$
68	-	-	(90)		$\tau(CSC)$
21	-	-	(27)		$\tau(CSC)$
295	-	-	-	E_2	$\delta(CSC)$
717	-	-	-		$\nu(CSC)$
736	739	-	-		$\nu(CSC)$
745	748	-	-		$\nu(CSC)$

* IR results The bands arising from vibrations of amosphous structures

$\Delta\nu$ 420-, 590-, 585-, 876-, 1124-, 1200-, 1229-, 1279-, 1318-, 1404-, 1420-, 1440-, 1450-, 1468 cm^{-1}.

shown below:

$$15\ cm^{-1}(S),\ 21\ cm^{-1}(MS,(Sh)),\ 47\ cm^{-1}(M),\ 68\ cm^{-1}(W)$$

Since E_2 modes are inherently too weak to be observed usually, the above bands may be assigned to A_1 and E_1 species considering their relative intensities and frequencies. The bands belonging to A_1 species are expected to be stronger than those associated with E_1 species. Thus $\Delta\nu$ 15- and 47 cm^{-1} bands probably belong to A_1 and those occurring at $\Delta\nu$ 21- and 68 cm^{-1}, to E_1 species.

On the whole, a considerable disagreement between the calculated and the observed frequencies reveals the inadequacy of the normal coordinate treatment (see Table 4.3) as observed in the case of POM (see section 4.2.1).

Probing the origin of some spurious bands

The dotted bands in spectra (a) and (b) (Fig. 4.3), arise when an aged specimen (3 years) was examined. These bands disappeared on solvent extraction of the latter specimen. Annealing at 140°C for 2 hours caused the same effect. These bands which occur at $\Delta\nu$ 284-, 379-, 1184- and 1355 cm^{-1}, are stronger and sharper than the neighbouring bands at $\Delta\nu$ 296-, 354-, 1177- and 1375 cm^{-1}. Since they disappear on solvent extraction of the specimen or on its annealing, they seem to arise from degradation products crystallized on the surface of the sample. These degradation products, probably polymer fragments of various chain lengths, are expected to cause a breakdown of the selection rules applicable to the established structure of the polymer. As a result, degeneracy of the E_1 or E_2 species will be lifted and the corresponding bands would split into doublets. Thus the band pairs: ($\Delta\nu$ 296-, 284 cm^{-1}), ($\Delta\nu$ 354-, 379 cm^{-1}), ($\Delta\nu$ 1177-, 1184 cm^{-1}) and ($\Delta\nu$ 375-, 1355 cm^{-1}) may be regarded

as resulting from the lifting of degeneracy in the case of $\Delta\nu$ 296 $cm^{-1}(E_2)$, $\Delta\nu$ 354 $cm^{-1}(A_1+E_1)$, $\Delta\nu$ 1177 $cm^{-1}(A_1+E_1)$ and $\Delta\nu$ 1375 $cm^{-1}(A_1+E_1)$ bands. This would also seem to support the assignment of the latter bands to their respective species. Further these bands may be regarded as "regularity bands" since these are the only bands which split on ageing. It may also be concluded that ageing may be cured by either solvent extraction or annealing at elevated temperatures. Whilst in the former case, the oxidation products would go into solution, in the latter case they would volatilize.

Annealing the specimen within $5^{o}C$ of T_m or melting seems to degrade the polymer to an irrepairable extent since in this case not only the scission of the polymer chain but also the breakdown of the whole chemical structure seems to take place. A partial spectrum of a melt quenched specimen is shown in Fig. 4.8(c).

Bands originating from amorphous structures

A number of bands have been observed which may not be reasonably assigned to fundamental modes. They are weak and appear in the reported IR spectrum as well. Many of these may be attributed to chemical faults of the molecular chain e.g. bands near $\Delta\nu$ 420-, 509-, and 585 cm^{-1} seem to arise from structures like -S S- and S-S-S, whereas bands near $\Delta\nu$ 1404-, 1420-, 1440 and 1450 cm^{-1} may originate from structures like $\{(CH_2)_m-S\}$ where $m \geq 3$.

4.3.2 Conclusion

The measurement of the detailed Raman spectrum has resulted in the following observations:

(i) Raman spectrum has been fully assigned on the basis of the recently calculated frequencies. As observed in the case of POM, a considerable disagreement exists between the calculated and the observed

frequencies thus indicating the inadequacy of the force field used in calculations.

(ii) Regularity bands have been identified which are highly sensitive to chain conformation.

(iii) Some bands arising from amorphous structures have been observed.

4.4 Polyethylene oxide - PEO, $+[(CH_2)-O]+_n$

The structural parameters of PEO are given in Table 4.1. It has been established by means of X-ray diffraction and vibrational analysis that the line group of PEO is isomorphous to the point group $D(4\pi/7)$[142,143]. The unit cell is translated by 4 molecular chains but their exact packing symmetry within the cell i.e. space group is not known.

The vibrational spectrum of PEO has been analysed by several groups under a number of conditions[142-148]. The Raman spectrum which is of interest in the present study has also been measured using laser sources recently[147,148]. Although all but a few bands belonging to Raman-active A_1 and E_1 species have now been observed and assigned to the predicted modes, the bands belonging to E_2 species have been scarcely detected probably because of their inherent weakness. The vibrational analysis so far has tended to be based only upon line group symmetry. Nevertheless it has successfully interpreted the observed features at ambient temperature. The present study, however, has resulted in the observation of a number of bands at ambient as well as at cryogenic temperature which may not be explained in terms of line group symmetry i.e. they may not be reasonably assigned to the Raman active species A_1, E_1 or E_2 or to vibrations originating from amorphous structures. These features may, however, be explained if the space symmetry is considered.

The purpose of the present study is to make detailed Raman measurements at ambient as well as cryogenic temperatures. The results thus obtained will be analysed in view of the previous assignments made for the vibrations of an isolated molecular chain and also considering the interchain interactions. It is hoped that the latter would be helpful in the prediction of the crystal symmetry (space group) and the magnitude of interchain forces tentatively.

4.4.1 Results and discussion

Raman spectra measured at 25°C (a) and -180°C (b) are shown in Fig. 4.4 and for comparison the spectrum reported by Koenig et al (c)[148] is also included.

It is clear that several new Raman bands have been observed which may originate from molecular vibrations in one of the following situations.

Isolated chain - regular structure

Isolated chain - amorphous structures

Interchain - correlation splitting

4.4.1(a) Isolated chain - regular structure

In this connection the previous assignments have been assumed to be reliable with the exception of a few ones which need some comments in view of the present evidence. The new bands appear close to the calculated frequencies of the A_1 and E_1 species and have been assigned correspondingly. The assignments to the E_2 species have been made by considering the frequency-phase relations given in Fig. 4.5.[145] The revised line group assignment of the Raman spectrum from present study is given in Table 4.4 together with the calculated and observed results from references 148 and 146.

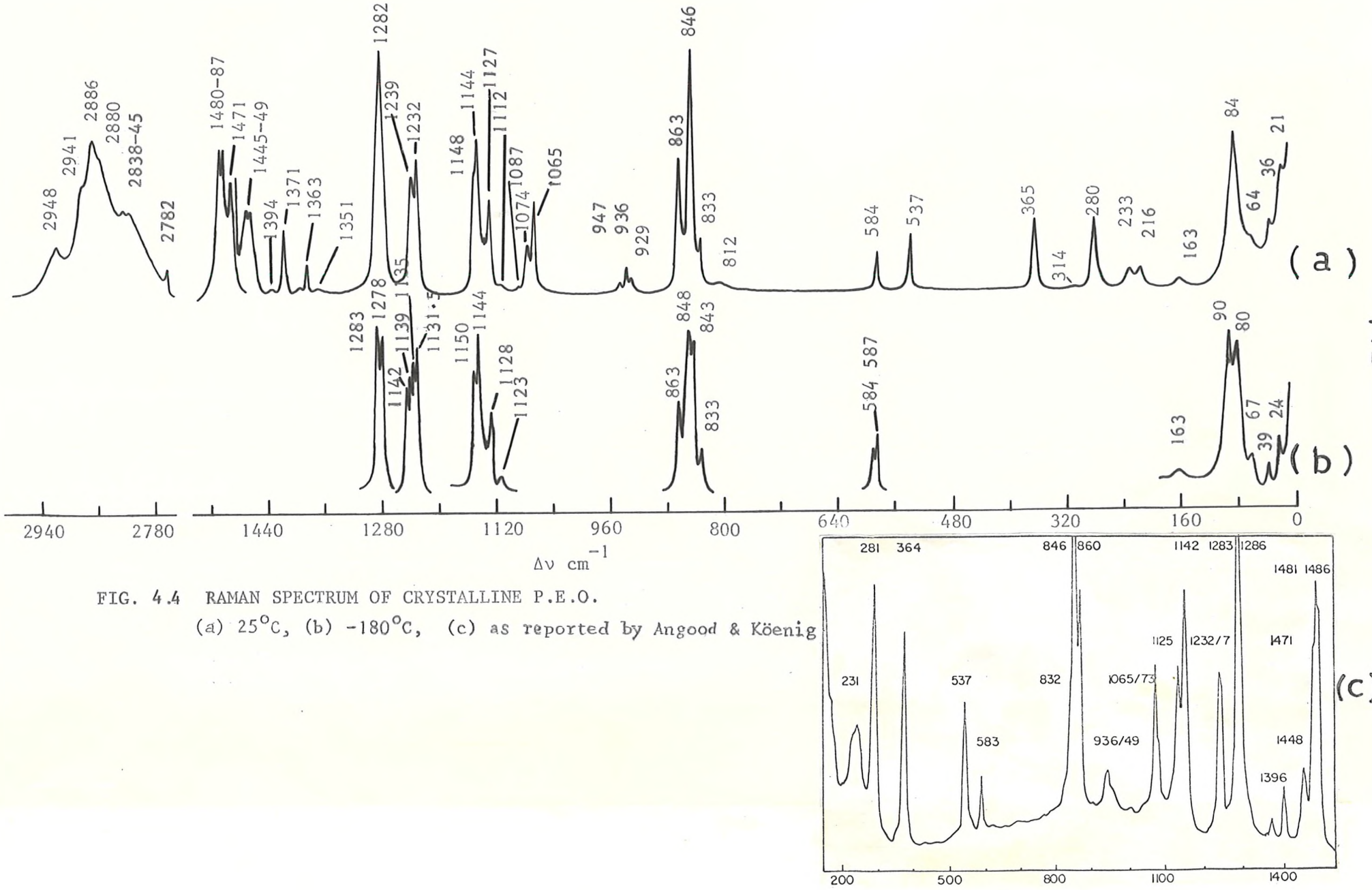

FIG. 4.4 RAMAN SPECTRUM OF CRYSTALLINE P.E.O.
(a) 25°C, (b) -180°C, (c) as reported by Angood & Köenig

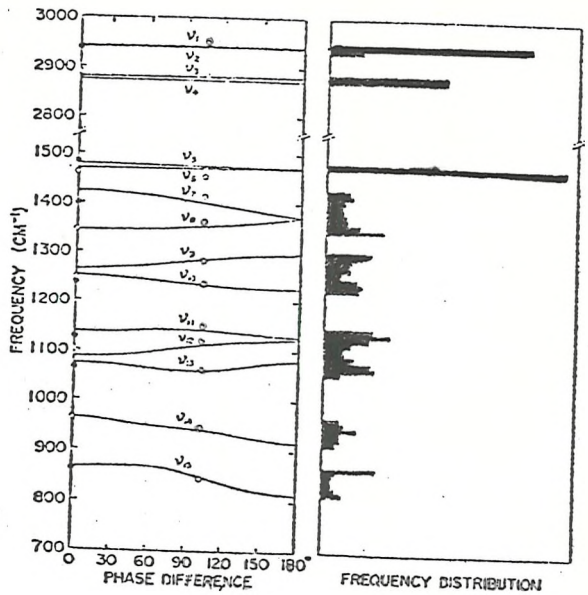

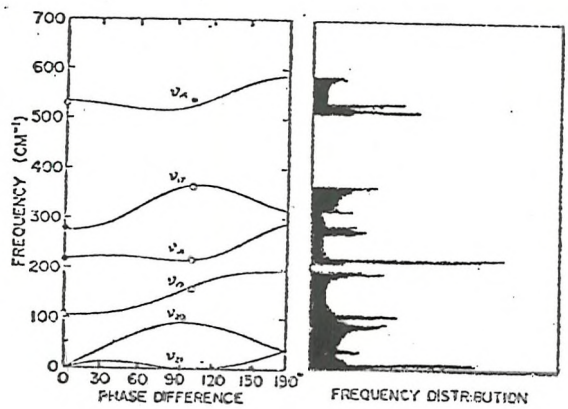

FIG. 4.5[145] FREQUENCY-PHASE RELATIONS OF PEO

4.4.1(b) Amorphous structures

The band at $\Delta\nu 314$ cm^{-1} may not be assigned to the A_1, E_1 or E_2 species. It may, however, be attributed to an amorphous structure or to some combination mode. Since no IR band has been observed near this frequency which would have suggested its assignment to a vibration of an amosphous structure, it may be assumed to arise from some combination like $\Delta\nu$ 84 cm^{-1}(S) + 233 cm^{-1}(W) = 317 cm^{-1}.

The spectral region between $\Delta\nu$ 810 - 950 cm^{-1} shows seven bands near 812-,833-, 844-, 929-, 936- and 947 cm^{-1}. (Fig. 4.4(a)). However, only those near 944-, 863- and 947 cm^{-1}, may be assigned to the predicted E_1, A_1 and E_1 species respectively. The remaining ones do not shift on cooling and hence they might not have arisen from correlation splitting. The calculations predict two IR bands in this region both belonging to E_1 species. These were observed near 846- and 946 cm^{-1}. at room temperature, and showed splitting at -130°C.[54] The total number of split bands as well as their frequencies are comparable to the above Raman bands as shown below:

Raman - $\Delta\nu$ 812, 833, 846, 863, 929, 936, 947 cm^{-1} at 25°C

IR - ν 821, 837, 846, 860, 929, 935, 946 cm^{-1} at -130°C

Tadokoro et al[54] attributed the splitting of IR spectral bands at low temperature to correlation splitting. Since the Raman and IR spectral bands are nearly coincident (as shown above) and further the Raman bands show no temperature dependence, the unpredicted bands occurring in the region between ν 810- and 965 cm^{-1} both in the Raman and IR spectra may not be ascribed to correlation splitting. Instead, they

Table 4.4

Raman spectrum of crystalline PEO
(a revised assignment)

Present study ($\Delta\nu$ cm^{-1})	Koenig et al[148] ($\Delta\nu$ cm^{-1})	Calculated[146] (ν cm^{-1})	Species	Mode
2941	-	2940	A_1	$\nu(CH_2)_a$
2845	-	2874		$\nu(CH_2)_s$
1487	1486	1479		$\delta(CH_2)$
1397	1396	1423		$W(CH_2)+\nu(CC)$
1232	1232	1252		$T(CH_1)$
1144	1142	1142		$\nu(CO)+R(CH_2)$
1127	1125	1137		$R(CH_2)+\nu(CO)$
1074	1073	1073		$\nu(CO)+\nu(CC)$
863	860	866		$\nu(CO)+R(CH_2)$
280	281	274		$\delta(CCO)+\tau(CC)+\delta(COC)$
233	231	218		$\delta(COC)+\tau(CO)$
2948(Broad)	-	2943	E_1	$\nu(CH_2)_a$
	-	2940		$\nu(CH_2)_a$
2888	-	2883		$\nu(CH_2)_s$
2838	-	2873		$\nu(CH_2)_s$
1471	1471	1476		$\delta(CH_2)$
1449	1448	1471		$\delta(CH_2)$
1416	-	1401		$W(CH_2)$
1363	1376	1353		$W(CH_2)$
1282	1283	1286		$T(CH_2)$
1239	1237	1234		$T(CH_2)$
1112	-	1112		$\nu(CO)+\nu(CC)$
1065	1065	1060		$\nu(CO)+R(CH_2)+\nu(CC)$

Table 4.4 (Contd)

948	947	941		$R(CH_2)+\nu(CC)+\nu(CO)$
846	846	847		$R(CH_2)+\nu(CO)$
537	537	524		$\delta(CCO)+\delta(COC)+R(CH_2)$
365	364	366		$\delta(CCO)+\delta(COC)$
216	-	216		$\delta(CCO)+\tau(CC)+\delta(COC)$
163	-	164		$\tau(CC)+\tau(CO)+\delta(CCO)$
1480	1481	-	E_2	$\delta(CH_2)$
1376	-	-		$W(CH_2)$
1351	-	-		$W(CH_2)$
1087	-	-		$R(CH_2)+\nu(CO)+\nu(CC)$
584	-	-		$\delta(COC)$

Bands arising from amorphous structures

$\Delta\nu$ 812-, 833-, 929- and 936 cm^{-1}.

may be attributed to vibrations of amorphous structures. These amorphous structures are likely to be associated with chemical or structural faults of the molecular chain since polypropylene[149] and polyoxacyclobutane (see section 4.6) give rise to spectral bands at similar positions. The splitting of the IR bands at -130°C, however, may be attributed to the increased resolution, made possible by the suppression of hot bands. Bands arising from amorphous structures have been listed at the bottom of Table 4.4.

4.4.1(c) Some previous assignments

Previously, a medium intensity band observed near $\Delta\nu$ 584 cm^{-1} (Fig. 4.4(a)), was assigned to E_1 species resulting from a combination between A_1 and E_1 species having calculated frequencies of 216- and 363 cm^{-1} respectively. An IR band observed near ν580 cm^{-1} was quoted to substantiate this assignment. This assignment, however, may only be justified if the assignment of the band near $\Delta\nu$ 216 cm^{-1} to A_1 species is considered to be correct. Calculations predict two bands in the spectral range $\Delta\nu$ 212 to 216 cm^{-1} belonging to A_1 and E_1 species. In the previous studies, however, only one band was resolved near this spectral range at $\Delta\nu$ 216 cm^{-1} and subsequently assigned to A_1 species. Since a band near $\Delta\nu$ 233 cm^{-1} has been observed in the present study in addition to that at $\Delta\nu$ 216 cm^{-1}, the former may be assigned to the A_1 whilst the latter to the E_1 species. This would imply a combination frequency 233-(A_1)+363 cm^{-1}(E_1) = 596 cm^{-1}(E_1), which is considerably higher than the observed one. Further, the observed band seems to be too strong to be associated with a combination mode.

It may, however, be reasonably assigned to an E_2 mode from the frequency phase relations of Fig. 4.5.

Similarly, the E_1 mode calculated at ν 1353 cm^{-1} was previously associated with an IR band observed at ν 1364 cm^{-1} and a Raman band observed at $\Delta\nu$ 1376 cm^{-1}. Since a Raman band has been observed in this study at $\Delta\nu$ 1363 cm^{-1}, the calculated E_1 mode may now be associated with the latter band rather than that observed at $\Delta\nu$ 1376 cm^{-1}. The $\Delta\nu$ 1376 cm^{-1} band may instead be assigned to an E_2 species from frequency-phase relations (Fig. 4.5).

4.4.1(d) Correlation splitting

As mentioned already, the unit cell of PEO is translated by 4 molecular chains but their exact packing geometry is not known. Since each line group mode can be in-phase and out-of-phase with identical modes of the neighbouring chains, it may split into a quadruplet. Whilst the number of split components observed in the Raman or IR spectrum would depend upon the optical activity of the space group modes, the magnitude of splitting between the components would depend upon interchain forces.

Fig. 4.4 shows the Raman spectrum measured at 25°C (a) and -180°C (b). The details of the results are listed in Table 4.5 with reference to the line group modes. It may be seen that a number of bands split into doublets and a few band pairs show increased separation at -180°C. The splitting thus observed may be attributed to correlation splitting since only one of the components in each doublet can be associated with a line group mode.

It may be noted that no Raman band splits into more than two bands. Although the IR spectrum was not measured in this study, it has been reported that the IR band occurring near ν 1282 cm^{-1} (E_1) splits into a doublet (ν 1282- 1285 cm^{-1}) at liquid N_2 temperature[148]. Since the corresponding Raman band occurs at the same frequency ($\Delta\nu$ 1282 cm^{-1})

at 25°C [Fig. 4.4(a)] and splits into a doublet ($\Delta\nu$ 1279.5 + 1283.5 cm^{-1}) at -180°C. [Fig. 4.4(b) , also see Table 4.5], it may be concluded that out of the 4 space group modes resulting from a line group mode two are Raman active only whilst the other two are IR active only. Comparison between the crystal structures of PEO and that of isotactic polypropylene may be useful in deducing the observed optical activity of the space group modes of PEO. Isotactic polypropylene like PEO, has 4 molecular chains per unit cell and the unit cell is of symmetry $P2_1/c(^5C_{2h})$ i.e. one in which two of the chains are in the "up" direction and two in the "down" direction[150]. The factor group of the space group in this case, is isomorphous to the point group C_{2h}. If the same space symmetry is assumed in the case of PEO, the line group modes would transform as follows:

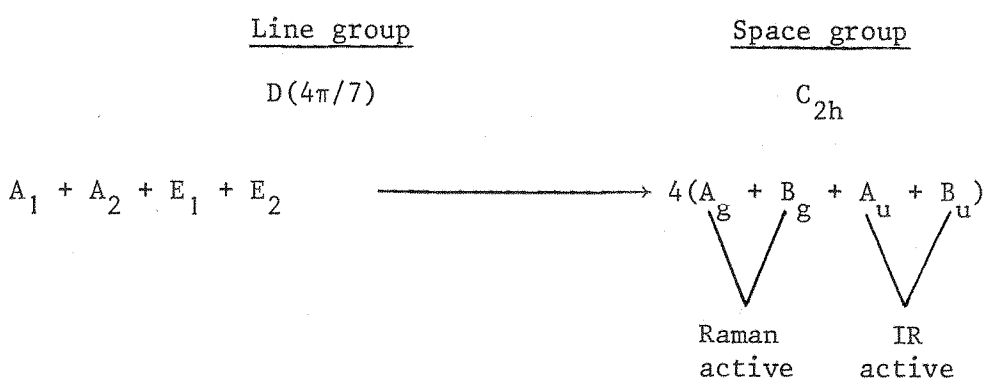

Thus the Raman bands observed as doublets in the present study, belong to A_g and B_g species whilst those appearing in the IR spectrum would be ascribed to A_u and B_u species.

As seen in Table 4.5, the magnitude of splitting between the components of correlation doublets varies between $\Delta\nu$ 3-6 cm^{-1} on the average. This magnitude is comparable to that observed in the case of polyethylene. Also like polyethylene, all the bands do not split at liquid N_2 temperature. Thus it may be concluded that interchain forces in PEO are almost as strong as in polyethylene.

Table 4.5

Correlation band splittings in the Raman spectrum of PEO

Line group mode	Species	25°C ($\Delta\nu$ cm^{-1})	-180°C ($\Delta\nu$ cm^{-1})	Magnitude of splitting ($\Delta\nu$ cm^{-1})
-	(Lattice mode(?)	84	80+90	10
$\delta(CCO)+\delta(COC)$	E_2	584	584+587	3
$R(CH_2)+\nu(CO)$	E_1	846	843+848	5
$R(CH_2)+\nu(CO)$	A_1	1127	1123+1128	5
$\nu(CO)+R(CH_2)$	E_1	1144-48	1144+1150	6
$T(CH_2)$	E_1	1232	1231.5+1235	3.5
$T(CH_2)$	A_1	1239	1239+1242	3
$T(CH_2)$	E_1	1282	1278.5+1283.5	5

Lattice modes

A number of bands associated with lattice modes are expected in the vibrational spectrum because of the crystal structure of this polymer.

The bands associated with lattice modes are expected to increase in frequency on cooling[151]. The low frequency Raman spectrum in Fig. 4.4(a) shows a number of bands below $\Delta\nu 100$ cm^{-1} (21-, 34-, 64- and 84 cm^{-1}) which shift to higher frequencies by 3-6 cm^{-1} at -180°C. The band occurring at 84 cm^{-1} (25°C) is the strongest in this region which not only shifts but also splits into a doublet at -180°C ($\Delta\nu$ 80-90 cm^{-1}) [See Fig. 4.4 and Table 4.5] . In view of low frequencies of these bands and shifting to higher frequencies on cooling, they may be assigned to the lattice modes. Although the lowest frequency calculated for a line group mode i.e. CO internal rotation (E_1) falls near ν 92 cm^{-1}, the band at $\Delta\nu$ 84 cm^{-1} may not be assigned to this mode due to the following reason. The predicted E_1 mode is both Raman as well as IR active. Since no IR band has been observed near the calculated frequency, corresponding Raman band may not be comparable in intensity to that observed at $\Delta\nu$ 84 cm^{-1}.

A Raman band observed by Schaufele at $\Delta\nu$ 126 cm^{-1} and later tentatively assigned to a lattice mode has not been observed in this study.

4.4.2 Conclusion

A number of new Raman bands have been resolved in this study at 25°C. These have been assigned to the line group species A_1, E_1 or E_2 or to vibrations of the amorphous structures.

Several bands showed doublet splitting at -180°C. This phenomenon has been attributed to correlation splitting. On the basis of an

analogy between the crystal structures of PEO and isotactic polypropylene, the space group of the former has been assumed to be similar to that of the latter i.e. C_{2h}.

The low frequency bands between $\Delta\nu$ 20-90 cm^{-1} have been tentatively assigned to lattice modes.

4.5 Polyethylene sulphide - PES, $\left[(CH_2)_2-S\right]_n$

The crystal structure of PES was determined by Tadokoro et al[120], using X-ray diffraction and IR vibrational analysis and is shown in Table 4.1. Angood and Koenig[140] measured its vibrational spectrum and concluded that the molecule has a centre of symmetry by applying the mutual exclusion rule, which supported the structural results of Tadokoro et al. They also made tentative assignments of the observed bands. Recently Tadokoro et al[141] have carried out normal coordinate analysis and assigned the observed vibrational bands on the basis of calculated frequencies and their sensitivity to thermal treatment. When the latter report was published, the present work was in progress. The findings from this work supported a number of conclusions drawn by Tadokoro et al but it was felt that a more detailed study was still required to investigate some of the structural characteristics of this polymer left unattended in the previous studies. This polymer is of great interest for a number of reasons i.e. 2 chains per unit cell, high degree of crystallinity (> 85%), high T_m (> 200°C) etc.

The factor group analysis on the basis of line, site and space groups is given in Table 4.6. Provided that the interchain forces are quite strong (at least as strong as in polyethylene)[74,75] the observation of correlation doublets predicted under the space group symmetry seems very likely due to a high degree of crystallinity. Further the

high melting point of this polymer affords a convenient study of the features e.g. "regularity or conformational bands", bands arising from disordered structures, LA modes etc. over a wide range of temperature. Whilst LA modes have been discussed in Chapter 6, other features will be considered in the following sections.

Table 4.6

Factor group analysis of PES[141]

Line (C_{2h})	Site (C_{2h})	Space (D_{2h})
$A_g^{a}(10)$	A_g	$A_g(10)$
		$B_{1g}(10)$
$B_g^{b}(10+R_x)$	B_g	$B_{2g}(11)$
		$B_{3g}(11)$
$A_u^{c\ d}(9+T_y)(\perp)$	A_u	$A_u(10)(\perp)$
		$B_{1u}(10+T_a)(\perp)$
$B_u^{e}(9+T_x)(\parallel,\perp)$	B_u	$B_{2u}\ 10+T_a\ (\perp)$
		$B_{3u}\ 10+T_c\ (\parallel)$

a - Number of symmetry species; b - Rotation about x axis;

c - Translation along y axis; d - perpendicularly polarized;

e - polarized in parallel direction.

4.5.1 Results and discussion

4.5.1(a) Factor group analysis

Line group modes

Fig. 4.6 shows Raman spectrum (a) and polarized IR spectrum (c) of PES measured at 25°C. These spectra closely resemble those reported

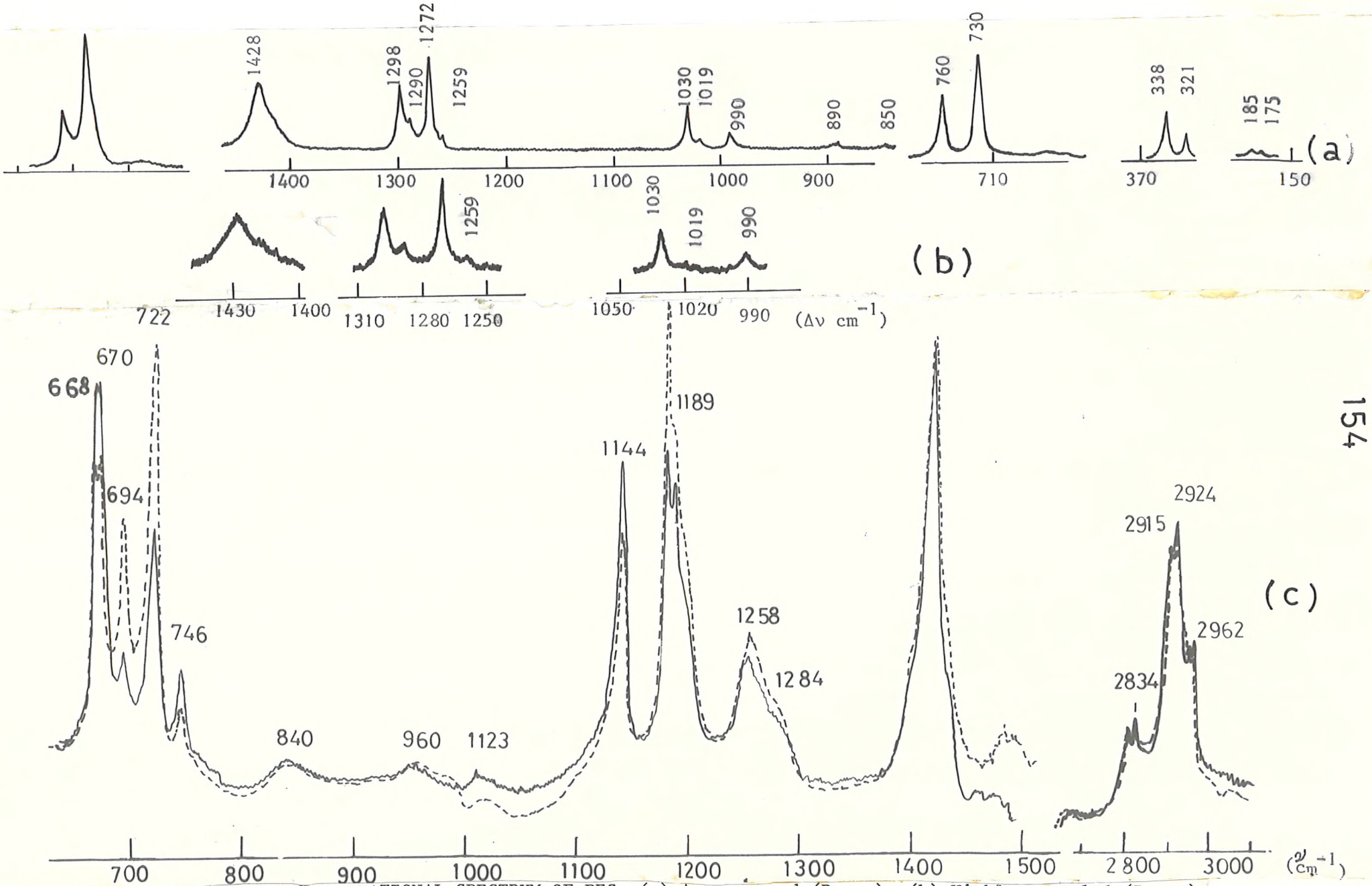

FIG. 4.6 VIBRATIONAL SPECTRUM OF PES (a) As prepared (Raman), (b) Highly annealed (Raman); (c) Polarized IR [(——)⊥ , (----)∥]

by Tadokoro et al[141] except in their greater resolution and detail by comparison. Tadokoro et al did not observe a number of bands predicted in the Raman spectrum including those at ν 1427-, 1111-, 1106-872- and 152 cm^{-1}. Whilst ν 1111- and 1106 cm^{-1} bands have not been observed even now probably because of their extremely weak intensity, the other predicted bands have resolved themselves near the calculated frequencies and may be assigned accordingly as follows:

Observed ($\Delta\nu$ cm^{-1})	Calculated (ν cm^{-1})	Assignment (Species)	(Mode)
1419,M,Sh	1427	B_g	$\delta(CH_2)_a$ -$W(CH_2)_a$
850,W	872	B_g	$r(CH_2)_a$
175	152	B_g	$\tau(CS)_a$

IR doublet near 671 cm^{-1} - Correlation splitting?

An IR doublet with bands at ν 669- and 671 cm^{-1} (see Fig. 4.8), seems to arise from correlation splitting since calculations[141] predict a single band in this spectral region near ν 680 cm^{-1}. The latter band belongs to A_u symmetry species of the line group which splits into $A_u + B_{1u}$ under the factor group of the space group. Since A_u is optically inactive and only B_{1u} is active in the latter case, the ν 680 cm^{-1} band is not expected to split into a correlation doublet. It has been observed that bands associated with line and space group modes may appear simultaneously in the spectrum; the band associated with the forbidden mode, however, appears with diminished intensity [see section 5.3.1(a), PTHF] .

The bands at ν 669- and 671 cm^{-1} appear with almost equal intensity at 25°C. The intensity of the ν 669 cm^{-1} band, however, decreases

considerably at -180°C relative to that of ν 671 cm^{-1} band, whilst the separation between the two increases by 2-3 cm^{-1}. Further, splitting between the two decreases on increasing the temperature so that near 180°C there remains a single band with the maximum near ν 671 cm^{-1} (Fig. 4.8). Thus the doublet may be attributed to correlation splitting but only with some reservation because of the predicted spectral behaviour in this region.

Lattice modes

Apart from correlation splitting, several lattice vibrational modes are to be expected, as a result of two chain per unit cell structure of PES. Tadokoro et al[141] observed two Raman bands near Δν 36- and 65 cm^{-1} and tentatively assigned them to lattice modes. Whilst the band near Δν36 cm^{-1} is not observed in the present study, the band near Δν 60 cm^{-1} (Fig. 6.6) is thought to have its origin in this type of motion and thus to involve the movement as an entity of one chain with respect to its neighbour within the unit cell. This hypothesis is confirmed by cooling the specimen to -180°C when the band at Δν 62 cm^{-1} shifts to Δν 67 cm^{-1}. On the other hand, when the specimen is heated to 180°C, the Δν 62 cm^{-1} band falls in frequency to Δν 52 cm^{-1}. In this experiment, cooling causes the lattice to contract, stiffening the force field and hence forcing up the frequency of the lattice type vibrations; the reverse happens on heating.

4.5.1(b) Vibrational studies over the temperature range: -180 to +200°C

The present study has resulted in the observation of a number of bands in the Raman spectrum whose frequencies show temperature-dependence (Fig. 4.7). These bands occur as doublets with the component bands varying in intensity and separated from each other by ∿ 10 cm^{-1}.

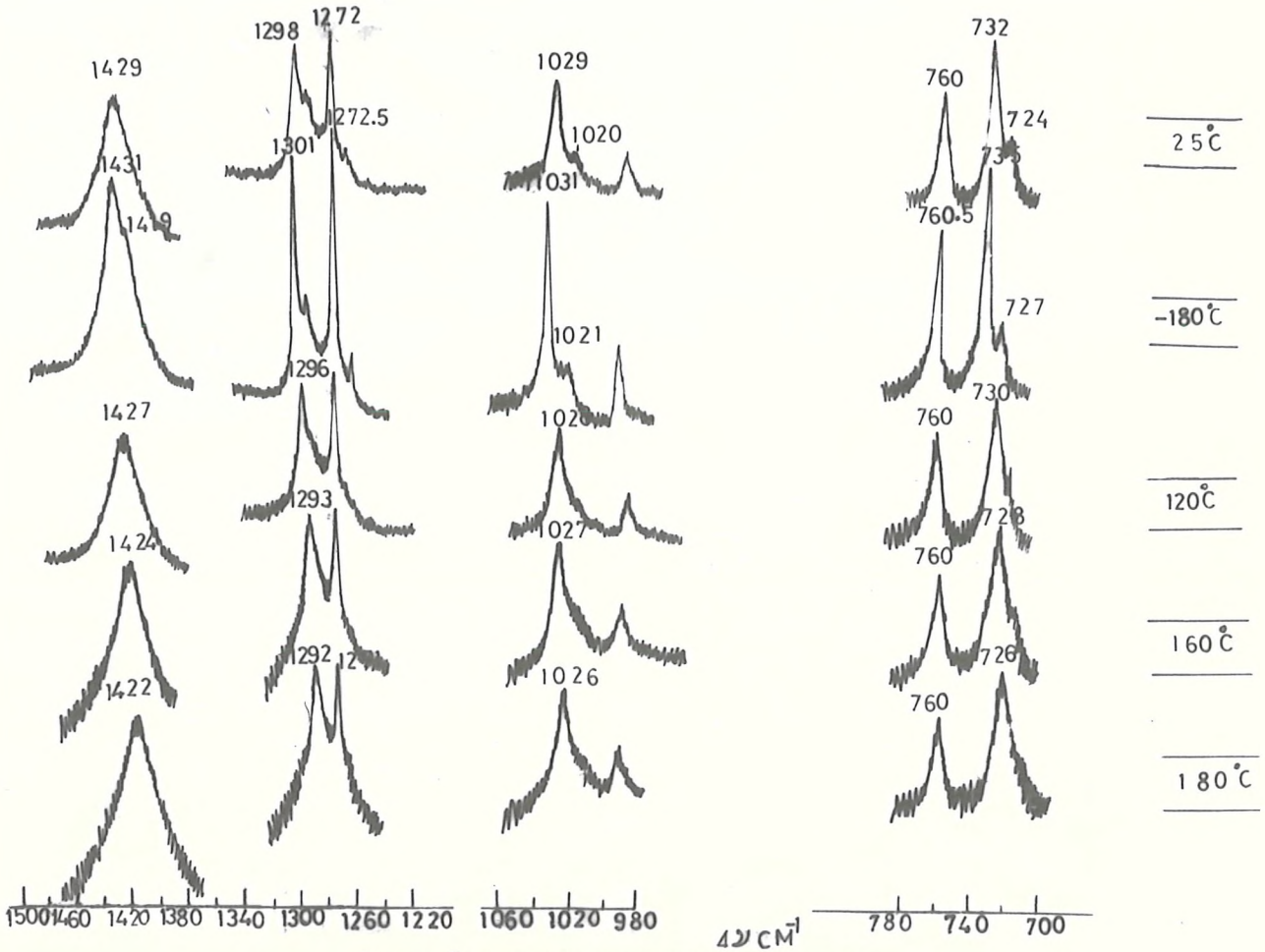

FIG. 4.7: RAMAN SPECTRUM OF P.E.S. OVER THE TEMPERATURE RANGE -180 TO 180°C.

(SEE FIG. 6.6 ALSO)

They are listed in Table 4.7 as AB doublets where the higher frequency stronger band has been labelled as A, whilst the lower frequency weaker band as B. The temperature-dependence of the frequencies of A and B bands may be attributed to one of the following effects or to a combination of two or more of them:

(i) Variation in the population of high vibrational energy levels or hot bands.

(ii) Correlation splitting predicted under the factor group analysis (Table 4.6).

(iii) Variation in the molecular conformation (one dimensional polymorphism)

The following discussion is intended to look for the origin of A and B bands and the cause of temperature-dependence of their frequencies over the temperature range: -180 to +180°C.

The origin of A and B bands

The A bands occur close to the calculated frequencies of the line group modes. As such they are associated with the long range order conformation of the molecular chain ($TG\bar{G}$). In contrast, B bands have not been predicted from normal coordinate analysis. It may, however, be seen from Fig. 4.6(a),(c) that B bands occur not only in the Raman spectrum but also in the IR spectrum at almost the same frequencies. Since this can only happen by a breakdown of the mutual exclusion rule, these bands may be attributed to the disordered structures belonging to the short range order of the molecular chain.

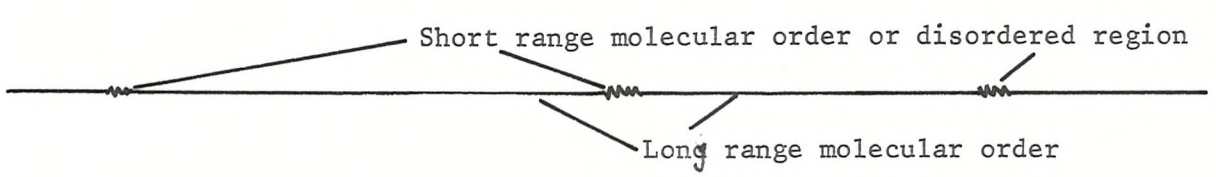

Table 4.7

Temperature-dependent frequencies of some Raman bands over the range: -180 to +180°C.

Species	Assignment	Label	-180°C ($\Delta\nu cm^{-1}$)	25°C ($\Delta\nu cm^{-1}$)	120°C ($\Delta\nu cm^{-1}$)	160°C ($\Delta\nu cm^{-1}$)	180°C ($\Delta\nu cm^{-1}$)	Overall shift ($\Delta\nu cm^{-1}$)
A_g	$(CH_2)+W(CH_2)$	A	1431,VS	1429	1427	1423.5	1422	9
-	-	B	1419,Sh	1418	-	-	-	
A_g	$W(CH_2)-\delta(CH_2)$	A	1301,VS	1298	1296	1293	1292	9
-	-	B	1290,MW	1288	-	-	-	
B_g	$W(CH_2)-\delta(CH_2)$	A	*1272.5,VS	1272	1271	1271	1271	1-2
		B	1267,MW	1264	-	-	-	
		B	1260.5,MW	1260	-	-	-	
B_g	(C-C)	A	1031,MS	1029	1028	1027	1026	5
		B	1021,W	1020	1019	-	-	
A_g	(CSC)+ (SCC)	A	732,VS or 735	730 or 732	728	726	725	10
		B	727,Sh	724	724	-	-	

* Since the frequency of this band is not temperature dependent, it may not be assigned to regularity or conformational band.

This view is further supported from the Raman spectrum of a highly annealed specimen (Fig. 4.6(b)), and the IR spectrum of the melt (Fig. 4.8). Whereas the intensities of these bands seem to be little affected by annealing, they increase considerably by melting as expected from their association with the disorder of one dimensional crystallinity. Since the frequencies of these bands are close to those of A bands, they may be considered as associated with the same type of vibrational modes as the latter.

Thus it seems that the origin of AB doublets lies in the conformational disorder of the molecular chain rather than in correlation splitting. Nevertheless, this explanation does not offer any interpretation of the temperature dependence of frequencies of these bands. In order to establish the origin of this behaviour, therefore, it is still imperative to consider correlation splitting among one of the following possible causes:

The cause of variation in the frequency of A and B bands with temperature

(i) Hot bands

Cooling or heating may cause slight increase or decrease respectively, in the frequency of A and B bands due to the decreased or increased intensity of hot bands. Therefore, slightly increased frequencies of both bands at low temperature may be attributed to the suppression of the hot band intensities. However, large decreases in the frequencies of A bands at elevated temperatures may not be ascribed to the increased intensities of hot bands alone. This is firstly because the frequency decreases occur only in the case of A bands whilst B bands are hardly affected and secondly the magnitude of splitting (5-10 cm^{-1}) is too large to be due to this effect.

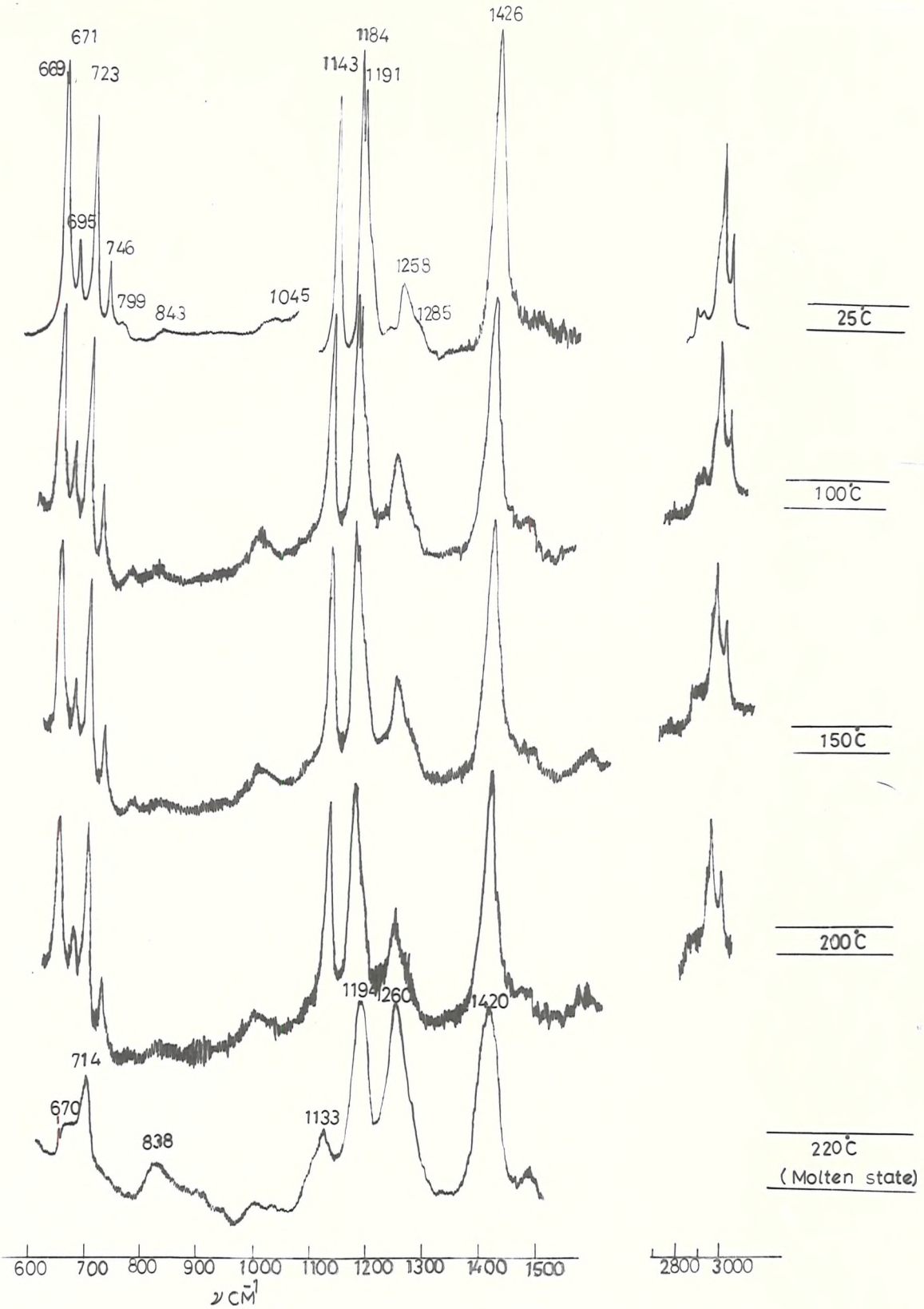

FIG. 4.8 IR SPECTRUM OF P.E.S. OVER THE TEMPERATURE RANGE 25- to 220°C

(ii) Correlation splitting

It has been shown in the last section that AB doublets may not be ascribed to correlation splitting predicted under the factor group analysis, since B bands arise from short range order amorphous structures. Nevertheless, it is interesting to see whether correlation splitting offers some explanation of the large downward shifts of A bands on heating. It may be assumed that each A band represents one of the components of a correlation doublet whose other component is too weak to be observed. In this case, the separation between A and the imaginary component of a correlation doublet would be over 10 cm^{-1} at room temperature, since A bands show downward shifts of around 10 cm^{-1} on heating. This is rather inconceivable since it implies very strong interchain forces. In the presence of such forces other spectral bands are also expected to show some frequency variations with temperature. Such variations, however, do not occur.

(iii) Variation in the molecular conformations

It seems that large downward shifts of A bands may be adequately explained if it is assumed that heating causes variation in the molecular conformation i.e. one dimensional polymorphism. There are a number of reasons which substantiate this assumption.

The frequencies of A bands measured at the highest temperature i.e. 185°C approach those of B bands. It appears that had the temperature been allowed to rise above 185°C, A bands would have overlapped B ones thus arriving at virtually the same frequencies as those of the latter. Although high background scattering above 185°C prevented such measurements to be made, extrapolation of the observed results predicts a similar deduction near 200°C (T_m). Further the frequencies

of these bands revert to their normal values on cooling to room temperature. These observations imply that the decreasing frequencies of A bands are probably connected to the slow transformation of $TG\bar{G}$ conformation into the high energy conformations as the temperature rises until near T_m, the conformation resembles the one associated with B bands. Further, the sequence of high energy conformations reverts on cooling until at room temperature the $TG\bar{G}$ conformation is resumed.

Bands characteristic of low and high energy conformations have also been observed in the spectra of other polymers e.g. polyvinyl chloride[151], polytetrafluoroethylene[69], gutta percha[152] and have been termed as "regularity bands". The A bands may be similarly identified as "regularity bands". The behaviour of these bands in the case of PES, however, is somewhat different from similar bands of other molecules. Whilst the frequencies of the former revert to the values at room temperature when room temperature is reached, those of the latter bands do not revert under similar conditions.

It is now possible to clearly distinguish between A and B bands as associated with molecular long and short range orders respectively. Thus as proposed in an earlier section, the reason for their occurrence as doublets is not that they originate from correlation splitting but from conformational splitting. The unique feature of these observations is, that the temperature dependent frequencies of A bands indicate a one dimensional polymorphism in which a certain high energy conformation is stable only if the corresponding temperature is maintained.

It may be noted that the IR spectrum shows no regularity band over the range 25-200 ^{o}C. It is only in the spectrum of the melt that the bands at ν 1143- and 723 cm^{-1} may be recognised as regularity bands in

view of their considerably decreased frequencies as well as intensities (Fig. 4.9).

4.5.1(c) Raman spectrum as a function of the degree of crystallinity

Whilst the half band width of all Raman bands decreases to some extent as a function of annealing i.e. as a result of the increasing degree of crystallinity, the behaviour of the AB doublet near $\Delta\nu$ 723 - 732 cm^{-1} is particularly interesting.

Fig. 4.9 shows variation in the frequency and the shape of the doublet as a function of annealing temperature (T_{ann}).

Fig. 4.10 shows the plot of density against the half band width of the doublet in various spectra of Fig. 4.9 .

It may be seen that whilst the frequency of the $\Delta\nu$ 732 cm^{-1} band increases on melt quenching and decreases on annealing, the frequency of the $\Delta\nu$ 723 cm^{-1} shoulder remains relatively unaffected under similar conditions. The intensity of the latter, however, decreases characteristically as a function of annealing temperature.

Clearly these characteristic changes are brought about by variations in the degree of crystallinity with varying thermal treatments.

Thus it is possible to use the half band width of the doublet: $\Delta\nu$ 723 - 732 cm^{-1}, as a measure of the degree of crystallinity in PES, after calibration with some standard measurement.

4.5.2 Conclusion

A number of new bands resolved in this study have been assigned to the previously predicted line group modes.

An IR doublet near ν 671-669 cm^{-1} seems to arise from correlation splitting. A Raman band near 62 cm^{-1} has been assigned to a lattice mode.

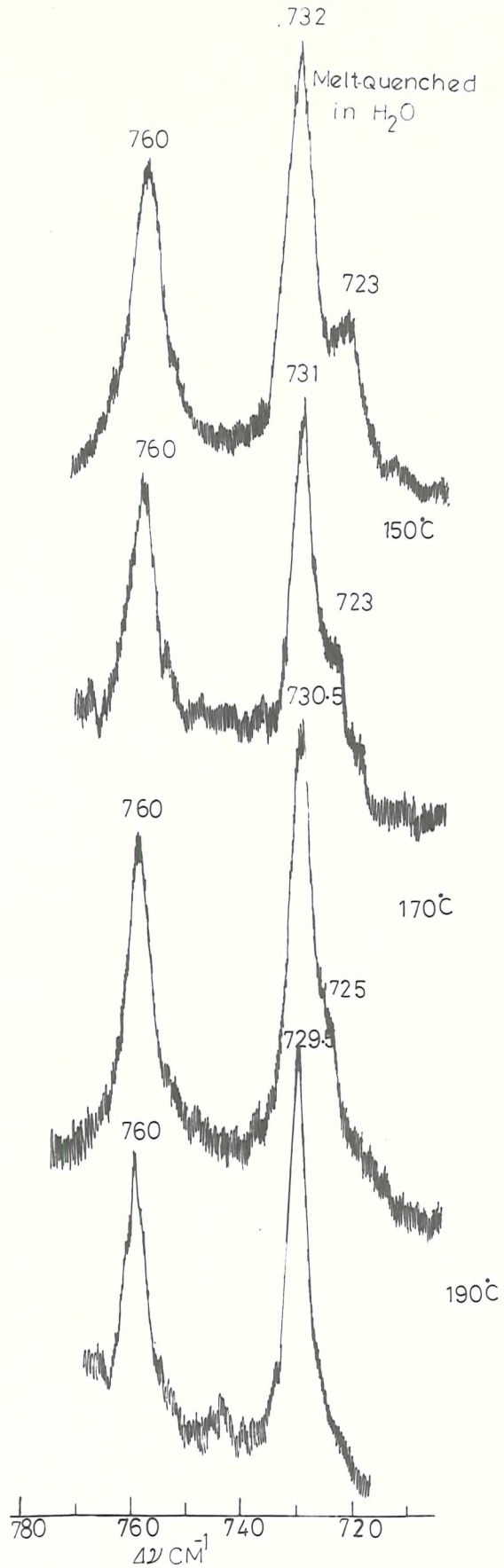

FIG. 4.9 :THE FREQUENCY & THE SHAPE OF THE DOUBLET ($\Delta\nu$ 723–732 CM^{-1}) AS A FUNCTION OF T_{ann}.

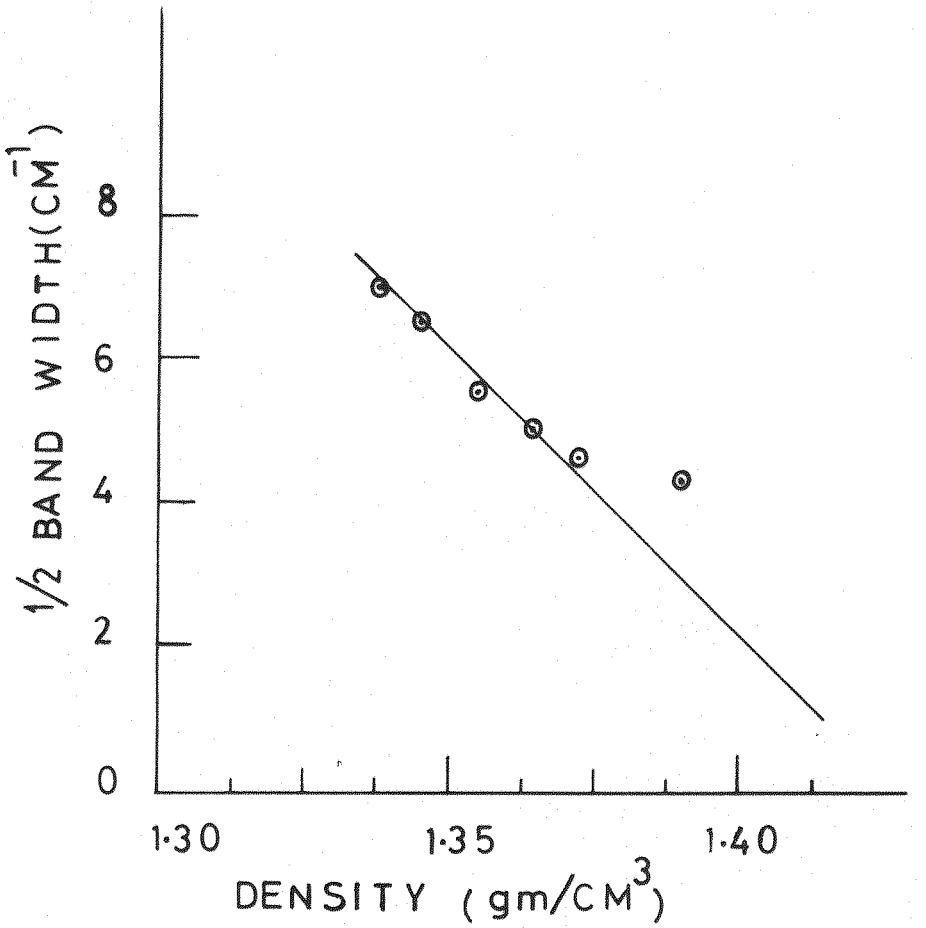

FIG. 4.10 DENSITIES OF ANNEALED P.E.S. SPECIMENS AGAINST ½ BAND WIDTHS OF THEIR DOUBLETS ($\Delta\nu$ 732–724 CM^{-1})

Whilst interchain interactions seem to be very weak, intra-chain interactions are considerably strong. As a result of conformational splitting "regularity" bands have been recognised. The temperature-dependence of the frequencies of these bands results from one dimensional polymorphism at elevated temperatures.

The band shape, frequency, and ½ band width of a Raman doublet near $\Delta\nu 732 - 723\ cm^{-1}$ is highly characteristic of the degree of crystallinity.

4.6 Polyoxacyclobutane - POCB, $+(CH_2)_3-O+_n$

POCB is the third member of polyether series with m=3. It exists in three crystalline forms usually known as modifications I, II and III respectively.[55] The preparative procedure for these modifications has been given in the experimental chapter and their crystal parameters in Table 4.1. Tadokoro et al[153] measured the IR spectra of all three modifications and assigned the observed bands by carrying out normal coordinate analysis. However, no Raman spectrum of any of these modifications has yet been reported.

It has been the purpose of this study to measure detailed Raman spectra of these modifications and to complete the vibrational assignments which were previously made solely on the basis of IR results.

Owing to the insurmountable problem of fluorescence and absorption, however, it has not been possible to make such measurements on all except modification III which is the most stable one.

The molecular vibrations of POCB III may be treated under the factor group D_2. In this case, the 14 vibrations of A species are Raman active only whereas 14 of each of B_1, B_2 and B_3 are both Raman and IR active.[153]

4.6.1 Results and Discussion

The Raman spectrum from present study and the reported IR spectrum[153] are shown in Fig. 4.11, and assignments of the observed Raman bands are given in Table 4.8 together with the calculated frequencies and the previous IR assignments. In the normal coordinate treatment giving the calculated frequencies in Table 4.8, the methylene groups contained in one chemical unit $O(-CH_2-CH_2-CH_2-O-)$ were denoted as M_I, M_{II} and M_{III} respectively. M_I and M_{III} are adjacent to the oxygen atoms while M_{II} has methylene groups on both sides. Owing to similar local symmetry of M_I and M_{III}, they were treated as M_I while M_{II} was treated differently.

It appears [see Table 4.8] that the observed Raman bands fit well against the calculated results. Since no calculations exist for the A species, the assignments in this case, have been made tentatively. For this prupose, it has been assumed that corresponding bands would be absent in the IR spectrum and stronger than those associated with B_1, B_2 or B_3 species in the Raman spectrum. The assignments to the vibrational modes were then made using group frequency correlations.

Some explanations concerning various spectral regions are as follows:

CH_2 stretching region (ν 3000-2800 cm^{-1})

While making assignments of the observed IR spectra of POCB, Tadoloro et al applied vibrational analysis of PTHF[154] as a guideline. The latter had shown that both symmetric and asymmetric vibrations associated with M_{II} have higher frequencies than similar vibrations of M_I.

Since the observed Raman bands in this region are fewer than the

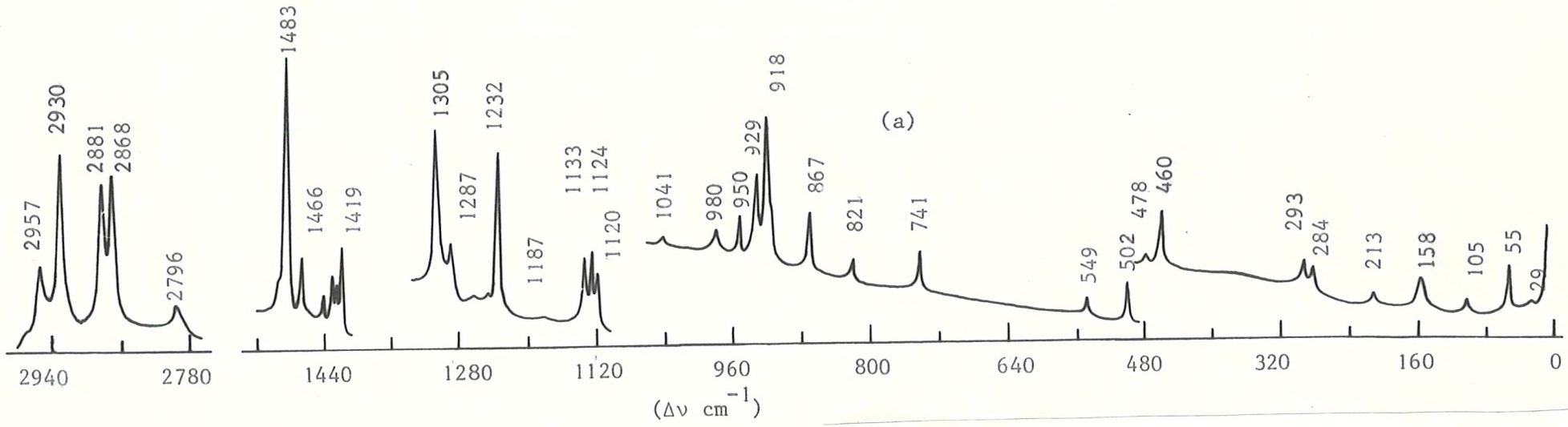

FIG. 4.11 VIBRATIONAL SPECTRUM OF POCB III:
(a) Raman (b) reported I_R

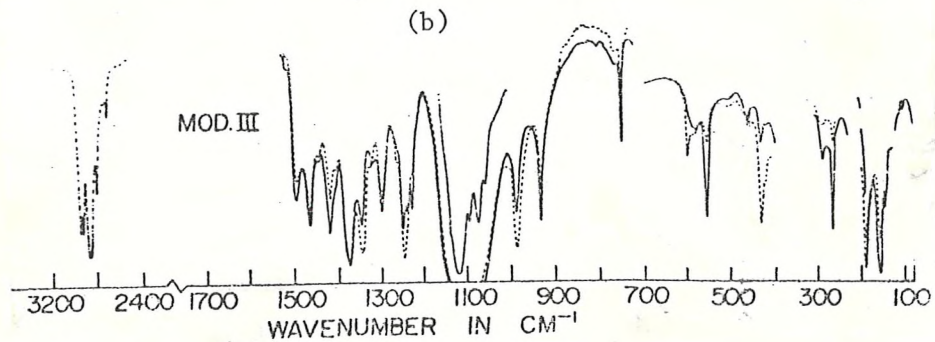

Table 4.8

Vibrational spectrum of crystalline POCB III
(Assignment of the Raman bands)

Raman (Present data) ($\Delta\nu$ cm^{-1})	IR (Reported data*) (ν cm^{-1})	Calculated* (ν cm^{-1})	Species	Mode*
2951,M	2951,VS	2946	B_1	$\nu_a(CH_2)_{II}$ (98)
2930,VS	2928 VS	2913		$\nu_a(CH_2)_{I}$ (98)
2868,W	2863 VVS	2858		$\nu_s(CH_2)_{I}$ (99)
1494,W,Sh	-----	1492		$\delta(CH_2)_{I}$ (93)
----	1375,VS	1415		$W(CH_2)_{I}$ (63)+$W(CH_2)_{II}$ (27)
----	1341(11),S	1321		$W(CH_2)_{II}$ (45)-$(CH_2)_{I}$ (23)-ν(CC)(20)
1245,VW,Sh	1244(11),S	1249		$T(CH_2)_{I}$ (84)
1120,MW	1116,VS	1121		ν(CO)(49)-ν(CC)(40)
1064	1070(11),VS	1057		ν(CC)(35)+$R(CH_2)_{II}$ (23)+ν(CO)(22)
980,W	983(11),M	983		$R(CH_2)_{I}$ (50)-ν(CO)(23)+$R(CH_2)_{II}$ (14)
819,W	-----	816		$R(CH_2)_{II}$ (45)-$R(CH_2)_{I}$ (36)
----	431(11),M	430		δ(CCO)(74)
----	186(11),M	187		τ(CC)(79)
105,MW	105,VW	103		τ(CO)(88)
2930,WS	2928,VS	2915	B_2	$\nu_a(CH_2)_{I}$ (97)
2886,S	2879,VVS	2888		$\nu_s(CH_2)_{II}$ (84)
2801,MW	2803,S	2854		$\nu_s(CH_2)_{I}$ (86)
1494,W,Sh	1495(⊥),M	1494		$\delta(CH_2)_{I}$ (92)
1461,MW	1458(⊥),M	1463		$\delta(CH_2)_{II}$ (94)

Table 4.8 (Contd)

1405,VW	1405,Sh	1386		$W(CH_2)_I$ (79)
1290,W,Sl	1297(⊥)M	1253		$T(CH_2)_I$ (94)
1215,W,Sl	1221(⊥),W	1201		$T(CH_2)_{II}$ (84)
1100,VW	1090,S	1094		ν(CO)(38)-ν(CC)(24)-$R(CH_2)_I$ (20)
1047,VW	1053(⊥),S	1002		ν(CO)(44)+$R(CH_2)_I$ (31)
868,MW	----	876		ν(CC)(53)-$R(CH_2)_I$ (35)
549,W	551(⊥),M	561		δ(CCO)(56)-δ(CCC)(32)
267,VW	264(⊥),M	245		δ(CCC)(49)+δ(CCO)(41)
158MW (Broad)	153(⊥),M	162		τ(CC)(55)+τ(CO)(44)
2951,MS	2951,VS	2946	B_3	$\nu_a(CH_2)_{II}$ (98)
2930,VVS	2928,VS	2913		$\nu_a(CH_2)_I$ (98)
2868,VS	2863,VVS	2859		$\nu_s(CH_2)_I$ (99)
1494,W,Sh	1495(⊥),M	1494		$\delta(CH_2)_I$ (93)
1424,W	1416(⊥),M	1434		$W(CH_2)_I$ (78)
----	----	1343		$W(CH_2)_{II}$ (56)-ν(CC)(29)
1227,M	1234(⊥),W	1223		$T(CH_2)_I$ (88)
1132,M	1132,Sh	1155		ν(CO)(28)-δ(CCO)(18)-δ(COC)(15)
1120,MW	1116,VVS	1120		ν(CC)(51)-ν(CO)(35)
929,M	929(⊥),M	942		$R(CH_2)_I$ (55)-ν(CO)(19)
741,MW	743(⊥),M	789		$R(CH_2)_{II}$ (55)-$R(CH_2)_I$ (28)
459,MW	461(⊥),W	454		δCOC(60)+ν(CC),(19)
284,W	289(⊥),W	281		τ(CC)(36)-δ(CCO)(35)
158,W	153(⊥),M	165		τ(CO)(41)-δ(CCO)(31)-τ(CC)(19)

Table 4.8 (Contd)

				Suggested assignment)
1485,VS	F	-	A	$\delta(CH_2)$
1441,W	F	-		$\delta(CH_2)_{II}$
1429,MW	F	-		$W(CH_2)_{I}$
1419,M	F	-		$W(CH_2)_{II}$
1305,VS	F	-		$T(CH_2)_{I}$
1232,S	F	-		$T(CH_2)_{II}$
1124,M	F	-		$\nu(CO)$ $\nu(CC)$
950,W	F	-		$R(CH_2)_{I}$
918	F	913		$R(CH_2)_{II}$
502	F	-		$\delta(CCO),\delta(CCC)$
293	F	-		$\tau(CC),\delta(CCO)$

* Reference 153

the predicted ones, it has not been possible to assign any band to the A species.

Spectral region between ν 1500-700 cm^{-1}.

The bands in this region arise from CH_2 bending, wagging, twisting, CC and CO stretching and CH_2 rocking vibrations. In contrast to CH_2 stretching vibrations, the PTHF results for this region showed that vibrations associated with $(CH_2)_I$ give rise to higher frequencies than those belonging to M_{II}.

The calculated frequencies for bending vibrations of B_1, B_2 and B_3 species associated with $(CH_2)_I$ fall close to ν 1490 cm^{-1}. There are two Raman bands near $\Delta\nu$ 1483-(VS) and 1494 cm^{-1}(MW). Since the latter band occurs near the calculated frequencies and is weaker than the former, it has been assigned to bending vibrations of the B species whilst the former to that of the A.

The bands belonging to CH_2 wagging and twisting vibrations seem to be very weak in the Raman spectrum and perhaps due to this reason some of them have not been observed. Those of the A species are, however, strong enough to justify their assignment.

Calculations predict 3 bands between ν 1120 and 1155 cm^{-1} which belong mainly to coupled CO and CC stretching vibrations of B_1 and B_2 species. IR spectrum showed a strong band near ν 1116 cm^{-1} with a shoulder near ν 1132 cm^{-1}. In contrast, Raman spectrum has shown three well resolved bands near $\Delta\nu$ 1120-, 1124- and 1133 cm^{-1}. Thus the bands at $\Delta\nu$ 1120- and 1133 cm^{-1} have been assigned to the same vibrational modes as the corresponding IR ones. The $\Delta\nu$ 1124 cm^{-1} band, however, has been assigned to the A species, since it is stronger than the neighbouring bands and does not occur in the IR spectrum.

The frequency region between ν 1060- and 750 cm^{-1} mainly belongs to CH_2 rocking modes with some mixing of skeletal modes in the high frequency region. It was shown by Tadokoro et al. on the basis of their IR results (Table 4.8) that frequencies of rocking vibrations associated with adjacent CH_2 units are similar to those of a simply coupled oscillator model of CH_2 units. The frequency-phase relation curve thus obtained approximated to ν_8 curve of polyethylene (See Fig. 1.15).

Conclusion

The above analysis indicates that normal coordinate treatment developed by Tadokoro et al. offers reasonable interpretation of the observed Raman spectrum of POCB III. The bands attributed to the A species, however, need further explanation on more rigorous basis.

4.7 Polytri methylene sulphide - PTrMS, $\{(CH_2)_3-S\}_n$

PTrMS is the counterpart of POCB in the polythioether series $\{(CH_2)_m-S\}_n$. The molecular and crystal structure has been given in Table 4.1. The latter was determined by Tadokoro et al using the X-ray diffraction method and mentioned without details in the proceedings of a conference[121]. Neither Raman nor IR spectrum of this polymer has yet been published.

This polymer has a number of characteristics e.g. all gauche molecular conformation, 2 chains per unit cell, high molecular weight, moderate melting point ($\sim 63^{\circ}C$), moderate crystallinity($\gtrsim$ 75%), which form an interesting basis for the study of its vibrational spectrum.

In view of this, detailed Raman and IR spectra have been measured

and analysed using the factor group analytical approach.

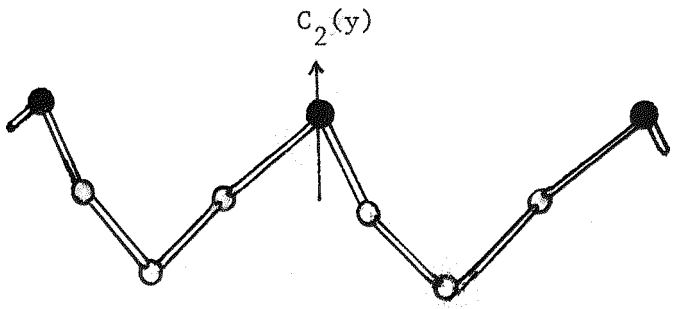

Fig. 4.12 The symmetry elements of the molecular chain of PTrMS.

● = S; o = C

The polymer chain is of G_4 type which has a C_2 rotation axis as the only symmetry element apart from the trivial identity operation as shown in Fig. 4.12. Thus molecular vibrations of PTrMS may be treated under the factor group isomorphism to the point group C_2. The details of the factor group analysis are given in Table 4.9.

Table 4.9

Factor group analysis of PTrMS under the group C

C_2[a]	N[b]	IR[c]	Raman[c]
A	$16 - R_y$	A(⊥)	A
B	$14-R_x,R_z$	A(∥)	A

a = Molecular group; b = Number of symmetry species

c = Optical activity.

4.7.1 Results and discussion

4.7.1(a) Molecular vibrations

The observed Raman and polarized IR spectra are shown in Fig. 4.13(a) and (b) respectively. The proposed assignments have been collected in Table 4.10. These are based upon the following premises which are thought to apply to this molecule.

i) Analogous to the case of POCB[153], it would be possible to treat M_I and M_{III} as M_I and M_{II} differently.

ii) The vibrations associated with $(CH_2)_{II}$ would have higher frequencies than those associated with $(CH_2)_I$ in the ν 3000- 2800 cm^{-1} region. On the contrary, the latter would have higher frequencies than the former in the ν 1500-700 cm^{-1} region.

iii) The calculated and observed frequencies for CH_2 vibrations of POCB would serve as a useful guideline in assigning the corresponding bands.

iv) Each vibration associated with $(CH_2)_I$ or $(CH_2)_{II}$ would give rise to a band of A and another of B species. Since A and B species are both IR and Raman active, the frequencies of the corresponding bands would be coincident in both spectra.

v) The IR dichroism would be reliable in making distinction between the bands of A and B species. Further, the bands of A species would be strong in the Raman but weak in the IR, whereas those of B species would be weak in the Raman but strong in the IR spectrum.

Thus in each of the following Raman and IR spectral regions, $(CH_2)_I$ and $(CH_2)_{II}$ are expected to give rise to a pair of bands each i.e. 2 pairs of bands in total:

CH_2 stretching (ν3000-2800 cm^{-1}), CH_2 bending (ν1500-1410 cm^{-1}),

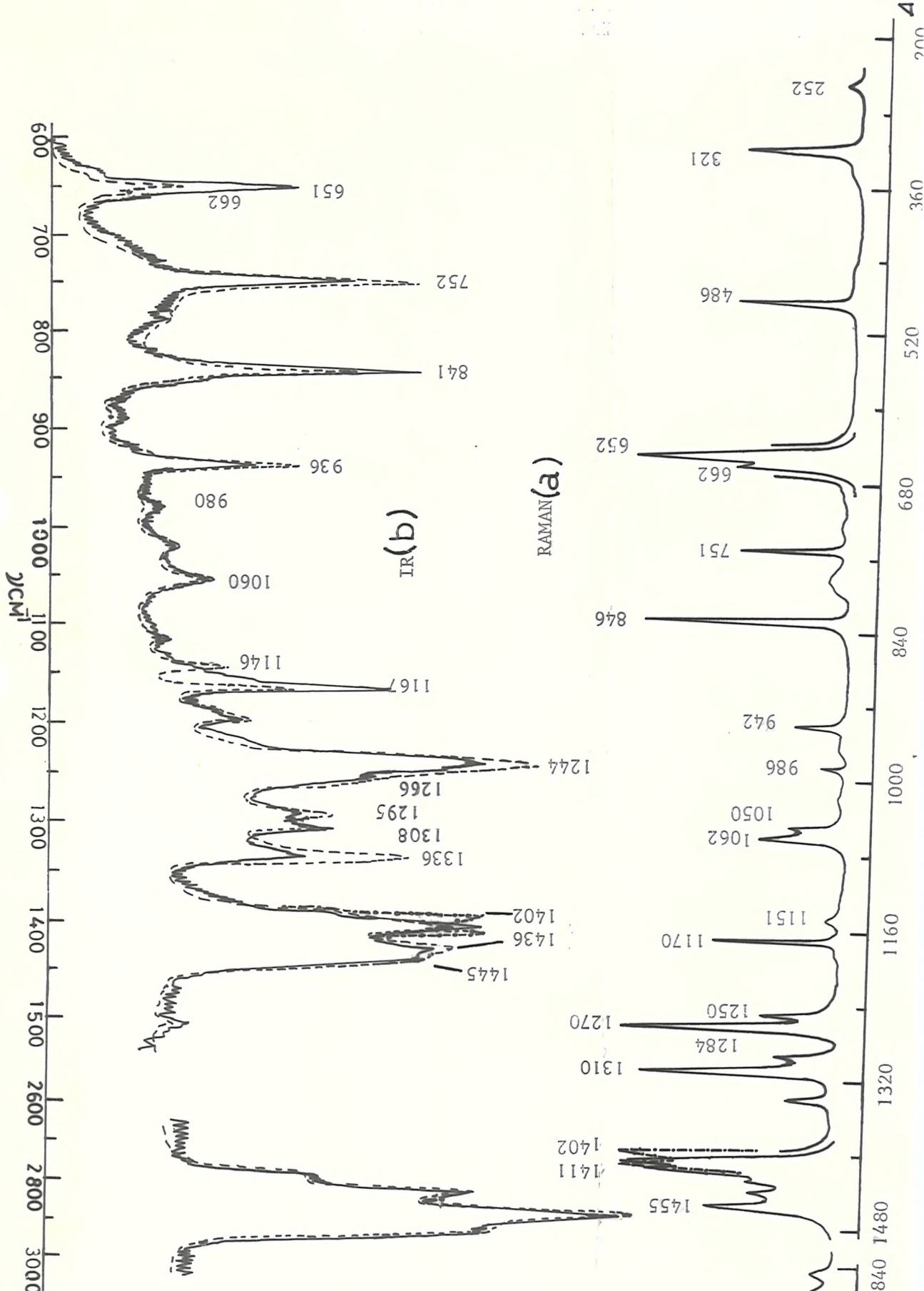

FIG.v.13 Vibrational spectrum of PTrMS
(a) Raman (b) IR
dotted line (-·-·-·-) at -180°C
solid line (———) in (b): ⊥
broken line (- - - - - - -) in (b): ∥

Table 4.10

The vibrational spectrum of PTrMS

(A tentative assignment)

Raman ($\Delta\nu cm^{-1}$)	IR (νcm^{-1})	Species	Mode
2869,M	2867,S,⊥,∥	A	$\nu_s(CH_2)_{II}$
2847,M	2842,S,⊥,∥		$\nu_s(CH_2)_{I}$
1455,VS	1455,W,Sh,⊥		$\delta(CH_2)_{I}$
1442,S	1445,M,⊥,∥		$\delta(CH_2)_{II}$
1409,S	1408,S,⊥,∥		$W(CH_2)_{I}$
1310,VS	1308,MW,⊥		$W(CH_2)_{II}$
1262,VS	1266,W,Sh,⊥		$T(CH_2)_{I}$
1170,M	1167,MS,⊥		$T(CH_2)_{II}$
1062,M	1060,W,⊥		$\nu(CC)$
986,W	980,W,⊥		$R(CH_2)_{I}$
846,S	841,S,⊥		$R(CH_2)_{II}$
652,VS	651,MS,⊥		$\nu_s(CSC)$
662,M	662,MW,⊥		
2955,M	2952,M,⊥,∥	B	$\nu_a(CH_2)_{II}$
2910 VS 2920	2908 Vs,⊥ ∥ 2920		$\nu_a(CH_2)_{I}$
1430,MS,Sh	1430,S,⊥,∥		$\delta(CH_2)_{I}$
1416,S	1418,S,Sh,⊥,∥		$\delta(CH_2)_{II}$
1340,MW	1336,MS,∥		$W(CH_2)_{I}$
1294,MW	1295,W,∥		$W(CH_2)_{II}$
1250,MW	1244,S,∥		$T(CH_2)_{I}$
1151,VW	1146,W,∥		$\nu(CC)$
1050,MW	1050,M,⊥,∥		$\nu(CC)$

Table 4.10 (Contd)

942,M	936,MS,II	B	$R(CH_2)_I$
751,M	752,S, II		$\nu(CSC)+R(CH_2)_{II}$

Bands arising from amorphous structures

ν 1200-, 1187-, 1127-, 990-, 958-, 917-, 890-, 851-, 821-, 790-, 785-, 725-, 676 cm^{-1}.

CH_2 wagging (ν1410-1280 cm^{-1}), CH_2 twisting (ν1280-1150 cm^{-1}), CH_2 rocking (ν1000-750 cm^{-1}).

Each pair of bands would consist of components belonging to A and B species which would have reciprocal intensities in Raman and IR spectra.

vi) Correlation splitting would be indicated, if a band splits into a doublet or the separation between two bands increases at -180°C.

The observed Raman and IR spectra seem to be in good agreement with these expectations. A few points concerning various spectral regions, however, need further comments as follows:

CH_2 stretching (ν3000-2800 cm^{-1})

Tentatively 4 bands are expected in this region i.e. 2 each for symmetric and asymmetric stretching vibrations according to the following scheme:

Asymmetric (ν_a): ν3000-2880 cm^{-1}) (S)

Symmetric (ν_s): ν2880-2800 cm^{-1} (W)

Five prominent bands have been actually observed. The doublet (ν 2910-, 2920 cm^{-1}), however, may be treated as associated with a single vibrational mode since the component bands are very close to each other and seem to arise from Fermi interaction. Such doublets have also been observed in the case of POCB against the calculated frequencies of single vibrational modes.

Since IR dichroic data is ambiguous in this case, bands assigned to symmetric vibrations have been considered to be of the A species, whereas those assigned to asymmetric ones to be of the B species.

Spectral region between ν1500-1150 cm^{-1}.

The bands in this region arise from CH_2 bending, wagging and twisting modes in an analogy with the case of POCB[153], but the fre-

quencies seem to be rather lower than the similar vibrations of POCB. This may be due to the different characteristics of ether and thioether linkages or of the molecular conformations associated with POCB and PTrMS. This view is supported from the fact that similar vibrations of POM[130,131] and PEO[142,146] occur at higher frequencies than those of their counterparts in polythioether series i.e. PTM[138] and PES[141] respectively (see sections 4.2-4.6).

The bands of B species are typically weak and some of them seem to be too weak to be resolved. As in the case of CH_2 stretching region, the IR dichroic data for the CH_2 bending region is not decisive. Thus corresponding assignments have been made on the basis of band intensities.

Spectral region between ν 1150 and 640 cm^{-1}.

This region shows the bands arising from C-C stretching, CH_2 rocking and C-S stretching vibrations. If the feequency-phase relation of CH_2 rocking modes observed in the case of POCB[153] (see section 4.6) is assumed to apply to PTrMS, CH_2 rocking modes would fall between $\sim$ 750- and 1000 cm^{-1}. Similarly C-C stretching frequencies are expected to occur between 1000-1150 cm^{-1}. Since the local symmetry of C-S-C linkages is analogous in PTM and PTrMS, (See Table 4.1) the associated vibrations of PTM would be comparable to those of PTrMS with respect to symmetry, frequency and intensity. The activity of these vibrations, however, would be different in these two cases because of different selection rules. PTM gives rise to two bands near $\Delta\nu$ 647- add 734 cm^{-1} in the Raman spectrum and two near ν 708- and 734 cm^{-1} in the IR spectrum which are associated with C-S-C stretching vibrations of A_1, E_1, E and A_2 species respectively (see Table 4.3 section 4.3). On the other hand, PTrMS gives rise to two bands near ν 651- and 751 cm^{-1} in both Raman and IR spectra. Obviously, the

latter bands are comparable to the Raman and IR spectral bands of PTM at $\Delta\nu 647\ cm^{-1}$ and $\nu 734\ cm^{-1}$ respectively. Since IR dichroism and relative intensities of these bands also support this view, they may be assigned to the A and B species respectively. It is to be noted that the $\Delta\nu\ 751\ cm^{-1}$ band has already been assigned to a CH_2 rocking mode. Thus it seems that this band arises from coupling between CH_2 rocking and C-S-C stretching vibrations.

Bands below $\nu\ 650\ cm^{-1}$.

It is difficult to assign a medium intensity Raman band near $\Delta\nu\ 486\ cm^{-1}$ which falls within the frequency range for S-S stretching vibrations i.e. $\Delta\nu\ 450 - 550\ cm^{-1}$ (Author's own results)
It may be assumed that it originates from chemical faults of the molecular chain such as S-S linkages. It, however, does not seem to be the case, since the intensity of this band does not vary with specimens of different origins and molecular weights.

The far IR spectra of polyethers with $m \geq 4$ have shown a number of bands in the region between ~150- to $600\ cm^{-1}$, which have been identified as frequency-phase modulated progressions arising from skeletal bending and torsional modes[155]. Similar bands also seem to arise in Raman spectra of polyethers as well as Raman and IR spectra of polythioethers with $m \geq 4$ (see Chapter 5). In view of this, the $\Delta\nu\ 486\ cm^{-1}$ Raman band together with other Raman and IR bands observed down to $\Delta\nu\ 200\ cm^{-1}$, may be assigned to skeletal bending and torsional modes. Since IR dichroism was not measured in this region, assignment of these bands to the A and B species may not be made. Nevertheless the bands at $\Delta\nu$ 486- and $435\ cm^{-1}$ seem to belong to the A and B species respectively since they appear with recirpocal intensities in the Raman and IR spectra.

4.7.1(b) Correlation splitting

As indicated in Table 4.1, the unit cell of PTrMS is translated by 2 molecular chains. The factor group of the space group is isomorphous to the point group C_s and may be correlated with site (C_1) and line (C_2) groups as follows:

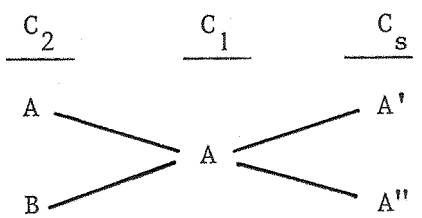

Thus each line group mode is expected to be split into 2 space group modes and a doublet would appear for every single band associated with A or B species. The split components would be both Raman and IR active.

Generally, it has been observed that when IR and Raman spectra were measured at -180°C, the half band widths decreased enormously. Typical half band width decreases in the IR spectrum were upto 8 cm^{-1}. Nevertheless only the band near ν 1408 cm^{-1} (See Table 4.10 and Fig. 4.13) splits into a doublet under these conditions giving rise to component bands near ν 1402 and ν 1411 cm^{-1} in both Raman and IR spectra.

The band near ν 660 cm^{-1} in both Raman and IR spectra was suspected to arise from correlation splitting of the 651 cm^{-1} band. The components of the doublet (ν 1651-, 660 cm^{-1}) , however, showed negligible increase in separation at -180°C , thus indicating its origin from some other phenomenon e.g. Fermi interaction.

Lattice mode

The Raman band occurring near $\Delta\nu$ 46 cm^{-1} at 25°C seems to arise from a lattice mode because of its low frequency and the fact that it shifts to a higher frequency by $\sim$ 9 cm^{-1} at -180°C.

Bands arising from amorphous structures

A number of broad, ill defined, weak bands have been observed in both the Raman and IR spectra at almost the same frequencies. These have been listed at the bottom of table 4.13. Since their intensities showed dependence on thermal treatment, they may be attributed to amorphous structures. Their exact nature however, may be clarified only by carrying out more rigorous vibrational analysis.

4.7.2 Conclusion

The vibrational spectrum of polytrimethylene sulphide finds reasonable interpretation on the basis of G_4 model having a C_2 rotation axis and 2 chains per unit cell. A rigorous assignment of the observed bands, however, needs complete vibrational analysis.

Correlation splitting has been observed in Raman as well as IR spectrum but the interchain interactions seem to be very weak.

4.8 General Conclusion

A number of newly resolved bands in the Raman spectra of POM, PEO and PES have been assigned to the previously calculated frequencies, whilst Raman spectra of PTM and POCB, and Raman and IR spectra of PTrMS have been fully assigned. It has emerged that while the previous normal coordinate treatments can satisfactorily explain the observed vibrational features of PEO, PES and POCB, they are not satisfactorily compatible with the observed spectrum of POM and PTM. Further, the

vibrational spectrum of PTrMS finds reasonable explanation on the basis of factor group analysis.

Both PTM and PES give rise to highly characteristic conformation sensitive"regularity" bands. PES, in addition, shows one dimensional polymorphism at elevated temperatures. These observations suggest strong intrachain interactions in these molecules.

Correlation splitting has been observed in the case of PEO, PES and PTrMS. Nevertheless interchain interactions seem to be sufficiently strong in the case of PEO only.

C H A P T E R V

STRUCTURAL STUDIES OF POLYETHERS AND POLYTHIOETHERS WITH $m \geq 4$

5.1 Introduction

The X-ray diffraction analysis of the higher members of polyether series $\text{-}(CH_2)_m\text{-}O\text{-}_n$ (m = 4,6,8-10,12) has shown that these molecules take essentially extended planar zig zag conformation and that there are two types of molecular packings: the monoclinic PTHF-type and the orthorhombic PE-type[52] (Table 4.1). In Fig. 5.1 are shown the molecular packings (c projection) of (a) PTHF-type and (b) PE-type[92]. Van der Waal's radii of the chain atoms are indicated by circles. In these two types, two essentially planar zig zag chains pass through the centre and the corner of the unit cell. The molecular arrangement is, however, different in each type; the zig zag planes of the molecular chains are parallel to the bc plane in the PTHF type whilst the zig zag planes make an angle of about 41° with bc plane in the PE type. The PTHF type is generally more stable in the case of the lower m members (m = 4,6 and 8) and the PE-type is stable in the higher m members (m = 8-10 and 12), though the occurrence of the crystal modifications depends upon the preparation conditions. The relationships between the preparation conditions and occurrence of crystal modifications are summarized in Table 5.1.

Table 5.1[52]

The relationship between preparation conditions and the occurrence of crystal modifications of polyethers $\text{-}(CH_2)_m\text{-}O\text{-}_n$. (m = 6-12)

m	From solution	From melt
6	PTHF type (+ PE type)	PTHF type
8	PE type (+ PTHF type)	PTHF type
9	PE type	PE type
10	PE type (+ PTHF type)	PE type (+ PTHF type)
12	PE type	PE type

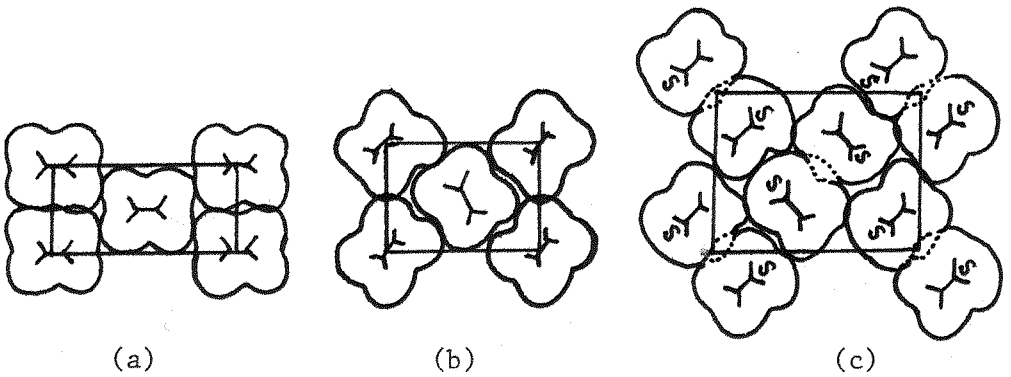

FIG. 5.1 MOLECULAR PACKING (C-axis projections) OF (a) PTHF-TYPE (b) PE-TYPE AND (c) PPMS UNIT CELLS. VAN DER WAALS RADII OF THE CHAIN ATOMS ARE INDICATED BY CIRCLES

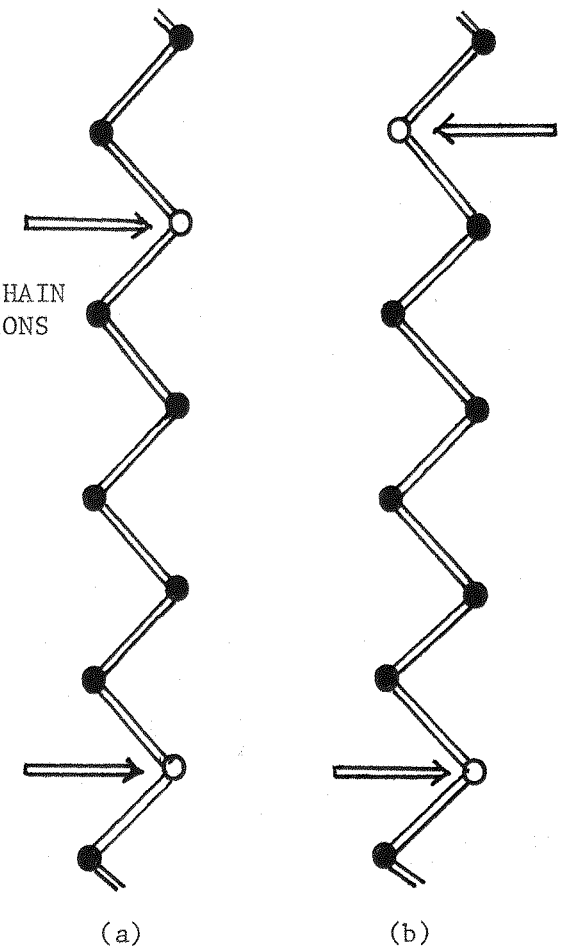

FIG. 5.2 ARRANGEMENTS OF THE CHAIN ATOMS AND THE DIRECTIONS OF THE DIPOLE MOMENTS

a = m = odd

b = m = even

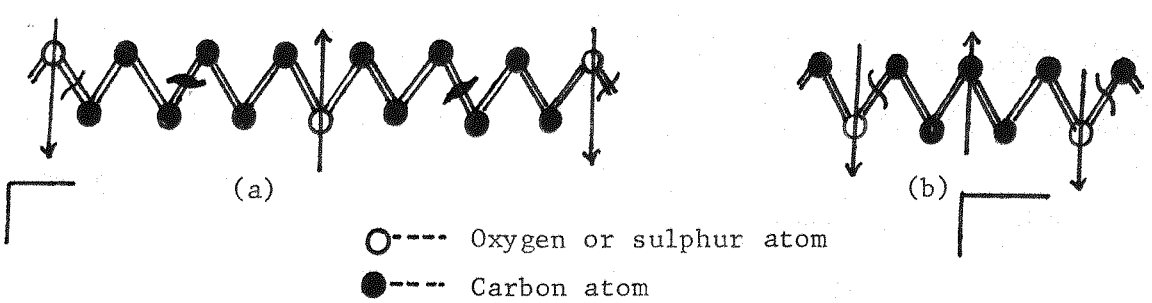

FIG. 5.3 SYMMETRY ELEMENTS OF AN EXTENDED PLANAR ZIG ZAG MOLECULAR CHAIN (a) m = even (b) m = odd

The stability of these crystal structures is generally attributed to the electrostatic and Van der Waal's interactions. Thus, it has been proposed[92] that the crystal structures of these polyethers are produced by the stronger effects of the dipole-dipole interactions between the C-O-C groups with the PTHF type and the Van der Waal's interactions between the methylene sequences in the PE type.

The molecular and crystal structure of the polythioether series $\{(CH_2)_m-S\}_n$ with $m \geq 4$ has not been determined as yet, with the exception of polypentamethylene sulphide[92] (PPMS), m = 5 (Table 4.1). The latter has 4 molecular chains per unit cell which take essentially planar zig zag conformation. The molecular packing in the lattice is, however, different from both PTHF- and PE-types, belonging to the polyether series. In this case two neighbouring molecular chains are arranged in parallel to each other like those of the PTHF type due to the dipole-dipole interactions of C-S-C bonds, and are packed as a whole like the PE-type due to the Van der Waal's interactions (Fig. 5.1c). This difference arises from the fact that PPMS has m = odd. The polyethers mentioned above have m = even, in which the oxygen atoms in the molecular chains are located alternately on both sides of the zig zag chain. Thus, antiparallel array of the C-O-C dipole moments contributes to the stabilization of the planar zig zag conformation (Fig. 5.2a). On the other hand, in PPMS all the sulphur atoms are located on one side of the zig zag chain because of m = odd and the C-S-C dipole moments are set in a parallel array to each other (Fig. 5.2b). Therefore, the planar zig zag conformation of PPMS may be unstable in an isolated molecular chain, but stabilized as a whole by the arrangement of the two molecular chains whereby the zig zag planes are parallel and the dipole moments are antiparallel to each other.

From these considerations, it is clear that whilst the molecular conformation of polythioethers with m = 4, 6 and 10 is expected to be similar to that of polyethers and PPMS, i.e. planar zig zag, the crystal structure is likely to be similar to that of polyethers (referred above) because of m = even i.e. PE- or PTHF-type.

The purpose of this study is to deduce the molecular and crystal structures of polythioethers (with m = 4, 6 and 10) by a comparative study of their vibrational spectra and those of polyethers in general and PTHF and PDMO in particular under various conditions. This study would also reveal the crystallization behaviour of polyethers and polythioethers.

5.2 Molecular structure

5.2.1 Introduction

An infinitely extended planar zig zag chain of a polyether or a polythioether would have symmetry elements as shown in Fig. 5.3(a) and (b) depending upon m = even or odd respectively. The fibre period has been assumed to be 1 and 2 repeat units for model (a) and (b) after the molecular structures of PPMS[92] and PDMO[52] respectively. The factor group of the molecular group would, therefore, be isomorphous to the point group c_{2v} for m = odd and to d_{2h} for m = even. In Table 5.2 are given the symmetry species number of normal modes (N) and selection rules [activity in the IR and Raman effects i.e. A (active), F (forbidden)] obtained from the factor group analysis.

Table 5.2

Factor group analysis under the molecular groups d_{2h} and c_{2v}

Group	Symmetry species	N	IR	Raman
d_{2h}	a_g	$\frac{1}{2}(5m+2)$	F	A
	b_{1g}	$\frac{1}{2}(5m+2)$	F	A
	b_{2g}	$2m$	F	A
	b_{3g}	$2m+1(R_x)$	F	A
	a_u	$2m$	F	F
	b_{1u}	$2m+1(T_z)$	A($\perp$)	F
	b_{2u}	$\frac{1}{2}(5m+2)(T_y)$	A($\perp$)	F
	b_{3u}	$\frac{1}{2}(5m+2)(T_x)$	A($\parallel$)	F
c_{2v}	A_1	$\frac{1}{2}(5m+3)(T_y)$	A($\perp$)	A
	A_2	$2m-1$	F	A
	B_1	$\frac{1}{2}(5m+1)(T_x)$	A($\parallel$)	A
	B_2	$\frac{1}{2}(5m-1)(T_z,R_z)$	A($\perp$)	A

5.2.2 Results and discussion

The Raman and polarized IR spectra of polythioethers with m = 4-6 and 10 are shown in Fig. 5.4(a) and (b) respectively. On the other hand, the Raman spectra of polyethers with m = 4 and 10 are shown in Fig. 5.5(a) and the IR spectra of polyethers with m = 4,6-10,12 in Fig. 5.5(b). The latter IR spectra refer to Tadokoro et al[52]. For comparison, the Raman and IR spectra of polyethylene are presented in Fig. 5.6 .

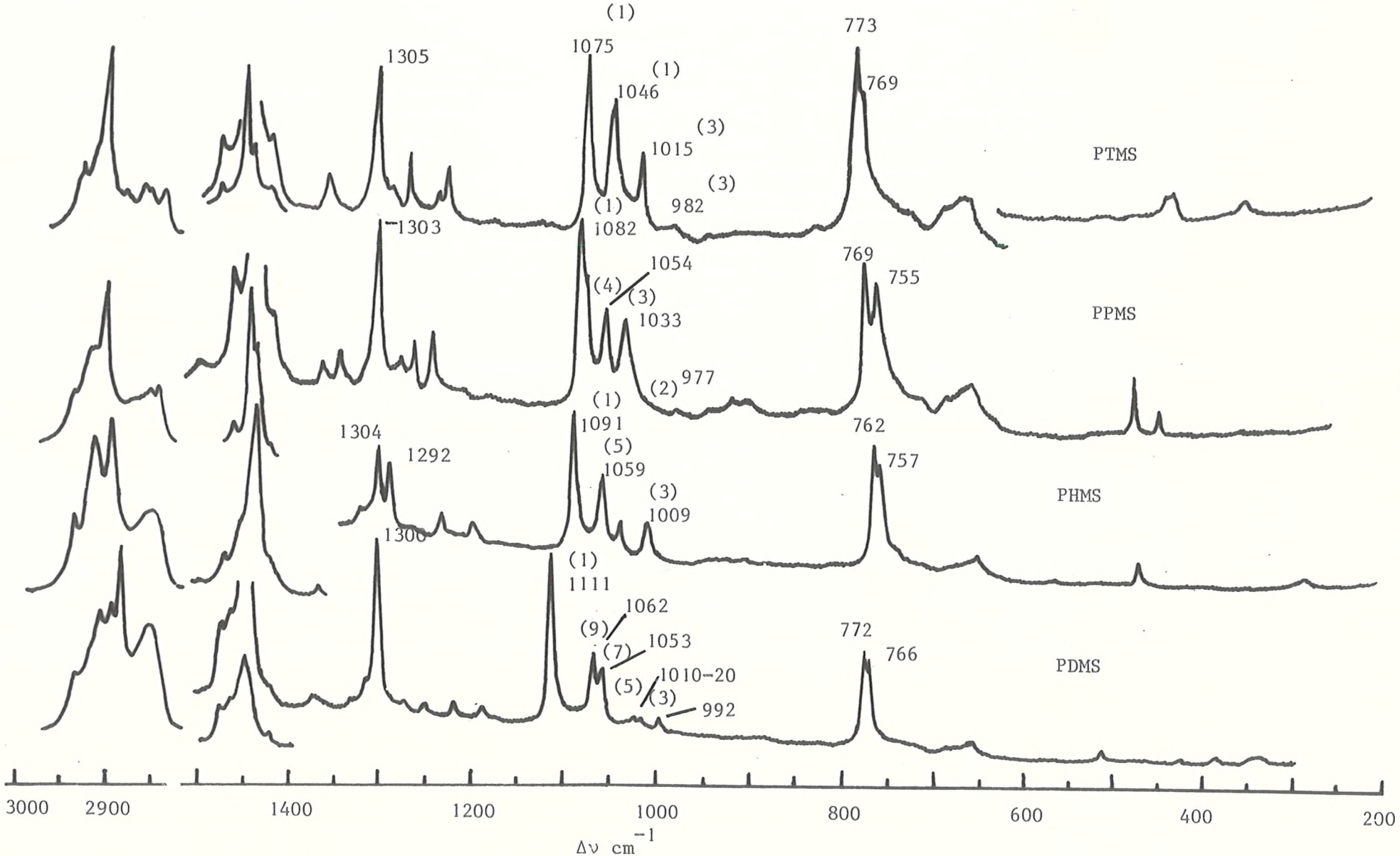

FIG. 5.4(a) RAMAN SPECTRA OF POLYTHIOETHERS

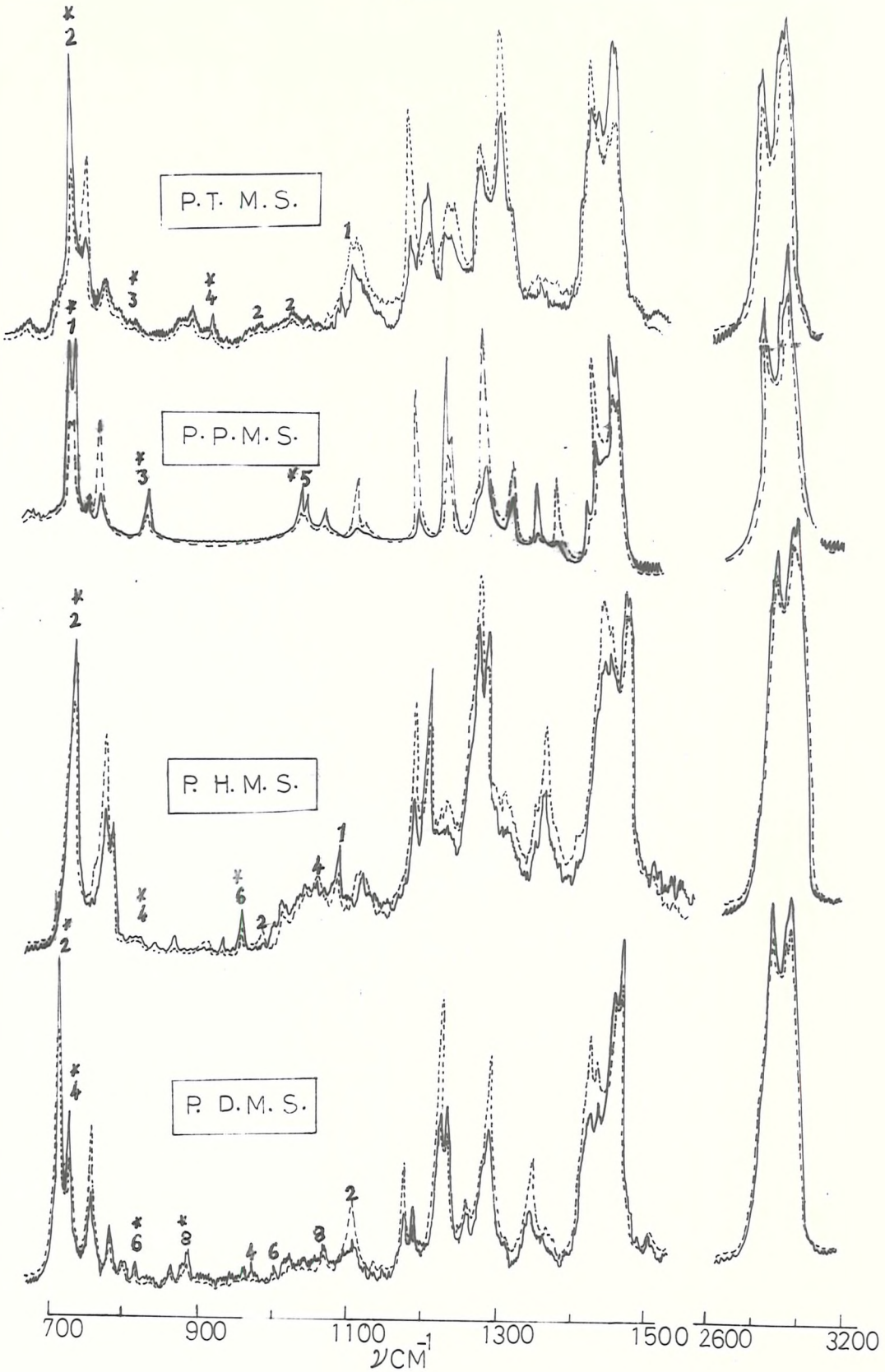

FIG.5.4(b) : I R SPECTRA OF POLYTHIOETHERS

solid line(——) : perpendicularly Polarised

broken line(----) : parallal Polarised

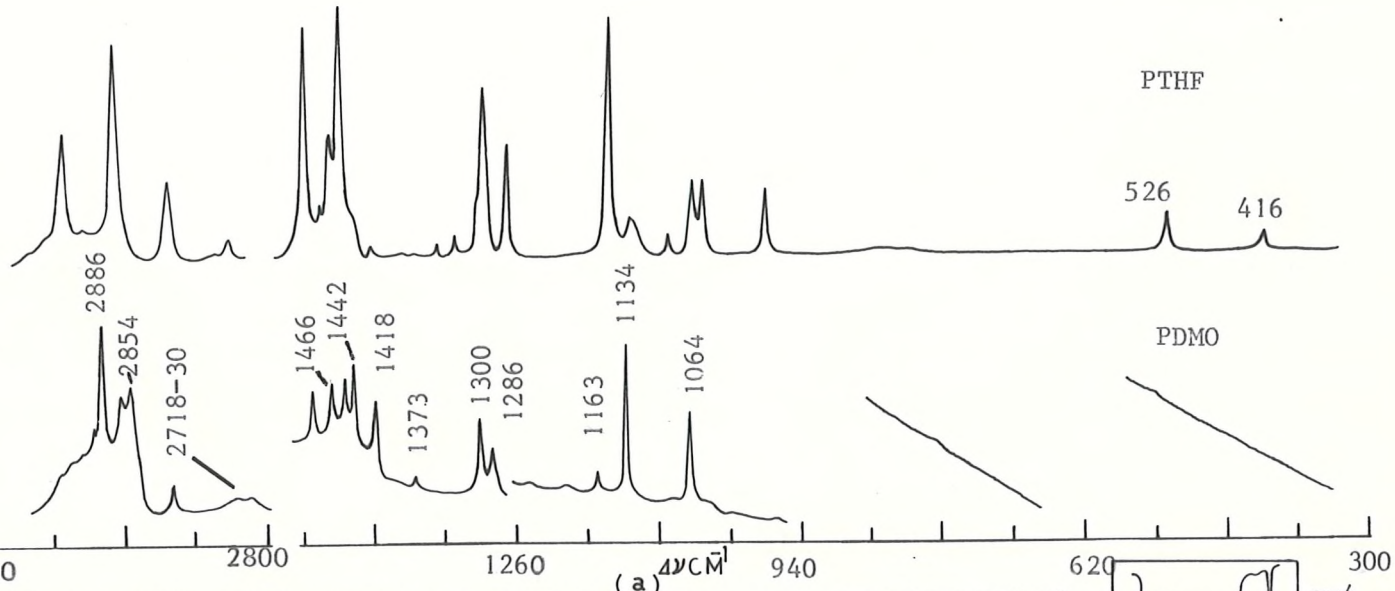

FIG.5.5 VIBRATIONAL SPECTRA OF POLYETHERS
(a) Raman (m=4,10)
(b) Reported IR (m=4,6-10,12)

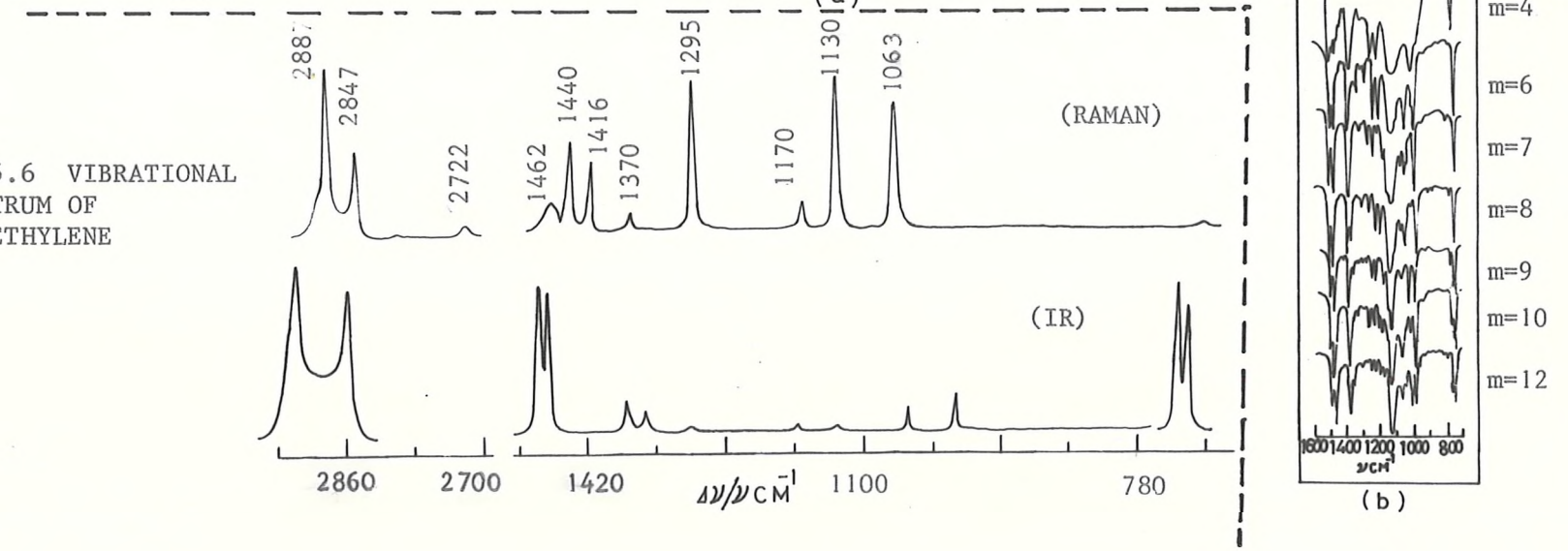

FIG. 5.6 VIBRATIONAL SPECTRUM OF POLYETHYLENE

It is clear from Fig. 5.4(a) and (b), that the band profiles appearing in various spectral regions of one polymer are comparable to those appearing in the spectra of other polymers in terms of frequency, intensity and IR dichroism. Further, the major bands in the spectrum of one polythioether are close in frequency not only to similar bands in the spectra of other polythioethers, but also to the major bands in the spectra of polyethers Fig. 5.5(a) and (b), (with the exception of certain bands probably arising from localized modes e.g. νC-S-C, νC-O-C). These major bands in the spectra of polythioethers and polyethers also seem to correspond to the vibrational bands of polyethylene (Fig. 5.6) i.e. those associated with the limiting frequencies of the $(CH_2)_m$ sequence [See Table 1.2].

Thus the spectral features of polythioethers with m = 4, 6 and 10, clearly indicate that these molecules take the same molecular conformation as associated with polythioether with m = 5, polyethers with m = 4, 6-10, 12 and polyethylene i.e. the planar zig zag one.

Further support to this fact may be obtained from a rather detailed analysis of the spectral features as given below.

It may be seen from Fig. 5.4 (a),(b) and 5.5 (a),(b) that apart from prominent bands observed in various regions of the spectra of each polymer as mentioned above, a series of weaker bands also appear in these spectral regions. The number of spectral bands in each region of these polymers, however, depends upon the number m. Thus, these series of bands may be regarded as arising from the frequency-phase relations of the adjacent methylene groups in the $(CH_2)_m$ sequences similar to the case of planar zig zag n-alkanes[62], and may similarly be called as "progression bands". The correspondence of the spectral regions in which these bands appear, to similar spectral regions of n-alkanes suggests the

following frequency ranges for them [See Table 1.2] .

C-C bending: 200 - 600 cm^{-1}

CH_2 rocking: 700 - 1050 cm^{-1}

C-C stretching: 950 - 1150 cm^{-1}

CH_2 twisting: 1170 - 1300 cm^{-1}

CH_2 wagging: 1300 - 1420 cm^{-1}

CH_2 deformation: 1420 - 1500 cm^{-1}

CH_2 stretching: 2800 - 3000 cm^{-1}

CH_2 rocking and C-C stretching modes

These progression modes have been found to be very sensitive to molecular structure[62]. Tadokoro et al have analysed the bands arising from IR-active CH_2 rocking modes of polythioethers with m = 5, on the basis of simply coupled oscillator model[92] . It was shown that the frequencies of these bands corresponded approximately to points on the dispersion curve for CH_2 rocking modes of the planar zig zag polymethylene chain calculated by Tasumi et al[63] (see Fig. 1.15). A similar approach to the progression bands arising from CH_2 rocking and C-C stretching modes of polythioethers with m = 4,6 and 10, and polyethers with m = 4 and 10, is worth considering.

Molecules with m = even and m = odd give rise to $\frac{n}{2}$ and $\frac{n+1}{2}$ IR active CH_2 rocking modes respectively[62,158]. On the other hand, these molecules give rise to a total of n-1 Raman and IR active C-C stretching modes[62,158]. The k values may be assigned to the observed bands approximately by counting their number in the appropriate spectral regions with regard to their intensity and IR dichroism, and taking into account the selection rules described in Table 1.2. A plot of the frequencies

of IR-active CH_2 rocking modes, and Raman and IR active C-C stretching modes against $\frac{\theta}{\pi} = \frac{k}{m+1}$ has been presented in Fig. 5.7(a) and (b) respectively. The k values assigned to the concerned bands, have been shown by numbers 1, 2, 3, etc. in Fig. 5.4(a) and (b). It is clear that analogous to the case of polythioether with m = 5, the progression bands in the CH_2 rocking and C-C stretching spectral regions of polythioethers with m = 4, 6 and 10 and polyethers with m = 4 and 10, correspond approximately to points on the frequency-phase curves (ν_8 and ν_4 respectively) of the polymethylene chain [Fig. 1.15].

It may be remarked that in the case of lower members, the interacting effect of S or O atoms seem to perturb the frequency-phase relations. This is reflected by the difficulty of assigning k values to the observed bands in these cases. This behaviour is, however, expected since the lower members of n-paraffins have been found to behave similarly[62].

C-C bending and torsional modes

The C-C bending and torsional modes are forbidden in the Raman spectrum of an infinite polymethylene chain whilst in the IR absorption they have zero frequencies[63]. Since polyethers and polythioethers have finite methylene sequences, the features due to these modes would appear both in their Raman and IR spectra.

Todokoro et al have analysed the IR active C-C bending and torsional modes of polyethers with m = 4, 6, 8-10, and 12, using the simply coupled oscillator model[155]. According to their results, the band progressions between ν550 - 300 cm^{-1} and ν250 - 150 cm^{-1} arise from C-C bending and C-C torsional modes respectively and correspond to ν_5 and ν_9 branches of the polymethylene chain calculated by Tasumi et al[63]. [See Fig. 1.15].

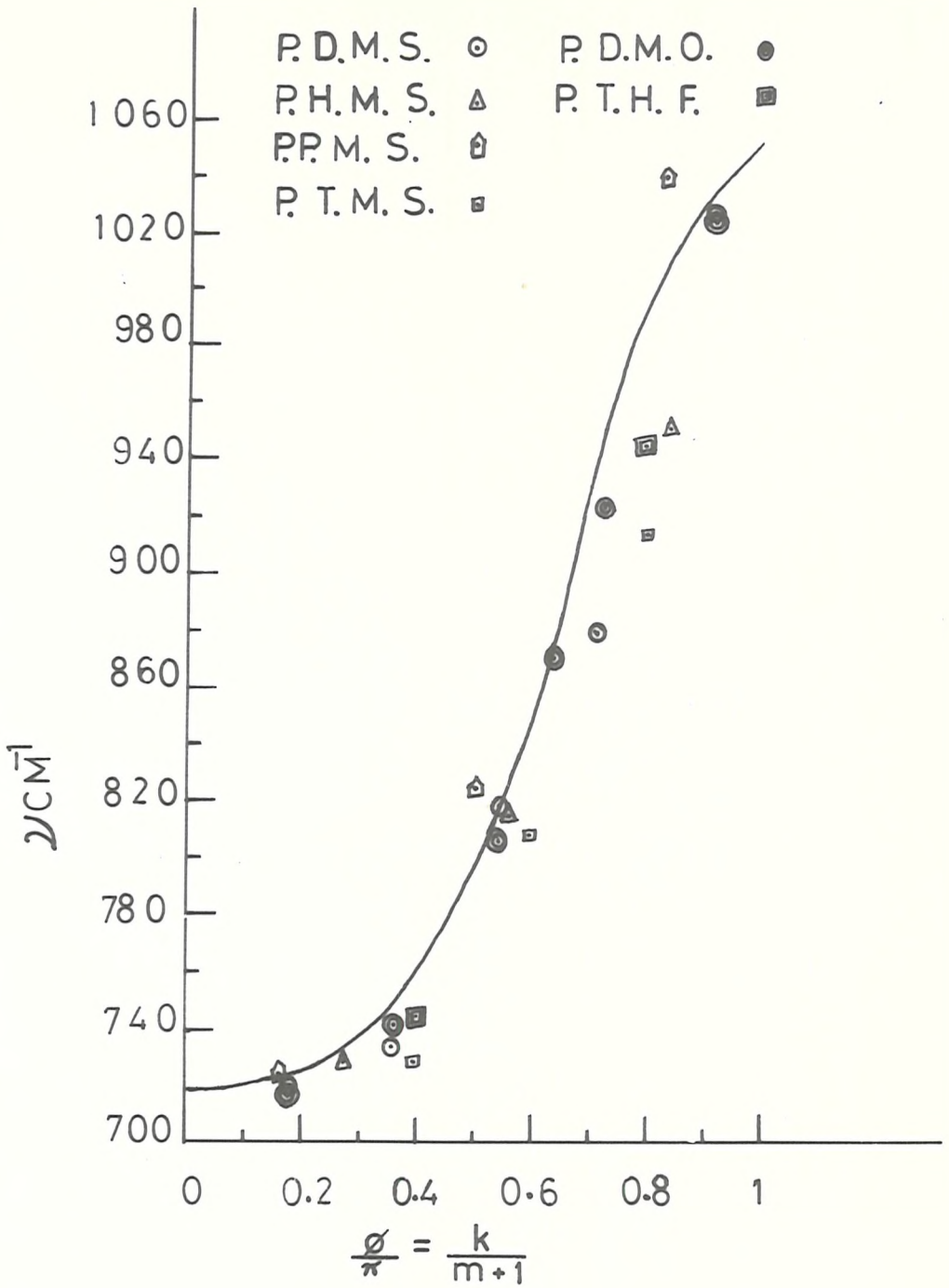

FIG. 5.7(a) FREQUENCY-PHASE CURVE FOR IR-ACTIVE CH_2 ROCKING-TWISTING MODES OF POLY-ETHERS & POLYTHIOETHERS

(Solid line of the curve represents ν_8 of polyethylene see Fig. 1.15)

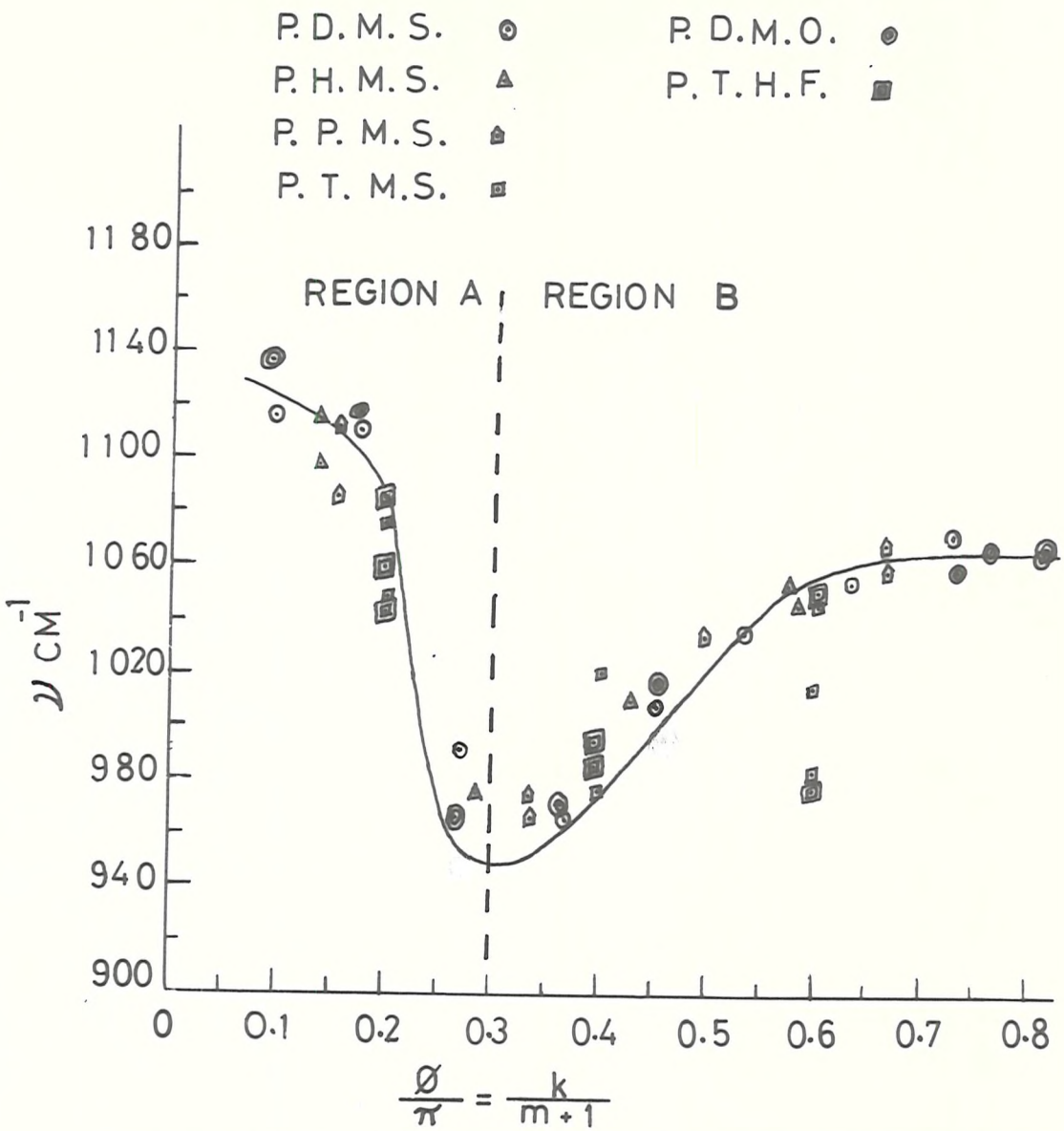

FIG.5.7(b): FREQUENCY-PHASE CURVE FOR C-C STRETCHING MODES OF POLYETHERS & POLYTHIOETHERS

(Solid line of the curve represents ν_4 of polyethylene see Fig. 1.15)

Raman spectra of polyethers with m = 4 and 10, and polythioethers with m = 4, 5, 6 and 10, also show progressions of bands in the above frequency ranges and may be regarded as arising from similar modes [Fig. 5.4(a),(b) and 5.5(a),(b)].

Localized modes

The behaviour of the modes associated with C-O-C bonds in polyethers and C-S-C ones in polythioethers, also reflects the molecular structure.

The stretching modes associated with these bonds cannot couple with CH_2 rocking modes when the conformation is planar zig zag[154]. Further, the C-O-C bond is more polar than the C-S-C bond. Thus the former would have a greater change in the transition moment than the latter and would give rise to stronger features in the IR spectrum. On the contrary the C-S-C bond would have a greater change in polarizability during the vibration than the C-O-C one, and would give rise to stronger feature in Raman spectrum. [See Section 1.3.1]

It seems, however, that molecular conformation does not perturb the frequency of the C-O-C stretching mode appreciably e.g. PTHF[154], POCB[153], PEO[142-146], POM[124-131], [See Sections 4.2 - 4.4 and 4.6 also] but it causes a considerable change in the frequency of C-S-C stretching modes as indicated in Sections 4.3, 4.5 and 4.7. [see reference 152 also]

A comparison of the frequencies of concerned modes is given below for the sake of convenience.

Molecule	$\Delta\nu/\nu$ cm^{-1}	Species	Mode
PTM (G_{18})	648	A_1	νCSC, δSCS
	735	A_2	νCSC
	708	E	νCSC
	671	E	νCSC, δSCS
PES(TG$\bar{G}$)	731	A_g	$\nu(CSC)_s - \delta(CCS)_s$
	760	B_g	$\nu(CSC)_a - \delta(CCS)_a$
	672	A_u	$\nu(CSC)_s + R(CH_2)_s$
	723	B_u	$\nu(CSC)_a + R(CH_2)_a$
	695	B_u	$R(CH_2)_a + \nu(CSC)_a$
PTrMS(G_4)	651	A_1	νCSC
	752	B_1	νCSC, RCH_2

Since the frequencies of C-S-C stretching modes of PES are higher than the frequencies of similar modes of PTM and PTrMS, it may be suggested that as the chain conformation straightens, the frequencies of these modes increase.

Polythioethers with m = 4,5,6 and 10, show strong and medium intensity doublets respectively in the following frequency ranges as shown in Fig. 5.4(a) and (b).

Raman: $\Delta\nu 775 - 755$ cm^{-1}

IR : $\nu 785 - 745$ cm^{-1}

The intensity, IR dichroism and the frequency ranges of both of these sets of bands indicate that they arise from C-S-C stretching modes. As usual the lower frequency band in each case may be assigned to the symmetric and higher frequency one to the asymmetric stretching mode[14]. This is also supported by the decreased parallel dichroism of the latter.

A considerable increase in the frequencies of both Raman and IR active C-S-C stretching modes indicate that the associated molecular conformation is probably planar zig zag.

The overall effect of C-O-C and C-S-C stretching modes on the spectra of polyethers and polythioethers respectively.

At this point it would be worth considering the cause of detailed differences in the spectra of corresponding members of polyether and polythioether series.

Although the spectra of both polyethers and polythioethers resemble more closely to that of polyethylene as m increases, Raman spectra of polyethers tend to be so more than those of polythioethers [See Fig. 5.4(a),(b) and 5.5(a),(b)]. Thus the Raman spectrum of polydecamethylene oxide seems to be a close copy of polyethylene. This difference arises basically from the electrical behaviour of C-O-C and C-S-C groups as mentioned above. Further, since the mass and potential of oxygen and carbon atom is similar, strong coupling between methylene sequences and oxygen atoms takes place and the polyether chain behaves like the polymethylene chain during vibration[155]. On the other hand, the mass and potential of the sulphur atom is widely different from that of the carbon atom which results in strictly frequency-phase modulated vibrations of the $(CH_2)_m$ sequences in polythioethers. Consequently the band progressions are highly developed even in higher polythioethers such as polydecamethylene sulphide, whereas these are weak or absent in the case of polydecamethylene oxide.

Finally it may be concluded from the above analysis that polythioethers with m = 4, 6 and 10 take planar zig zag conformations similar to the zig zag structures of polyethers with $m \geq 4$ and polypentamethylene sulphide.

Further, as m increases, the Raman spectra of polythioethers and polyethers with m $\geq$ 4 become closer and closer to that of polyethylene. This is especially so in the latter case i.e. polyethers.

Molecular group associated with the polythioether chain

As indicated earlier, the symmetry elements of planar zig zag polyether and polythioether chain would be those belonging to d_{2h} or c_{2v} symmetry groups, according to whether m = even or odd, respectively. Thus it should be possible to reasonably explain the Raman and IR spectra of corresponding molecules on the basis of factor group analysis. As expected, Raman and IR spectra of polythioether with m = 5, show several coincidences and the spectral features may be assigned to the symmetry species of the c_{2v} group, by considering coincidences, relative intensities and IR dichroism (Table 5.3).

The rule of mutual exclusion, however, should apply to Raman and IR spectra of polythioethers with m = 4, 6 and 10, since in this case, the molecular group is expected to be d_{2h}. Contrary to the expectation these spectra also show some coincidences. Apart from some coincidences of weak bands which may be attributed to irregular structures those due to more prominent ones are as follows:

PTMS		PHMS		PDMS	
Raman ($\Delta\nu cm^{-1}$)	IR(νcm^{-1})	Raman ($\Delta\nu cm^{-1}$)	IR(νcm^{-1})	Raman ($\Delta\nu cm^{-1}$)	IR(νcm^{-1})
1238,W	1241(∥)M			1111,VS	1113(∥)MW
1305,VS	1304(∥)VS	1304,M	1299(∥)MW	1300,VS	1291,M(∥) 1302,MW,Sh(∥)
1422,M	1425(∥)S	1438-42,VS	1439(∥)MS	1422,M	1425(∥)S
1455,VS	1452(⊥)VS	1456 , VS	1455(⊥)VS	1464,S	1466(∥,⊥)VS

These coincidences may be regarded as accidental since these are few in number and the frequencies of the concerned bands in Raman and IR progressions may be too close to be differentiated except by carrying out normal

Table 5.3

A proposed assignment of the prominent vibrational features of polypentamethylene sulphide

Raman ($\Delta\nu$ cm^{-1})	IR (ν cm^{-1})	Species	Approx. Mode
717,W	723,S, ⊥	B_2	$R(CH_2)$
734,W	728,S, ⊥	B_2	$R(CH_2)$
754,VS	751,W, ∥	A_1	$\nu_s(C-S)$
768,S	765,MW, ∥	B_1	$\nu_a(C-S)$
815 VW 829 VW	827,MW, ⊥	B_2	$R(CH_2)$
1032,M	-	A_2	$R(CH_2)$, $\nu(C-C)$
1054,M	1042-48,MW, ⊥	B_2	$R(CH_2)$, $\nu(C-C)$
1075-82,VS	1077,W, ⊥	A_1	$\nu(C-C)$
1239-43,M	1236-1241,S, ⊥	B_2	$T(CH_2)$
1278,W	1278 VS, ∥	B_1	$T(CH_2)$
1303,VS	1300 MW, ∥	A_1	$T(CH_2)$
1337,W	-	A_2	$W(CH_2)$
1347 MW	1346 MW, ⊥	B_2	$W(CH_2)$
1363-67,MW	1362 W, ∥	B_2	$W(CH_2)$
1422,M	1419 MW, ∥	B_2	$W(CH_2)$ or $\delta(CH_2)$
1436,MS	1433,S, ∥	B_2	$\delta(CH_2)$
1445,VS	1442,MS, ∥	A_1	$\delta(CH_2)$
1458,MW	1457,VS ⊥	B_1	$\delta(CH_2)$
1465,M	1464 VS, ⊥	B_1	$\delta(CH_2)$

Table 5.4

A proposed assignment of the prominent vibrational features arising from $(CH_2)_n$ sequences of polythioethers with m = 4,6 and 10 and polyether with m = 10.

PTMS m =4 ($\Delta\nu$/νcm^{-1})	PHMS m =6 ($\Delta\nu$/νcm^{-1})	PDMS m=10 ($\Delta\nu$/νcm^{-1})	PDMO m=10 ($\Delta\nu$/νcm^{-1})	PE[62,63,66] m =∞ ($\Delta\nu$/νcm^{-1})	Species	Mode
2907,vS	2893,VS	2886,VS	2886,VS	2883(2899)*		$\nu_a(CH_2)$
2866,M	2860,S	2863,S	2864,S	2848(2845)		$\nu_s(CH_2)$
1422,M	1421,W,Sh	1422,M,Sh	1419,M	1418(1437)	A_g	$\delta(CH_2)$
–	–	1139,W	1169,W	1168(1164)		$T(CH_2)$
1074,VS	1091,VS	1111,VS	1138,VS	1131(1127)		Skeletal
1359,M	1370,W	1366,MW	1373,W	1370(1408)		$W(CH_2)$
1305,VS	1304,MS	1300,S	1300,S	1295(1308)	B_{1g}	$W(CH_2)$
1046,MS	1059,S	1065,S	1064,MS	1061(1051)		Skeletal
1359,MW	1370,W	1372,MW	1373,W	1370(1413)		$W(CH_2)$
1288,W	1292,M	1300-12,VS	1286,M	1295(1303)	B_{2g}	$T(CH_2)$
1046,MS	1059,S	1065,S	1074,MS	1061(1051)		Skeletal
2907,VS	2893,VS	2886,VS	2886,VS	2883(2904)		$\nu_a(CH_2)$
2854,M	2850,MS	2854,S	2853,S	2848(2838)		$\nu_s(CH_2)$
1442,S 1451,VS	1438 1442 VS	1446,VS	1442,VS 1451,S	1441(1455)	B_{3g}	$\delta(CH_2)$
–	–	1139,W	1169,W	(1168)(1164)		$R(CH_2)$
1074,VS	1091,VS	1111,S	1138,S	1131(1127)		Skeletal
2924,VS,⊥	2933,VS, ⊥	2924,VS,⊥	2921,VS,⊥	2929(2919)		$\nu_a(CH_2)$
2838,VS,⊥	2851,VS, ⊥	2844,VS,⊥	2855,VS,⊥	2851(2874)	B_{1u}	$\nu_s(CH_2)$
1460,VS,⊥	1462,VS, ⊥	1466,VS,⊥	1485,S, ⊥	1473(1489)		$\delta(CH_2)$
728,VS,⊥	725-27,VS,⊥	733,M, ⊥	730,MS,⊥	731 (749)		$R(CH_2)$
2910,VS,⊥	2918,VS, ⊥	2912,VS,⊥	2920,VS,⊥	2929(2917)		$\nu_a(CH_2)$
2848,VS,⊥	2851,VS, ⊥	2844,VS,⊥	2855,VS,⊥	2851(2877)		$\nu_s(CH_2)$
1455,VS,⊥	1455,VS, ⊥	1457,S , ⊥	1462-66,VS,⊥	1463(1479)	B_{2u}	$\delta(CH_2)$

Table 5.4 (Contd)

728,VS,⊥	725-27,VS,⊥	719,VS,⊥	719,VS,⊥	720 (737)		$R(CH_2)$
1304,VS,∥	1262,VS, ∥	1226,S, ∥	1278,S, ∥ 1370,S, ∥	1175(1175)	B_{3u}	$W(CH_2)$
1181,S, ∥	1178,S, ∥	1179,M, ∥	1193,W, ∥	1050(1059)		$T(CH_2)$

* Calculated

coordinate analysis. This is further supported from the fact that such coincidences also exist in Raman and IR spectra of polydecamethylene oxide whose molecular group is known to be d_{2h} from X-ray diffraction analysis[52]. Nevertheless, it is not possible to make detailed assignments of the observed bands since only b_{3u} species have unique IR dichroism and the spectral behaviour of Raman bands is not predictable on the basis of the present data. However, since the molecular group of PE is also d_{2h}, the assignments of Raman and IR bands of PE may be correlated with the corresponding bands of these molecules, with regard to relative intensities and IR dichroism. A "close fit" of this type has been presented in Table 5.4. This indicates that the molecular group associated with polythioethers having m = 4, 6 and 10 is very likely to be isomorphous to the point group d_{2h}.

Further, it is clear that vibrational spectrum of PDMO also finds explanation on the basis of the factor group analysis under the molecular group d_{2h}.

5.3 Crystal structure and correlation band splitting

5.3.1 Introduction

As already stated, polyethers with $m \geq 4$ assume two types of packings of two molecular chains i.e. PTHF- or PE-type, depending upon the number m and the modes of preparation (see Table 5.1). Since in the PTHF-type lattice, two chains become equivalent by a simple translation, the Bravais unit cell or the spectroscopic unit cell is half the size of crystallographic unit cell thus containing only a single molecular chain. On the other hand, the spectroscopic unit cell is identical with the crystallographic unit cell in the case of the PE-type polyether. The space and line groups in both of these cases are related as follows:

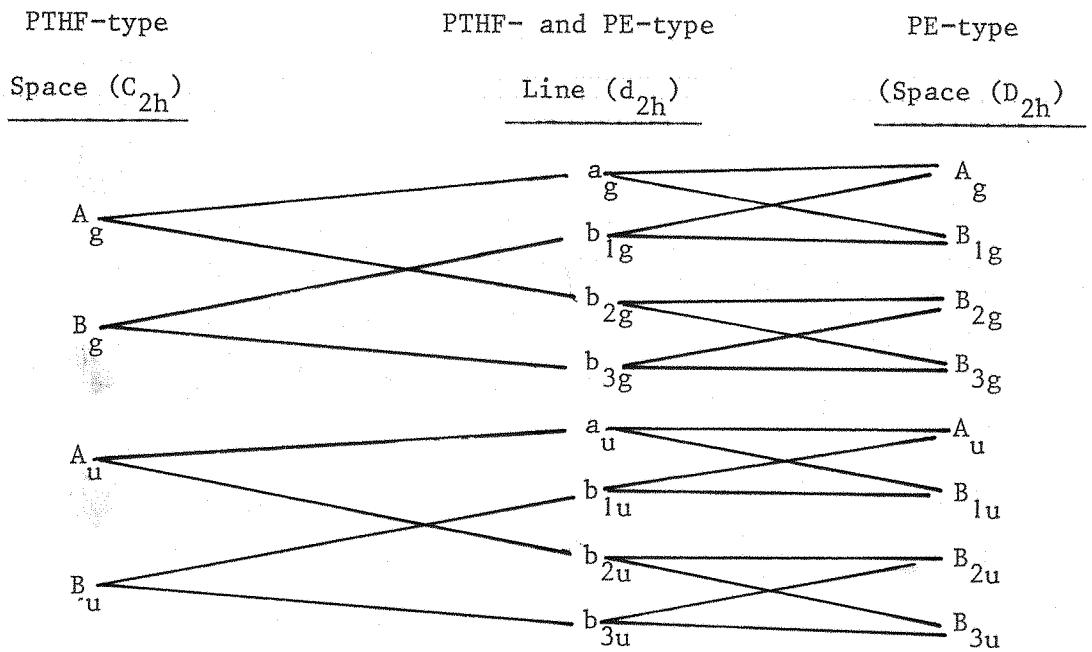

Consequently the spectral changes caused by the intermolecular interactions (correlation band splitting and appearance of the bands due to lattice vibrations) should be expected only in the polyethers of the PE type lattice. In fact, in the spectra of polyethers with m = 8,9,10 and 12 (PE-type), the doublet splittings of the IR-active CH_2 rocking modes have been observed at almost the same positions as in polyethylene[52] Further, the IR active skeletal torsional modes of these molecules between ν200-100 cm^{-1}, have also showed splitting. On the contrary, in the spectra of polyethers with m = 4,6 and 8 (PTHF-type), the band splitting has not been observed. The magnitude of splitting has been found to increase gradually with the number m (about 7 and 11 cm^{-1} in polyethers with m = 8 and 12 respectively).

The correlation effects in other parts of the vibrational spectra of polyethers have not been investigated as yet. These are expected to be similar to those observed in the case of polyethylene and n-paraffins because of the structural similarity of polyethers to the latter molecules.

As explained in the introductory chapter [Section 1.4.3c], the band shape in the CH_2 deformation region of Raman spectra of n-paraffins and polyethylene is of special significance, since it reflects 1 chain or 2 chains per unit cell structure.

Polythioethers with $m \geq 4$ have similar chemical and molecular structure as polyethers with $m \geq 4$. It is, therefore, to be expected [as argued in section 5.1] that the molecular packing of the former would also be similar to that of the latter i.e. PE- or PTHF-type.

So far, molecular packing of the polythioether with m = 5 only has been determined, which as already mentioned, is different from both the PE- and PTHF-type[92] . In the spectroscopic sense, however, it is also a 2 chain per unit cell structure, and would, therefore, show similar correlation effects as a PE-type polyether or polyethylene. This has been confirmed by the splitting of IR bands arising from CH_2 rocking modes into doublets[92] . Like polyethers, correlation splitting in the Raman spectrum of this molecule, however, has not yet been investigated.

Thus it may be concluded that if polythioethers with m = 4,6 and 10 (even) give rise to correlation band splitting, they would have similar crystal structure as polyethers with $m \geq 4$ (even) having 2 chains per unit cell i.e. PE-type. On the contrary, the absence of correlation splitting in their spectra would be indicative of a single chain per unit cell structure i.e. PTHF-type.

5.3.2 Results

PTHF and PDMO (polyethers): The CH_2 deformation and stretching regions of the Raman spectra of PTHF and PDMO are shown in Fig. 5.8(a) and (b) respectively at 25°C and -180°C.

PTMS, PPMS, PHMS and PDMS (polythioethers): Various regions of the Raman spectra and CH_2 rocking regions of the IR spectra of PTMS, PPMS, PHMS and PDMS are shown in Fig. 5.9(a),(b),(c) and (d) respectively at 25°C and -180°C. The corresponding data are collected in Table 5.5.

It is clear from Fig. 5.8(a) and (b), and Fig. 5.9(a),(b),(c) and (d), and Table 5.5 that either band splitting occurs or separation between the components of some doublets increases at -180°C in a number of cases in the spectra of all molecules except PTHF. As a result, a band near 1420 cm^{-1} occurs only in the spectra of PDMO, PTMS, PPMS, PHMS and PDMS. The vibrational behaviour of PTHF is peculiar under the influence of temperature, since the relative intensities of the bands near $\Delta\nu$1454-,1491- and 2869 cm^{-1} vary with temperature.

5.3.3 Discussion

PTHF and PDMO: The occurrence of a band near $\Delta\nu$1420 cm^{-1} in the spectrum of PDMO and its absence in that of PTHF in Fig. 5.8(a) and (b) indicates that correlation splitting occurs only in the case of PDMO. This view is further supported by the fact that separation between $\Delta\nu$ 1418- and 1442 cm^{-1} bands in the case of PDMO [Fig. 5.8(a)] increases at -180°C. Since doublet splitting has already been observed in the case of the IR-active CH_2 rocking modes of PDMO[52], the vibrational behaviour of this molecule seems to be connected with the factor group analysis of the space group D_{2h} [Section 5.3.1].

As expected, no band splitting has been observed in the case of PTHF because of the 1 chain per unit cell structure. Nevertheless, the relative intensities of the bands near $\Delta\nu$1454-,1493- and 2869 cm^{-1} vary as a function of temperature and the band near $\Delta\nu$1493 cm^{-1} increases in frequency by 3 cm^{-1} at -180°C. This behaviour may be explained on the

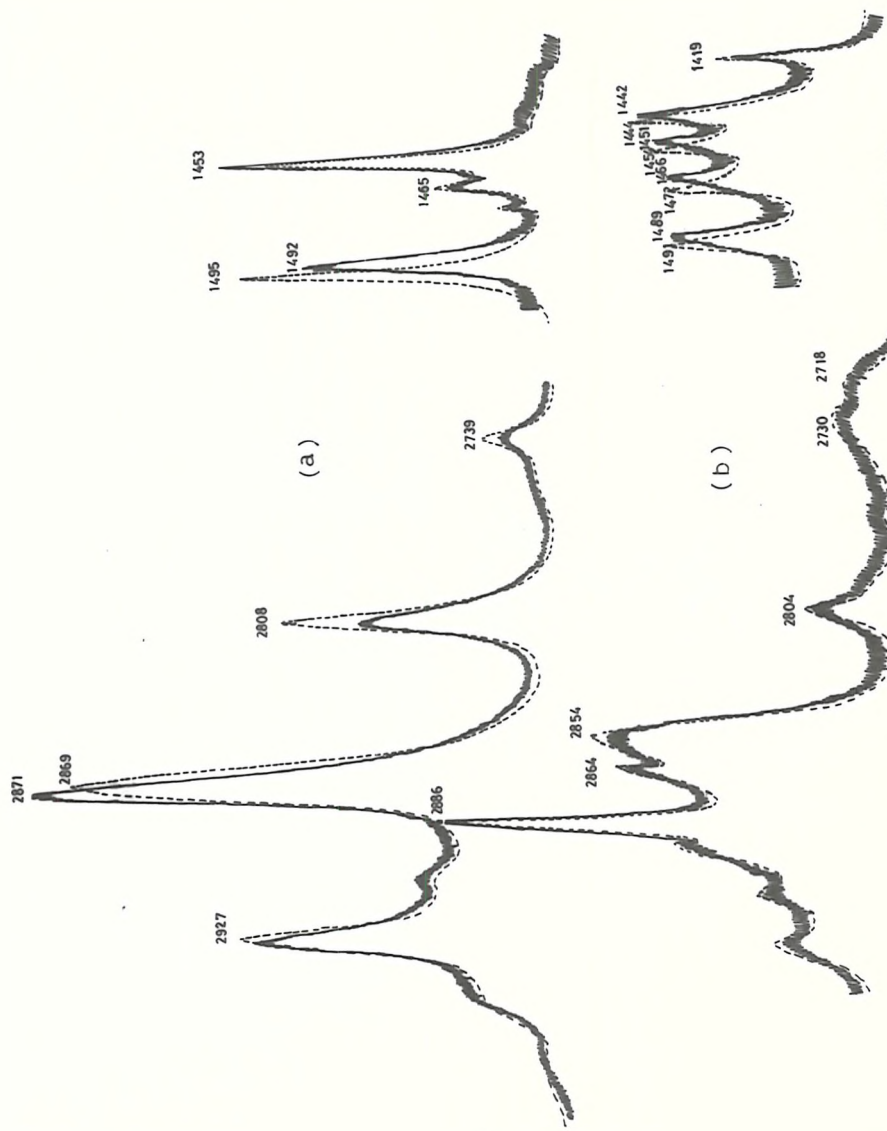

FIG. 5.8 : RAMAN SPECTRA OF(a) P.T.H.F & (b) P.D.M.O. AS A FUNCTION OF TEMP.
solid line(——): 25C
broken line(- - -): -180C

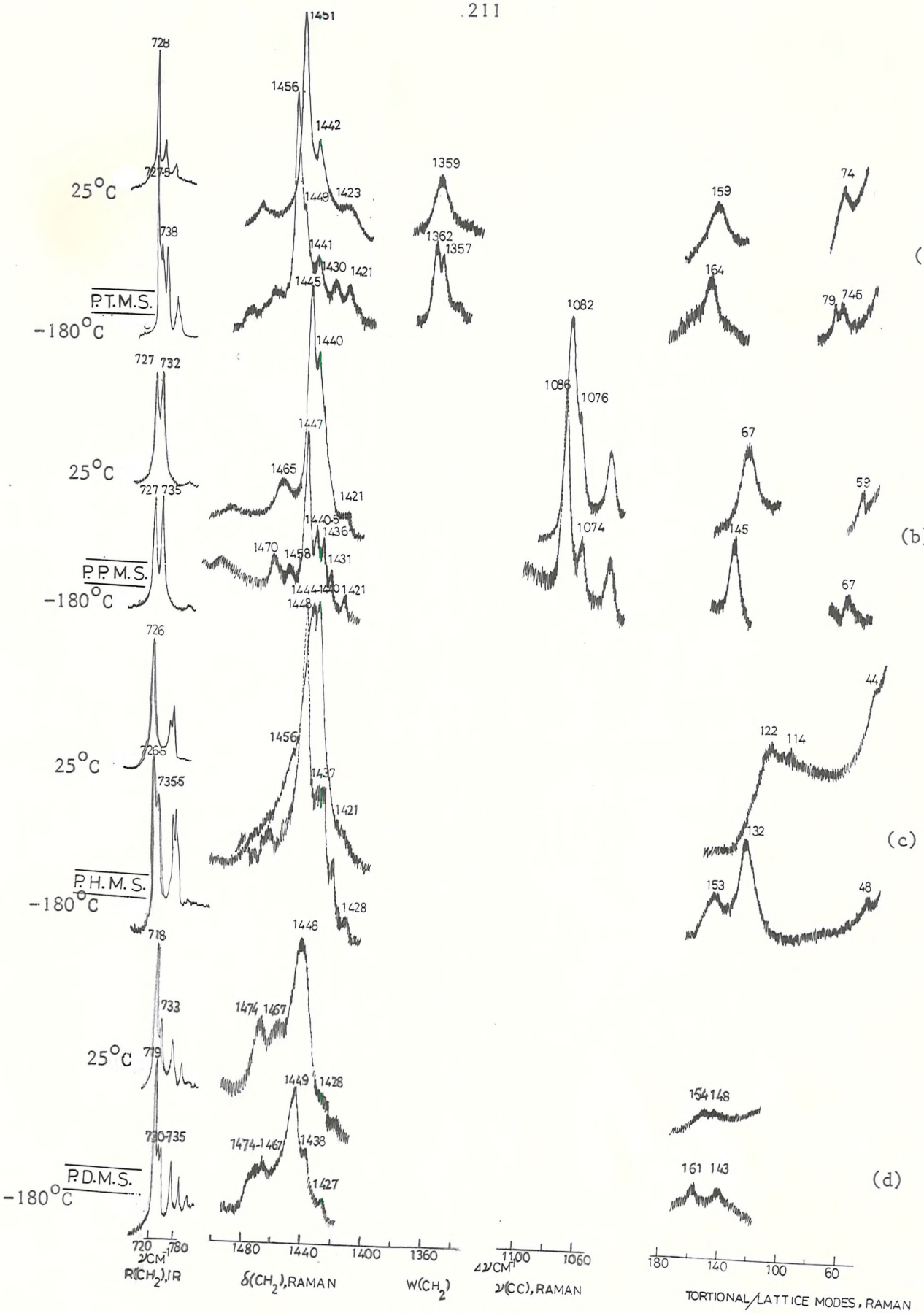

FIG. 5.9: VIBRATIONAL SPECTRA OF POLYTHIOETHERS AS A FUNCTION OF TEMPERATURE.

Table 5.5

Vibrational spectra of polythioethers with m = 4 (PTMS), 5 (PPMS), 6 (PHMS) and 10 (PDMS) as a function of temperature.

	Mode	PTMS $(\Delta\nu/\nu cm^{-1})$		PPMS $(\Delta\nu/\nu cm^{-1})$		PHMS $(\Delta\nu/\nu cm^{-1})$		PDMS $(\Delta\nu/\nu cm^{-1})$	
		25°C	-180°C	25°C	-180°C	25°C	-180°C	25°C	-180°C
Raman	δCH_2	1423	1421	1421	1421 1431 1436	1421	1418 1428	1428	1427
		1442	1438 1442	1440	1440.5	1440(16)[a]	1436 1448] 22 [a]	1448 14 [a]	1438 1448.5] 20 [a]
		1451(b)[a]	1449 1456] 8 [a]	1445(14)[a]	1447(4.5)[a]	1456			
					1458				
		1479	1471	1465	1470	1480	1472	1467	1467
			1486	1500	1504		1488	1474	1474
	WCH_2	1359(8)[a]	1357 1362] 10 [a]						
	ν C-C	-	-	1076 1082] 8 [a]	1074 1086] 7 [a]				
	Torsional or Lattice	159 69 69	163 76 76	137 59 59	145 67 67	114 122 44	132 153 48	154	143
IR	RCH_2	728(5)[a]	727.5 738] 6 [a]	727[b] 735[b]	727.5[b] 735[b]	726 728] 11 [a]	726.5 735.5] 19 [a]	718 733] 7 [a]	719 730 735] 13 [a]

(a) half band width (b) ref. 122

basis of the factor group analysis as follows:

The relationship between the line and space groups has been given in section 5.3.1. The line group symmetry is likely to be predominant at 25°C. Therefore, the bands at $\Delta\nu$1454- and 1493 cm^{-1} may be assumed to be of a_g and b_{2g} species respectively in view of their relative intensities. On the other hand, the space group symmetry is likely to be predominant at -180°C. In this case, the line group species $a_g + b_{2g}$ will transform to the space group species A_g thus giving rise to a strong band at $\Delta\nu$1496 cm^{-1} and weakening the intensities of the bands near $\Delta\nu$1454- and 1493 cm^{-1}. The decreased relative intensity of the strong band near $\Delta\nu$2869 cm^{-1} and its increased ½ band width from 13- to 16 cm^{-1} at -180°C also seems to reflect the same effect.

It is worth noting that the band shapes of the CH_2 deformation spectral regions of PDMO and PTHF resemble closely to those of the corresponding spectral regions of n-paraffins and polyethylene having 2 and 1 chain per unit cell structures respectively [See section 1.4.3c].

PTMS, PPMS, PHMS and PDMS: The band splitting observed in the case of these molecules [Fig. 5.9(a),(b),(c) and (d) and Table 5.5] may be attributed to interchain interactions and not to the increased resolution produced by cooling since:

(i) the components of some doublets show increased separation at -180°C e.g. skeletal stretching in PPMS and CH_2 rocking in PPMS and PHMS [Table 5.5].

(ii) the relative half band widths of those bands which split increases considerably at -180°C. On the other hand, the relative ½ band widths of those bands which do not split decreases at -180°C [Table 5.5].

(iii) A band near $\Delta\nu$ 1420 cm^{-1} occurs in all cases which is characteristic of correlation splitting in the CH_2 deformation regions of this type of molecule . Further band splitting in this region becomes increasingly complex at $-180^{\circ}C$, due to the joint effect of Fermi resonance and correlation splitting.

The observed correlation splitting may be explained on the basis of factor group analysis of the space group D_{2h} in the case of PTMS, PHMS and PDMS (m = even) and C_{2h} in the case of PPMS (m = odd) [Section 5.3.1 and Ref. 92]. According to this analysis, every line group mode should split into a doublet in the space group. Although band splitting in the CH_2 deformation regions seems to be rather complex due to the joint effect of Fermi resonance and correlation splitting, no band splits into more than two components in other spectral regions.

The correlation effects in the case of these molecules, however, seem to be somewhat different from those observed in the case of PDMO and other PE-type polyethers, and polyethylene as follows:

(i) The splitting of CH_2 rocking modes of polyethers and polyethylene has been observed even at $25^{\circ}C$, whereas corresponding splitting of polythioethers has been observed mostly at $-180^{\circ}C$. Nevertheless, the magnitude of splitting is about the same as in polyethers and polyethylene i.e. $\sim$ 10 cm^{-1}.

(ii) Similar to polyethers band splittings are fewer than in the case of polyethylene.

Among other similarities in the spectra of polythioethers, and polyethers, e.g. PDMO [Fig. 5.9(a-d) and Fig. 5.8(a) respectively], the band shapes in the CH_2 deformation regions are worth noting. The similarity of these band shapes together with the occurrence of a common

feature near $\Delta\nu 1420\ cm^{-1}$ is also suggestive of the 2 chain per unit cell structure

5.4 Polymorphism in polyethers and polythioethers with $m \geq 4$.

5.4.1 Introduction

Tadokoro et al[52] studied the polymorphism in polyethers with $m \geq 4$ i.e. partial transformation of the PTHF type structure to PE type and vice versa under the conditions of melt and solution crystallization given in Table 5.1, using X-ray diffraction patterns and IR spectra. As the transformation proceeded, both the X-ray diffraction patterns and IR spectra showed characteristic variations.

It is worth investigating if annealing would have a similar effect on the transformation of crystal structure in polyethers.

Like polyethers, polythioethers e.g. PTMS, PHMS and PDMS may also show structural transformation or polymorphism under similar conditions.

5.4.2 Results

PDMO: The CH_2 rocking and deformation regions of the IR spectrum, and CH_2 deformation and stretching regions of the Raman spectrum of PDMO are shown in Fig. 5.10(a) and (b) respectively as a function of annealing temperature (T_{ann}).

Further, the X-ray counter curves at similar annealing temperatures are presented in Fig. 5.10(c).

PTMS, PHMS and PDMS: Fig. 5.11 shows CH_2 deformation regions of the Raman spectra and CH_2 rocking and deformation regions of the IR spectra of these molecules as a function of crystallization from solution and annealing close to T_m.

Further, the X-ray counter curves listed below are presented in Fig. 5.12 for a comparative study.

(a) PTMS, PHMS and PDMS

(i) Crystallized from solution

(ii) Annealed close to T_m

(b) (i) Polyethylene[50] and orthorhombic and monoclinic n-paraffins[160] (2 chains per unit cell structures)

(ii) PTHF[51] and a triclinic n-paraffin[160] (1 chain per unit cell structures)

The data from Fig. 5.12(a) and (b) are summarized in Table 5.6.

Since no variation occurs in the vibrational spectrum or X-ray diffraction curve of PPMS under similar conditions, corresponding data for this polymer have not been included.

5.4.3 Discussion

PDMO

It is clear from Fig. 5.10 (a) and (b), that the correlation doublets observed in various spectral regions merge into singlets as the temperature of annealing increases. A similar effect seems to occur on rolling as well, though a rather detailed study is required in this case. Further, annealing close to T_m i.e. 75°C results in a complete disappearance of the correlation effects as indicated by the complete loss of the 1418 cm^{-1} band in Raman spectrum and simplification of the CH_2 rocking and deformation regions of IR spectrum. Thus it may be concluded that the PE-type structure of PDMO gradually transforms to the PTHF-type as T_{ann} increases and a complete transformation to the latter type occurs on annealing very close to T_m. This is supported from the characteristic variations in the X-ray counter curve which finally resembles that of PTHF-type [see Fig. 10(c)].

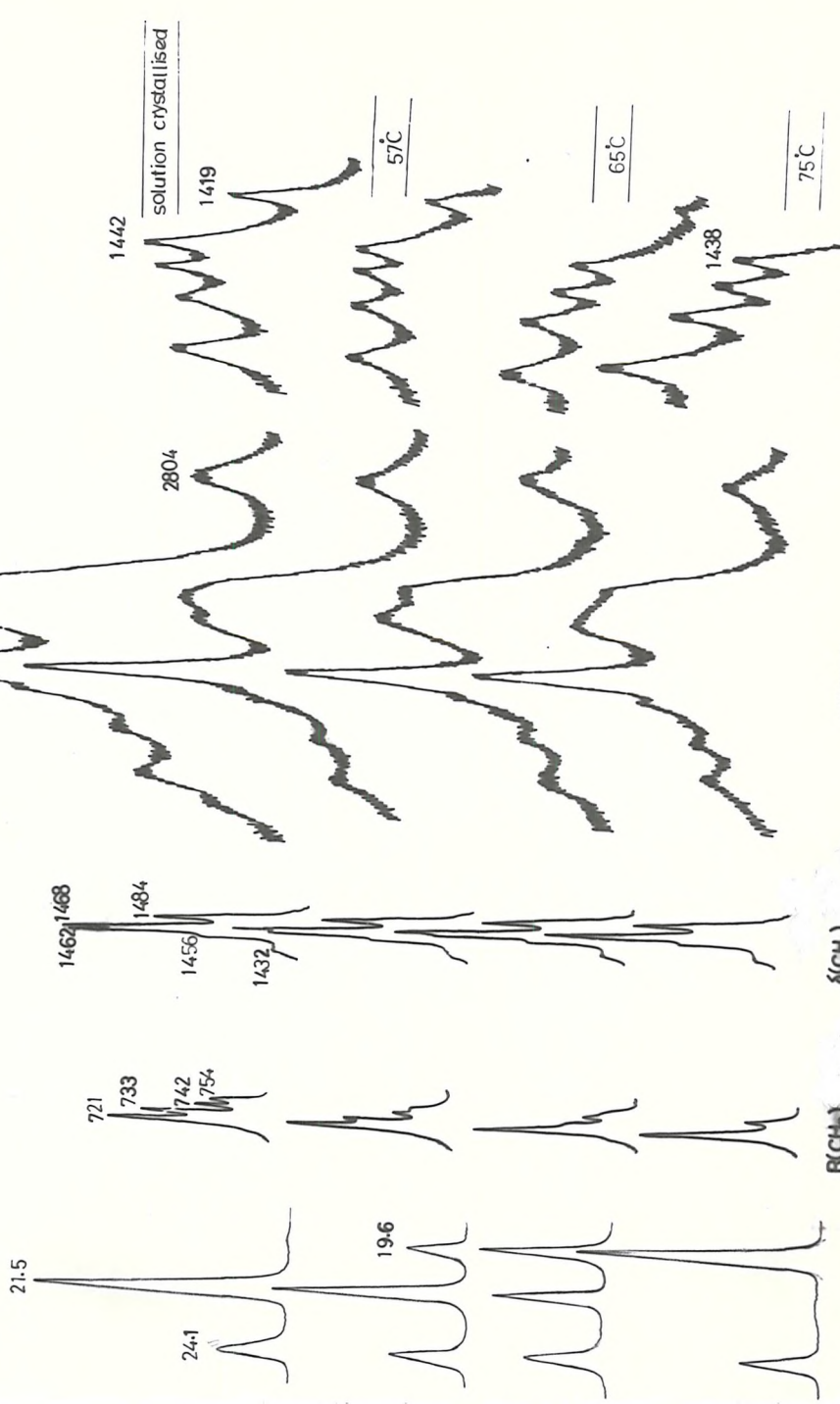

FIG. 5.10 IR (a) AND RAMAN (b) SPECTRA, AND X-RAY DIFFRACTOGRAM (c) OF PDMO AS A FUNCTION OF T_{ann}

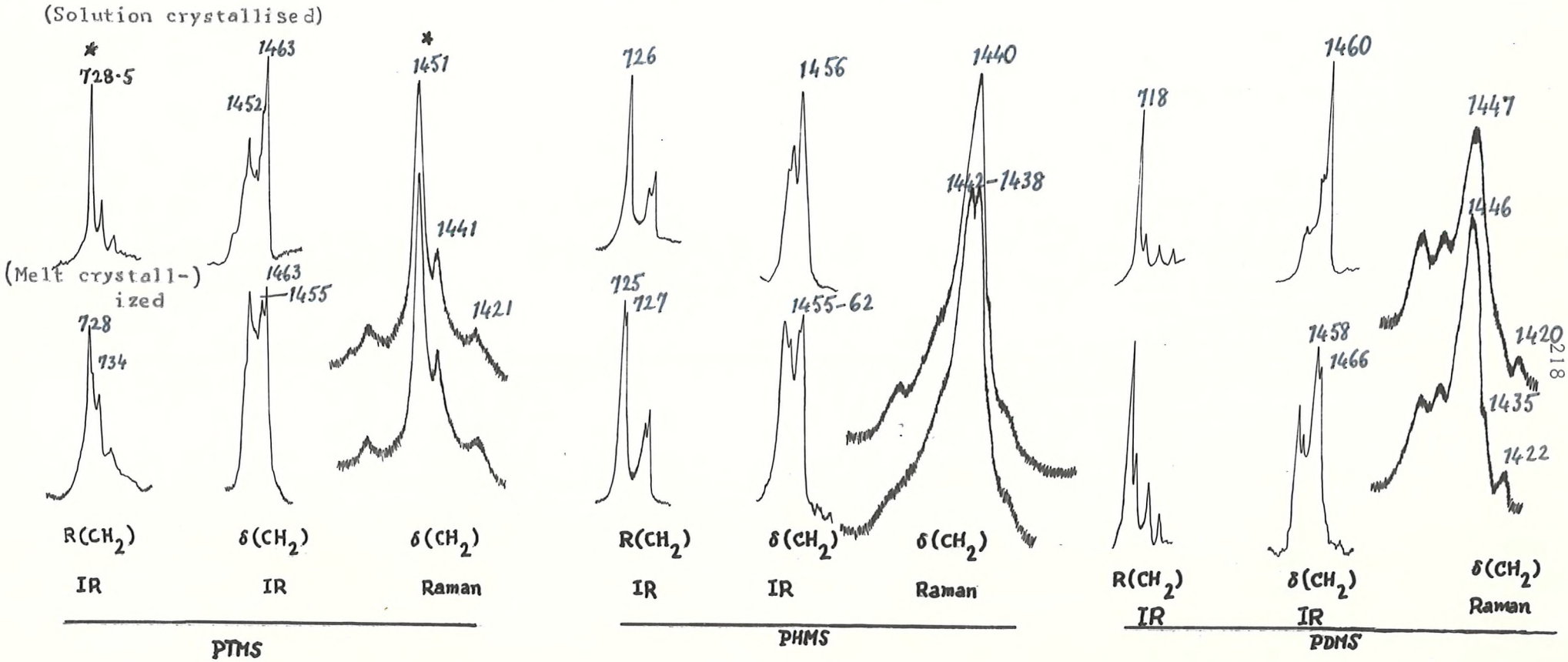

FIG. 5.11 PARTIAL IR AND RAMAN SPECTRA OF PTMS, PHMS AND PDMS AS A FUNCTION OF SOLUTION CRYSTALLIZATION AND MELT-CRYSTALLIZATION

* $\nu/\Delta\nu$ cm^{-1}

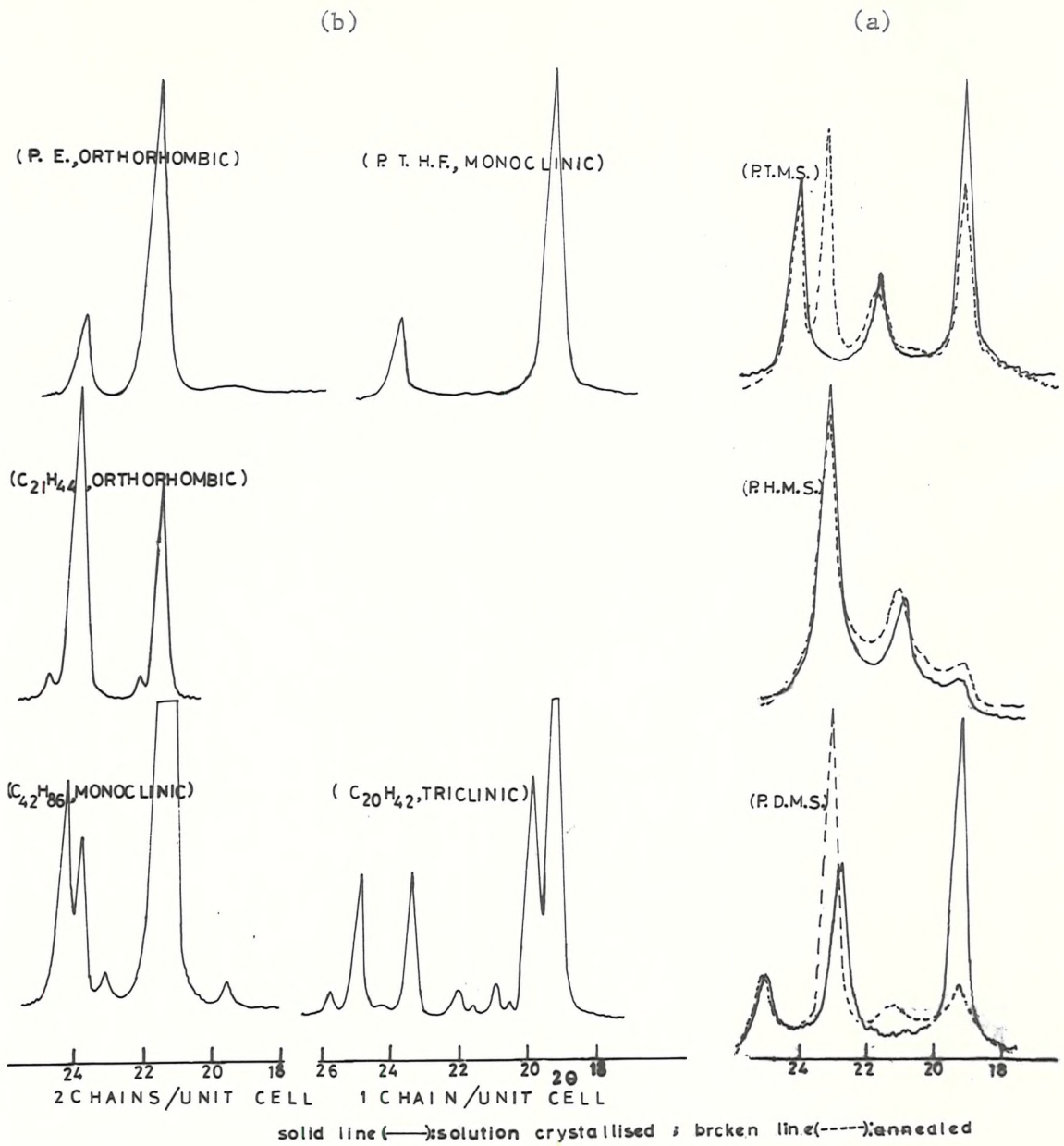

FIG. 5 12: X-RAY DIFFRACTION CURVES OF THE MOLECULES WITH 1&2 CHAINS/ UNIT CELL STRUCTURES&OF POLYTHIOETHERS

Table 5.6

(a) Main X-ray peaks for polythioethers i.e. PTMS, PHMS and PDMS crystallized from solution and annealed close to T_m.

(b) Crystallographic data and main X-ray peaks for polyethylene, n-paraffins and PTHF.

(a)

Molecule	Crystallized from Solution (2θ)	Annealed (2θ)
PTMS	19.4(S), 21.8(W),24.2(MS)	19.4(M),21.9(MW),23.4(S),24.2(M)
PHMS	194.(W),21(MW),23.2(W),∿25(VW)	19.4(W),21.2(MW),23.3(S),∿25VW
PDMS	194.(S),22.9(MS),∿25(W)	19.4(W),23.2(S), ∿25(W)

(b)

Molecule	Crystal type and space group	Chains/ unit cell	2θ
PE	Orthorhombic - D_{2h}	2	21.8(S),23.9(M)
$C_{21}H_{44}$	Orthorhombic - D_{2h}	2	21.5(M),23.8(S)
$C_{42}H_{86}$	Monoclinic - C_{2h}	2	19.6(VW),21.4(S), 23.9(MW),24.2(M)
PTHF	Monoclinic - C_{2h}	1	19.4(S),23.9(M)
$C_{20}H_{42}$	Triclinic - C_2 or C_1	1	19.3(S),23.4(M), 24.9(M)

Recently Balt Kaleja et al[159] have carried out similar studies on PDMO using the X-ray diffraction method. Their findings partly support the present conclusions.

PTMS, PHMS and PDMS

It is clear from Fig. 5.11 that the spectral regions which show correlation splitting at -180°C [See Fig. 5.9 (a-d) and Table 5.5] , also show splittings on annealing close to T_m. The splittings in the latter case are, however, fewer than in the former. Melt crystallization and rolling also seem to cause similar effect. Further, correlation splitting appears to decrease as m increases e.g. in the case of PDMS. This tendency reflects a decreasing content of the 2 chain per unit cell structure in higher polythioethers as m increases.

These results are further supported from an empirical assessment of the X-ray counter curves shown in Fig. 5.12(a).

A comparison of the X-ray counter curves [Fig. 5.12 (b)] and corresponding crystallographic data in Table 5.6(b) for polytheylene n-paraffins and PTHF indicates that characteristic modes of crystallization in these molecules give rise to the following unique peaks:

Crystal Type	Chains/unit cell	2θ
Orthorhombic or PE-type	2	∿21.6(S-M),∿24(M-W (1 peak)
Monoclinic	2	∿21.6(S-M),∿24(M-W (2 peaks)
PTHF-type	1	∿19.4(S)
Triclinic	1	∿19.4(S),∿25(W)

When these results are compared with the X-ray counter curves of PTMS, PHMS and PDMS and corresponding data in Table 5.6 (a), the following conclusions may be drawn:

	PTMS	PHMS	PDMS
(Solution crystallized)	PE- + PTHF-type	PE- +Triclinic-type	Triclinic-type
(Annealed or melt crystallized)	PE- + PTHF- + Triclinic-type	PE- + Triclinic-type	Triclinic- + PE-type

These observations indicate a reverse crystallization behaviour of polythioethers in comparison with polyethers. Whilst the former seem to crystallize preferably into a 2 chain per unit cell structure on annealing or melt crystallization, the latter crystallize preferably into a 1 chain per unit cell under similar conditions. Further, the ratio: $\frac{\text{2 chains per unit cell}}{\text{1 chain per unit cell}}$ seems to decrease with m in poly--thioethers whilst it increases with m in polyethers.

5.5 Final conclusion

Polythioethers with m = 4, 6 and 10 i.e. PTMS, PPMS and PDMS, assume planar zig zag conformation which belongs to the symmetry group d_{2h}.

They seem to show polymorphism having 2 or more types of coexisting crystal structures. The contents of the coexisting structures seem to vary with m as well as with the conditions of crystallization e.g. solution and melt crystallizing, annealing and rolling. Generally 2 chain per unit cell structure is predominant for the lower members whereas 1 chain per unit structure predominates in the case of higher members. The factor group of the space group seems to be isomorphous to the point group D_{2h} in the case of 2 chain per unit cell structures.

The transformation of the PE-type structure into the PTHF-type in PDMO may be controlled by annealing at various temperatures below T_m, and a complete transformation from the PE- to the PTHF-type structure

may be affected by annealing at or very close to T_m. Rolling also causes the transformation of the PE-type structure into the PTHF-type.

PPMS does not show polymorphism.

The vibrational spectra of polythioethers with m = 4-6, and 10 and polyethers with m = 4 and 10 find reasonable explanation on the basis of the factor group analysis. The correlation splitting in polythioethers with m = 4,6 and 10 becomes prominent only at cryogenic temperature thereby reflecting weak interchain interactions.

CHAPTER VI

INVESTIGATION OF CRYSTALLINE LAMELLAR STRUCTURE IN POLYETHERS AND POLYTHIOETHERS (m = 1 - 10) USING LOW FREQUENCY RAMAN SPECTRA

6.1 Introduction

In the last two chapters, the so called internal and external modes of polyethers and polythioethers with m = 1-6, 10, were considered whilst little attention was paid to longitudinal acoustic modes of their crystalline lamellar structures. The study of LA vibrations of these polymers is significant not only to demonstrate the potentiality of Raman technique for such measurements but also because lamellar structures of these polymers are unknown in most cases.

In the introductory chapter, LAM frequencies of n-paraffins and polyethylene were discussed to show how these could be related to the chain length in the case of n-paraffins and to the chain stem length between the folds in the case of polyethylene using equation 1. The relation between the chain stem length thus derived and the LAXD long spacing was also discussed briefly.

When passing on to other polymers different from polyethylene chemically as well as conformationally, it should be realized that low frequency Raman bands can appear due to a variety of reasons. The present discussion is, however, concerned with those bands only which are associated with the physical parameters of the crystal thickness and not with the chemical nature of the molecule or with the crystal lattice intrinsically. In the search for a suitable material, equation 1 should be of guidance. In order to have a ν value as large as possible to facilitate its detection for the L values in the range of the usual crystal lamellae, E the Young's modulus should be large. Polyethylene is one of the most favourable materials in this respect; because of the planar zig zag conformation of the chain within the crystal coupled with a low value of ρ, it should give a high frequency per unit chain length easily detectable with the present technique. Conditions are expected to be less favourable for polymers with lower chain moduli such as

pertain to helical conformations where correspondingly lower frequencies are expected for identical L values.[190]

Owing to these reasons, the existing reports on the observation of LA modes in polymers other than polyethylene were very scarce at the start of this work. Calculations exist for the α helix of poly-l-alanine,[157,161] but no experimental confirmation has been quoted. Olf and coworkers[78] reported their failure to observe LA modes in several polymers. Keller et al[86] have recently obtained some results on a low melting polyester-polydecamethylene sebacate. On the other hand, a low frequency band has been observed at low temperatures in cis 1-4 polybutadiene at $\Delta\nu 3\text{-}5$ cm^{-1}, depending upon the sample treatment.[162]

Polyethers and polythioethers of the series $\{(CH_2)_m\text{-}Y\}_n$ may be viewed as suitable and promising materials for this study because of their chemical resemblance to polyethylene. Lower members of these series ($m \leq 3$), however, have helical conformations and high densities (see Table 4.1), and are, therefore, not likely to conform to the requirements of equation 1. On the other hand, higher members with $m \geq 4$ are close to polyethylene chemically as well as structurally. Since their crystal structures and the densities resemble that of polythylene (see Chapter 5 and Table 4.1), the LAM frequencies associated with the straight stems of lamellae should not be substantially different from those pertaining for polyethylene of identical stem lengths.

6.1.1 The influence of specific chemical nature on the fold length value

Since planar zig zag polyethers and polythioethers are chemically different from polyethylene, it is possible that their chemical nature would have a marked influence on the fold length values. Keller et al[163] have shown in a series of recent studies that chain folding in polyamides

crystallized in solution can be influenced by the specific chemical groups situated along the chains thus giving rise to characteristic fold length values. Nevertheless, only those fold length values would be permitted which are compatible with the crystal structure[164]. The specific chemical nature of the end groups can also strongly affect the folded crystal structure in short chain molecules[165]. For example, polar groups tend to build up associations of regularly arranged chain ends inducing a sharply folded structure whereas bulky end groups which are not capable of forming chemical associations are rejected as cilia from the crystalline lamellae giving rise to rather disordered layer surfaces.

The planar zig zag polyethers and polythioethers exist as follows due to their method of preparation [see section 2.6.1]:

$$X\left[Y\text{-}(CH_2)_m\right]_n YX \qquad \begin{matrix}(Y = O \text{ or } S)\\(X = H \text{ or } Na)\end{matrix}$$

(a)

The fractions of (a) with various number average molecular weights (Mn) offer the double feature of a model with (i) an n distribution of chains of varying lengths with two YX end groups and (ii) a specific regular distribution of chemical groups (O or S atoms) situated along the main chain. Thus the effects associated with short chains having end groups and specific chemical nature may be reflected in the fold length values of these polymers. As regards the effect of crystal structure, (a) crystallizes in 1 or 2 chains per unit cell structures [see Table 5.1 and Section 5.3.1]. Since the value of the fibre period is the same for both crystal structures[52], the influence of crystal structure on the value of fold length is likely to be similar in both cases.

Recently the chain folded structure of PDMO has been investigated using the LAXD method with the above implications in mind[166]. Four fractions of PDMO having molecular weights $\bar{M}_n$ = 1358, 1503, 2906 and 4074

were examined. All the fractions exhibited various coexisting characteristic values of L_x which were independent of the crystallization temperature and the molecular weight. The conspicuous intensity changes with the crystallization or annealing temperature and eventual disappearance of certain diffraction peaks, however, indicated that the population of crystals with larger fold length values gradually increased at the expense of the population of crystals having smaller fold length values, as a function of crystallization or annealing temperature.

The characteristic long period (L_x) was explained on the basis of a model involving a regular chain folded structure, which preserved the unit cell. (Fig. 6.1) According to this model, the L_x in (Å) fits with the assumption $L_x = 13.75 \times n\ (L_c) + 8(2L_f)$ [see Section 1.4 for the definitions of L_c and $2L_f$] where n represents the number of monomeric units across the crystal, 13.75 Å is the length of one repeating unit and 8Å is the contribution of the interlamellar gap plus fold. The packing of stems according to this model, has an alternate sequence of n and n-1 extended monomeric units yielding a layer thickness equal to the length of n monomers. This packing mode excludes the oxygen atoms from the folds and assumes a well defined 3-dimensional superstructure of these atoms within the lattice. Further, the chain ends are not excluded from the crystal lattice.

In view of the chemical and structural similarity of PDMO to planar zig zag polyethers and polythioethers, they are expected to have a similar chain folded structure.

6.1.2 This study

The chemical and structural implications discussed above, form an interesting basis for the study of lamellar structures of polyethers and

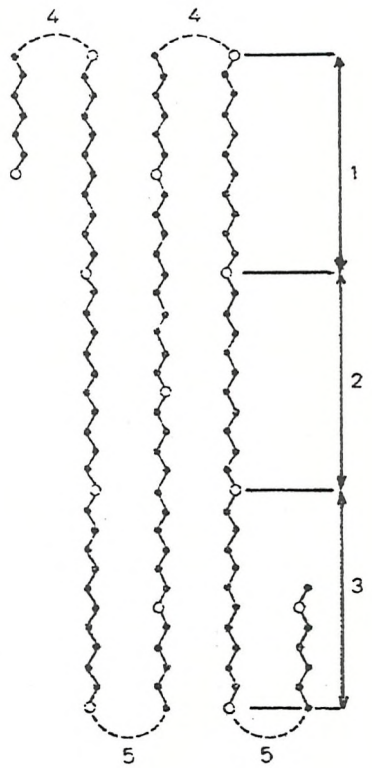

FIG. 6.1[166] CHAIN FOLDED STRUCTURE OF PDMO

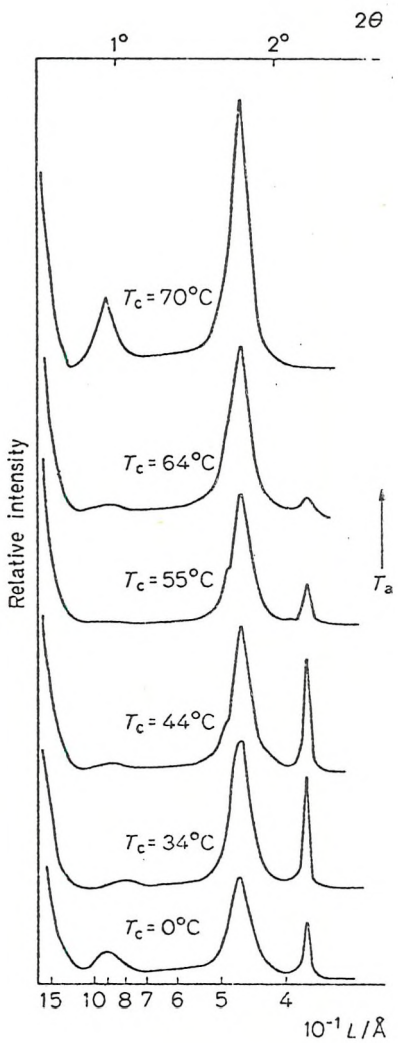

FIG. 6.5[166] LOW ANGLE X-RAY DIFFRACTOGRAM OF PDMO (Solution crystallized) AS A FUNCTION OF T_{ann} (T_c).

polythioethers. Thus crystallization in polyethers and polythioethers with m = 1-6, 10, which include both helical and planar zig zag molecules has been investigated in this study using the Raman technique.

Solution crystallized and in some cases melt quenched specimens were annealed for 3 hour-durations unless stated otherwise. The frequency of LA mode in the case of planar zig zag molecules has been correlated to the chain stem length using equation 1 with a Young's modulus value similar to that of n-paraffins and polyethylene i.e. $3.58 \pm 0.25 \times 10^{12}$ dynes/cm^2. The chain lengths thus computed henceforth called Raman lengths (L_R)* have been compared with those derived from LAXD long spacing (L_x) wherever possible.

An increase in lamellar thickness is usually accompanied with a subsequent increase in the degree of crystallinity thus causing a simultaneous increase in density and T_m as well. The variations achieved in lamellar thickness as a function of annealing temperature (T_{ann}) have, therefore, been further substantiated from the measurement of density and D.S.C. derived melting points (T_m).

The results have been discussed under the following main titles:

1 Polyethers with m = 1-4,6,10

2 Polythioethers with m = 1-6,10

6.2 Results and discussion

6.2.1 Polyethers with m = 1-4,6,10

6.2.1a m = 1-3

Polyethers with m = 1-3 give rise to a number of low frequency bands, nonetheless they are not attributable to LA modes because of their indifference towards thermal treatment (see Chapter 4).

* $L_R = L_c$ (see Section 1.4)

6.2.1 b m = 4,6,10

The low frequency Raman spectra of PTHF, PHMO and PDMO have been shown in Fig. 6.2, 6.3 and 6.4 respectively and the corresponding data have been summarized in Tables 6.1, 6.2 and 6.3.

Table 6.1

Low frequency Raman data of PTHF

Sample	T_{ann} (°C)	$\Delta\nu$ cm^{-1}		L_R (Å)	*L_x (Å)
		25°C	-180°C		
Solution crystallized	-	29,M	29.5 M	113	164
Bulk material	-	20,VS	20.5,VS	154	235
		56,W,B	∿60,W,B		
		96,W,B	∿100,W,B		
"	38	No change	-		
Melt quenched in liquid N_2	-	30	-	106	-
"	25 (for 7 days)	25	-	123	

* Please see Chapter 2 (section 2.8)

Table 6.2

Low frequency Raman data of PHMO

Sample	T_{ann} (°C)	$\Delta\nu$ cm^{-1}		L_R (Å)	L_x (Å)
		25°C	-180°C		
Solution crystallized	-	32	32.5	97	100
"	48, for 24 hours	20	-	156	168
					-

Table 6.3

Low frequency Raman data of PDMO

Sample	T_{ann} (°C)	$\Delta\nu$ cm^{-1} 25°C	$\Delta\nu$ cm^{-1} -180°C	L_{oR} (Å)	L_{ox} (Å)	* $\sim n$
Solution crystallized	-	21,W,Sh	-	153		
		32,S,B	~33	98	102	7 11
		59,W	~59	54	65	4
		78,W	~79	41	47	3
"	57	17,W,Sh	-	188	-	
		29,S	-	110	118	8 14
		62,W	-	52	65	4
		75,W	-	42	47	3
"	64	15.5,S	-	206	-	15
		25,M	-	128	-	9
		48,W	-	67	-	5
		64,W	-	50	65	4
"	68	~15,S	-	213	-	15
		~24,W	-	134	-	10
		41,W	-	78	90	6
"	75	12.5,S	-	265	-	19
		23,W	-	139	-	10
		52,W	-	62	65	4

* n = number of repeating units.

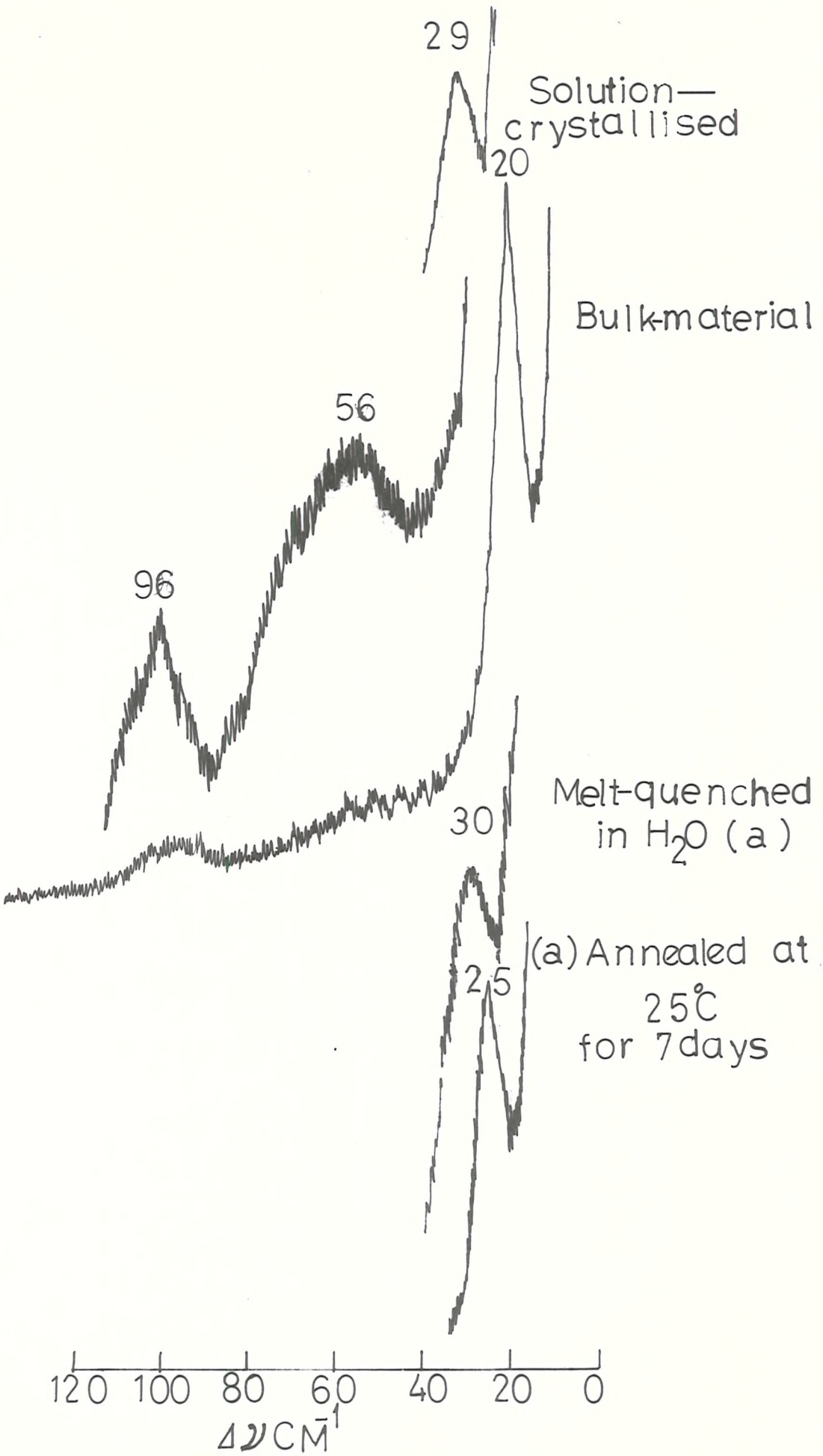

FIG. 6.2 LOW FREQUENCY RAMAN SPECTRA OF PTHF

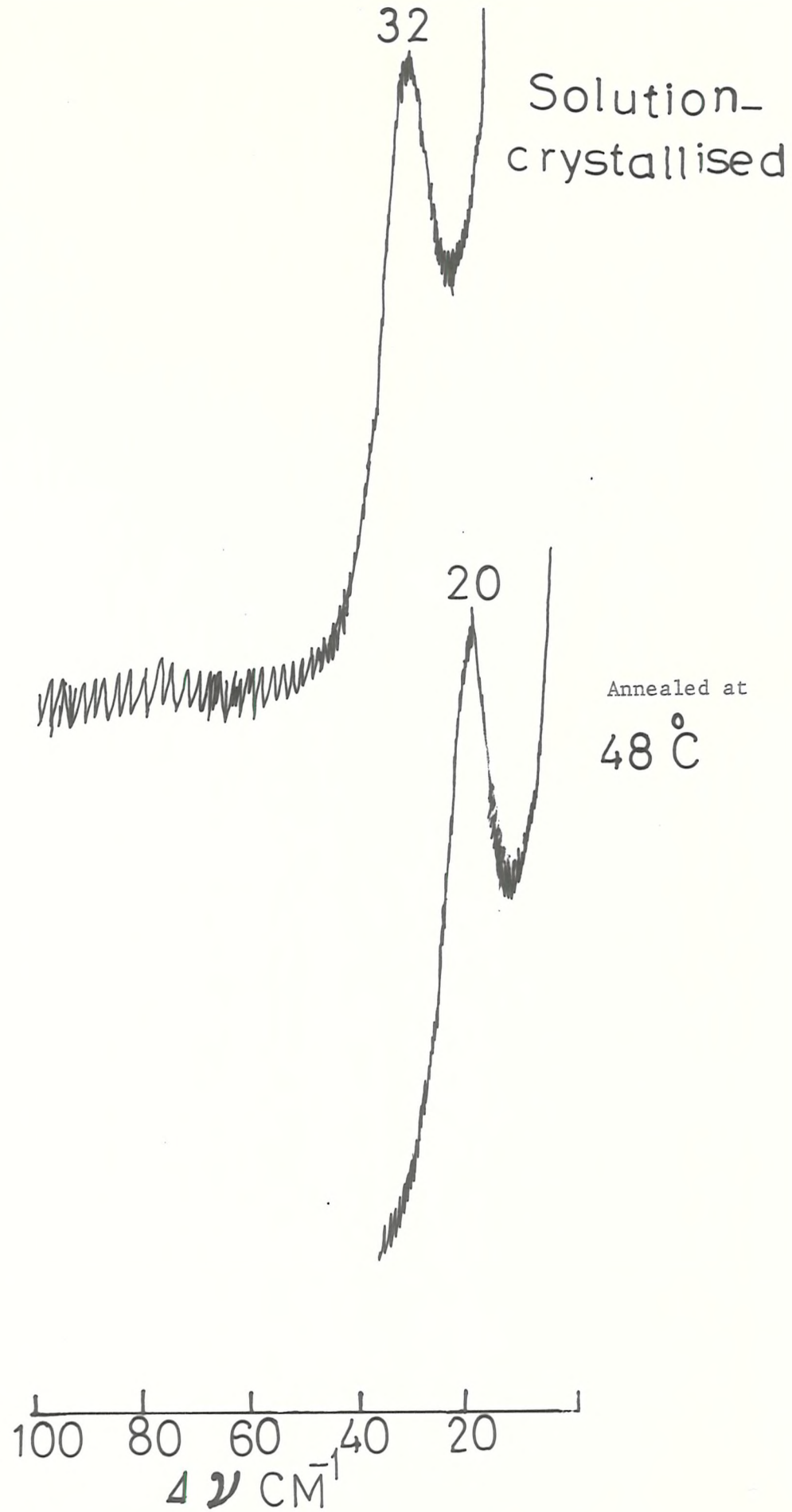

FIG. 6.3 LOW FREQUENCY RAMAN SPECTRUM OF PHMO

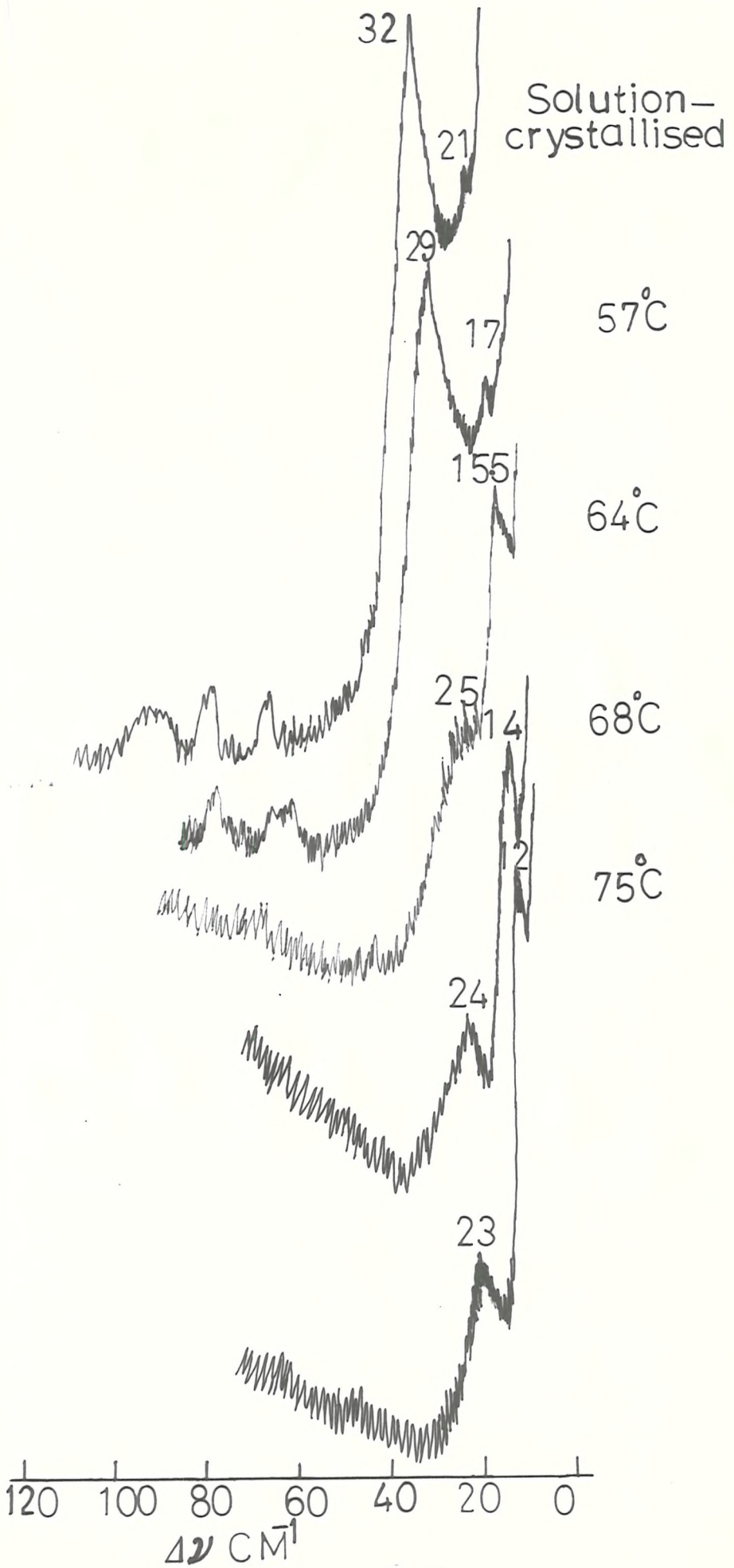

FIG. 6.4 LOW FREQUENCY RAMAN SPECTRUM OF PDMO AS A FUNCTION OF T_{ann}

Polytetrahydrofuran

The bulk specimen of this polymer gave rise to a very strong Raman band near $\Delta\nu 20$ cm^{-1} which was invariant in position as a function of temperature or T_{ann}. This, however, shifted to $\sim\Delta\nu$ 30 cm^{-1} when the specimen was melt quenched in liquid N_2 or crystallized from solution [Fig. 6.2 and Table 6.1]. Since this polymer has a low T_m ($\sim$ 40°C) its annealing should be possible at a very low temperature. This view was supported from the fact that the Raman band of the melt quenched specimen fell from $\Delta\nu$ 30- to 25 cm^{-1} when examined after 7 days, during which it was kept at $\sim$ 25°C. Thus low frequency of the Raman band of bulk specimen may be ascribed to its annealing at the ambient temperature. These observations clearly indicate that $\Delta\nu$ 20 cm^{-1} band of the bulk specimen and $\sim\Delta\nu$ 30 band of the solution crystallized or melt quenched specimens have their origin in the LA modes.

In addition to the $\Delta\nu$ 20 cm^{-1} band of the bulk specimen, two weak and broad bands have also been observed near $\Delta\nu$ 60- and 100 cm^{-1} which show slight variations in frequency at -180°C (see Table 6.1). The factors ($\Delta\nu$ 20 cm^{-1}) × 3 = $\Delta\nu$ 60 cm^{-1} and ($\Delta\nu$ 20 cm^{-1}) × 5 = $\Delta\nu$ 100 cm^{-1} suggest the association of the latter bands with 3rd and 5th order LA modes.

A considerably large difference between the calculated Raman lengths (L_R) and LAXD long spacings (L_x) reveals that Young's modulus of PTHF should be substantially different from that of polyethylene.

Poly Hexamethylene oxide

PHMO is a highly crystalline and brittle material with a T_m close to 52°C and a density 1.04 g/cm^3. The specimen, however, happened to be somewhat fluorescent thus allowing a rather limited study of its low frequency Raman spectrum. The LAXD data has been adopted from Tadokoro et al[52] with the assumption that these would compare with the present

results since the specimens have been prepared in a similar manner as reported by the latter authors. The band near $\Delta\nu$ 32 cm^{-1} in the solution crystallized specimen is clearly associated with an LAM because of its behaviour towards temperature and thermal treatment [See Table 6.2, Fig. 6.3]. The comparison between L_R and L_x seems to be quite agreeable thus indicating that Young's modulus in this case would be close to that of polyethylene.

Polydecamethylene oxide

PDMO is a highly crystalline, slightly greyish substance which melts near 76°C. The calculated and the observed densities 1.025 g/cm^3 and 1.03 g/cm^3 respectively, are close to that of polyethylene.

Fig. 6.4 and Table 6.3 show a number of low frequency bands between $\Delta\nu$ 80- and 10 cm^{-1} in the Raman spectra of both solution crystallized as well as subsequently annealed specimens whose frequency as well as intensity vary as a function of T_{ann}. The solution crystallized specimen gives rise to the strongest band near $\Delta\nu$ 32 cm^{-1} which is accompanied by a weak shoulder near $\Delta\nu$ 21 cm^{-1}. Both $\Delta\nu$ 32 cm^{-1} band and the shoulder near $\Delta\nu$ 21 cm^{-1} gradually fall in frequency but reciprocate in intensity as a function of increasing T_{ann} until at 75°C, these bands occur near $\sim\Delta\nu$23- and 12 cm^{-1} respectively with completely reversed intensities. The half band widths of these bands also decrease during this process. Further, the higher frequency weaker bands also behave similarly. The thermal behaviour of these bands clearly indicate their association with the LA modes of various chain stem lengths. This implies that the lamellar structure of PDMO involves various coexisting stem lengths (L_c). As the annealing temperature is increased, the population of lamellar structures having lower stem length values decreases at the expense of the population of those having higher stem

length values. Further, annealing close to T_m brings about a considerable increase in the lamellar core thickness when stem lengths in the vicinity of 267 Å or 19n predominate [see Table 6.3].

These conclusions furnish further support to those derived from the LAXD results[166] mentioned previously. A rigorous comparison between the LAXD results given in Fig. 6.5 and the Raman features given in Fig. 6.4 and Table 6.3, however, indicate a number of differences as follows:

The L_x values near 47 Å are associated with strong peaks whereas corresponding values of L_R are associated with weak Raman features. On the contrary, the L_x values of 90 Å, 102 Å and 118 Å are associated with relatively weak LAXD peaks, whereas corresponding L_R values are associated with the strong Raman features near $\Delta\nu 30$ cm^{-1}. Further very high values of stem lengths e.g. 139 Å, 267 Å [see Table 6.3] are detected by the Raman technique only.

Whereas the difference in the population of certain lamellar structures as determined from the two techniques may be attributed to different origins of the samples used, the detection of extra number of coexisting lamellar structures using Raman technique, may be ascribed to the better resolution offered by the latter.

It is significant to note a common feature in the low frequency Raman spectra of PTHF, PHMO and PDMO i.e. the frequency of the strongest band associated with LAM occurs near $\Delta\nu$ 30 cm^{-1} thus reflecting the similarity of crystal structure.

6.2.2 Polythioethers with m = 1-6 and 10

6.2.2 a m = 1-3

Like the first three members of polyether series [see Section 6.2.1a], the first member of polythioether series i.e. PTM, gives rise to a number

of low frequency Raman bands which are invariant in frequency with thermal treatment. The second and third members of this series i.e. PES and PTrMS, however, give rise to well defined low frequency bands whose frequencies vary as a function of annealing temperature. Therefore, these latter molecules will be considered in detail.

Polyethylene sulphide

PES is known to solidify with a high degree of crystallinity (> 85%) and has one of the highest T_m in the polythioether series. The morphological structure of the 'as prepared' polymer has been investigated using the EM technique[167]. It has been observed that PES obtained by anionic polymerization in THF assumes the shapes of platelets (lamellae), microhedrites, microspherulites or particles of irregular structure depending upon the molecular weight. At low molecular weights (500-1000), the lamellar form is observed whose thickness varies considerably over a range of 50-300 Å. Further, at higher molecular weights (1500-5600), microhedrites and microspherulites are observed whilst at a molecular weight of 14,280, particles of irregular structure are formed and lamellae appear rarely.

The crystallization mode of the melt quenched material, however, has not yet been investigated. In this study, the structure of high molecular weight melt quenched material will, therefore, be investigated using the Raman technique. The significance of this investigation centres on the fact that repeated attempts to apply LAXD technique in several laboratories to this material have failed to produce viable patterns.

The Raman spectra at low energies of various specimens of PES have been shown in Fig. 6.6 (a), (b), (c) and (d). The bands of interest are those which change from spectrum to spectrum i.e. those lying between $\Delta\nu$ 5- and 25 cm^{-1}. The relevant data have been summarized in Table 6.4.

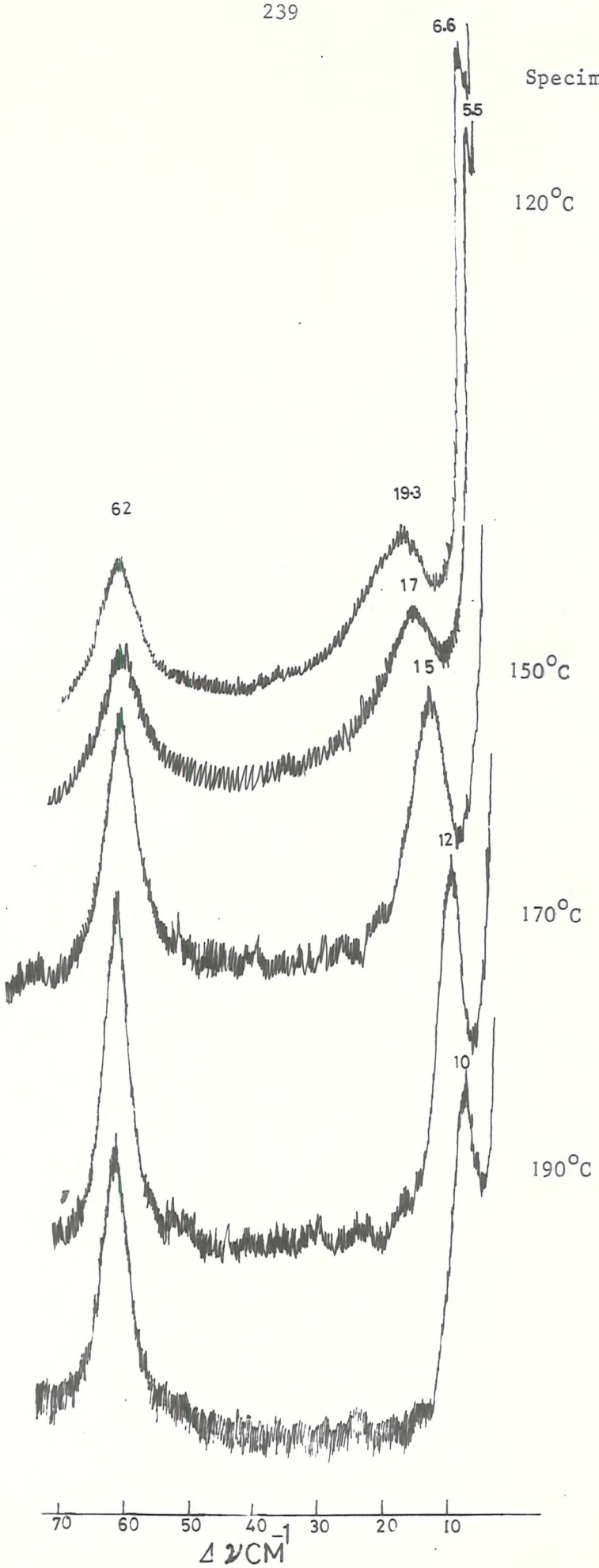

FIG. 6.6(a) LOW FREQUENCY RAMAN SPECTRUM OF PES (SPECIMEN A) AS A FUNCTION OF T_{ann}

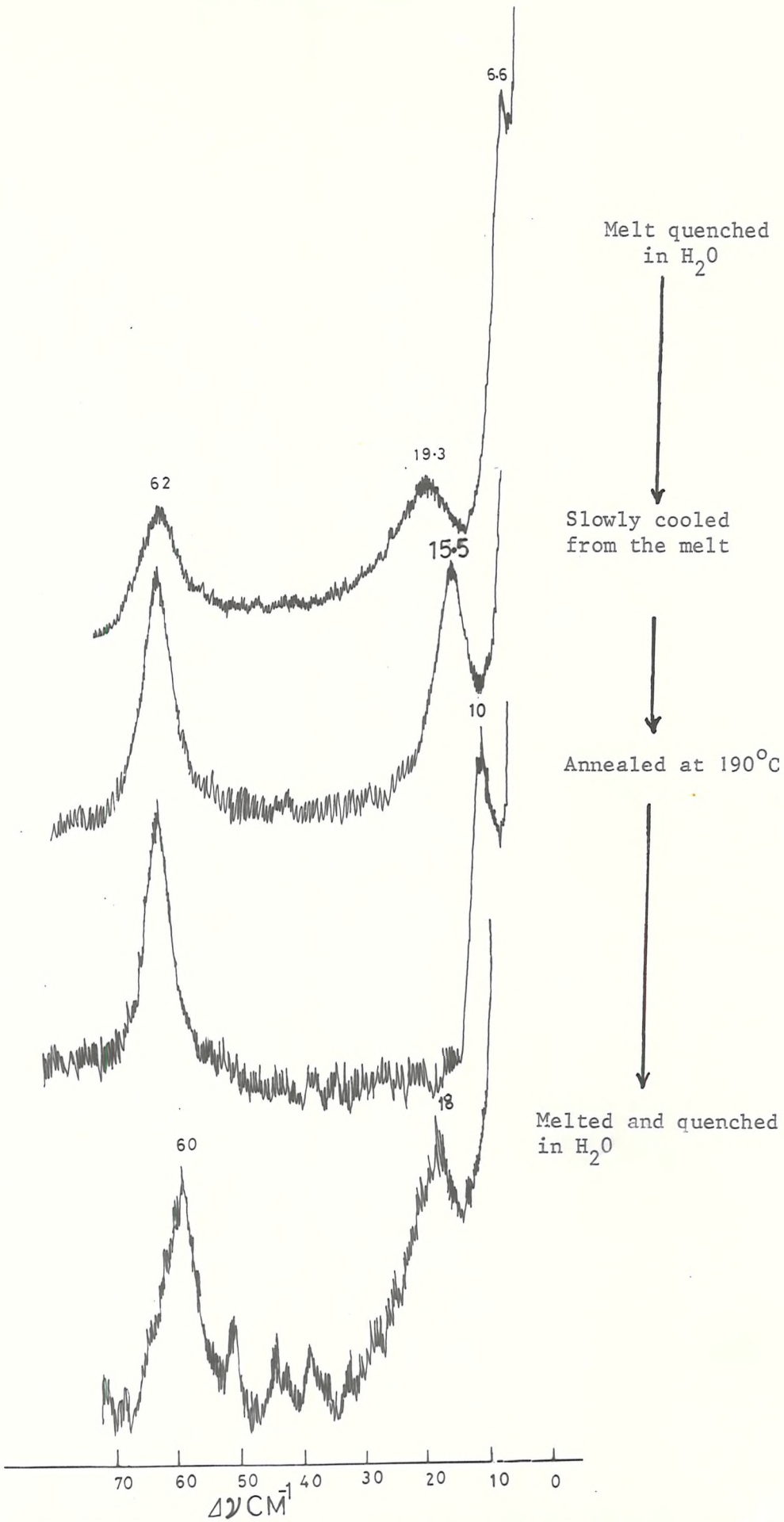

FIG. 6.6(b) LOW FREQUENCY RAMAN SPECTRUM OF PES UNDER VARIOUS TREATMENTS

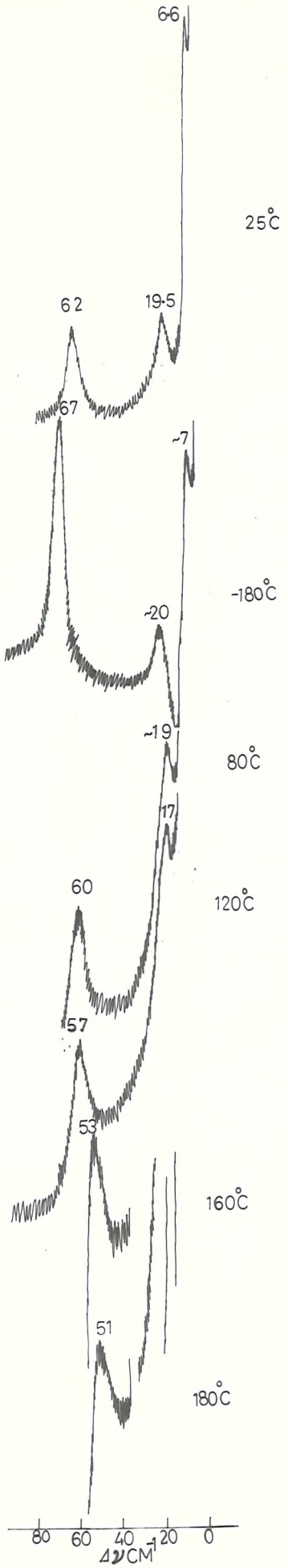

FIG. 6.6(c) LOW FREQUENCY RAMAN SPECTRUM OF PES (SPECIMEN A) AS A FUNCTION OF TEMPERATURE

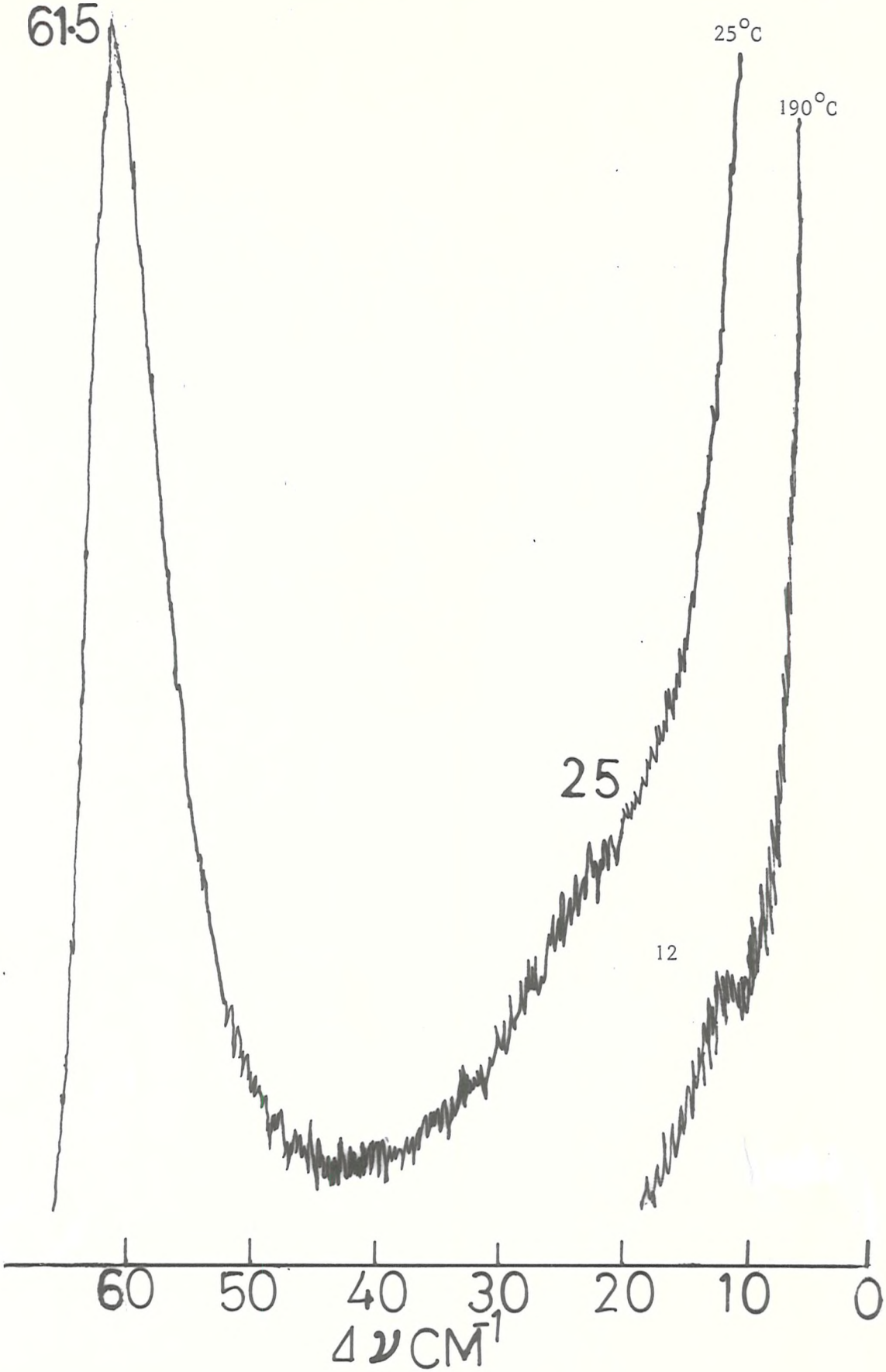

FIG. 6.6(d) LOW FREQUENCY RAMAN SPECTRUM OF PES (AS PREPARED) AS A FUNCTION OF T_{ann}

Table 6.4

Low frequency Raman data of PES

Sample	T_{ann} (°C)	$\Delta\nu$ cm^{-1}				
		25°C ($\frac{1}{2}$W)	-180°C	100°C	120°C	180°C
A (Melt-quenched in H_2O)	-	6.6,19.6 (7)	∿7,∿20	∿19	∿17	-
"	120	5.5,17 (6.5)	-	-	-	-
"	150	-, 15(5.5)	-	-	-	-
"	170	- ,12.5(4)	-	-	-	-
"	190	-,10(4.5)	-	-	-	-
Slowly cooled from the melt	-	- ,16(6)	-	-	-	-
"	190	- ,10(4)	-	-	-	-
Melt quenched in H_2O	-	∿6,18	-	-	-	-
As prepared	-	∿15-35	25	-	-	-

Fig. 6.6 (a) shows the spectrum of a melt quenched specimen, hereafter called specimen A, as a function of T_{ann}: 120-, 150-, 170- and 190 °C. It is clear that a strong band near $\Delta\nu$ 20 cm^{-1} falls gradually in frequency as a function of annealing temperature until at 190°C it shifts to 10 cm^{-1} . Another strong and sharp band occurs near $\Delta\nu$ 7 cm^{-1} in the first stages but disappears in the background at high annealing temperatures. Fig. 6.6(b) shows the spectrum of specimen A for step by step treatments involving (i) slow cooling from the melt (ii) then annealing at 190°C (iii) then remelting and quenching in H_2O. It is shown that the frequencies of the $\Delta\nu$ 20- and 7 cm^{-1} bands are lowered or raised by varying the conditions of crystallization. Fig. 6.6(c) shows the spectrum of specimen A at -180-, 100-, 120- and 180°C indicat-

ing that frequencies of the $\Delta\nu$ 20- and 7 cm^{-1} bands are invariant with temperature until the annealing temperature is reached i.e. near $120^{o}C$. Fig. 6.6(d) shows the spectrum of the as prepared specimen having a weak broad feature which extends over the range $\Delta\nu$ 15-35 cm^{-1}, with the maximum near $\Delta\nu 25$ cm^{-1}. The position of the maximum is invariant with temperature i.e. on cooling to $-180^{o}C$, but falls as a function of T_{ann}.

These observations point convincingly to the fact that the bands below $\Delta\nu$ 25 cm^{-1} originate from L.A. vibrations. The relative positions of the bands in Fig. 6.6(a), (b) and (c) further suggest that the lowest frequency band arises from the first order LAM and the highest frequency one from the third order LAM. These assignments are, however, tentative. It is quite possible that these bands might have originated from two coexisting lamellar structures with different stem length values. As such both would be associated with the first order LAM.

The weak and broad feature near $\Delta\nu 25 cm^{-1}$ in Fig.6.6(d) reflects poorly developed lamellar structures with a wide range of stem lengths in the as prepared specimen, thus supporting the results from EM studies . The strong intensities and narrow half band widths of the bands in Fig. 6.6(a), (b) and (c), however, indicate highly developed lamellar structures with a narrow range of stem length distribution, in the melt crystallized specimen.

The relationship between frequency (ν) and stem length in the case of this polymer is difficult to establish because of the non planar backbone, but it can be concluded with confidence that annealing causes a gradual increase in lamellar thickness as a function of T_{ann} until at $190^{o}C$, the original thickness has doubled.

If one assumes that Young's modulus for the isolated chain in PES is close to that in PE, the Raman data would indicate a lamellar core

thickness (L_R) in the specimen A of ~400 Å. It is far more likely, however, that the modulus is lower than this value by a factor of two or more since the backbone is non planar. It is, therefore, assumed that (L_R) and hence approximately (L_X) in the specimen A lies in the range 100 to 300 Å.

The plot of density against the third order LAM (see Fig. 6.7), and the increase of D.S.C. derived T_m within the range 202 to 217 °C as a function of annealing, provide further evidence for the existence of lamellar structures and their thickening.

Thus it may be given as a conclusion that Raman data provide novel evidence for the existence of lamellar structures in the melt crystallized as well as the "as prepared" specimens of PES. Whereas the lamellar structures are highly developed in the former case, they seem to be only poorly so in the latter case. Whilst the latter result is in accordance with the EM studies, the existence of lamellae in the melt crystallized PES has been indicated for the first time. The lamellar structures in both thicken on annealing at temperatures in excess of 120°C.

Polytrimethylene sulphide

Polytrimethylene sulphide is an elastomer having a moderately high degree of crystallinity (> 65%). The crystallization mode of this polymer has not yet been investigated. In view of its helical structure (G_4), it is interesting to note that a Raman band near $\Delta\nu$ 16 cm^{-1} shows sensitivity to thermal treatment. Its low frequency Raman spectrum is presented in Fig. 6.8 and the relevant data are summarized in Table 6.5.

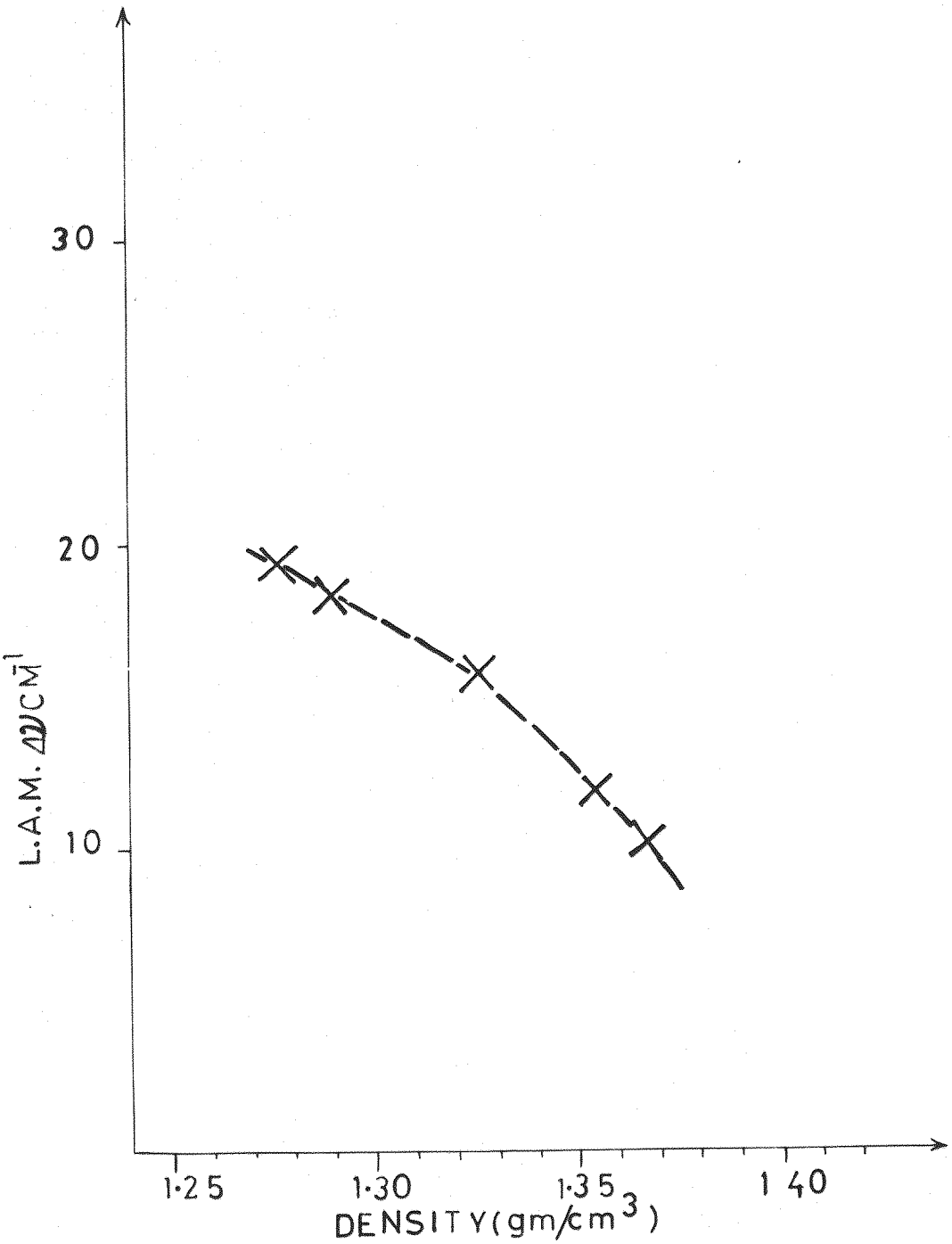

FIG.6.7: DENSITIES OF ANNEALED P.E.S. SPECIMENS AGAINST THEIR L.A.M. FREQUENCIES

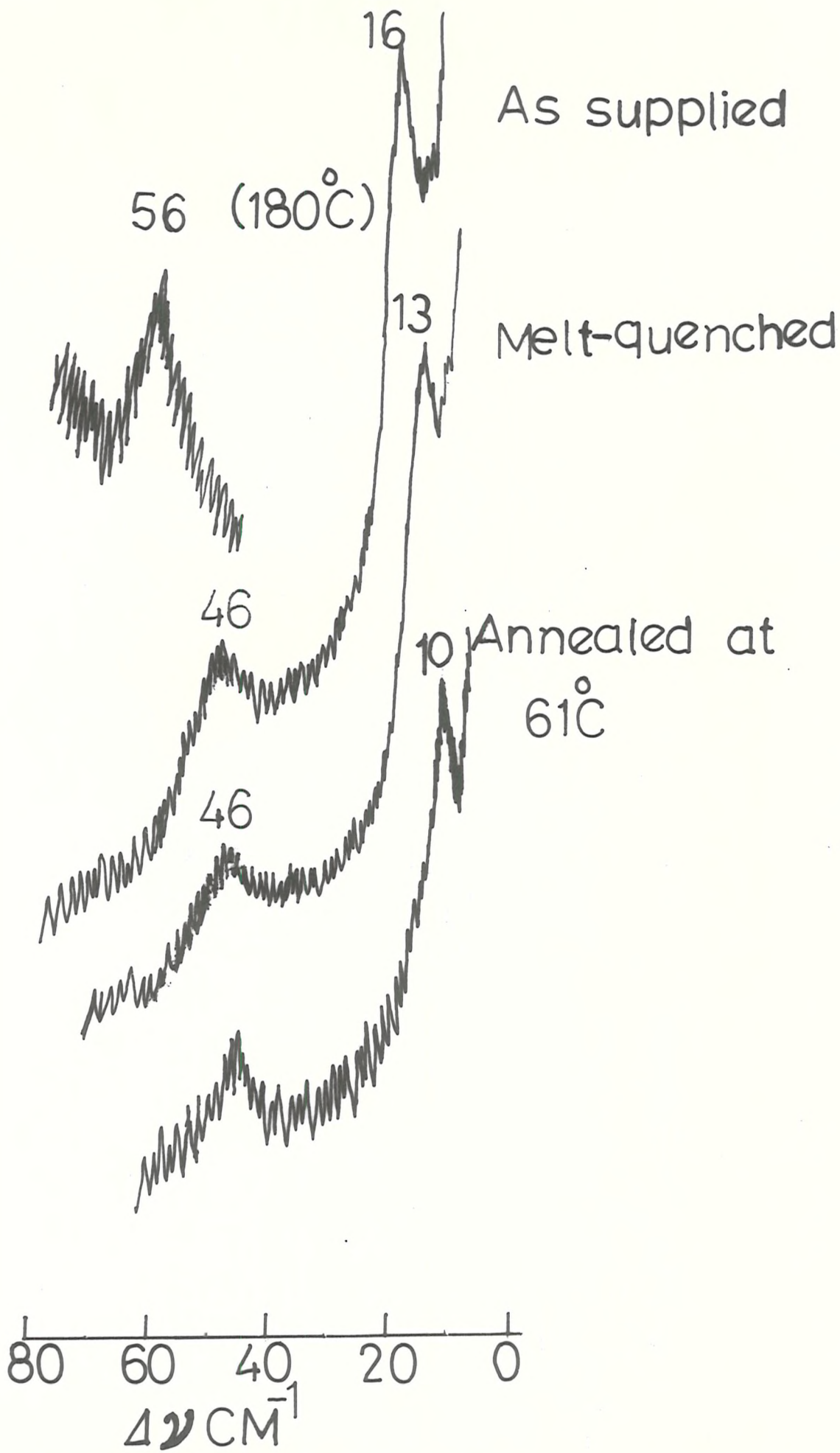

FIG. 6.8 LOW FREQUENCY RAMAN SPECTRUM OF PTrMS

Table 6.5

Low frequency Raman data of PTrMS

Sample	T_{ann} (°C)	$\Delta\nu$ cm^{-1}		Density (g/cm^3)	T_m (°C)
		25°C	-180°C		
As supplied	-	16	16.5	1.250	62
Melt quenched in H_2O	-	13	13.5	-	-
"	61	10	-	1.125	70

Clearly, the band near $\Delta\nu$ 16 cm^{-1} in Fig. 6.8 falls in frequency as a function of thermal treatment, thus indicating a gradual increase in lamellar thickness (L_R). Since a considerably low value of Young's modulus is postulated in the case of this polymer due to helical conformation, a correspondingly low frequency was expected for the LA mode. Thus the sensitivity of the observed band to thermal treatment (which occurs at higher than the expected frequency) was thought to have resulted from a structural transformation and not from variations in lamellar thickness. The lowered density [see Table 6.5] of the material after annealing treatment furnished support to this view. Nevertheless, high frequency vibrational spectra as well as X-ray diffraction counter curves for the annealed and unannealed specimens were found to be similar, thus revealing that no such transformation had occurred. It may, therefore, be concluded that the $\Delta\nu$ 16 cm^{-1} band originates in LA vibrations of the lamellar segments. The lowering of density due to thermal treatment may be attributed to degradation of the specimen at high temperatures. The increased T_m under similar conditions [see Table 6.5], in contrast reflects increased crystallinity due to lamellar thickening.

As in the case of PES, no relationship between ν and L_R may be established, since neither Young's modulus, nor such information as LAXD long spacing is available.

6.2.2 b Polythioethers with m = 4,5,6 and 10

The method of preparation yielded two fractions of each of these polymers i.e. a low molecular weight fraction (soluble in the reaction medium of dry benzene-ethanol mixture) and a high molecular weight one (insoluble in the reaction medium, see Chapter 2). Both fractions had similar characteristics of T_m and crystallinity and were obtained as highly crystalline powders melting between 64 - 92°C.

In contrast to PTMS, PPMS and PHMS the high molecular weight fraction of PDMS, was only slightly soluble in common solvents e.g. $CHCl_3$, CH_2Cl_2.

Since spectral features of both low and high molecular weight fractions are similar, the results will not be discriminated against molecular weights. The low frequency Raman spectra of PTMS, PPMS, PHMS and PDMS, are shown in Figs. 6.9, 6.10, 6.11 and 6.12, and the corresponding results are summarized in Tables 6.6, 6.7, 6.8 and 6.9 respectively.

Table 6.6

Low frequency Raman data of PTMS

Sample	T_{ann} (°C)	$\Delta\nu$ cm^{-1}		L_{oR} (A)	Density (g/cm^3)	T_m (°C)
		25°C	-180°C			
Solution crystallized	-	36	36.5	84	1.090	64
Melt-quenched in H_2O	-	32	-	94	-	-
Solution crystallized	57	29	-	104	-	66
Melt quenched in H_2O	62	27	-	111	-	68
"	64	25	-	121	1.125	70

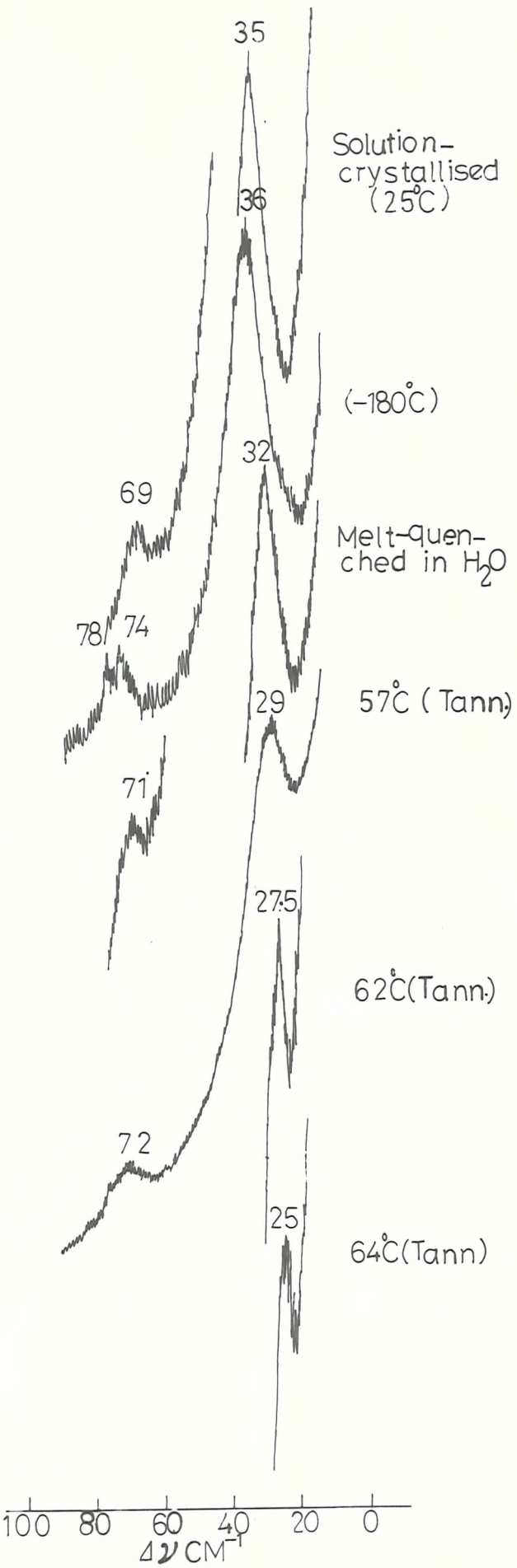

FIG. 6.9 LOW FREQUENCY RAMAN SPECTRUM OF PTMS

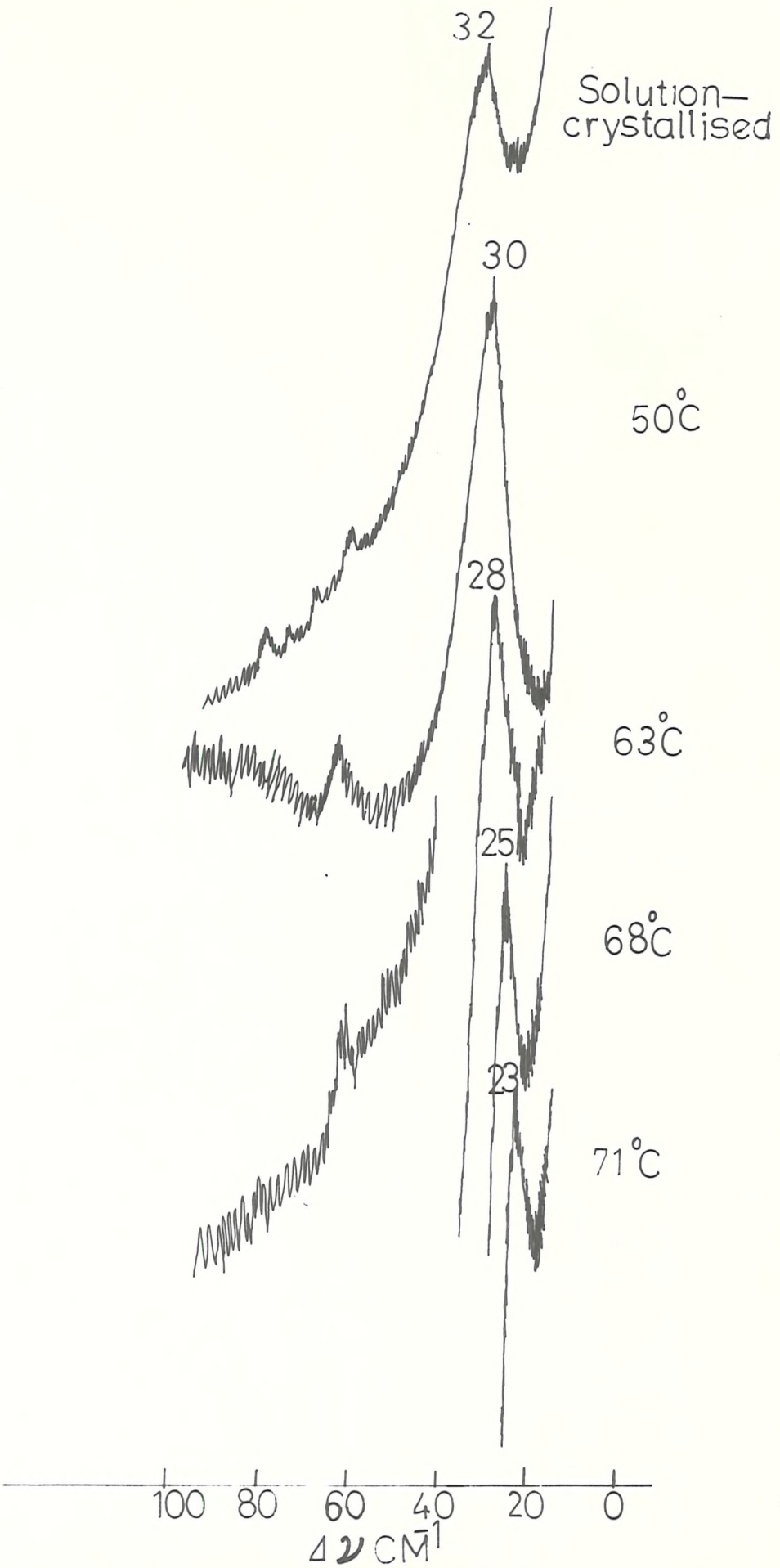

FIG. 6.10 LOW FREQUENCY RAMAN SPECTRUM OF PPMS AS A FUNCTION OF T_{ann}

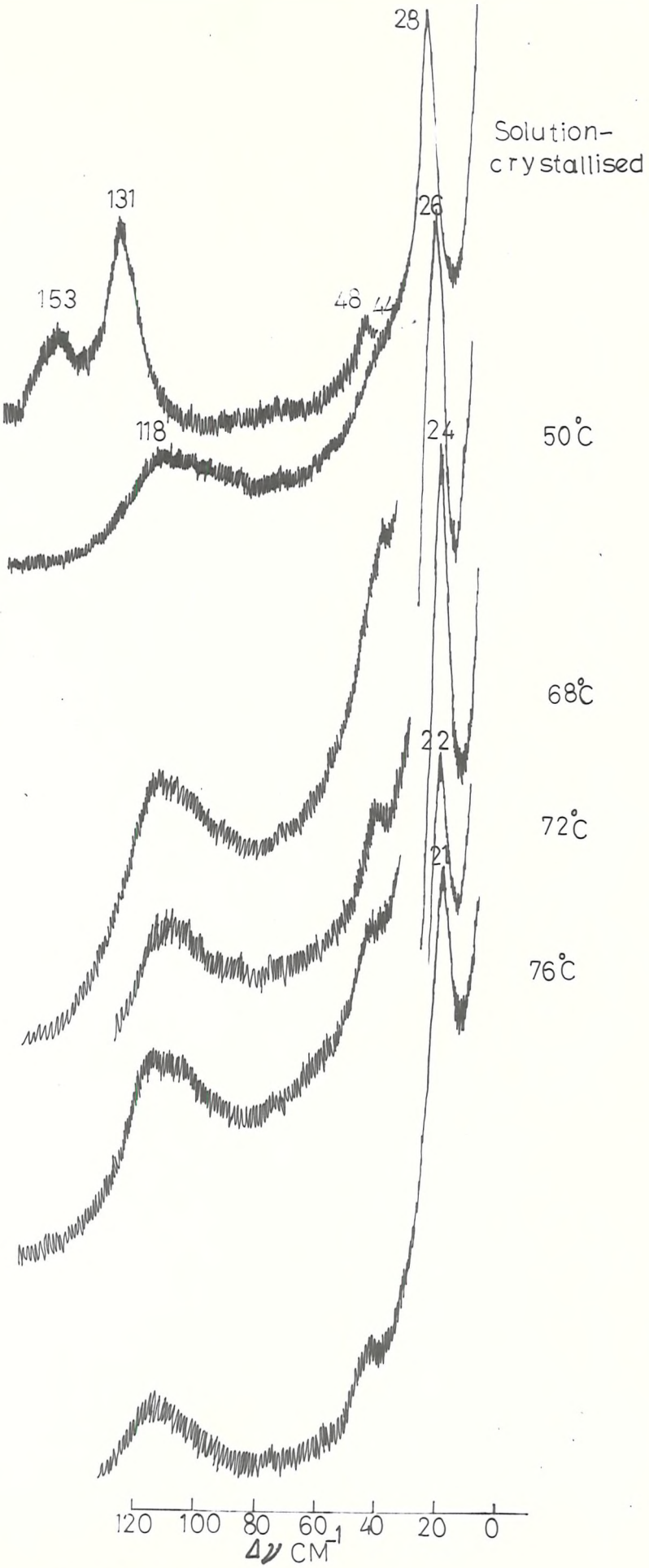

FIG. 6.11 LOW FREQUENCY RAMAN SPECTRUM OF PHMS AS A FUNCTION OF T_{ann}

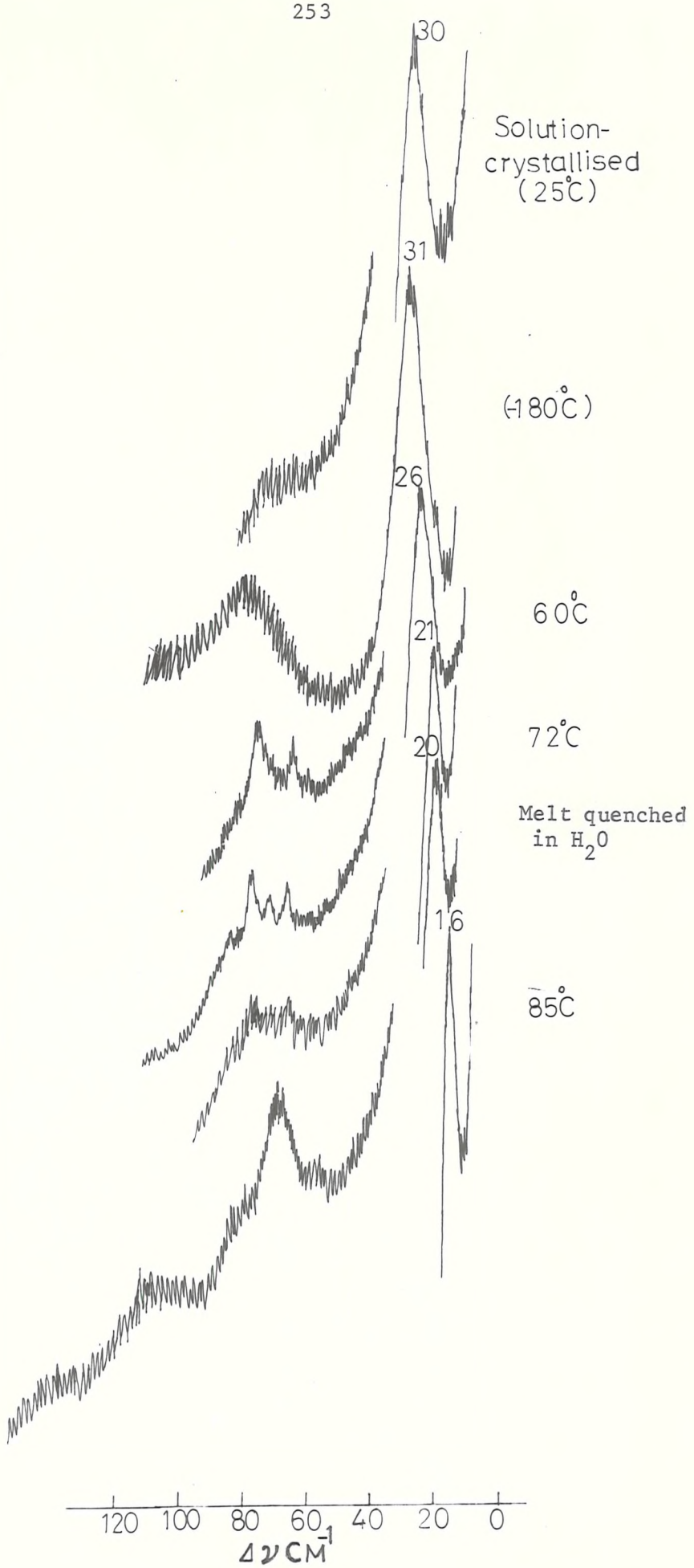

FIG. 6.12 LOW FREQUENCY RAMAN SPECTRUM OF PDMS AS A FUNCTION OF T_{ann}

Table 6.7

LA vibrational data of PPMS

Sample	T_{ann} (°C)	$\Delta\nu$ cm^{-1}		L_{oR} (A)	Density (g/cm^3)	T_m (°C)
		25°C	-180°C			
Solution crystallized	-	32	32.5	90	1.110	72
"	50	30	-	97	-	-
"	63	28	-	104	1.150	-
"	68	25	-	117	1.180	75
"	71	23	-	125	-	76

Table 6.8

Low frequency of Raman data of PHMS

Sample	T_{ann} (°C)	$\Delta\nu$ cm^{-1}		L_{oR} (A)	Density (g/cm^3)	T_m (°C)
		25°C	-180°C			
Solution crystallized	-	28	28.5	106	1.090	76
"	50	26	-	114	-	-
"	68	24	-	122	-	-
	72	22	-	135	-	78
"	76	21	-	142	1.140	81

Table 6.9

Low frequency of Raman data of PDMS

Sample	T_{ann} (°C)	$\Delta\nu$ cm^{-1} 25°C	$\Delta\nu$ cm^{-1} -180°C	L_{oR} (A)	L^*_{ox} (A)	Density (g/cm^3)	T_m (°C)
Solution crystallized	-	30,S	31	107	114	1.038	87
"		85-80,W,B	∿85-80	36-38	-		
"	60	26,S	-	120	-	-	-
		67,W	-	46	-	-	-
		78,W	-	40	-		
		85,W	-	36	-		
	72	21.S	∿21,S	148,S	-	-	-
		69,W	∿69,W	42,W	-		
		76,W	∿76,W	41,W	-		
		80,W	∿80,W	39,W	-		
Melt-quenched in H_2O	-	20,S	-	156	170	-	-
Solution crystallized	85	16,S	-	194	193	1.050	92
		59,W	-	53	-		
		71,MW	-	44	-		
		90,W	-	35	-		
		110,W	-	29	-		

* see Chapter 2. (section 2.8)

It is clear that polythioethers with m = 4,5,6 and 10 give rise to a very strong band in the frequency range of $\Delta\nu$ 28 to 36 cm^{-1}. The frequency of this band varies as a function of T_{ann} so that an increase in the latter results in a corresponding fall in frequency. The magnitude of maximum downward shift, however, depends upon molecule to molecule being greater for those whose crystal structures are affected more with thermal treatment [PTMS and PDMS] and smaller for those whose crystal structures are either unaffected or less affected with the latter treatment [PPMS and PHMS] , [see Section 5.3.1 b]. Further,maximum value of the frequency of this band also varies in a similar manner being highest for PTMS ($\Delta\nu$ 36 cm^{-1}) and lowest for PHMS ($\Delta\nu$ 28 cm^{-1}).

Nevertheless, the sensitivity of this band to thermal treatment and indifference to variation in temperature [see Fig. 6.9 - 6.12 and Tables 6.6 - 6.9] clearly indicate its origin in an LA mode of the chain stems within lamellar structures. This is further supported from an increase in density as well as T_m on annealing.

The LAXD results have been available in the case of PDMS only. A close agreement between the values of L_R and L_x in this case, suggests that Young's modulus of PDMS must be very close to that of polyethylene. This would independently suggest that the frequency of LA modes is associated with all trans chain stems.

Apart from the strongest band below $\Delta\nu$30 cm^{-1}, the low frequency Raman spectrum of PDMS shows a number of weaker bands in the range $\Delta\nu$ 60- to 110 cm^{-1} whose frequency as well as intensity varies as a function of T_{ann}. These bands may, therefore, be assigned to the LA vibrations of various coexisting lamellar structures with characteristic values of stem lengths. This result is similar to that observed in the case of PDMO. Thus it may be concluded that the chain folding model proposed for PDMO[166], would apply to the chain folded structure of PDMS as well.

Although less prominent, it appears from a close study of Figs 6.8 - 6.11 that lower members of the polythioether series also give rise to higher frequency Raman bands ($\Delta\nu$ 100 - 40 cm^{-1}) which may be associated with various coexisting lamellar structures.

Further, it may be noted that the highest frequency of LA mode in PTMS, PPMS, PHMS and PDMS occurs within a narrow range i.e. $\Delta\nu$28 - 35 cm^{-1}.

These observations furnish further support to the conclusions drawn in Chapter 5 which suggest a close relationship among the crystal structures of polythioethers with $m \geq 4$.

6.3 Conclusion

The potential of Raman technique in general, has been demonstrated for the diagnosis of lamellar crystallization in polymers. Polyethers with m = 4, 6 and 10 and polythioethers with m = 2-6 and 10 give rise to well defined low frequency Raman features whose frequencies ν are associated with the LA vibrations of chain stem lengths L_R constituting the lamellae. The value of ν is a function of lamellar thickness and varies with the conditions of crystallization.

The most prominent feature in the spectra of solution crystallized polyethers and polythioethers with $m \geq 4$ i.e. L.A.M. 1 falls within a narrow frequency range i.e. $\Delta\nu$ 28-35 cm^{-1}, reflecting close resemblance of their structures. Incidentally, the reported L.A.M. frequency of polydecamethylene sebacate also falls within this range when crystallized from solution. Although the value of Young's modulus of polyethylene may be approximately applied when calculating L_R in these polymers, it is clear that the frequency of L.A.M.1 in polyethylene ($\sim$ $\Delta\nu$ 16 cm^{-1}) and these polymers is widely different in similar circumstances. This difference may be attributed to dissimilarities in chemical structure

(see section 6.1.1). In contrast, the frequency of L.A.M.1 in non planar molecules i.e. PES and PTrMS is relatively lower ($\sim \Delta\nu$ 20 cm^{-1}) indicating the influence of molecular conformation.

Half band widths and relative intensities of these features seem to reflect the distribution of various lamellar thicknesses in a particular specimen.

Higher members of the polyether and polythioether series i.e. PDMO and PDMS crystallize into various coexisting lamellar structures with characteristic stem length values thus indicating a similar model of chain folding in these polymers. The evidence for the occurrence of various co-existing lamellar structures in lower members is less prominent.

The failure to observe LA modes in helical polymers i.e. POM, PEO, POCB and PTM indicates that using present technique, lamellar crystallization can be detected only in those polymers which give rise to LAM frequencies down to$\Delta\nu$ 5 cm^{-1}.

CHAPTER VII

CONCLUSIONS

The contents of this thesis describe a section of the work of a research group engaged in the application of a wide range of structural techniques e.g. Vibrational spectroscopy, X-ray diffraction, NMR, DSC etc. to problems in polymer science. Within the group, the responsibility of the author has been to develop the application of Raman technique in the analytical fields of simpler organic compounds and polymers in collaboration with other techniques.

The project described in Chapter III was started to develop characteristic Raman frequencies for a variety of molecular groups with a basic purpose in mind i.e. their application to vibrational analysis of polymer systems having particularly an aromatic backbone. Thus group frequency correlations were developed from an analysis of ~300 organic compounds, most of them being substituted benzenes. Mono, di and tri substituted benzenes gave rise to highly characteristic Raman features, though tetra, penta and hexa substituted benzenes did not yield any satisfactory correlations. Apart from this, various molecular groups also gave rise to characteristic Raman frequencies. It has been noted that although Raman characteristic frequencies are more useful than IR ones, the joint use of both of these frequencies can yield better results than the application of any of them alone (Chapter III).

The following two polymeric systems were selected primarily for a comparative study using these correlations:

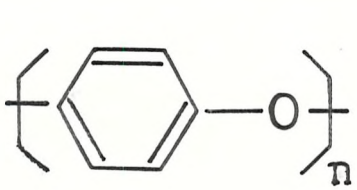

(i)

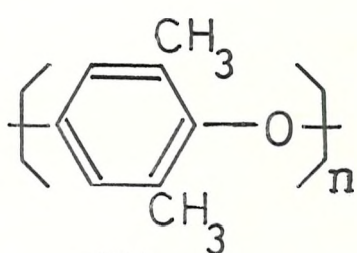

(ii)

The crystal structure of (i) has been recently determined.[94] It has a planar zig zag conformation and two chains translate the unit cell - space group: pbcn, D_{2h}^{14} . Thus interest centred not only on the spectral features arising from the vibrations of an isolated molecular chain but also on those arising from interchain interactions and LA vibrations of the chain segments within crystalline lamellae.

Unfortunately, however, it emerged from subsequent experimentation that (i) was not amenable to Raman studies because of the insurmountable problem of fluorescence. A number of efforts were made to suppress this nuisance but without success (see section 2.7).Thus, although this polymer yielded no results, the project as a whole was not a failure. It has achieved a useful purpose i.e. considerable contribution to the development of Raman spectroscopy has been made in the analytical field as a result of deducing characteristic frequencies for a variety of molecular backbones and groups. Further, it assisted to fix the direction of the project which forms the central body of this thesis i.e. vibrational analysis of polymers with particular emphasis on the investigation of features arising from interchain interactions and LA modes. The latter features are very important in following the crystallization behaviour of polymers. Polyethylene has been the subject of a number of such studies. Thus, in view of the feasibility of this project, it was necessary to embark on those polymers which have a close chemical as well as structural resemblance to polyethylene. Aliphatic polyethers and polythioethers of the series $\left[(CH_2)_m-Y\right]_n$, [Y=O or S] are suitable candidates for these investigations in view of the latter characteristics (see Chapters 4 and 5).

Considerable experimental expertise has been developed in this project,by the synthesis of a large number of polymers and by devising

ways to suppress fluorescence in difficult samples. Although the real cause of fluorescence is still not clear, considerable evidence has emerged from this study to support the view that it is mainly rooted in impurities.

The vibrational analysis of polyethers with m = 1-4,6 and 10, and polythioethers with m = 1-6 and 10, in conjunction with supplementary techniques e.g. D.S.C., X-ray diffraction, density measurements etc., has resulted in the assessments given below:

Molecular vibrations

Prior to the study of band splitting caused by interchain interactions, it is necessary to carefully analyse the vibrational features belonging to an isolated molecular chain. This has been greatly facilitated in this study, by the available high degree of resolution. As a result, the following conclusions have been made:

POM, PEO, PTM, PES (Partial assignment)

A number of newly observed bands have been assigned to fundamental modes according to the reported calculations or on a tentative basis. It seems that a number of bands in the Raman spectrum of POM, particularly in the low frequency region, can not be explained on the basis of available normal coordinate analysis. Similarly, considerable disagreement exists between the calculated and observed frequencies of PTM. These discrepancies clearly indicate that the normal coordinate analysis of POM and PTM should be reassessed.

POCBIII, PTrMS (Full assignment)

Although calculations exist for those symmetry species of the molecular vibrations of POCBIII which have duel activity, i.e. B_1, B_2 and B_3, no Raman spectrum has yet been reported. The Raman spectrum from this study has been assigned not

only to B_1, B_2 and B_3 species but also to A ones which are Raman active only. The latter assignments, however, have been made on a tentative basis. On the whole, calculated and observed frequencies show good agreement.

Neither Raman nor IR spectrum of PTrMS has yet been reported. The present study has resulted in a tentative assignment of both Raman and IR spectra on the basis of C_2 factor group. The vibrational spectrum of this molecule then confirms that it has a C_2 rotation axis as suggested by Tadokoro.

PDMO, PTMS, PPMS, PHMS, PDMS. (Partial assignment)

Neither Raman nor IR spectra of these molecules have been reported except the IR spectra of PDMO and PPMS.

The molecular group of PDMO is similar to that of polyethylene i.e. d_{2h}. Assuming that the molecular group of PTMS, PHMS and PDMS is also d_{2h}, a comparison of the vibrational spectra of these molecules with those of PDMO and polyethylene has resulted in a tentative assignment of prominent spectral features.

The symmetry group associated with the molecular chain of PPMS is, however, different i.e. c_{2v}, which offers a reasonable explanation of the vibrational spectrum.

As a part of this project, vibrational spectra have also been studied with regard to various circumstances and have yielded the following results:

Conformational regularity

The effect of ageing on the spectrum of PTM and of elevated temperatures on the spectrum of PES has revealed that these polymers give rise

to highly conformation-sensitive bands. These bands which are termed as regularity bands by Zerbi arise from the so called conformational splitting. Further, PES shows one dimensional polymorphism at elevated temperatures. The polymorphs seem to be transitory in nature and normal conformation returns as soon as the ambient temperature is reached.

Melt quenching does not seem to affect the molecular conformation except in the case of PTM. In the latter case the molecular conformation seems to have broken down to an irrepairable extent.

Further polyethers and polythioethers with m = 1-3 give rise to a number of weak features in the vibrational spectrum which can not be assigned to fundamental modes thus indicating their origin from amorphous structures or short range order molecular conformation.

Molecular structure of PTMS, PHMS and PDMS

The structure of these molecules has not yet been reported. An analysis of the vibrational spectra of these molecules based upon analogies to other molecules of known structure has revealed that they take planar zig zag conformation. As mentioned above, the symmetry group associated with their molecular chain seems to be isomorphous with the point group d_{2h}.

Intermolecular vibrations

Correlation splitting

Polyethers and polythioethers having more than 1 chain per unit cell i.e. PEO, PDMO and PPMS, and those having unknown crystal structures i.e. PTMS, PHMS and PDMS give rise to distinct band splitting either at cryogenic or both at cryogenic and ambient temperature. The band splitting has been tentatively ascribed to interchain interactions with the follow-

ing implications:

(i) Although interchain interactions are generally weak, they are particularly weak in the case of PES and PTrMS.

(ii) PEO seems to have a space group isomorphous to the point group C_{2h} if configuration of the 4 molecular chains in the unit cell is assumed to be similar to that in the case of isotactic polypropylene.

(iii) Polythioethers with m = 4, 6 and 10 i.e. PTMS, PHMS and PDMS can have a 2 chain per unit cell structure.

Polymorphism

Polymorphism in PDMO has been studied as a function of T_{ann}. It has been shown that PE-type structure (2 chains/unit cell) transforms gradually to the PTHF type (1 chain/unit cell) with increasing T_{ann} until at a T_{ann} close to T_m ($\sim 75^{o}C$) the PE-type structure transforms completely to the PTHF-type.

Polythioethers i.e. PTMS, PHMS and PDMS have also shown polymorphism under similar conditions. The transformation, however, seems to occur in a reverse order in comparison with polyethers i.e. 1 chain per unit cell structure transforms gradually to the 2 chain per unit cell as a function of T_{ann} or melt crystallization. Further, the transformation occurs only partially.

The relationship between crystallization and longitudinal acoustic vibrations of polymers

Polyethers with m = 4, 6 and 10 and polythioethers with m = 2-6 and 10 give rise to well defined low frequency Raman features (typically between $\Delta\nu 10 - 35\ cm^{-1}$) whose frequencies ($\nu$) are associated with LA vibrations of the chain stems within lamellae. The lamellar core thickness or chain stem length (L_R) is a function of the mode of sample

preparation e.g. solution or melt crystallization, quenching, annealing etc. as indicated by variation in the frequency of LA mode under these conditions.

Raman bands due to fundamental modes (i.e. m=1) are relatively intense, but the higher order modes either give rise to weak bands or nothing at all. The intensity and width at half height of these bands seems to be related with the distribution of lamellar thicknesses within a narrow range. It has become evident, however, that conformational as well as chemical structure of a molecule also influences the frequency of LA mode.

It has not been possible to establish the relationship between lamellar core thickness (L_R) and ν in the case of non planar molecules i.e. PES and PTrMS, since neither the value of Young's modulus nor that of LAXD long spacing (L_x) is available. In the case of PES, however, it has been concluded that annealing a melt quenched specimen at 190°C results in doubling the original thickness. Further, it has been indicated that lamellar structures develop poorly during the polymerization of PES from the monomer. Crystallization from the melt, however, results in well developed lamellae.

The calculated values of L_R [using equation 1 with the observed value of ν and assuming that the value of Young's modulus for polyethylene, $(3.58 \pm 0.25) \times 10^{12}$ dynes/cm^2 applies] agree well with the values of L_x in the case of PHMO, PDMO and PDMS. This result is highly significant in view of the following implications:

(i) The value of Young's modulus of polyethylene can be applied confidently to other molecules having considerably long planar zig zag segments while calculating L_R approximately.

(ii) Although near equivalence between L_R and L_x has been indicated, minor differences between these quantities and their implications can be

understood only if the correct value of Young's modulus is known.

The significance of Raman measurements, has nevertheless been indicated from an independent technique i.e. LAXD in this way.

The higher members of polyether and polythioether series i.e. PDMO and PDMS crystallize into various coexisting lamellar structures with characteristic values of the stem length. This observation is consistent with the results derived from LAXD study of PDMO. The similarity of lamellar structure in PDMO and PDMS suggests that the chain folding model in the latter case would be similar to that reported for the former case.Such structures are,however, less prominent in lower members.

Finally the failure to observe LA modes in some helical polymers, i.e. POM, PEO, POCB and PTM, may be ascribed to the instrumental limitations of Raman technique i.e. inability to record signals below $\sim\Delta\nu$ 5 cm^{-1} since these polymers are expected to give rise to very low frequency LA modes.

These results constitute the first cumulative work on the observation of LA modes in polymers not only chemically but also in some cases structurally different from polyethylene. They generally demonstrate the potential of Raman technique for the diagnosis of lamellar crystallization in polymers. It is hoped that the present study would open a new avenue of interest encouraging further development of Raman technique in this field.

REFERENCES

1. A. Smekal, Naturwissenschaften, 11, 873 (1923)

2. C.V. Raman, Nature, 121, 501, 619, 721, (1928)

3. J.H. Hibben, The Raman Effect and Its Chemical Applications, Reinhold, New York, (1939)

4. K.W.F. Kohlrausch, Ramanspektren, Hand-und Jahsbuch der Chemischen Physik, Edwards Bros., Ann Arbor, (1945) Vol.9.

5. R.N. Jones and C. Sandorfy in "Chemical Applications of Spectroscopy" W. West, Ed. Interscience, New York, (1956)

6. J. Brandmüller and H. Möser, Einfiihrung in die Ramanspektroskopie, Steinkopff, Darmstadt, (1962)

7. G. Placzeck in E. Marx, Handbuck der Radiologie Akademische Verlagsgesellschaft, Leipzig (1934), Vol. IV/2

8. G. Herzberg, Molecular Spectra and Molecular Structure, Van Nostrand, Reinhold, New York, (1945), Vol.2

9. P.J. Hendra, C.J. Vear, Analyst, 95, 112, (1970)

10. B. Schrader, Angew. Chem., Internat. Edit., 12(11), 884, (1973)

11. H.A. Szymansky; Raman Spectroscopy, Theory and Practice, Plenum Press, New York, (1967) Vol.1; (1970) Vol.2

12. T.R. Gilson, P.J. Hendra, Laser Raman Spectroscopy, Wiley Interscience, London, 1970

13. M.C. Tobin, Laser Raman Spectroscopy, Wiley Interscience, New York, 1971

14. S.K. Freeman, "Applications of Raman Spectroscopy", J. Wiley and Sons Inc. New York (1974)

15. D.O. Hummel, Polymer Spectroscopy, Verlag-Chemie, GmbH, Weinheim/ Bergstr. (1974)

16. J.R. Durig, "Vibrational Spectra and Structure" Vol.2-4, Elsevier, Scientific Publishing Company, New York (1975)

17. K.J. Ivin, "Structural Studies of Macromolecules by Spectroscopic Methods," J. Wiley, London, 1976.

18. E.B. Wilson, Jr., J.C. Decius and P.C. Cross "Molecular Vibrations, The Theory of Infrared and Raman Vibrational Spectra" McGraw-Hill, New York, 1955

19. W.W. Coblentz, "Investigations of Infrared Spectra", Carnegie Institute Washington, 1905

20. L.J. Bellamy "The Infra red Spectra of Complex Molecules" (1954) and "Advances in Infra red Group Frequencies" (1966) Methuen and Co. Ltd. London

21. Fateley, Williams, G. U.S. Clearing House Fed. Sci. Tech. Inform. AD No.722487 (1971) 386 pp, Avail. NITS From Govt. Announc. (U.S.) (1971) 12, 80;
Gerald, L. Carlson, AD 762303, (1973) Avail. NTIS, U.S. Dept. of Commerce.

22. Dollish Francis R., Fateley Williams, G., Bentley, Freeman, F. "Characteristic Raman Frequencies of Organic Compounds", Wiley Interscience, New York, N.Y., (1973)

23. B. Schrader and W. Meier, Z. Anal. Chem. 260, 248 (1972)

24. R.A. Nyquist, Appl. Spectrosc. 26 81 (1972)

25. George E. McManis and Lyle E. Gast, J. Amer. Oil Chem. Soc. 51(5) 198-9, (1974)

26. H.J. Sloane, Amer. Chem. Soc. Div. Org. Coatings Plast. Chem. Pap. 30, 27 (1970)

27. B. Schrader and E. Steigner, Z. Anal. Chem. 254, 177 (1971);
B. Schrader and E. Steigner in E. Heftmann, "Modern methods of Steroid analysis", Academic Press, New York, 1973, Chapter 9, p.231.

28. N. Sheppard, J. Chem. Phys. 17, 79 (1949); Trans. Farad. Soc. 46, 527 (1950)

29. N.B. Colthup, L.H. Daly and S.E. Wiberley, "Introduction to Infra-red and Raman Spectroscopy", Academic Press New York, 1954, 2nd Ed. 1975

30. K. Nakamoto; Infra red Spectra of Inorganic and Coordination Compounds", 2nd Edit. Wiley-Interscience, New York, 1970.

31. P.J. Hendra and J.R. Mackenzie, Chem. Commun. 760 (1968)

32. M.I. Bank and S. Krimm, J. Polym. Sci. A2, 7, 1785-1809 (1969)

33. P.P. Shorygin, Uspekhi Khimii 19, 419 (1950)

34. K. Venkateswarlu and M. Radhakrishnan, Spectrochim. Acta, 18, 1433 (1962)

35. H.A. Szymansky, "Correlation of Infra red and Raman Spectra of Organic Compounds", Hertillon Press, Cambridge Springs Penn., 1969.

36. K. Herrmann, O. Gerngross and W. Abitz, Z. Physik. Chem. B10, 371 (1930); W. M.D. Bryant, J. Polym. Sci. 2, 547 (1947)

37. P. Ingram and A. Peterlin in Herman F. Mark, Norman G. Gaylord and Norbert M. Bikales, Ed., Encyclopedia of Science and Technology Vol. 9, Interscience Div., John Wiley and Sons, New York, pp.204-274, (1968)

38. P.H. Geil, "Polymer Single Crystals", Interscience Div. John Wiley and Sons. New York, 1963.

39. A. Keller, Kolloid Z. und Z. Polymere 197, 98-115 (1964)

40. D.A. Blackadder, J. Macromol. Sci-Rev. Macromol Chem. C1(2), 297-326 (1967)

41. Catalogue of Raman, Infra red, Ultraviolet and Mass Spectral Data, American Petroleum Institute Research Project 44 and Thermodynamics Research Centre Data Project, Texas A. and M. University, College Station, Texas, 77843 (USA); S.P. Sadtler, Raman Special Collection, Sadtler Research Laboratories, Philadelphia; Sadtler Raman Reference Spectra (5 volumes) Heyden and Son Ltd., London(1975); B. Schrader and W. Meier, Raman/IR Atlas, Verlag Chemie, Weinheim (1974)

42. B. Wunderlich, "Crystalline High Polymers: Molecular Structure and Thermodynamics", The American Chemical Society, Washington D.C. (1969)

43. A. Keller and S. Sawada. Makromol. Chem. 74, 190 (1964); R.A. Palmer and A.J. Cobbold, Makromol. Chem. 74, 174 (1964).

44. P.J. Hendra, E.P. Marsden, M.E.A. Cudby and H.A. Willis, Makromol. Chem. 176, 2443 (1975).

45. M.J. Folkes, A. Keller, J. Stejny, P.L. Goggin, G.V. Frazer and P.J. Hendra, Kolloid Z. und Z. Polymere, 253, 354 (1975)

46. B. Fanconi and J. Crissman, J. Polym. Sci., Polymer Letters, 13, 421 (1975)

47. G.V. Frazer, P.J. Hendra, M.E.A. Cudby and H.A. Willis, J. Materials Sci. 9, 1270 (1974)

48. L. Mandelkern, "Crystallization of Polymers", McGraw-Hill Book Co. New York, 1974. (also see Ref. 4).

49. A. Sharples, "Introduction to Polymer Crystallization", St. Martin's Press, New York, 1966

50. C.W. Bunn, Trans. Farad. Soc. 35, 482 (1939)

51. K. Imada, T. Miyazawa, Y. Chatani, H. Tadokoro and S. Murahashi, Makromol. Chem. 83, 113 (1965)

52. S. Kobayashi, H. Tadokoro and Y. Chatani, Makromol. Chem. 112, 225-241 (1968)

53. T. Uchida and H. Tadokoro, J. Polym. Sci., A-2, 5, 63 (1967); G.A. Carazzolo and M. Mammi, J. Polym. Sci. A-1, 965 (1963)

54. H. Tadokoro, Y. Chatani, T. Yoshihara, S. Tahara and S. Murahashi, Makromol. Chem. 73, 109 (1964)

55. H. Tadokoro, Y. Takahashi, Y. Chatani, and H. Kakida, Makromol. Chem. 109, 96, (1967); H. Kakida, Y. Chatani, M. Kobayashi and H. Tadokoro, Macromolecules 3, 369 (1970)

56. N.G. Gaylord and Herman F. Mark, "Linear and Stereoregular Addition Polymers", Interscience Publishers, New York, 1959

57. J.H. Schachtschneider and R.G. Snyder, Spectrochim.Acta 19, 117 (1963)

58. H. Lipson and H. Steeple, "Interpretation of X-ray Powder Diffraction Patterns, MacMillan, London, St. Martin's Press, New York, 1970

59. M.J. Gall, P.J. Hendra and D.S. Watson, Appl. Spectrosc. 25(4), 423, (1971)

60. J.L. Koenig, Appl. Spectrosc. 4(2), 233, (1971)

61. D.I. Bower in Structural prop. oriented polym. pp.187-218, Edit. W. I. Macmillan, Wiley New York, N.Y. (1975)

62. R.G. Snyder and J.H. Schachtschneider, Spectrochim. Acta 19, 85 (1963)

63. M. Tasumi, T. Shimanouchi and T. Miyazawa, J. Mol. Spectry. 9, 261 (1962); 11, 422 (1963)

64. H. Matsuura and T. Miyazawa, Spectrochim. Acta, 23A, 2433 (1967)

65. F.J. Boerio, J.L. Koenig, J. Macromol. Sci. - Rev . Macromol. Chem., C7(2), 209-249 (1972)

66. H. Tadokoro in reference 15.

67. D.O. Hummel in reference 15.

68. G. Zerbi, F. Ciampelli, V. Zamboni, J. Polym. Sci. C-7, 141-151 (1964)

69. E.S. Clark and L.T. Muus, Z. Krist. 117, 119 (1962)

70. S.W. Cornell and J.L. Koenig, J. Polym. Sci., A,7, 1965 (1969)

71. C.W. Bunn, Proc. Roy. Soc. (A), 180, 40-65 (1942)

72. S. Krimm, Adv. Polym. Sci. 1, 103, (1960)

73. P.J. Hendra, H.P. Jobic and K. Holland-Moritz, J. Polym. Sci., 13B, 365 (1975)

74. M. Tasumi and T. Shimanouchi, J. Chem. Phy. 43, 1245 (1965)

75. F.J. Boerio and J.L. Koenig, J. Chem. Phys. 52, 3425 (1970)

76. R.F. Schaufele and T. Shimanouchi, J. Chem. Phys. 47(9), 3605 (1967)

77. R.G. Snyder, J. Chem. Phys. 47, 1316 (1967)

78. A.F. Burmester and P.H. Geil in R.D. Pae, D.R. Morrow and Yu Chen "Advances in Polymer Science and Engineering", Plenum, New York, pp.42-100, 1972

79. P.H. Geil, Encyclop. Polym. Sci. Technol. 5, 662-9 (1966)

80. J.R. Overton and S.K. Haynes, J. Polym. Sci. 43, 9-17 (1973)

81. R. Bonart, R. Horemann and L.L. McCullough, Polymer, 4, 199, (1963)

82. A. Siegmann and P.H. Geil, J. Macromol. Sci. (Phys.) B4, 557,(1970)

83. B. Wunderlich, J. Polym. Sci., 43, 29-42 (1973)

84. J.R. Knox, J. Polym. Sci. 18C, 69-77, (1967)

85. H.G. Olf, A. Peterlin and W.L. Peticolas, J. Polym. Sci., B12, 359 (1974)

86. J.L. Koenig and D.L. Tabb, J. Macromol. Sci. Phys. B9, 141 (1974)

87. P.J. Hendra in R.G.J. Miller and B.C. Stace, Laboratory methods in infra red spectroscopy, II Edit., Chapter 15, pp.230-267, Heydon and Son Ltd., London,1973.

88. M. Schubert, Expt. Techn. Physik. 8, 1155 (1960)

89. J. Lal and G.S. Trick, J. Polym. Sci. 1, 13-19 (1961)

90. U.S. Patent 3, 320, 217, cl. 260-79, May 16, 1967

91. C.S. Marvel and A. Kotch, J. Amer. Chem. Soc. 70, 993 (1948)

92. Y. Gotoh, H. Sakakihara and H. Tadokoro, Polymer J. 4(1), 68 (1973)

93. P.J. Hendra and E.J. Loader, Chem. and Ind. 318 (1968)

94. J. Boon and E.P. Magré, Makromol. Chem. 126, 130 (1969)

95. R.H. Atalla, Private Communication (1971)

96. E. Steigner, Ph.D. Thesis, Westphalian Wilhalms University, Munich, Germany (1969)

97. B. Schrader and W. Meier, Z. Anal. Chem., 260 , 248 (1972)

98. C.G. Cannon and G.B.B.M. Sutherland, Spectrochim. Acta 4, 373 (1951)

99. H.L. McMurry and V. Thornton, Anal. Chem., 24,318 (1952)

100. C.W. Young, R.B. Duvall and N. Wright, Anal. Chem., 23, 709 (1951)

101. R.P. Bell, H.W. Thompson and E.E. Vago, Proc. Roy. Soc., A192, 498 (1948)

102. A.R.H. Cole and H.W. Thompson, Trans. Farad. Soc. 46, 103 (1950)

103. H. Fromherz, H. Buren and L. Thaler, Angew. Chem. A59, 142 (1947)

104. R.J. Bourguel and M.L. Piaux, Bull. Soc. Chim., 2(5), 1958 (1935)

105. B. Gredy, Bull. Soc. Chim. 2(5), 1029 (1935)

106. H.V. Risseghem, B. Gredy and M.L. Piaux, Compt. Rend., 196, 938 (1933)

107. D.A. McCaulay, A.P. Lien and P.J. Launer, J. Amer. Chem. Soc., 76, 2354 (1954)

108. L.J. Bellamy, R.F. Lake and R.J. Pace, Spectrochim. Acta, 19, 443 (1963)

109. D. Hadzi and N. Sheppard, Proc. Roy. Soc. A216, 247 (1953)

110. K.W.F. Kohlrausch and Kopple, Z. Physik. Chem., 24B, 370 (1934)

111. E.J. Hartwell, R.E. Richards and H.W. Thompson, J. Chem. Soc. 1436 (1948)

112. G.M. Barrow, J. Chem. Phys. 21, 2008 (1953)

113. H.C. Cheng, Z. Physik. Chem. 24B, 293 (1934)

114. R.N. Jones and F. Herling, J. Org. Chem. 19, 1252, (1954)

115. J.F. Grove and H.A. Willis, J. Chem. Soc., 877 (1951)

116. K.W.F. Kohlrausch, A. Pongratz and R. Seka, Ber. 66B, 1, (1933)

117. A.R. Kartritzky and N.A. Jones, J. Chem. Soc. 2067 (1959)

118. R.G. Cooke, Chemistry and Industry, 142 (1955)

119. G. Carazzolo and G. Valle, Makromol. Chem., 90, 66 (1966)

120. Y. Takahashi, H. Tadokoro and Y. Chatani, J. Macromol. Sci. (Phys.) B2(2), 361 (1968)

121. H. Sakakihara, Y. Takahashi and H. Tadokoro, Abstracts SPSJ 18th Annual Meeting, Tokyo, November 11, 1969, P407 (Japanese).

122. R.G. Snyder, J. Mol. Spectry., 7, 116 (1961)

123. C.Y. Liang and S. Krimm, J. Chem. Phys. 25, 563 (1956)

124. V. Zamboni and G. Zerbi, J. Polym. Sci. C(7), 153 (1964)

125. A.R. Philpotts, D.O. Evans and N. Sheppard, Trans. Farad. Soc., 51, 1051 (1955)

126. T. Miyazawa, K. Fukushima, and Y. Ideguchi, J. Chem. Phys. 37, 2764 (1962)

127. H. Tadokoro, M. Kobayashi, Y. Kawaguchi, A. Kobayashi and S. Murahashi, J. Chem. Phys., 38, 703 (1963)

128. Y. Matsui, T. Kubota, H. Tadokoro and T. Yoshihara, J. Polym. Sci., A3, 2275 (1965)

129. F.J. Boerio and D.D. Cornall, J. Chem. Phys., 56(4) (1972)

130. G. Zerbi and P.J. Hendra, J. Mol. Spectry. 27, 17 (1968)

131. H. Sugeta, T. Miyzawa and T. Kajiura, J. Polym. Sci. B7, 251 (1969)

132. T. Kitagawa and T. Miyazawa, International Symposium on Macromolecular Chemistry, Tokyo-Kyoto, 1966, Paper 2.5.04.

133. J.E. Preedy and E.J. Wheeler, Nature (Phys. Sci.), 236, 60 (1972)

134. H. Miyaji and Kenjiro Asai, J. Phys. Soc. Japan, 36, 1497 (1974)

135. J. Takeda, K. Hayashi and S. Okamura, J. Appl. Polym. Sci., 13, 1435 (1969)

136. D.O. Hummel, "Infra red Analysis of Polymers, Resins and Additives" (Atlas), Wiley Interscience, New York (1969)

137. P.J. Hendra, D.S. Watson and M. Mammi, Spectrochim. Acta, 28A, 351 (1972)

138. M. Ohsaku, Bull. Chem. Soc. Japan, 47(4), 965 (1974)

139. Zitomer Fred, Anal. Chem., 40(7) 1091 (1968)

140. A.C. Angood and J.L. Koenig, J. Macromol. Sci. (Phys.), B3(2), 321 (1969)

141. M. Yokoyama, H. Ochi, A.M. Ueda and H. Tadokoro, J. Macromol. Sci. (Phys.) B7(3), 465 (1973)

142. T. Miyazawa, K. Fukushima and Y. Ideguchi, J. Chem. Phys. 37(12), 2764 (1962)

143. T. Yoshihara, H. Tadokoro and S. Murahashi, J. Chem. Phys. 41(9), 2902 (1964)

144. H. Matsuura and T. Miyazawa, J. Polym. Sci. A2, 7, 1735 (1969).

145. H. Matsuura and T. Miyazawa, Bull. Chem. Soc. Japan, 42, 372 (1969)

146. H. Matsuura and T. Miyazawa, Bull. Chem. Soc. Japan, 41, 1798 (1968)

147. R.F. Schaufele, J. Opt. Soc. Am. 57, 105 (1967)

148. J.L. Koenig and A.C. Angood, J. Polym. Sci. A2 8, 1787 (1970)

149. G.V. Frazer, P.J. Hendra and D.S. Watson, M.J. Gall, H.A. Willis and M.E.A. Cudby, Spectrochim. Acta 29A, 1525 (1973)

150. Z. Mencik, Macromol. Sci. (Phys.), B6, 101 (1972)

151. M. Tasumi and S. Krimm, J. Chem. Phys. 46, 755 (1967)

152. N. Nogami; H. Sugeta and T. Mujazawa, Chem. Lett. (Chemical Society of Japan) 147 (1975).

153. D. Makino, M. Kobayashi and H. Tadokoro, J. Chem. Phys. 51(9), 3901 (1969)

154. K. IMada, H. Tadokoro, A. Umehara and S. Murahashi, J. Chem. Phys., 42(8), 2807 (1965)

155. D. Makino, M. Kobayashi and H. Tadokoro, Rep. Progr. Polym. Phys. Japan, 13, 169 (1970)

156. E.F. Lutz and S. Searles, J. Amer. Chem. Soc., 80, 3168 (1958)

157. B. Fanconi, E.W. Small and W.L. Peticolas, Biopolymers, 10, 1277 (1970)

158. G. Turrel, "Infra red and Raman spectra of crystals", Academic Press, London, 1972

159. F.J. Balta Calleja, J. Appl. Cryst., 7, 506 (1974)

160. Kitaigorsdski Organic Chemical Crystallography (Consultants Bureau 1961) p.177.; S.M. Ohlberg, J. Phys. Chem. 63, 248 (1959)

161. K. Itoh and T. Shimanouchi, Biopolymers, 9, 383 (1970)

162. J.B. Downes (Private communication)

163. P. Dreyfus, A. Keller, J. Macromol. Sci. (Phys.), B4, 811 (1970); P. Dreyfus, A. Keller, F.M. Willmouth, J. Polym. Sci. A2, 10, 857 (1972); E.D.T. Atkins, A. Keller, D.M. Sadler, J. Polym. Sci. A2, 10, 863 (1972)

164. N. Okui, Ph.D. Thesis, Tokyo Institute of Technology, 1973; J. Loboda-Cackovic, H. Cackovic, R. Hosemann, J. Polym. Sci., (in Press)

165. J.P. Arlie, P. Spegt, A. Skoulios, Makromol. Chem. 104, 212 (1967); B. Gilg, A. Skoulios, Makromol. Chem., 140, 149 (1970)

166. S. Fernandez-Bermudez, F.J. Balta Calleja and R. Hosemann, Makromol. Chem. 175, 3567 (1974)

167. E. Balcerzyk, H. Pstrocki and W. Wlodarski, J. Appl. Polym. Sci., 11, 1179 (1967)

168. G. Varsanyi, Vibrational Spectra of Benzene Derivatives, Academic Press, New York, 1969.

169. A.M. Bogomolov, Opt. Spectrosc., 9,162 (1960)

170. Ibid, 10, 162 (1961)

171. Ibid, 12, 99 (1961)

172. Ibid, 13, 90 (1962)

173. Ibid, 13, 183 (1962)

174. J.H.S. Green, W. Kynaston and A.S. Lindsey, Spectrochim. Acta, 17, 486 (1961)

175. J.H.S. Green, Spectrochim. Acta 17, 607 (1961)

176. Ibid, 18, 39 (1962)

177. Ibid, 24A, 1627 (1968)

178. J.H.S. Green and W. Kynaston, Spectrochim. Acta, 25A , 1677 (1969)

179. J.H.S. Green, Spectrochim. Acta, 26A, 1503 (1970)

180. J.H.S. Green, D.J. Harrison, W. Kynaston and D.W. Scott, Spectrochim. Acta, 26A, 1515 (1970)

181. J.H.S. Green, Spectrochim. Acta, 26A, 1523 (1970)

182. Ibid, 26A, 1913 (1970)

183. J.H.S. Green and D.J. Harrison, Spectrochim. Acta, 26A, 1925 (1970)

184. J.H.S. Green, D.J. Harrison and W. Kynaston, Spectrochim. Acta, 27A, 793 (1971)

185. Ibid, 27A, 807 (1971)

186. J.H.S. Green and H.A. Louwers, Spectrochim. Acta, 27A, 817 (1971)

187. J.H.S. Green, D.J. Harrison and W. Kynaston, Spectrochim. Acta, 27A, 2199 (1971)

188. Ibid, 28A, 33 (1972)

189. M. Margoshes and V.A. Fassel, Spectrochim. Acta, 7, 14 (1955)

190. I. Sakurada and K. Kaji, J. Polym. Sci., C31, 57 (1970)

APPENDIX I

NOTATIONS

ν (cm^{-1})	Frequency in wavenumbers
EM	Electron microscopy
DSC	Differential scanning calorimetry
f.a.	Fibre axis
I	Intensity
IR	Infra Red
LAM	Longitudinal acoustic mode
LAXD	Low angle X-ray diffraction
WAXD	Wide anlge X-ray diffraction
L_R	Raman length
L_x	LAXD long spacing
MS	Mass spectroscopy
NMR	Nuclear magnetic resonance spectroscopy
ρ	Density
M-	Meta
O-	Ortho
P-	Para
POM	Polyoxymethylene
PEO	Polyethylene oxide
POCB	Polyoxacyclobutane
PTHF	Polytetrahydrofuran
PHMO	Polyhexamethylene oxide
PDMO	Polydecamethylene oxide
PTM	Polythiomethylene
PES	Polyethylene sulphide
PTrMS	Polytrimethylene sulphide
PTMS	Polytetramethylene sulphide
PPMS	Polypentamethylene sulphide

PHMS	Polyhexamethylene sulphide
PDMS	Polydecamethylene sulphide
PE	Polyethylene
P	Polarized
dP	Depolarized
T_m	Melting temperature
T_{ann}	Annealing temperature
ν_s	Symmetric stretching
ν_a	Asymmetric stretching
δ	Deformation
W	Wagging
T	Twisting
R	Rocking
τ	Torsion
VS	Very strong
S	Strong
M	Medium
MW	Medium weak
W	Weak
VW	Very weak
V	Variable
ϕ	Phenyl
$\perp$	Pependicular
$\parallel$	Parallel
Sh	Shoulder

APPENDIX II

LIST OF ORGANIC COMPOUNDS

List of organic compounds analysed for deductions described in Chapter III. The compounds are arranged under the titles of their characteristic groups.

Monosubstituted Benzenes

1 Anisole
2 Aniline
3 Acetanilide
4 Azobenzene
5 Benzoic acid
6 Benzoin
7 Benzil
8 Benzoic anhydride
9 Bromobenzene
10 Benzylidine chloride
11 Benzene sulphonamide
12 Benzyl amine
13 Benzamide
14 Benzanilide
15 Benzpinacol
16 Tert. Butyl benzene
17 Benzaldehyde
18 Benzonitrile
19 Benzyl alcohol
20 Benzhydrol
21 Benzyl acetate
22 Benzoyl chloride
23 Benzophenone
24 Cumene (Isopropyl benzene)
24 Cinnamaldehyde
26 Cinnamic acid
27 Chlorobenzene
28 Dibenzyl
29 Diphenyl
30 Diphenyl acetylene
31 P-Diphenyl benzene
32 Diphenyl mercury
33 Diphenyl sulphone
34 Diphenyl sulphoxide
35 Diphenyl ether
36 Dibenzyl ether
37 Diphenyl acetylene
38 Diphenyl amine
39 Diphenyl disulphide
40 Sym. Diphenyl thiourea
41 Ethyl benzene
42 N-Ethyl aniline
43 Ethyl benzoate
44 Fluorobenzene
45 Hippuric acid
46 P-Hydroxy azobenzene
47 Isothiocyanatobenzene
48 Isobutylbenzene
49 Mendelic acid
50 Methyl phenyl acetylene
51 4-Methoxyazobenzene
52 Nitrobenzene
53 P-Nitrodiazoamine azobenzene
54 4-Nitronaphthalene diazoamine azobenzene
55 Phenol
56 Toluene
57 Triphenyl arsenic dibromide
58 O-Triphenyl
59 Triphenyl ammonia
60 Triphenyl amine
61 Triphenyl arsine
62 Triphenyl antimony
63 Triphenyl phosphine
64 Triphenyl phosphoxide

65 Thiophenol
66 Thioanisol
67 S-Benzene Thiouranium chloride
68 Thioacetanilide
69 Tetraphenyl boron
70 Tetraphenyl tin

Disubstituted Benzenes

(1) (O -) 1-2

1 Acetyl salicylic acid
2 O-Anisidine
3 O-Bromobenzoic acid
4 O-Catechol
5 O-Chloroaniline
6 O-Chloronitrobenzene
7 O-Chlorophenon
8 O-Cresol
9 O-Dichlorobenzene
10 O-Dimethoxybenzene
11 Diethyl phthalate
12 Guiacol (O-methoxyphenol)
13 O-Iodobenzoic acid
14 2-Mercaptobenzothiazol
15 O-Nitrobenzoic acid
16 Phthalic acid
17 Phthalic anhydride
18 Potassium hydrogen phthalate
19 Salicylic acid
20 Salicyldehyde
21 O-Triphenyl
22 O-Toluene thiol
23 Thiomersal
24 Salicyl sulphonic acid

---

(2) (M -) 1-3

1 M-Amino phenol
2 M-Bromonitrobenzene
3 M-tert. Butyl phenol
4 M-Chloroaniline
5 M-Chloronitrobenzene
6 M-Chloroperbenzoic acid
7 M-Cresol
8 M-Difluorobenzene
9 M-Dinitrobenzene
10 M-Dimethoxy benzene
11 Ethyl M-nitrobenzoate
12 M-Fluorotoluene
13 M-Hydroxybenzaldehyde
14 M-Hydroxybenzoic acid
15 M-Nitrotoluene
16 M-Nitrobenzoic acid
17 M-Nitrobenzene sulphonyl chloride
18 Resorcinol
19 M-Toluene thiol
20 M-Toluic acid
21 M-Toluidine

---

(3) (P -) 1-4

1 Acet-P-bromoanilide

2 P-Aminosalicylic acid sodium salt

3 Anisoin (4:4' Dimethoxy benzoin)

4 Anisic acid

5 P-Bromochlorobenzene

6 P-Bromobenzene sulphonic acid sod. salt

7 P-Bromoacetophenone

8 P-Bormophenacyl bromide

9 P-Carboxybenzosulphone dichloramide (Halozone)

10 P-Dichlorobenzene

11 P-Dimethoxy benzene

12 P-Dimethyl aminobenzaldehyde

13 P-Diphenyl benzene

14 P-Hydroxy benzaldehyde

15 P-Hydroxy benzoic acid

16 P-Hydroxy azobenzene

17 P-Methoxy azobenzene

18 P-Methoxy phenyl acetic acid

19 P-Nitrobenzyl alcohol

20 O-Nitrophenyl hydrazine

21 P-Nitrobenzoic acid

22 P-Nitrobenzene diazoaminoazobenzene

23 Metol

24 Quinol

25 Sulphaguanidine

26 P-Thiocresol

27 P-Dimethyl benzene

Trisubstituted Benzenes

1, 2, 3

1 2-6 Dimethoxy phenol
2 2-6 Dinitroaniline
3 2-3 Dichlorophenol
4 2-6 Dinitrophenol
5 2-6 Diethyl aniline
6 2-Hydroxy-M-toluic acid
7 3-Nitrophthalic acid
8 Pyrogallol
9 Salicyl sulphonic acid
10 1-2-3, Trimethoxy benzene
11 3-Nitrophthalic anhydride
12 1-2-3 Tricarboxylic acid
13 1-2-3 Trichloro benzene

1, 3, 5

1 3-5 Dichlorophenol
2 3-5 Dinitrobenzoic acid
3 3-5 Dinitrobenzoyl chloride
4 1-3-5 Trifluorobenzene
5 1-3-5 Trinitrobenzene
6 Phloroglucinol
7 Mesitylene

1, 2, 4,

1 1-2-4 Benzene tricarboxylic acid
2 1-Bromo 3-4 dimethoxy benzene
3 4-Bromo-M-Xylene
4 1-Chloro 2-4 dinitrobenzene
5 4-Chloro 2-nitroaniline
6 Bromo 2-4 dinitrobenzene
7 2-4 Dinitroaniline
8 2-4 Dibromophenol
9 2-4 Dinitrodiphenyl amine
10 3-4 Dimethoxy benzaldehyde
11 3-4 Dimethoxy phenyl acetic acid
12 2-5 Dichloronitrobenzene
13 2-4 Dinitrophenyl hydrazine
14 2-4 Dinitroanisole
15 2-4 Dinitrotoluene
16 O-Nitro P-toluidine
17 Orcinol (5-Methylresorcinol)
18 4-Nitrophthalamide
19 Safrole
20 Thymol
21 3-4 Xylidine
22 2-4 Xylidine
23 O-tert. Butyl catechol
24 Vaniline
25 4-Alkyl 1,2 dimethoxy benzene
26 1-2 Tri fluorobenzene

Tetrasubstituted Benzenes

1-2-3-4

1 3-6 Dihydroxy phthalonitrile
2 1-2-3-4 Tetrafluorobenzene
3 1-2-3-4 Tetramethyl benzene

1-2-3-5

1 4 Chloro-3-5 xylenol
2 2-6 Dibromo-4-nitrophenol
3 Picryl chloride
4 1-2-3-5 Tetrafluorobenzene
5 2-4-6 Tribromoaniline
6 2-4-6 Tribromophenol
7 3-4-5 Trihydroxy benzoic acid
8 2-4-6 Trimethyl phenol
9 2-4-6 Trinitrobenzoic acid
10 3-4-5 Trimethoxy benzoic acid
11 2-4-6 Trimethyl benzoic acid

1-2-4-5

1 2-5 Dichloro-P-quinone
2 2-5 ditert. Butyl quinone
3 1-2-4-5 Tetracarboxylic acid
4 1-2-4-5 Tetrachlorobenzene
5 1-2-4-5 Tetrafluorobenzene
6 1-2-4-5 Tetramethyl benzene

Pyridyl Compounds

1 2-Amino pyridine
2 3-Acetyl pyridine
3 4-Benzoyl pyridine
4 2-4-6 Collidine
5 2-2 Diphridyl
6 4-Ethyl pyridine
7 3-Hydroxy pyridine
8 3-Methyl pyridine
9 4-Nitropyridine-N-oxide
10 2-Benzoyl pyridine
11 2-3 Lutidine
12 α-Picoline
13 β-Picoline
14 γ-Picoline
15 Pyridine
16 3-Pyridyl acetic acid
17 Pyridinium chloride

Pentasubstituted Benzenes

1. Pentachlorobenzene
2. Pentafluorobenzene
3. Benzene pentacarboxylic acid
4. Pentamethyl benzene

Hexasubstituted Benzenes

1. Chloranil (Tertrchloroquinone)
2. Hexafluorobenzene
3. Hexamethyl benzene
4. Pentafluorochlorobenzene
5. 2,4,6 Trinitro 3-5 dimethyl tert. butyl benzene

Naphthalenes

1. Acet-1-naphthyl amide
2. 1-Bromonaphthalene
3. 2-Bromonaphthalene
4. 1-Chloro-4-naphthol
5. 1-Chloronaphthalene
6. 2-Isocyanatonaphthalene
7. 2-Hydroxy-3-naphthoic acid
8. 2-Hydroxy 1-4 naphthoquinone
9. Naphthalene
10. 1-Naphthol
11. 2-Naphthol
12. 2-Naphthoylchloride
13. 4-Nitronaphthalene diazoamino-azobenzene
14. 6-Bromo-2-naphthalene
15. 2-Nitro-1-naphthol
16. Octafluoronaphthalene
17. 2-Isocyanatonaphthalene
18. Nitroso R-salt($C_{10}H_4BH(SO_3Na)_2NO$)
19. 1-Chloro-2-naphthol
20. 1-4 Naphthoquinone
21. 1-Nitroso-2-naphthol

Cyclic and Open Chain Compounds

1. tert. Butyl amine
2. sec. Butyl amine
3. Cyclopentanone
4. Cyclohexanone
5. Cycloheptanone
6. Cyclohexane
7. n-Hexane
8. n-Pentane
9. n-Heptane
10. n-Octane
11. n-Dodecane
12. Octyl iodide
13. Octaldehyde
14. N-Butyramide
15. 1-Bromooctane
16. N:N Diethylcyclohexyl amine

Sulphur Compounds

Di and polysulphide and carbon-sulphide linkages

1 Allyl thiourea
2 L-Cystiene
3 L-Cystine
4 Ethyl potassium xanthate
5 N:N ethylene thiourea
6 S-Benzylthiouranium chloride
7 Dimethyl sulphoxide
8 Methionine
9 Polyethylene monosulphide
10 Polyethylene disulphide
11 Polyethylene trisulphide
12 Polyethylene tetrasulphide
13 Sod.dithiodiethyl carbamate
14 Sulphaguanidine
15 Sulpholane
16 3-Sulpholene
17 Thianthrene
18 Thioacetamide
19 Thioacetanilide
20 Thioanisole
21 Thiocaprolactam
22 Thiomersal
23 Thioglycollic acid
24 Thiodiglycollic acid
25 Thiophene
26 Thiourea
27 Thioformaldehyde
28 Sym. Diphenyl thiourea
29 Diphenyl sulphoxide
30 Diphenyl disulphide
31 Dimethylene sulphoxide
32 Isothiocyanato benzene
(plus already listed compounds)

Thiol linkages

1 P-Thiocresol
2 M-Toluene thiol
3 O-Toluene thiol
4 Thiophenol
5 Thioglycollic acid
6
7 2-Mercaptobenzothiazole
8 Mercaptoethanol
9 Cystiene
(plus already listed)

Anhydrides

1 Maleic anhydride
2 Succinic anhydride
3 Dichloromaleic anhydride
4 Benzoic anhydride
5 Phthalic anhydride
6 2-Nitro phthalic anhydride
7 Acetic anhydride
8 Propioanhydride
9 Butyranhydride
10 Pyromellictic dianhydride

APPENDIX III

PUBLICATIONS

The following published papers were included in the bound thesis. These have not been digitised due to copyright restrictions, but the links are provided.

https://doi.org/10.1007/BF00754475